

5. INNER NEARSHORE SEDIMENT CONCENTRATIONS AND SEDIMENT FLUXES

5.1 Introduction

In the previous chapter the surface wave hydrodynamics and cross-shore velocity field under waves were examined. These items were studied because they induce sediment transport which, in turn, results in morphological development of inner nearshore bars. To gain further insight in these sediment transport processes it is necessary to address the following research questions (cf. Chapter 2):

- what is the relative contribution of the high-frequency oscillating, suspended sediment transport, the low-frequency oscillating, suspended sediment transport, the mean suspended sediment transport and bedload transport to the total sediment transport in the nearshore?
- how does the relative contribution of these sediment transport mechanisms vary around a breakpoint, i.e. under different wave conditions?
- what is the order of magnitude and direction of the sediment transport around a breakpoint, i.e. under different wave conditions?
- what is the degree of convergence or divergence of the net sediment transport near the inner nearshore bar?

The sediment transport is considered to be the product of the velocity field and the sediment concentration. The character of the velocity field under different hydraulic conditions was discussed in Chapter 4. Hence, this chapter starts with a description of the sediment concentrations. The sediment transport is analysed in two ways: by an instantaneous approach and by a time-averaged approach. The instantaneous approach addresses the importance of intra-wave phenomena for suspended sediment transport by evaluating the relative contribution of high-frequency (wind) waves, low-frequency waves and net currents to the cross-shore suspended sediment transport. The net directions and volumes of the bed load transport are studied next and the section ends with an evaluation and discussion of the total sediment transport.

The measured time-averaged sediment concentration and the time-averaged sediment transport are also compared with the TRANSPOR model (Van Rijn, 1993) which is capable of computing concentration and sediment transport in a combination of currents and waves.

The sediment transport measurements were performed near the inter-tidal bar. In the first place, therefore, the results give insight into the sediment transport processes near the beach. The aim of this study is, however, to apply this knowledge to the morphological behaviour of the *inner nearshore bar*. The results of the sediment transport analysis are related, therefore, to the relative wave height which was measured near the inner nearshore bar. In this way, the results of the sediment transport analysis may also give insight into the spatial and temporal variability of the net sediment transport around the inner nearshore bar.

5.2 Data validation and calibration

The equipment used to take the measurements consisted of three Electromagnetic current meters (EMF), four Optical backscatter sensors (OBS), a pump sampling system and a capacitive wire (CW). These instruments were mounted on the measuring platform, the BERT (see Section 3.6). Calibration and validation of the EMF and CW data were treated in Section 4.3. This section presents the calibration and validation of the OBS data.

Before the field campaign, The OBS probes were calibrated in a laboratory using a calibration tank (Fig. 5.1). The water, first dehydrated to reduce the presence of air bubbles, in this calibration tank was circulated in a closed circuit by a pump capable of keeping sediment up to 1000 μm in suspension. A small vacuum pump, also to reduce air entrainment by creating an under pressure, was mounted on top of the perspex cylinder. The sediment was added to the water from above the cylinder and a suction nozzle was mounted near the sensor to take the samples.

The calibration was performed using sediment samples from the field site and by applying the following linear correlation:

$$C = \alpha V + b \quad (5.1)$$

where

- C = concentration [kg/m^3]
- α = gain of OBS
- V = voltage OBS
- b = offset OBS

The correlation coefficients between the concentrations in the tank and the output voltage of the OBS were generally high ($R^2 \approx 0.99$). However, the calibration turned out to be unsatisfactory and unreliable. After applying these calibration curves to the field measurements, the highest concentrations were found at the upper OBS and the lowest concentrations at the lowest OBS, a far from logical outcome that does not agree with what is generally accepted, i.e. that the concentration decreases with elevation above the bed. It is believed that the main reason for these unexpected results is that the calibration was performed with clear water. In the field, however, the IR-backscatter also originates from organic material and air entrainment induced by breaking waves. As these factors primarily affect the offset of the OBS (Greenwood et al., 1990), the offset was determined by using the data of the pump sampling system that was operating during the field measurements (see Section 3.6). The mean values of the pump sampler of each session were correlated with the time-averaged output voltage of the OBS sensors while using the gain from the laboratory calibration.

The combined use of the field data for determining the offset and laboratory calibration for the gain (α) resulted in calibration coefficients (R^2) of about 0.65-0.70. These coefficients were about of the same order as Kroon's (1994) OBS calibration curves which were established in 1990 at the same field site and with the same set of instruments. The correlation coefficients were lower than those obtained under laboratory conditions. In the field, however, the trapping efficiency of the pump sampler is affected by a variation in time and space of sediment size and eddy

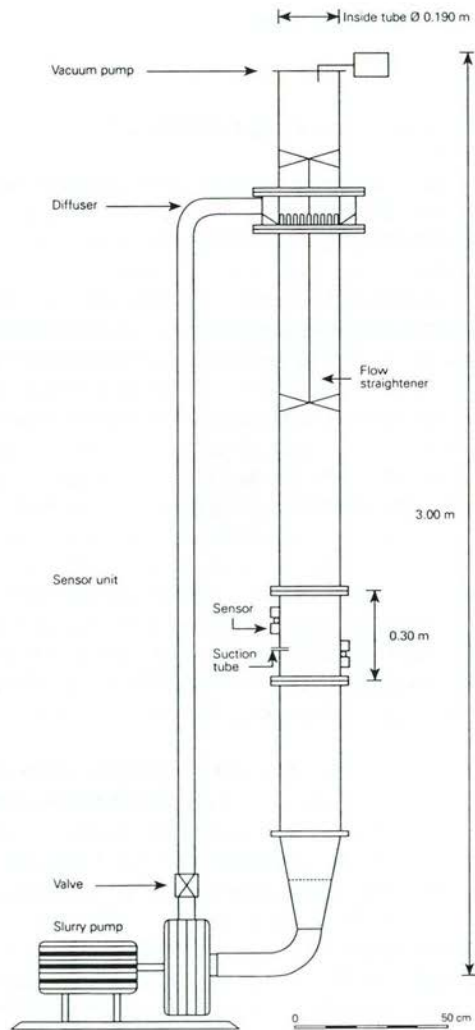


Figure 5.1 Calibration tank for the optical backscatter sensors (OBSS) (from Meene, 1994).

diffusivity. Moreover, the variation in sediment size and the higher levels of air bubbles also affects the OBS response (e.g. Black and Rosenberg, 1994). Hence the standard deviation of the session-averaged values of the pump sampler and the OBS is larger and results in lower correlation coefficients. Therefore, considering the turbulent environment, the results were satisfactory.

5.3 Sediment concentrations

5.3.1 Analysis and interpretation methods

The instantaneous relation between velocity and concentration was studied at 4 elevations above the bed (0.07, 0.12, 0.17 and 0.26 m) and the concentrations at these heights were recorded by the four OBSs. However, velocities were measured at only three elevations above the bed (0.1, 0.3 and 0.7 m). To make correlations between velocity and suspension events, the velocities at the OBS heights were calculated by linear interpolation and extrapolation using the EMFs at 0.1 and 0.3 m.

The relation between velocity and instantaneous concentration at a certain elevation was visualised in time-plots of measured velocity and concentration values and by calculation of the cross-spectra. A cross-spectrum resembles a frequency-dependent covariance function and reveals the velocity frequencies during which the bed sediment is actually dispersed from the bed into the vertical. In this way, a distinction can be made between the relevant conditions for sediment transport viz. high-frequency waves and low-frequency (infragravity) waves. Besides the cross-spectrum, coherence is also calculated, this being a measure of the frequency dependent correlation. The variation of the relation between velocity and concentration in the vertical is studied by applying the same analyses at the four elevations above the bed. In order to determine to what extent the concentrations at a higher level (0.26 m) are related to the near bed velocities (0.07 m), the correlations between the concentration at the four elevations were calculated using different time lags.

The concentrations obtained from the pump sampler were used to analyse the variation of time-averaged (over ca. 20 min) concentrations in the vertical, as these are likely to indicate the decay of concentrations higher in the vertical; they were obtained at elevations (0.035-0.6 m) higher than the OBS data (0.07-0.26 m). The time-averaged concentration was also used to verify the concentration profile model which is part of the TRANSPOR model (Van Rijn, 1993; Van Rijn and Kroon, 1993). The concentration profile model is based on a time-averaged convection-diffusion equation. A time-averaged model is used because a generally accepted modelling approach including both instantaneous and time-averaged effects is not yet available. The time-averaged convection-diffusion equation reads as follows:

$$cw_s + \varepsilon_s \frac{dc}{dz} = 0 \quad (5.2)$$

where

- w_s = particle fall velocity of suspended sediment in a fluid-sediment mixture [m s^{-1}]
- ε_s = sediment mixing coefficient [$\text{m}^2 \text{s}$]
- c = time-averaged concentration at elevation z above the bed [kg m^{-3}]

Originally, this equation was used to compute the equilibrium concentration in a steady flow. Here, it is assumed that the model is also valid for combined wave-current related mixing. Van Rijn (1993) proposed the following relationships for the wave-related sediment mixing coefficient for non-breaking waves:

$$\varepsilon_{s,w} = \varepsilon_{s,w,bed} = \alpha_b \cdot \delta_s \hat{U}_\delta \quad \text{for} \quad z \leq \delta_s \quad (5.3a)$$

$$\varepsilon_{s,w} = \varepsilon_{s,w,max} = \alpha_m h \frac{H_s}{T_p} \quad \text{for} \quad z \geq 0.5h \quad (5.3b)$$

$$\varepsilon_{s,w} = \varepsilon_{s,w,max} = \varepsilon_{s,w,bed} + \left[\varepsilon_{s,w,max} - \varepsilon_{s,w,bed} \right] \left[\frac{z - \delta_s}{0.5h - \delta_s} \right] \quad \text{for} \quad \delta_s < z < 0.5h \quad (5.3c)$$

where

- δ_s = thickness of the near bed mixing layer [m]
- α_b = 0.004 [-] = coefficient
- α_m = 0.035 [-] = coefficient
- \hat{U}_δ = peak orbital velocity at the edge of the wave boundary layer, based on significant wave height and wave peak period [m s^{-1}]
- H_s = significant wave height [m]
- T_p = peak wave period [s]
- z = elevation above the bed [m]
- h = water depth [m]
- $\varepsilon_{s,w,bed}$ = wave-related mixing coefficient near the bed [$\text{m}^2 \text{s}^{-1}$]
- $\varepsilon_{s,w,max}$ = wave-related mixing coefficient near the upper layer [$\text{m}^2 \text{s}^{-1}$]

The current-related sediment mixing coefficient over depth is calculated as:

$$\varepsilon_{s,c} = \kappa u_{*,c} z \left(1 - \frac{z}{h} \right) \quad \text{for} \quad z < 0.5h \quad (5.4a)$$

$$\varepsilon_{s,c} = 0.25 \kappa u_{*,c} h \quad \text{for} \quad z \geq 0.5h \quad (5.4b)$$

where

- κ = Von Karman constant (= 0.4) [-]
- $u_{*,c}$ = bed-shear velocity due to current [m s^{-1}]
- $\varepsilon_{s,c}$ = current related sediment mixing coefficient [$\text{m}^2 \text{s}^{-1}$]

Van Rijn (1989) proposed that equations 5.3 and 5.4 can be also be used for breaking waves. After analysis of concentration profiles in the surf zone of Egmond aan Zee, Kroon and Van Rijn (1993) suggested the following formula to calculate the thickness of the mixing layer under breaking waves.

$$\delta_s = 0.3h \left(\frac{H_s}{h} \right)^{0.5} \quad (5.5a)$$

$$\delta_{s,min} = 0.05 \text{ m} \quad (5.5b)$$

$$\delta_{s,max} = 0.2 \text{ m} \quad (5.5c)$$

The sediment mixing coefficient over depth for currents and waves combined is given by (Van Rijn and Kroon, 1993):

$$\varepsilon_{s,cw} = \left[(\varepsilon_{s,c})^2 + (\varepsilon_{s,w})^2 \right]^{0.5} \quad (5.6)$$

For the current-related and wave-related bed roughness ($k_{s,c}$ and $k_{s,w}$) a value of 0.01 m is used in the case of (non) breaking waves, breaking waves, breaking/swash and swash. The current- and wave-related bed roughness is set to 0.05 m for non-breaking waves. This higher value for non-breaking waves was chosen because ripples were more likely to be present, thereby increasing the roughness of the bed. However, ripples could not be observed during any of the measurements with the BERT because no appropriate instruments were available. The time-averaged velocity at the boundary layer was computed by the model, using linear wave theory and the measured significant wave height.

The bed boundary reference level was taken at the same height as the bed roughness height and the bed concentration is computed by (Van Rijn, 1993):

$$c_a = 0.015 \rho_s \frac{d_{50}}{a} \frac{T_a^{1.5}}{D_*^{0.3}} \quad (5.7)$$

where

- ρ_s = fluid sediment density [kg m^{-3}]
- a = reference level [m]
- T_a = dimensionless bed-shear stress for reference concentration at $z = a$ [-]
- d_{50} = median particle diameter of bed material [m]
- D_* = dimensionless particle diameter [-]
- c_a = reference concentration at the bed [kg m^{-3}]

For the suspended sediment size used to calculate fall velocity, Van Rijn (1993) suggests a value of 0.8 times the sediment size of the bed. This factor is also used in the present calculations where the sediment size of the bed was determined for each series using the bed load samples.

5.3.2 Results and discussion of instantaneous concentrations

Instantaneous concentrations near the bed

The analysis of the instantaneous concentrations first focuses on the lowest OBS (0.07 m above the bed). Thereafter, the variation of the concentration in the vertical will be discussed. The results are presented in Table 5.1.

Table 5.1 Hydrodynamic conditions and time-averaged concentrations

Series	h	H _a	T	Wave conditions	% breaking	H _a /L _a	H _a /h	Elevation nozzle 1 above bed [m]	Suspended Sediment Concentration [kg m ⁻³] at intake nozzle									
									1	2	3	4	5	6	7	8	9	10
	[m]	[m]	[s]		waves [-]	[-]	[-]											
2310-1	0.65	0.43	6.91	swash	-	0.055	0.66	0.082	3.400	4.789	3.880	2.673	3.475	2.975	2.175	1.708	+	+
2310-2	1.33	0.87	6.37	breaking	61.2	0.072	0.65	0.043	0.840	1.396	2.073	1.140	0.763	0.633	1.338	0.534	0.812	3.416
2310-3	1.34	0.90	6.72	breaking	70.1	0.071	0.67	0.044	4.025	3.368	2.204	0.673	2.143	1.596	1.480	1.271	+	+
2310-4	1.23	0.81	6.90	breaking	82.6	0.065	0.66	0.064	2.785	8.185	2.085	1.856	4.000	0.635	2.550	1.475	+	+
2310-5	1.03	0.73	7.36	breaking	74.6	0.057	0.71	0.055	*	*	*	2.940	2.490	2.556	2.870	1.270	+	+
2510-2	1.95	0.32	5.78	non breaking	0.0	0.056	0.16	0.060	0.141	0.158	0.222	0.102	0.099	0.073	0.068	0.006	+	+
2510-3	1.85	0.29	5.15	non breaking	0.0	0.056	0.16	0.067	0.080	0.090	0.050	0.050	0.040	0.030	0.050	0.015	+	+
2610-1	0.77	0.53	7.08	swash	-	0.058	0.69	0.071	5.055	4.923	4.075	2.400	2.290	2.044	1.284	+	+	+
2610-2	1.57	0.66	6.11	(non) breaking	3.4	0.069	0.42	0.067	0.568	0.343	0.578	0.440	0.317	0.265	0.107	0.087	+	+
2610-3	1.31	0.73	6.06	breaking	32.8	0.071	0.56	0.043	0.747	0.634	0.331	0.290	0.467	0.493	0.499	0.239	+	+
0411-1	0.87	0.49	8.04	swash	-	0.043	0.56	0.080	0.860	0.720	0.820	0.770	0.473	0.320	0.260	+	+	+
0411-2	1.21	0.66	7.72	breaking	84.9	0.051	0.54	0.035	2.030	2.400	1.100	0.984	0.766	0.849	0.725	0.430	+	+
0411-3	1.40	0.72	7.73	breaking	82.6	0.053	0.51	0.049	2.560	2.690	2.130	2.000	1.440	1.340	0.926	0.438	0.280	+
0411-4	1.37	0.70	7.71	breaking	84.6	0.052	0.51	0.033	2.040	1.700	2.010	1.630	1.500	1.190	1.110	0.639	0.190	+
0411-5	1.24	0.60	8.19	breaking	x	0.046	0.48	0.051	1.930	1.950	1.540	1.310	1.150	1.010	0.603	0.399	+	+
0411-6	1.05	0.47	8.28	breaking/swash	93.1	0.040	0.45	0.052	0.705	0.670	0.794	0.647	0.639	0.518	0.263	0.191	+	+
0511-1	1.00	0.64	7.04	swash	-	0.060	0.64	0.040	1.085	1.491	0.718	1.240	0.724	1.117	0.534	0.483	+	+
0511-2	1.20	0.74	6.52	breaking	84.9	0.065	0.61	0.040	1.783	1.773	1.825	1.538	1.361	1.131	1.070	0.789	0.493	+
0511-3	1.20	0.72	6.51	breaking	82.6	0.065	0.60	0.048	1.103	0.490	1.671	1.423	0.755	1.180	1.030	0.600	0.232	+
0511-4	1.08	0.67	6.73	breaking/swash	84.6	0.061	0.62	0.063	0.763	0.966	1.486	1.065	0.940	0.680	0.652	0.429	0.087	+
0511-5	0.89	0.58	6.77	breaking/swash	85.7	0.056	0.66	0.038	2.500	0.983	1.157	1.433	0.686	1.740	0.898	0.580	+	+
0611-1	0.97	0.57	6.98	breaking/swash	91.8	0.056	0.59	0.055	2.788	3.671	2.347	2.417	2.289	1.493	0.803	0.901	+	+
0611-2	1.50	0.81	5.81	breaking	71.2	0.079	0.54	0.070	0.992	0.462	0.568	0.679	0.889	0.458	0.522	0.372	0.197	+
0611-3	1.58	0.81	5.90	(non) breaking	64.1	0.078	0.51	0.050	0.626	0.064	0.482	0.389	0.145	0.232	0.136	0.109	0.099	+
0611-4	1.42	0.72	5.68	(non) breaking	69.1	0.075	0.51	0.050	0.905	0.319	0.077	0.783	0.645	0.998	0.893	0.808	0.272	+
0611-5	1.25	0.63	5.68	breaking	85.7	0.069	0.50	0.038	1.070	0.969	1.296	1.400	0.798	1.012	0.984	0.480	+	+
0711-1	1.06	0.68	6.64	swash	-	0.064	0.64	0.075	0.334	1.514	1.060	0.206	1.311	2.029	1.460	0.923	+	+
0711-2	1.61	0.88	6.26	breaking	35.5	0.075	0.55	0.063	1.174	2.033	1.495	0.885	2.185	1.850	1.290	1.130	0.639	+
0711-3	1.57	0.84	6.24	breaking	50.8	0.073	0.53	0.038	3.325	1.663	2.830	1.482	2.389	1.178	1.295	1.810	0.929	+
0711-4	1.29	0.68	6.31	breaking	-	0.065	0.53	0.040	2.320	2.643	4.114	4.444	2.570	1.930	1.109	1.340	0.520	+
0811-1	1.25	0.76	8.23	breaking	53.3	0.055	0.61	0.080	0.320	1.610	1.130	0.924	0.840	0.748	0.349	0.539	0.580	+
0811-2	1.62	0.80	8.20	(non) breaking	62.7	0.056	0.49	0.040	1.360	1.200	0.915	1.860	0.674	0.522	0.417	0.257	0.116	+
0811-3	1.43	0.79	8.06	breaking	78.0	0.056	0.55	0.040	1.194	1.900	1.432	0.616	1.173	0.610	0.464	0.332	0.232	0.340
0911-1	1.54	0.56	4.77	(non) breaking	36.0	0.084	0.36	0.057	0.720	0.573	0.480	0.314	0.205	0.134	0.081	0.157	0.064	0.009
0911-2	1.58	0.74	5.12	(non) breaking	10.4	0.087	0.47	0.037	0.531	0.756	0.255	0.453	0.267	0.087	0.052	0.006	0.003	+
0911-3	1.47	0.74	5.70	(non) breaking	23.1	0.077	0.50	0.040	1.526	1.165	1.163	0.978	0.658	0.679	0.463	0.155	0.163	0.142
1011-1	1.36	0.98	7.36	swash	-	0.065	0.72	0.025	2.880	2.170	1.700	1.940	1.070	1.530	1.320	1.170	0.669	+
1011-2	1.69	0.97	7.22	breaking	19.4	0.069	0.57	0.038	2.420	0.920	1.750	1.900	0.482	0.733	1.360	0.578	+	+
* = not determined because of pump failure									Intake nozzle number :									
+ = not measured because of low water level									1	2	3	4	5	6	7	8	9	10
x = not measured									Height above intake nozzle 1 [m] : -									
										0.015	0.035	0.065	0.115	0.215	0.365	0.585	0.815	1.06

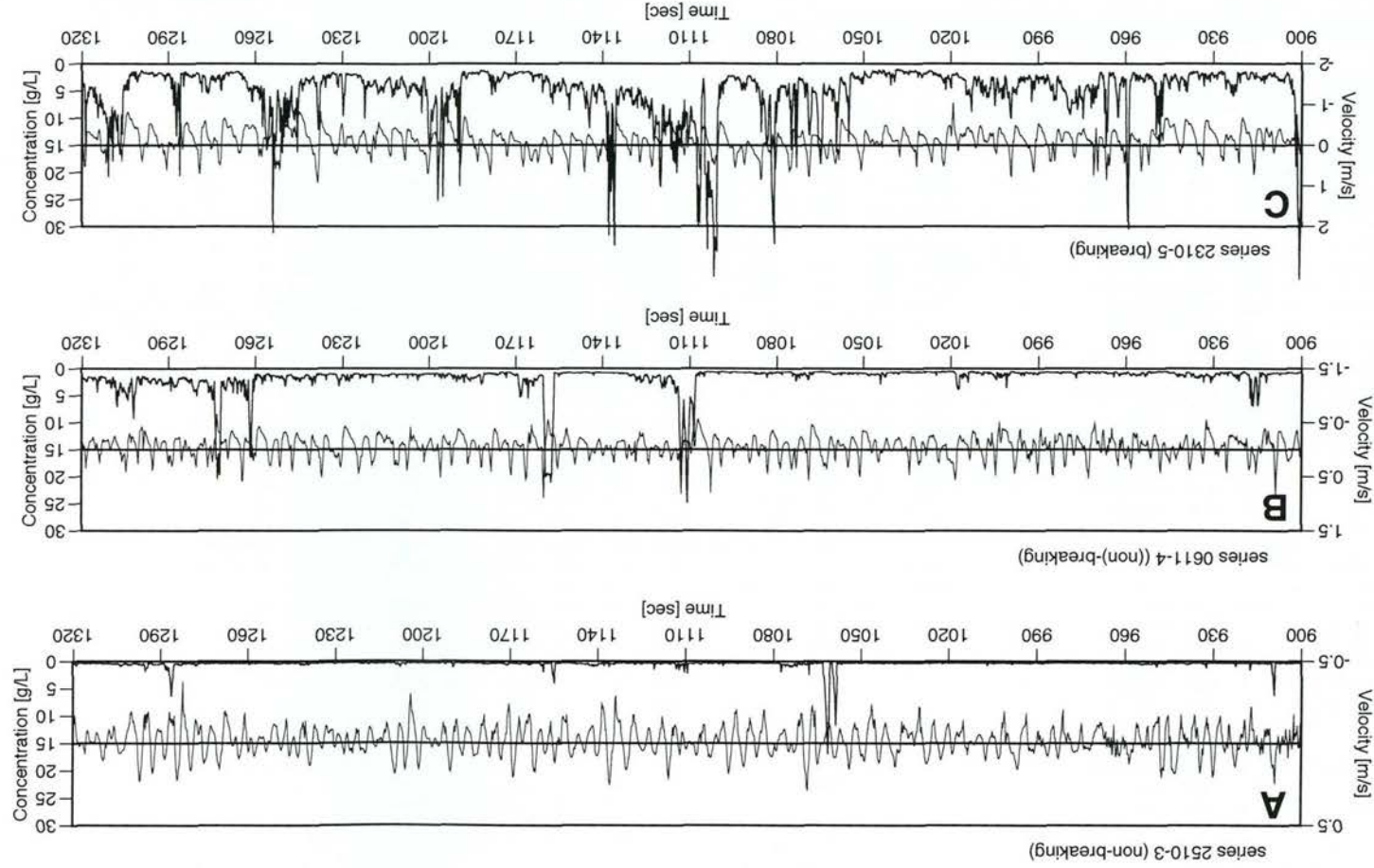


Figure 5.2 Time series of velocity (thin line) and concentration (thick line) at the lowest OBS level (0.07 m above the bed) in various hydrodynamic zones. Positive velocity is shown in the onshore direction, negative velocity in the offshore direction.

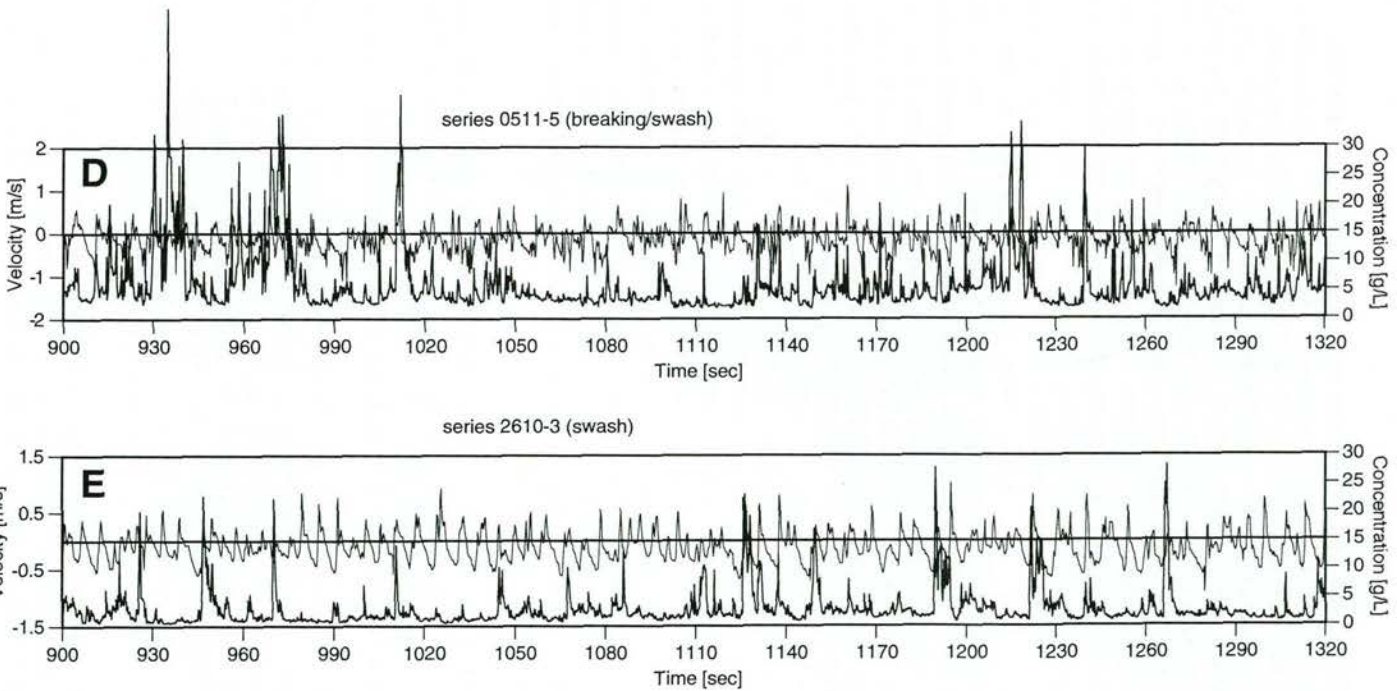


Figure 5.2

Time series of velocity (thin line) and concentration (thick line) at the lowest OBS level (0.07 m above the bed) in various hydrodynamic zones. Positive velocity is shown in the onshore direction, negative velocity in the offshore direction.

Figure 5.2 shows time-series of velocity and concentration near the bed for the five hydrodynamic zones, defined in Chapter 4. Intervals of 7 minutes starting at 10 minutes (900 seconds) and ending at 17 minutes (1320 seconds) were taken from the 40-minute time series. In all hydrodynamic zones, the sediment suspension is episodic. Periods of lower concentration, here named 'background concentration', are alternated by events in which the concentration may reach values of up to 40 times the background value. Note that these events are often not related to an increase in the velocity (wave height). The number of suspension events per time-interval, the concentration level reached in these events and the background concentration level all increase going from the non-breaking zone through the (non) breaking zone, the breaking zone to the breaking/swash zone. However, the transition from the breaking/swash zone to the swash zone shows a decrease in the number of suspension events and background concentration level; the concentration level reached in a suspension event remains about the same. The average duration of the time interval between two successive suspension events decreases from more than two minutes in the non-breaking zone to less than ten seconds in the breaking zone and in the breaking/swash zone. During the suspension events, the concentration reaches values from 15 kg m^{-3} (non-breaking zone) to 40 kg m^{-3} (breaking/swash zone) (Fig. 5.2d). The background concentration level in the non-breaking zone is about 0.05 kg m^{-3} and reaches levels up to 5 kg m^{-3} in the other zones. The above résumé shows that the importance of the suspension events increases when going from the non-breaking zone to the swash zone. The increase in concentration from the background level to the peak level and back takes places in a few seconds in the non breaking zone while in the breaker zone, the suspension event lasts a little bit longer. For instance, Figure 5.2c shows a larger suspension event at 1100 seconds, during which the background concentration rapidly increased from 2 to 10 kg m^{-3} . Only after some 60 seconds the original background concentration is reached again. The possible causes of this pattern are:

- a change of bedforms i.e. a change in the level and/or roughness of the bed;
- low-frequency hydrodynamic phenomena (e.g. variation in bound long waves, shear instabilities (cf. Bowen and Holman, 1989))
- rapid upward convection by vortices and slow downward settlement by gravity.

The effect of enhancing the background concentration level over a time scale longer than the time scale of the suspension events themselves may be caused by variation of the bed level, i.e. the presence of ripples. An increase of the bed level may be noticed by the lowest OBS, because it has a rather larger vertical looking angle of 50 degrees. For example, series 0911-3 shows a clear change in the background level at 1120-1140 seconds which may be caused by a ripple (Fig. 5.3). Note, however, that the presence or absence of ripples could not be verified visually.

An important argument against the possibility of low-frequency hydrodynamic phenomena being an important source for the low-frequency oscillation of the concentration is that the variation in the observed concentration is not sinusoidal. Rather, the concentration increases very rapidly and then decreases more slowly. Moreover, the relative contribution of low-frequency oscillations to the near-bed velocity field was found to be small (see previous chapter). Thus it is unlikely that the observed increase in concentration over longer time scales is caused by low-frequency motions.

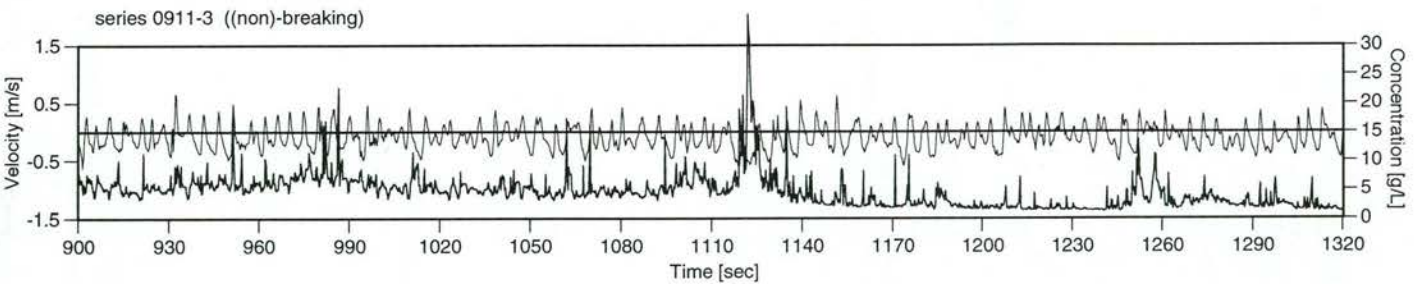


Figure 5.3

Time series of velocity (thin line) and concentration (thick line) at the lowest OBS level (0.07 m above the bed) in (non-) breaking zone. Positive velocity is shown in the onshore direction, negative velocity in the offshore direction.

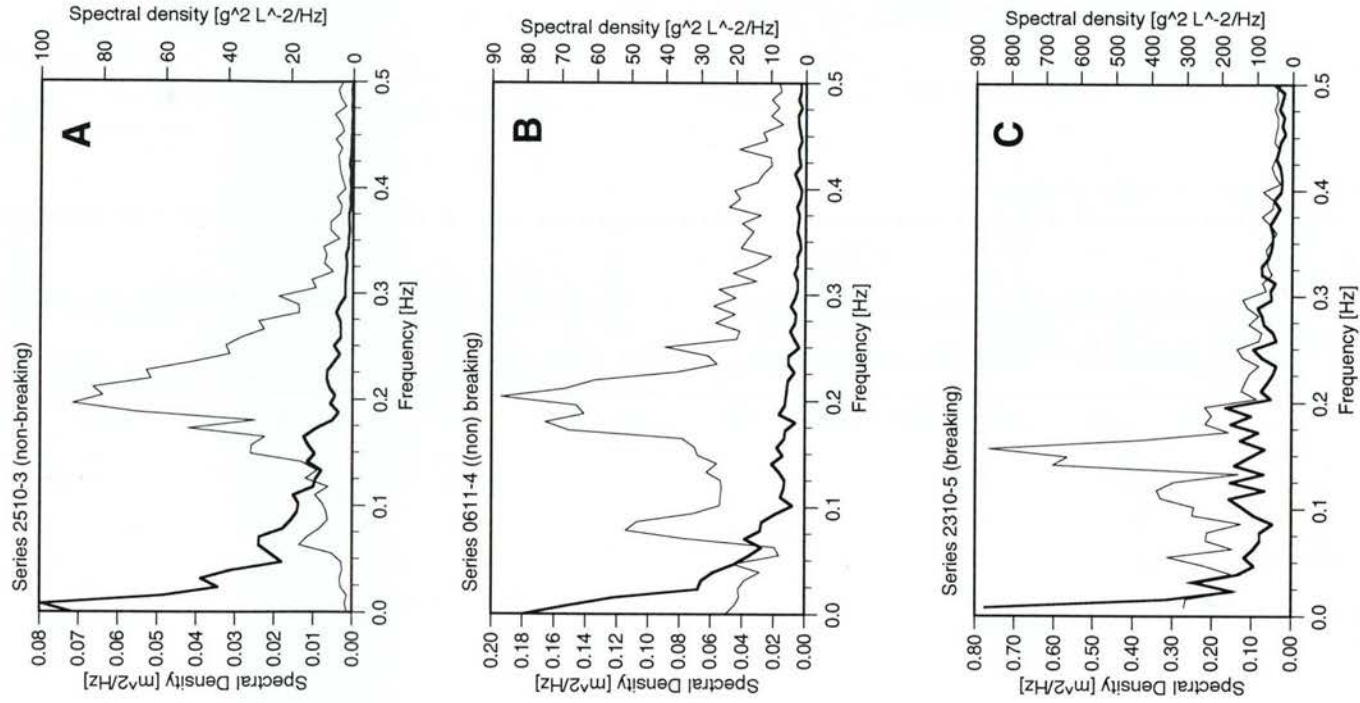


Figure 5.4

Velocity spectra (thin line, left vertical axis) and concentration spectra (thick line, right vertical axis) of lowest OBS (0.07 m above the bed).

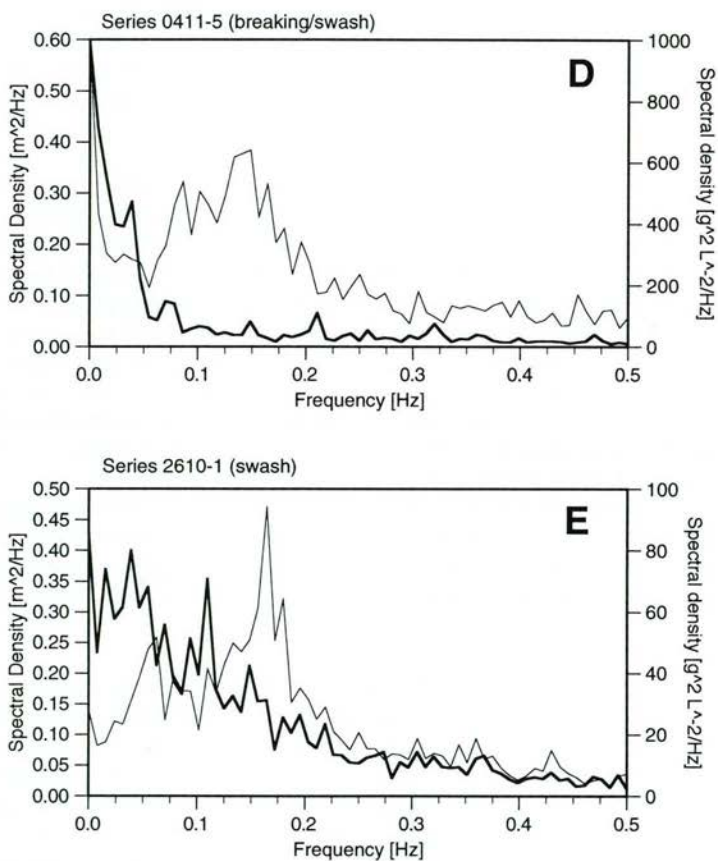


Figure 5.4 Velocity spectra (thin line, left vertical axis) and concentration spectra (thick line, right vertical axis) of lowest OBS (0.07 m above the bed).
(continued)

To examine the third possible cause for the observed concentration variation, i.e. differences of time scales of mixing and settling of the sediment, the vertical distribution of the instantaneous concentration has to be examined. This analysis is carried out further on in this section.

Further analysis of Figure 5.2 reveals that the individual suspension events show no clear relation to a particular phase of the individual wave cycles. In some cases the suspension occurs when the near-bed velocity direction changes from onshore to offshore. In other cases, suspensions occur during the following onshore movement. This observation is in line with the findings of other researchers (cf. Jaffe et al., 1994) who also found low correlations between instantaneous concentrations and velocities. Spectral analysis of the velocity and concentration series, including cross-spectra, may give more insight into the relationships.

The concentration spectra in all zones, except the swash zone, have a monotonically decreasing trend. As an example, Figure 5.4 shows the concentration spectra of the series in Figure 5.2. The spectral density is low at the higher frequencies (> 0.25 Hz) and increases towards the lower frequencies (< 0.25 Hz). The increase of the spectral density to the lower frequencies is at first rather gradual but increases very rapidly at the lowest frequencies. Therefore, the highest spectral densities are commonly found on the far left side of the spectrum. In addition, only a few peaks are visible in the concentration spectra of all zones, except that of the swash zone. Hence, the processes in these zones result more in an increase of the concentration over long periods (> 20 s) than in a variation in the concentration over short periods (< 20 s). It is in the swash zone that the spectral density at frequencies larger than 0.1 Hz seems to play an important role and that the spectral density changes more gradually when going from higher to lower frequencies. Although all spectra show an increase in spectral density towards the lower frequencies, the absolute spectral densities vary, a variation that is in agreement with those of the concentrations measured in the various hydraulic zones.

In spite of the rather uniform shape of the concentration spectra, the cross-spectra of velocity and concentration show large variations both in absolute values and in distribution over frequencies. Figure 5.5 shows the cross-spectra and coherence of the same five series also shown in Figures 5.2 and 5.4. To identify a significant influence of velocity on sediment (re-) suspension, both the cross-spectrum and the coherence must show high peaks. The significance level of the coherence is 0.16. The spectral densities vary between 0.025 (non-breaking), 0.1 ((non)breaking), 0.25 (breaking), 0.10 (breaking (swash)) and > 0.5 (swash). This means that the highest significant transports are found in the breaking and swash zones. Several significant spectral peaks are present in each zone which, however, do not occur at the incident wave velocity frequencies or higher harmonics of the incident wave frequency. This means that although a significant relation is present between the velocity and concentration at certain frequencies, it is not clear why these relations are only present at those particular frequencies.

In conclusion, the concentrations near the bed vary on time scales of the incident wave frequency and lower frequencies but a clear (linear) relation with the velocity is lacking. This is probably caused by the fact that a temporary increase in sediment concentration lasts longer than the period of the incident wave orbital motion. Hence, high concentrations may occur during zero velocity because the sediment -suspended

earlier- has not yet settled (cf. Jaffe et al., 1994). Peak and background concentration values increase from the non-breaking to the swash zone.

Vertical distribution of instantaneous concentrations

The previous two paragraphs dealt with instantaneous concentrations near the bed (0.07 m). The sediment is, however, also suspended higher up in the vertical. To obtain an understanding of the depth-integrated suspended sediment transport, it is important to examine to what extent the instantaneous concentration near the bottom compares with the values at higher elevations. As an example, Figure 5.6 shows time series of velocity and concentration at four elevations (0.07-0.26 m) for the series 2310-5 (breaking zone, Fig. 5.2c). This figure shows that the concentrations at all heights show a similar trend in time. Short periods of higher concentration alternate with long periods of lower concentrations. Even the background concentration does not vary much in the vertical. The absolute value of the peak concentrations, however, decreases somewhat with distance from the bed (from 20-25 to 10-15 kg m⁻³). An increase in the concentration near the bed occurs simultaneously with an increase in concentration at the other elevations. There seems to be no time lag between the increase of concentration at the bed (0.07 m) and further above the bed. Calculations of correlation diagrams for all series between the lowest and highest OBS confirm this. The highest degree of correlation is found at a zero time lag (Fig. 5.7) although the correlation diagrams of 0.07 m and 0.12 m show a higher degree of correlation at zero time lag than those of 0.07 m and 0.26 m. Apparently, there is a large vertical exchange of sediment in breaking waves between 0.12 and 0.26 m, i.e. the local vertical sediment diffusivity is large.

Figure 5.6 shows that the process whereby near-bed, incident wave-related suspension causes a temporal increase in the background concentration over larger time scales is also present higher up the vertical (0.12-0.26 m). This phenomenon, therefore, is not always caused by an increase of the bed level as suggested in the previous paragraph but may also be explained by the sediment settling as it passes the upper OBS sensors. This effect is present until the sediment suspended between 0.26 m above the bed (upper OBS) and the water-level has reached the bed again, as can be illustrated by the following computations. The sediment diameter (D_{50}) of the bed is about 400 μm (Table 4.1). According to Van Rijn (1993) the diameter of the suspended sediment is then about $0.8 \cdot 400 = 320 \mu\text{m}$. The fall velocity of sediment with a D_{50} of 320 μm is circa 0.04 m s⁻¹ (Wolf, 1992) and the average depth during the series 2310-5 was 1.03 m (Table 4.3). Thus, the time scale associated with the settling of the sediment is $1.03/0.04 \approx 25$ seconds, which is in the order of the time-scale of the temporal increment of the background concentration (Fig. 5.6) and therefore may be caused by the settling of sediment originating from above 0.26 m above the bed, by an increase in the bed-level or by a change in roughness of the bed or a combination of these features.

The vertical variation of the instantaneous concentrations in the case of non-breaking, (non) breaking, breaking/swash and swash series reveals a similar picture to that of the series with breaking waves. In all the series the suspension of sediment at the lowest OBS is almost immediately followed by an increase in the suspension load recorded by the other OBS sensors. Hence, the lack of a correlation between the instantaneous velocity and concentration is not the result of a time lag caused by the

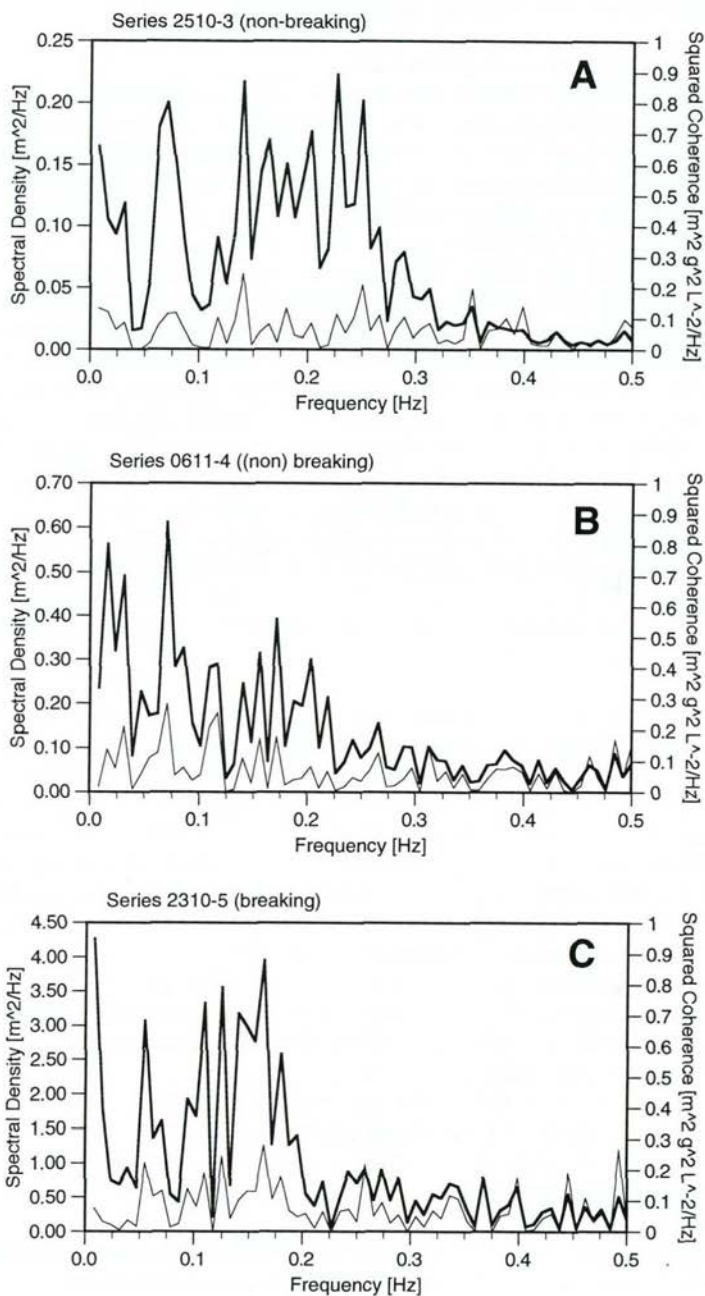


Figure 5.5 Cross-spectra (thick line) and squared coherence (thin line) of lowest OBS (0.07 m above the bed).

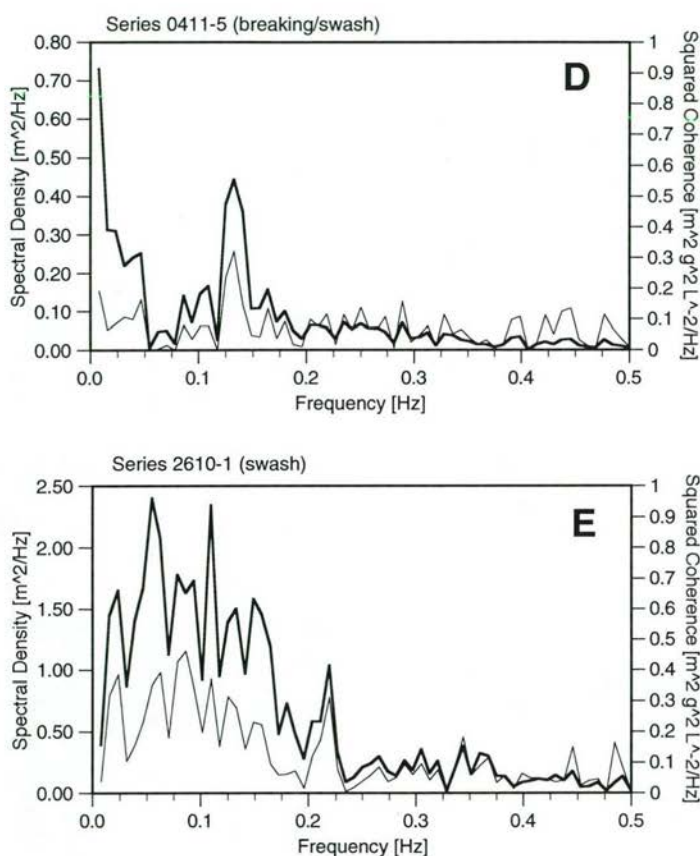


Figure 5.5 Cross-spectra (thick line) and squared coherence (thin line) of lowest OBS (continued) (0.07 m above the bed).

time needed for the sediment to travel from the bed to the highest OBS (Greenwood et al., 1990; Jaffe et al., 1994).

The degree of correlation between the lowest and highest OBS at zero time-lag varies over all hydrodynamic zones, but with no particular trend (not shown). The peak and background concentration decrease above the bed in all zones, and all series show that, up to 0.26 m, the suspension of sediment is an episodic process.

The variation of concentration spectra and cross-spectra in the vertical is studied by comparing the results of the lowest and highest OBS, with the exception of the cross-spectra of those in the non-breaking zone, which are not relevant because of the very low concentrations and low spectral densities observed. In the remaining zones, the concentration spectra of the highest OBS have lower absolute spectral densities compared with those of the lowest OBS (e.g. Fig. 5.8). The shape of the concentration spectra measured at the highest OBS is about the same as that for the lowest OBS, with the spectral densities increasing towards the lower frequencies though Individual spectral peaks may disturb this general trend. Individual spectral peaks in the cross-

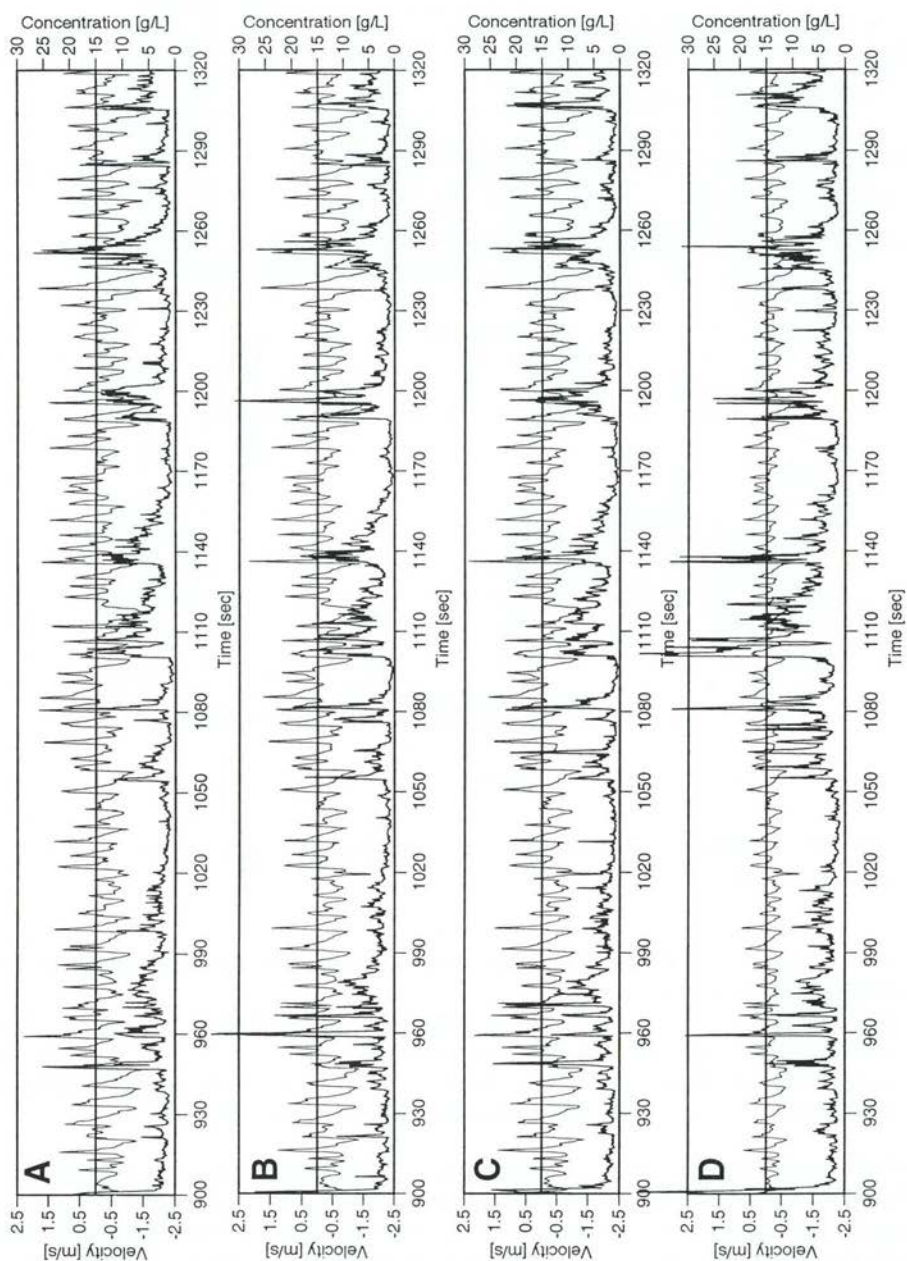


Figure 5.6 Time-series of velocity (thin line) and concentration (thick line) of EMF and OBS at 0.07, 0.12, 0.17 and 0.26 m above the bed of series 2310-5 (breaking conditions). Negative velocity is in the offshore direction, positive velocity in the onshore direction.

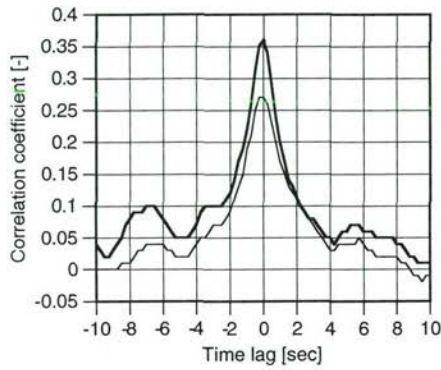


Figure 5.7 Correlation between suspended sediment concentration at 0.07 and 0.12 m (thick line) and between suspended sediment concentration at 0.07 and 0.26 m (thin line); series 2310-5 (breaking line).

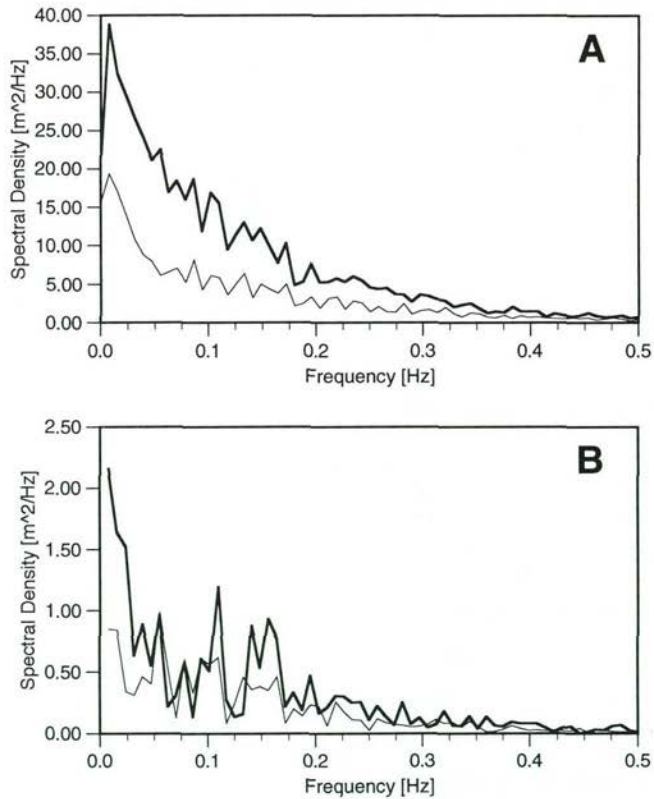


Figure 5.8 Concentration spectra (A) and cross-spectra (B) at upper OBS level (0.26 m above the bed; thin line) and lowest OBS (0.07 m above the bed; thick line); series 0411-3 (breaking waves).

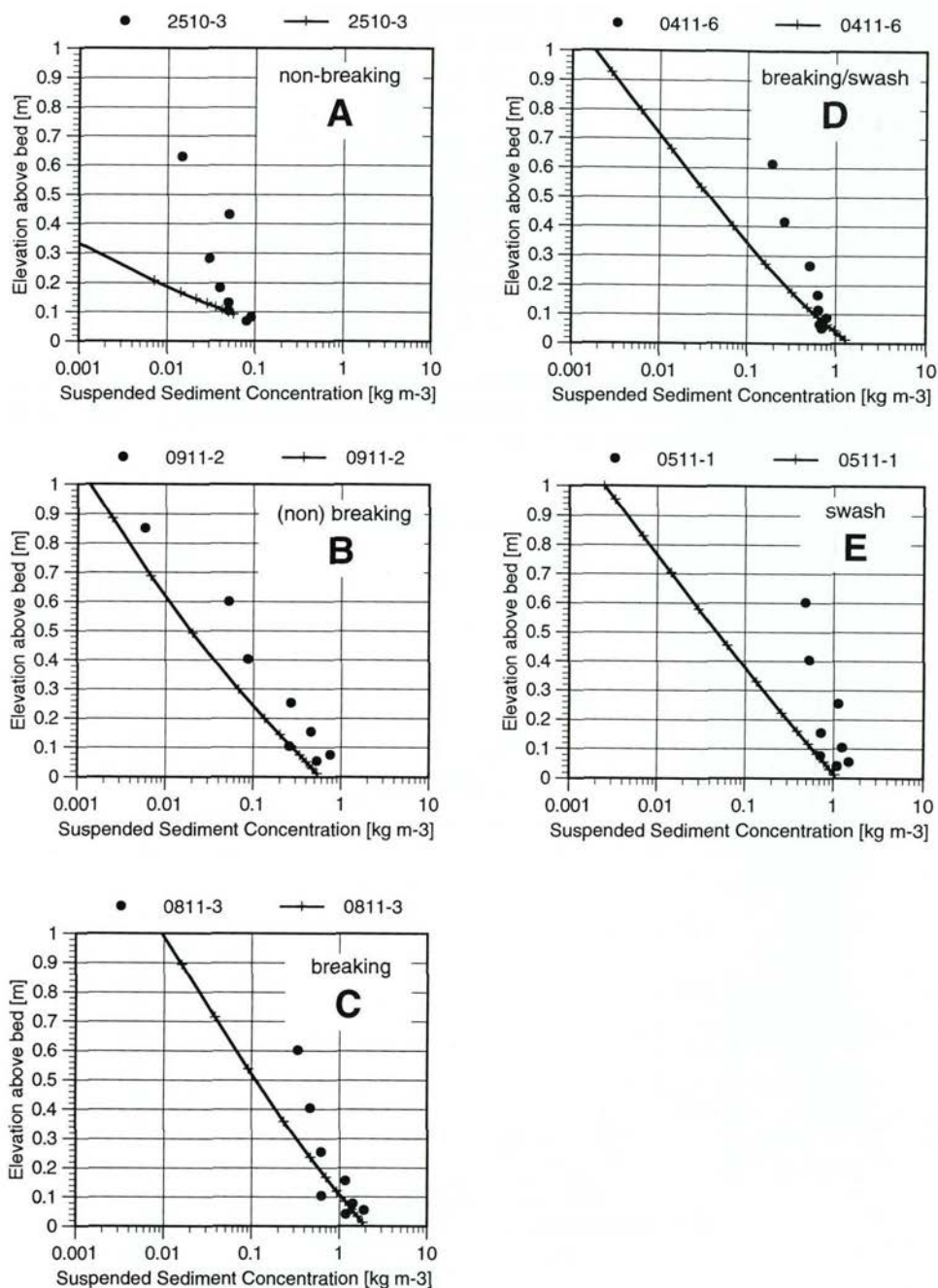


Figure 5.9 Examples of sediment concentration profiles, measured and theoretical. Dots are measured values, crosses are computed values according to the TRANSPOR model (Van Rijn, 1993).

spectra at the lowest OBS with a high squared coherence are also largely absent in the cross-spectrum at the highest OBS. Thus, the concentration and cross-spectra do not vary much between 0.07 m and 0.26 m.

In conclusion, the temporal variability in concentration is about the same for both the highest OBS (0.26 m above the bed) and the lowest one (0.07 m above the bed). For all hydrodynamics zones, the correlation between the lowest and highest OBS is the largest at zero second time lag. Thus, an increase in the concentration at the lowest OBS is followed, within a second, by an increase at the highest OBS. The concentration spectra and the cross-spectra have the same shape within a 40-minute measuring session, but differ in detail over the vertical. Clearly, the suspension of sediment is an episodic process in all hydrodynamic zones and at different distances from the bed, and, moreover, a clear correlation between the instantaneous velocity and the concentration is not present between 0.07 m and 0.26 m above the bed.

5.3.3 Results and discussion of time-averaged concentrations

Measured time-averaged concentration profiles

The time-averaged concentration profiles obtained with the pump sampler for five series are illustrated in Figure 5.9. These five series represent the five hydrodynamic zones. Table 5.1 shows the results of all measurements.

The following concentrations were observed (lowest - highest values) :

- non-breaking zone : 0.01 - 0.1 kg m⁻³
- (non) breaking zone : 0.5 - 1 kg m⁻³
- breaking zone : 0.5 - 3 kg m⁻³
- breaking/swash zone : 0.5 - 2 kg m⁻³
- swash zone : 0.5 - 5 kg m⁻³

The observations regarding the time-averaged concentrations in the vertical and in the different hydrodynamic zones reveal that the shapes of these profiles are more variable and thus less representative near to the bed than higher in the vertical.

The time- and depth averaged concentrations increase from the non-breaking zone to the breaking zone by a factor 20, while in the transition from breaking waves to breaking/swash, a slight decrease in the concentration near the bed and higher in the vertical can be detected. An increase to above the breaking zone level can again be seen in concentrations over the entire vertical when the hydrodynamic conditions change from breaking/swash to swash. The highest time-averaged concentrations are, therefore, found in the swash zone, conclusions which are in line with Kroon's (1994) findings.

Comparison between measured and computed time-averaged concentration profiles

The measured concentration profiles were compared with the computed concentration profiles according to the TRANSPOR model (Van Rijn, 1993) (Fig. 5.9).

Generally, the measured and computed near bed concentrations (< 0.2 m) are reasonably well predicted by the model and their ratio, with a few exceptions, is within a factor 2. Higher in the water column, however, this ratio may increase to a factor 5 to 10. This means that although the TRANSPOR model predicts the concentration

near the bed fairly well, the distribution of the sediment mixing coefficient over the depth is less well predicted, and, in almost all cases, the decrease of the suspended sediment concentration with height above the bed is overpredicted.

The largest deviation between the model and the measured time-averaged concentrations near the bed is found in the non-breaking zone (Fig. 5.9a) and may be attributed to an underprediction of the roughness related to the ripple dimension. Ripples were not observed before or after the measurements although they may have been present during them but were wiped out by the swash or breaking waves. Thus, ripples may have been present during the non-breaking wave conditions resulting in a higher bed roughness than for breaking conditions. The current- and wave-related roughness, therefore, was estimated to be about 0.05 m in the case of non-breaking waves, caused by, for instance, ripples 0.02 m in height and 0.15 m in length. Increasing the ripple height by 0.01 m and the length by 0.05 m results in a bed roughness of 0.09 m (Van Rijn, 1993), which in the case of non-breaking waves, leads to more satisfactory results for the near bed concentration. Figure 5.10 shows that the predicted near-bed concentrations are now more in line with the measured ones in the non-breaking zone. However, large differences are found in the upper part (elevation > 0.5 h) of the water column. So, clearly the decrease of concentration with elevation above the bed is overestimated by the TRANSPOR model. This means that either the vertical sediment-mixing coefficient in the upper layers present during non-breaking waves is underestimated by the model and/or the fall velocity of the suspended sediment is overestimated.

The decrease in concentration with elevation above the bed is not very satisfactory predicted by the TRANSPOR model in the non-breaking, breaking/swash and swash zones. However, in the breaking- and (non) breaking zones, the results are more satisfactory than in the non breaking zone (e.g. Fig. 5.9). This is somewhat peculiar because the sediment mixing coefficient used in the TRANSPOR model was originally designed for use in non-breaking waves (Van Rijn, 1993). The above results suggest, however, that the model is most reliable when applied near to the breaking waves, possibly because of the reduction in the D_{50} values of the sediment in the vertical (cf. Van der Graaff, 1988; Kroon, 1994). This decrease may be different for each zone because the D_{50} and the sorting of the bed material also vary between the series. The D_{50} of the bed varied between 300 μm and 530 μm with an average D_{50} of 380 μm . The sorting of the bed material was not investigated. So, the estimated D_{50} of the suspended sediment ($0.8 * D_{50}$, bed, suggested by the model) may not be valid for all zones or at all elevations above the bed. Figure 5.11 shows that a lower D_{50} value of the suspended sediment leads to a more uniform suspended sediment profile. Thus, the variation in the D_{50} of the suspended material could have been responsible for the observed discrepancies between the measured and computed suspended sediment profiles. To verify this hypothesis, three series of suspended sediment, sampled by the pump sampler, were analysed in a visual accumulation tube, but the D_{50} value of the suspended grains was shown to vary little in the vertical (Fig. 5.12). The ratio between the D_{50} of the suspended material and that of the bed material varies between a factor 0.5 and 0.6. Thus the differences between the computed and the measured concentrations may be reduced by choosing a lower value for the factor determining the ratio between the D_{50} of the bed material and that of the suspended sediment.

Another possible reason, explaining the differences between the time-averaged concentrations predicted by the TRANSPOR model and measured concentrations, is

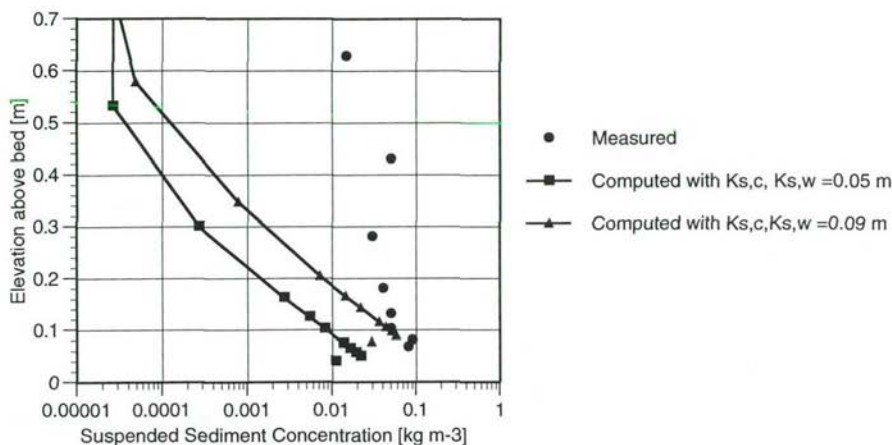


Figure 5.10 Influence of current- ($K_{s,c}$) and wave- ($K_{s,w}$) related bed roughness on computed (TRANSPOR model) suspended-sediment profile; series 2510-3 (non-breaking).

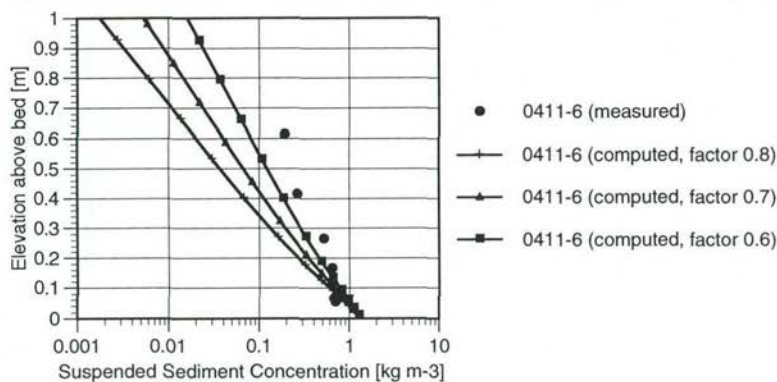


Figure 5.11 Effect on using different factors for estimating the D_{50} of the suspended sediment from the D_{50} of the bed sediment on the computed (TRANSPOR model) concentration for series 0411-6 ($D_{50,sus} = \text{factor} * D_{50,bed}$).

that the TRANSPOR model is a local model, i.e. it does not incorporate advection processes. Horizontal transport of suspended sediment is, however, very likely under field conditions. As shown by Figure 5.13, sediment may be brought into suspension by plunging breakers at the shoreline, and this sediment may be transported by undertow to the measuring location, where non-breaking waves are observed, thereby increasing the suspended sediment concentration recorded by the instruments.

Under comparable conditions and at the same field site, Kroon (1994) found reasonable agreement between the TRANSPOR model and measured concentrations in the inner surf zone at Egmond. Nevertheless, the model also both under- and overestimated some measurements. The differences between the computed and measured results of Kroon's study (1994) and this study are in the same order. The

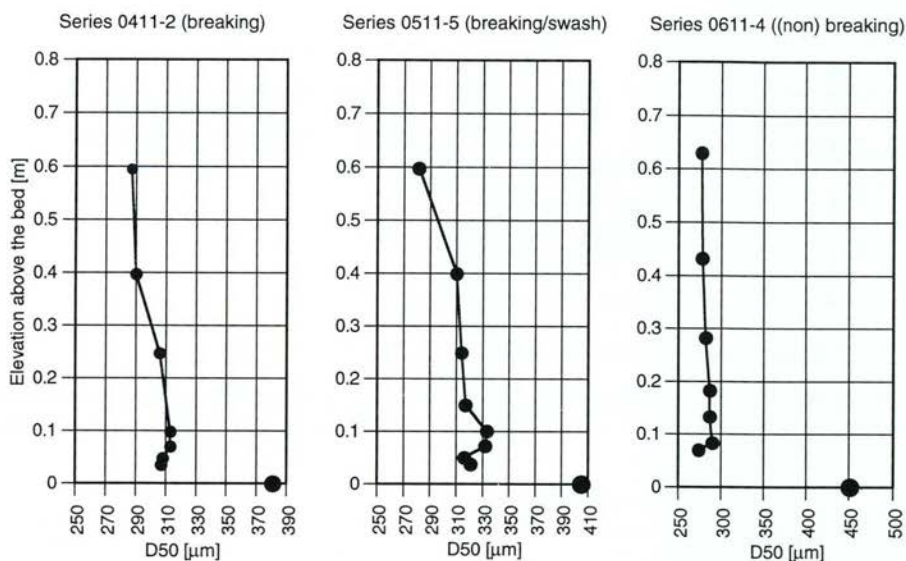


Figure 5.12 Mean grain size (D_{50}) of the bedload sediment and of the suspended sediment as a function of the elevation above the bed.

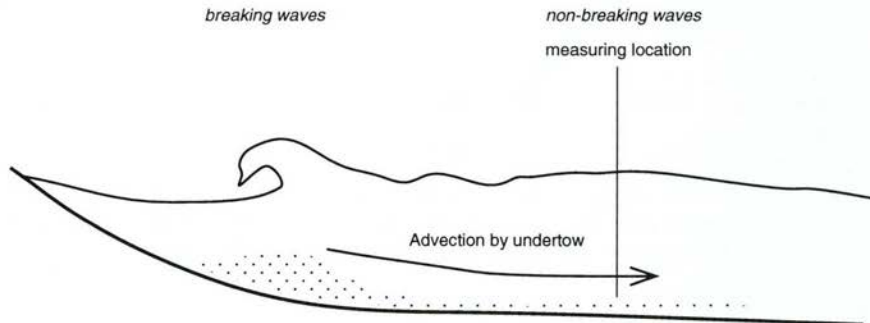


Figure 5.13 Explication of advective sediment transport. A combination of breakers at the landward side of the measuring location and a strong undertow may lead to higher sediment concentrations than expected from local conditions at the measuring location.

observed trends in the vertical distribution of the D_{50} of the suspended sediment found in this study were also found by Kroon (1994).

It is concluded that the TRANSPOR model generally underestimates the observed suspended sediment profiles and that the best agreement between the model and the measurements occurs in the near bed layer. Higher in the vertical, the ratio between the observed and computed concentration may increase up to a factor of 10. To

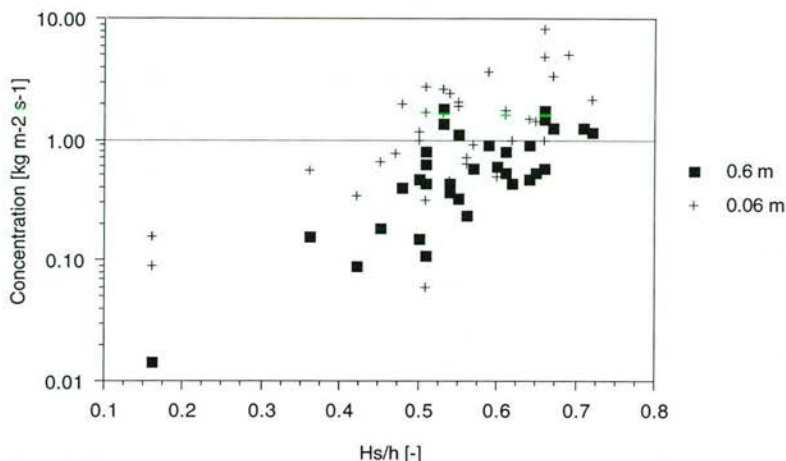


Figure 5.14 Relation between relative wave height (H_s/h) and concentration at 0.06 m and at 0.6 m above the bed.

improve the results of the TRANSPOR model in the upper layers, it is suggested to lower the relative depth at which the maximum vertical mixing is reached (Van Rijn uses $0.5 h$, Formula 5.3b and 5.3c). Other possibilities are to increase the factor α_m (Formula 5.3b) used to calculate the maximum sediment mixing coefficient or to decrease the factor determining the ratio suspended- to bedload sediment size to give a more uniform profile (Van Rijn, 1993). To verify these suggestions, more research on wave-related sediment mixing is necessary, especially under non-breaking conditions.

Relation between time-averaged concentration profiles and wave characteristics

The results presented in the previous section show that the time-averaged concentration near the bed and the decrease in the concentration vary in the different hydrodynamic zones.

The results of these concentration measurements will be used to try and explain the sediment-transport patterns and observed morphological changes of the inner nearshore bar (Section 5.8). However, because no concentration measurements were carried out at the inner nearshore bar itself, it is necessary to determine to what extent the observed tendencies in the concentration can be related to wave characteristics, i.e. the relative wave height.

It is clear that the magnitude of the time-averaged concentration in the entire vertical is related to the hydrodynamic zone. Therefore, a relation between the relative wave height and the suspended sediment concentration can be expected because the hydrodynamic zone is related to the relative wave height (H_s/h ; Fig. 4.5). Figure 5.14 shows that the concentration increases with the relative wave height; this trend can be observed at all elevations of the intake nozzles of the pump sampler. The same trend was also found by Kroon (1994) but there the relation between the relative wave height and the time-averaged concentration showed a much higher degree of correlation. The most likely reason for this discrepancy is that the suspended sediment concentration is also linked to the breaker type (e.g. Miller, 1976). Plunging

breakers are associated with larger suspended sediment concentrations because their vortex reaches the bottom whereas the vortices of spilling breakers remain limited to the surface thereby giving lower suspended sediment concentrations. Kroon (1994) found a good correlation between breaker type and relative wave height and, consequently, also between the relative wave height and the time-averaged suspended sediment concentration. This study found no relation between relative wave height and breaker type (Section 4.4.2) and therefore a lower degree of correlation between relative wave height and time-averaged concentration may be anticipated. Information about the breaker type in determining time-averaged suspended sediment concentration is of lesser value for this study, because of the large number of series with both plunging and spilling breakers and because of the high variation in sediment concentration of series with both breaker types (compare Tables 4.3 and 5.1).

In conclusion, the time-averaged suspended sediment concentration in the different hydrodynamic zones shows a weak relation with relative wave height, probably due to the presence of both plunging and spilling breakers within the same measurement series.

5.3.4 Conclusions

Instantaneous concentrations

- The concentrations near the bed vary on time scales of the incident wave frequency and lower frequencies.
- The instantaneous concentration during a suspension event reaches values from 15 kg m^{-3} in the non-breaking zone to 40 kg m^{-3} in the breaking/swash zone.
- After a suspension event, the instantaneous concentration reduces to background values from about 0.05 kg m^{-3} in the non-breaking zone to 5 kg m^{-3} in the breaking zone.
- The concentration spectra in all hydrodynamic zones show an increase in spectral density towards the lower frequencies.
- Cross-spectra of velocity and concentration vary largely over the different hydrodynamic zones.
- There is no clear (linear) relation between instantaneous velocity and concentration.

Vertical distribution of instantaneous concentrations

- The temporal variations of the instantaneous concentrations at 0.07 m (lowest OBS) and 0.26 m (highest OBS) above the bed show no time lag.
- The shape of the concentration spectra and cross-spectra at 0.07 m and 0.26 m are generally the same but may show individual peaks at different frequencies.

Measured time-averaged concentration profiles

- The time-averaged concentrations vary between $0.01\text{-}0.1 \text{ kg m}^{-3}$ (non-breaking zone), $0.5\text{-}1 \text{ kg m}^{-3}$ ((non)-breaking zone), $1\text{-}3 \text{ kg m}^{-3}$ (breaking zone), $0.5\text{-}2 \text{ kg m}^{-3}$ (breaking/swash zone) and $1\text{-}5 \text{ kg m}^{-3}$ (swash zone).
- A larger near bed (0.05 m) concentration also implies a higher concentration in the remaining part of the vertical (0.1-0.6 m).

- A higher near bed concentration is also associated with a larger vertical diffusivity, i.e. a steeper and more uniform vertical concentration profile.

Comparison between measured and computed time-averaged concentration profiles

- The TRANSPOR model (Van Rijn, 1993) reasonably predicts the measured concentrations near the bed.
- The ratio between the measured and computed concentration increases with distance from the bed up to a factor 10. This discrepancy may be reduced by decreasing the computed suspended sediment size.

Relation between time-averaged concentration profiles and wave characteristics

- An increasing relative wave height (H_w/h) results in a larger time-averaged concentration; a strong correlation is lacking though.

5.4 Instantaneous suspended sediment transport

5.4.1 Analysis and interpretation methods

The suspended sediment transport is related to the instantaneous values of the velocity and the concentrations. The concentrations were measured at four elevations above the bed (0.07, 0.12, 0.17, 0.26 m) while the velocities at these four elevations were linearly interpolated using the measured velocities at 0.1 and 0.3 m. The instantaneous sediment concentration data offer the opportunity to investigate the relative contribution of the oscillatory to the mean fluxes. It is assumed that the total time-averaged net cross-shore suspended sediment flux may be computed by adding together the mean and oscillating parts (e.g. Beach and Sternberg, 1988; Aagaard and Greenwood, 1994). The oscillating components are further decomposed into high-frequency and low-frequency oscillating components. Hence the instantaneous velocities and concentrations are composed of the following elements:

$$u_t = \bar{u} + \tilde{u}_{low} + \tilde{u}_{high} \quad (5.7a)$$

$$c_t = \bar{c} + \tilde{c}_{low} + \tilde{c}_{high} \quad (5.7b)$$

in which

$$\begin{aligned} \bar{u}, \bar{c} &= \text{time-averaged values of the velocities (u) and concentration (c)} \\ \tilde{u}_{low}, \tilde{c}_{low} &= \text{low-frequency oscillations} \\ \tilde{u}_{high}, \tilde{c}_{high} &= \text{high-frequency oscillations} \end{aligned}$$

The time-averaged net cross-shore flux then becomes:

$$\begin{aligned} \langle u_t \cdot c_t \rangle &= \langle (\bar{u} + \tilde{u}_{low} + \tilde{u}_{high}) \cdot (\bar{c} + \tilde{c}_{low} + \tilde{c}_{high}) \rangle = \\ &= \langle \bar{u} \cdot \bar{c} + \bar{u} \cdot \tilde{c}_{low} + \bar{u} \cdot \tilde{c}_{high} + \tilde{u}_{low} \cdot \bar{c} + \tilde{u}_{low} \cdot \tilde{c}_{low} + \tilde{u}_{low} \cdot \tilde{c}_{high} + \\ &+ \tilde{u}_{high} \cdot \bar{c} + \tilde{u}_{high} \cdot \tilde{c}_{low} + \tilde{u}_{high} \cdot \tilde{c}_{high} \rangle = \\ &= \langle \bar{u} \cdot \bar{c} \rangle + \langle \tilde{u}_{low} \cdot \tilde{c}_{low} \rangle + \langle \tilde{u}_{low} \cdot \tilde{c}_{high} \rangle + \langle \tilde{u}_{high} \cdot \tilde{c}_{low} \rangle + \langle \tilde{u}_{high} \cdot \tilde{c}_{high} \rangle \\ &= \text{[term 1]} \quad \text{[term 2]} \quad \text{[term 3]} \quad \text{[term 4]} \quad \text{[term 5]} \end{aligned} \quad (5.8)$$

After carrying out a comparable analysis in the inner surf zone of Egmond, Kroon (1994) showed that the third and fourth term may be neglected. Formula 5.8 then reduces to:

$$\langle u_t \cdot c_t \rangle = \langle \bar{u} \cdot \bar{c} \rangle + \langle \tilde{u}_{low} \cdot \tilde{c}_{low} \rangle + \langle \tilde{u}_{high} \cdot \tilde{c}_{high} \rangle \quad (5.9)$$

By comparing these net, mean and oscillating terms one can analyse whether it is justified to neglect the third and fourth term of Formula 5.8. The last two terms of Formula 5.8 are calculated by applying a high- and low-pass filter on the measured time series (cf. Kroon, 1994). The cut-off frequency used was 0.05 Hz, because the spectral density is often low around this frequency (see Aagaard, 1990; Kroon, 1994).

A similar approach is followed for the analysis of the longshore suspended sediment fluxes. The time-averaged, net longshore flux is:

$$\langle v_t \cdot c_t \rangle = \langle \bar{v} \cdot \bar{c} \rangle + \langle \tilde{v}_{low} \cdot \tilde{c}_{low} \rangle + \langle \tilde{v}_{high} \cdot \tilde{c}_{high} \rangle \quad (5.10)$$

5.4.2 Results and discussion

The relative contribution of the mean and oscillating fluxes to the net fluxes was analysed using the instantaneous concentrations and interpolated velocities at 0.17 m above the bed to minimise the influence of small ripples. Migrating ripples could be interpreted as an increase in the background concentration and an influence on the mean fluxes.

Kroon (1994) stated that the third and fourth term of Formula 5.8 could be neglected because of their minimal contribution to net sediment transport. This assumption was verified in this study by computing all terms of Formula 5.9. It is concluded from Table 5.2 that the contribution of the terms 3 and 4 of Formula 5.8 are indeed very low, which supports Kroon's findings. The average difference between the term on the left hand side and the three terms at the right hand side of Formula 5.9 was about 3 percent.

Figure 5.15 shows the relative contribution of the oscillating cross-shore fluxes to the net cross-shore suspended sediment transport. The ratio between the oscillating fluxes and the mean fluxes varies between 0.05 and 1.70, with an average ratio of 0.46. In most cases the suspended sediment transport is slightly dominated by the mean fluxes which are all offshore directed, in line with the offshore directed mean currents (undertow) (Section 4.5.3). The oscillating sediment fluxes mostly result in onshore transport which is probably caused by the asymmetry of the orbital velocity. A clear relation between either the duration- or amplitude-asymmetry of the orbital velocity and oscillatory fluxes was, however, not found. It are the mean fluxes that dominate the suspended sediment transport and because these are, except for one series, always directed offshore the net transport is also directed offshore. However, the oscillating components can not be neglected. The magnitude of the oscillating fluxes increases with the relative wave height while their direction is either on- or offshore for $H_s/h < 0.6$. Higher relative wave heights generally result in onshore directed oscillating fluxes.

Table 5.2 Hydrodynamic conditions and suspended sediment transport modes at 0.17 m above the bed

date	h	H _s	T	Wave conditions	% br. waves	H _g /L _s	H _g /h	<U>	<U> * <C>	<U _{osc,lo} * C _{osc,lo} >	<U _{osc,hi} * C _{osc,hi} >	<U _{osc,lo} *C _{osc,hi} > +
	[m]	[m]	[s]		[-]	[-]	[-]	[kg m ⁻¹ s ⁻¹]	[kg m ⁻¹ s ⁻¹]	[kg m ⁻¹ s ⁻¹]	[kg m ⁻¹ s ⁻¹]	<U _{osc,hi} *C _{osc,lo} > [kg m ⁻¹ s ⁻¹]
2310-1	0.65	0.43	6.91	swash	-	0.055	0.66	-0.0906	-0.9996	0.1071	0.7370	-0.0649
2310-2	1.33	0.87	6.37	breaking	61.2	0.072	0.65	-0.2565	-0.1396	-0.0520	-0.0602	0.0047
2310-3	1.34	0.90	6.72	breaking	70.1	0.071	0.67	-0.0769	-0.2636	0.0730	0.1100	-0.0037
2310-4	1.23	0.81	6.90	breaking	82.6	0.065	0.66	-0.2267	-0.3895	0.0513	0.1079	-0.0036
2310-5	1.03	0.73	7.36	breaking	74.6	0.057	0.71	-0.3600	-0.7165	0.1180	0.2396	0.0011
2510-2	1.95	0.32	5.78	non breaking	-	0.056	0.16	-0.0238	-0.0186	0.0023	-0.0079	-0.0004
2510-3	1.85	0.29	5.15	non breaking	-	0.056	0.16	-0.0408	-0.0255	-0.0005	-0.0154	-0.0006
2610-1	0.77	0.53	7.08	swash	-	0.058	0.69	-0.0429	-0.3308	-0.0108	0.3255	0.0268
2610-2	1.57	0.66	6.11	(non) breaking	3.4	0.069	0.42	-0.2175	-0.0784	-0.0093	-0.1239	0.0059
2610-3	1.31	0.73	6.06	(non) breaking	32.8	0.071	0.56	-0.2108	-0.1492	-0.0091	-0.0521	0.0004
0411-1	0.87	0.49	8.04	swash	90.9	0.043	0.56	0.0572	-0.1638	0.0965	0.1240	-0.0005
0411-2	1.21	0.66	7.72	breaking	84.9	0.051	0.55	-0.2385	-0.4185	0.0804	0.0943	-0.0053
0411-3	1.40	0.72	7.73	breaking	82.6	0.053	0.51	-0.2820	-0.3515	0.0473	0.0194	-0.0028
0411-4	1.37	0.70	7.71	breaking	84.6	0.052	0.51	-0.2221	-0.3054	0.0364	0.0436	-0.0033
0411-5	1.24	0.60	8.19	breaking	x	0.046	0.48	-0.1506	-0.1932	0.0305	0.0115	-0.0006
0411-6	1.05	0.47	8.28	breaking	93.1	0.040	0.45	-0.0768	-0.1066	0.0173	0.0116	-0.0009
0511-1	1.00	0.64	7.04	swash	-	0.060	0.64	-0.1121	-0.3208	0.0630	0.1240	-0.0217
0511-2	1.20	0.74	6.52	breaking	84.9	0.065	0.62	-0.1801	-0.1757	0.0358	-0.0227	0.0175
0511-3	1.20	0.72	6.51	breaking	82.6	0.065	0.60	-0.1933	-0.0973	0.0057	-0.1036	-0.0019
0511-4	1.08	0.67	6.73	breaking/swash	84.6	0.061	0.62	-0.0579	-0.1017	-0.0089	0.0563	0.0036
0511-5	0.89	0.58	6.77	breaking/swash	85.7	0.056	0.65	-0.0774	-0.2999	0.0756	0.1550	0.0081
0611-1	0.97	0.57	6.98	breaking	91.8	0.056	0.59	-0.3305	-0.4757	0.0513	0.0914	-0.0025
0611-2	1.50	0.81	5.81	breaking	71.2	0.079	0.54	-0.0750	-0.0783	0.0039	0.0033	0.0039
0611-3	1.58	0.81	5.90	(non) breaking	64.1	0.078	0.51	-0.0367	-0.0463	0.0098	0.0004	0.0006
0611-4	1.42	0.72	5.68	(non) breaking	69.1	0.075	0.51	-0.0900	-0.0860	-0.0096	0.0043	-0.0013
0611-5	1.25	0.63	5.68	breaking	85.7	0.069	0.50	-0.1610	-0.2138	0.0144	0.0390	0.0006
0711-1	1.06	0.68	6.64	swash	-	0.064	0.64	-0.0911	-0.3440	0.0644	0.1885	0.0000
0711-2	1.61	0.88	6.26	breaking	35.5	0.075	0.55	-0.4037	-0.5055	-0.0302	0.1367	0.0047
0711-3	1.57	0.84	6.24	breaking	50.8	0.073	0.54	-0.4817	-0.5175	-0.0056	0.0421	0.0007
0711-4	1.29	0.68	6.31	breaking	-	0.065	0.53	-0.4895	-0.6654	0.1164	0.0569	-0.0026
0811-1	1.25	0.76	8.23	breaking	53.3	0.055	0.61	-0.2498	-0.1405	-0.0212	-0.0649	0.0232
0811-2	1.62	0.80	8.20	(non) breaking	62.7	0.056	0.49	-1.3220	-0.9647	0.1119	-0.4613	0.0079
0811-3	1.43	0.79	8.06	breaking	78.0	0.056	0.55	-0.7013	-0.5540	-0.0356	-0.1117	0.0000
0911-1	1.54	0.56	4.77	(non) breaking	36.0	0.084	0.36	-0.0519	-0.0488	0.0049	0.0068	0.0148
0911-2	1.58	0.74	5.12	(non) breaking	10.4	0.087	0.47	-0.1046	-0.0673	-0.0171	-0.0228	-0.0026
0911-3	1.47	0.74	5.70	(non) breaking	23.1	0.077	0.50	-0.2967	-0.2886	-0.0442	0.0293	-0.0068
1011-1	1.36	0.98	7.36	swash	-	0.065	0.72	-0.0927	-0.1366	-0.0464	0.0872	-0.0031
1011-2	1.69	0.97	7.22	breaking	19.4	0.069	0.57	-0.1570	-0.1880	0.0083	0.0193	-0.0034

- = not applicable

<> = time-averaged

x = not measured

osc = oscillating part

lo = low-frequency

hi = high-frequency

U = velocity

C = concentration

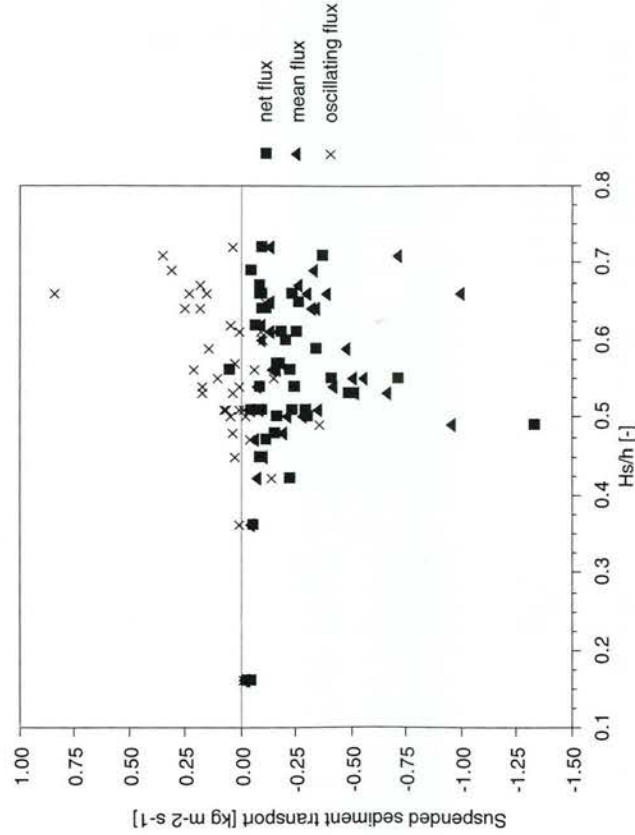


Figure 5.15 Relation between net, mean, and oscillating suspended sediment fluxes in the cross-shore direction at 0.17 m above the bed and the relative wave height (H_s/h). Positive transport onshore directed, negative transport offshore directed.

Figure 5.15 shows that, in general, the offshore directed mean fluxes increase between a relative wave height of 0.35 and 0.55. These relative wave heights represent the non-breaking, (non) breaking and breaking zones. The effect of a further increase in the relative wave height from 0.55 to 0.75, i.e. the transition from the breaker zone to the swash zone, on the mean fluxes is less clear. All but two series show a decrease in the mean fluxes with an increase in the relative wave height from 0.55 to 0.75. The two series that deviate from this general trend show an increasing mean flux with an increasing relative wave height between 0.55 and 0.75, but no particular reason for this deviation was found.

The net suspended sediment fluxes at 0.17 m above the bed follow the trend of the mean fluxes. Thus, they increase from the non-breaking wave zone to the breaking zone ($H_s/h = 0.35 - 0.55$) and generally decrease from the breaking zone to the swash zone ($H_s/h = 0.55 - 0.75$). These results are not entirely in agreement with Kroon's (1994) study. He found that when the relative wave height increased from 0.2 to 1.2 both the mean and net suspended sediment flux increased, resulting in increasing offshore transport. However, Kroon's analysis of the different transport modes was applied to series measured at 0.02 - 0.09 m above the bed and the above results are based on measurements at 0.17 m above the bed, a difference which may explain why the results in this study differ from those of Kroon's (1994). To verify this suggestion, the influence of elevation above the bed on the contribution of the different transport modes to the sediment transport will be evaluated.

The oscillating suspended sediment transport is further divided into a low-frequency and high-frequency component. Figure 5.16 shows that every combination regarding

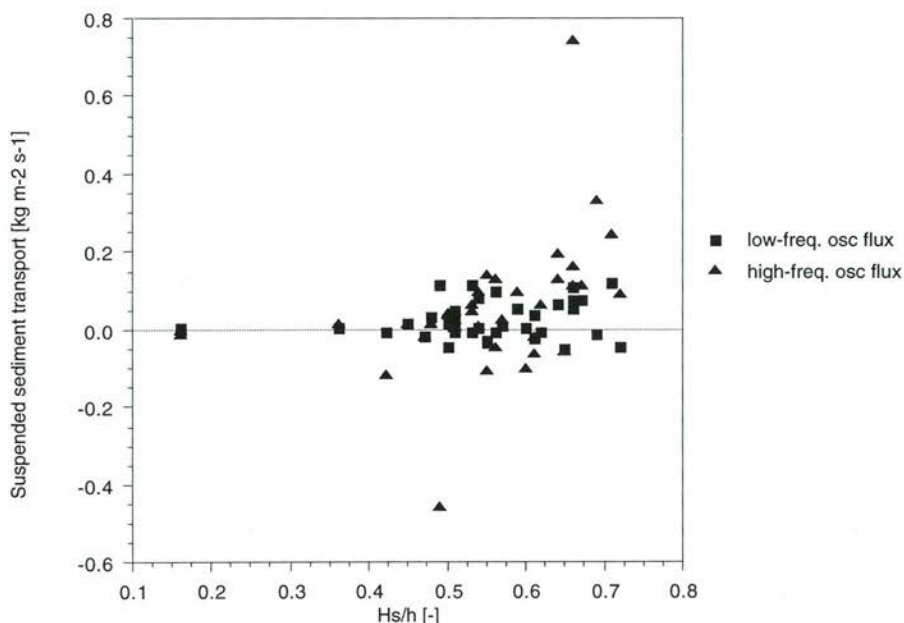


Figure 5.16 Relation between low-frequency (< 0.05 Hz) and high-frequency oscillating (> 0.05 Hz) suspended sediment fluxes in the cross-shore direction at 0.17 m above the bed and the relative wave height (H_s/h). Positive transport is onshore directed, negative transport offshore directed.

the direction of the high- and low-frequency transport is present. The majority of the series show an onshore transport in both the high and low frequencies. Generally, it was found that the high-frequency transport is about twice that of the low-frequency transport and that the high-frequency oscillating transport increases for high (> 0.6) values of the relative wave height whereas for low frequencies there is no trend in relation to the relative wave height.

The influence of the distance from the bed on the direction and magnitude of the different modes of the cross-shore, suspended sediment transport is illustrated in Figure 5.17. This figure shows that the largest changes in the magnitude of the different transport components occur between 0.12 and 0.07 m above the bed. Between these elevations, the mean sediment transport increases while the high- and low-frequency oscillating transport decreases towards the bed. No clear vertical trends between 0.07 and 0.26 m are visible.

The same figure seems to indicate that the series-averaged mean transport is much higher than the oscillating sediment transport but this is the result of the fact that these values are averaged over all series. If the ratio oscillating to mean sediment transport is computed per series and thereafter averaged, then a more realistic ratio becomes apparent, being 0.63, 0.46, 0.45 and 0.35 at 0.26, 0.17, 0.12 and 0.07 m, respectively. Note that the standard deviations of these averaged values are rather high, being 0.32, 0.32, 0.36 and 0.99 respectively. Nonetheless, it can be concluded that the suspended sediment transport between 0.07 and 0.26 m is dominated by the

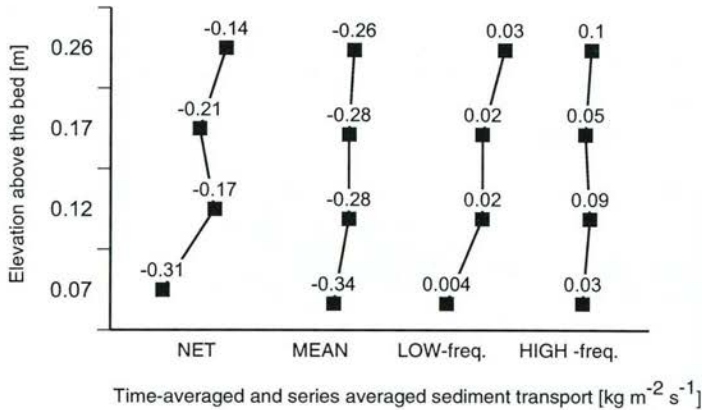


Figure 5.17 Vertical distribution of cross-shore suspended sediment transport modes.

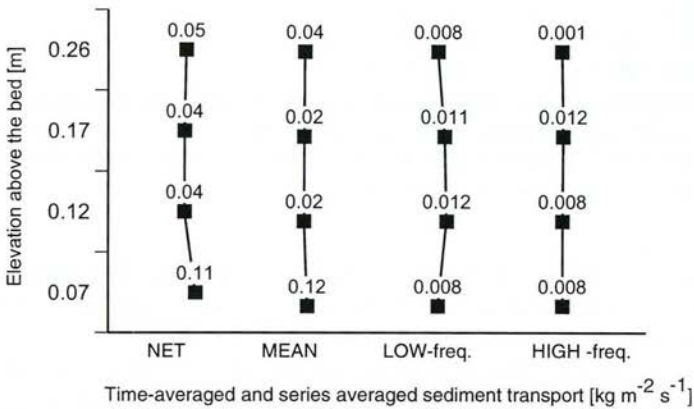


Figure 5.18 Vertical distribution of longshore suspended sediment transport modes.

mean suspended sediment transport while the contribution of the oscillating suspended sediment transport to the total transport decreases towards the bed.

The series-averaged magnitudes of the different transport modes to the longshore sediment transport in the vertical is presented in Figure 5.18. In the longshore direction, the mean transport is clearly larger than the oscillating transport. The mean sediment transport increases towards the bed with the largest increase occurring between 0.12 and 0.07 m above the bed but there is no large vertical variation between the low-frequency and high-frequency sediment transport. The ratio oscillating to mean sediment transport, computed per series and thereafter averaged, is 15, 28, 25 and 19 percent at 0.26, 0.17, 0.12 and 0.07 m, respectively. Hence, the contribution of the oscillating suspended sediment transport to the total suspended sediment transport shows no trend in the vertical and is lower in the longshore direction than in the cross-shore direction.

In conclusion, the net suspended sediment transport between 0.07 and 0.26 m above the bed and in the cross-shore direction is near the bed dominated by the mean suspended sediment transport while the relative contribution of the oscillating suspended sediment transport decreases towards the bed. The relative contribution of the oscillating, suspended load components in the longshore direction is smaller than in the cross-shore direction and shows no vertical trend.

5.4.3 Conclusions

The following conclusions are based on the analysis of the instantaneous suspended sediment transport at elevations of 0.07 - 0.26 m above the bed and in the inner nearshore zone.

Cross-shore

- The net sediment transport at 0.17 m above the bed is slightly dominated by the mean sediment transport and the average ratio between the oscillating transport and the mean transport is 0.46.
- The low-frequency oscillating suspended sediment transport at 0.17 m is about half that of the high-frequency oscillating suspended sediment transport.
- The average contribution of the sum of the high-frequency velocity - low-frequency concentration term and the high-frequency concentration - low-frequency velocity terms to the net sediment transport is very small (about 3%).
- The mean sediment transport increases for a relative wave height between 0.35 and 0.55 (non-breaking wave - breaker zone) and the highest mean suspended sediment transport is found in the breaking zone. The mean sediment transport decreases from the breaking zone to the swash zone.
- The high-frequency oscillating suspended sediment transport increases with relative wave height and is increasingly onshore directed while the low-frequency oscillating sediment transport shows no cross-shore trend.
- The cross-shore suspended sediment transport is dominated by the mean suspended sediment transport; the contribution of the oscillating suspended sediment transport to the sediment transport decreases towards the bed.

Longshore

- The net longshore suspended sediment transport is dominated by the mean suspended sediment transport and the oscillating component shows no vertical trend

5.5 Depth-integrated, time-averaged suspended sediment transport

5.5.1 Analysis and interpretation methods

Depth-integrated, time-averaged suspended sediment transport is defined as the integration between 0.05 m above the bed and the water-level of the product of the time-averaged velocity and the time-averaged sediment concentrations. A value of 0.05 m above the bed was chosen because bedload transport is regarded here to be all transport below 0.05 m above the bed (see Section 5.6).

To calculate the depth-integrated, time-averaged suspended sediment transport it is necessary to interpolate and extrapolate the measured velocities and measured concentrations over depth. The velocities were measured at 0.1, 0.3 and 0.7 m above the bed and the time-averaged concentration at 10 positions between 0.05 and 1.06 m above the bed.

It is assumed that the concentration decreases logarithmically with elevation above the bed. A logarithmic profile is fitted through the measured points using a least squares solution. The assumed profile has the form:

$$c = a \ln(z) + b \quad \text{for } 0 < z < h \quad (5.11)$$

where

c = concentration [kg m^{-3}]
 z = elevation above the bed [m]
 a, b = regression coefficients.

The use of Formula 5.11 occasionally resulted in negative concentrations in the upper part of the water column. These negative concentrations are replaced by a concentration of zero kg m^{-3} .

It is assumed that the velocity at elevation 0 ("bed") is 0 m s^{-1} . Furthermore, the time-averaged velocity between 0.7 m and the time-averaged water level is assumed to be equal to the velocity measured at 0.7 m above the bed. The cross-shore velocities in between the bed and the measured velocities at 0.1, 0.3 and 0.7 m above the bed were calculated using a third order function, giving a cross-shore velocity profile of:

$$v = az + bz^2 + cz^3 \quad \text{for } 0 < z_i < h \quad (5.12)$$

where

v = velocity at elevation z above the bed [ms^{-1}]
 z = elevation above the bed [m]
 a, b, c = regression coefficients.

A third order function (5.12) or the logarithmic function (5.11) was used to determine longshore velocity. Which profile was used for the interpolation was determined by the highest regression coefficient.

Finally, the depth-integrated, suspended sediment transport is calculated with:

$$S_s = \sum_{i=1}^N \frac{1}{2} (v_i c_i + v_{i-1} c_{i-1}) (z_i - z_{i-1}) \quad \text{for } 0.05 < z < h \quad (5.13)$$

where

S_s = depth-integrated, suspended sediment transport [$\text{kg s}^{-1} \text{ m}^{-1}$].

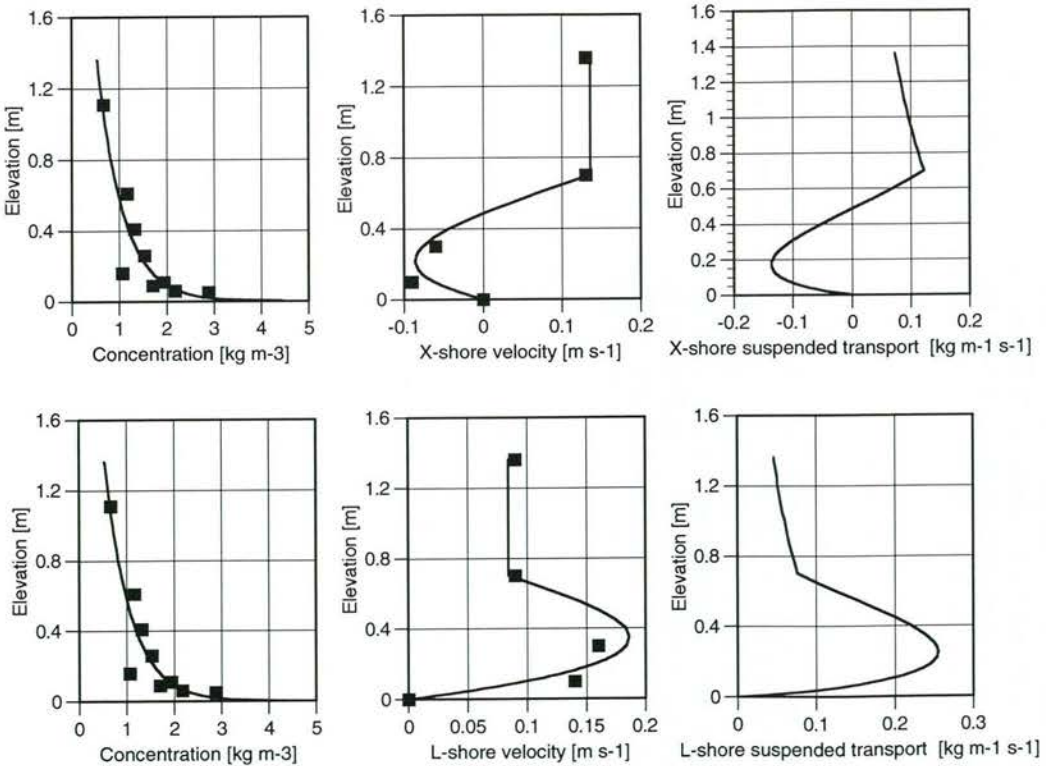


Figure 5.19 Example of computed concentration profiles, velocity profiles and the resulting suspended sediment transport profiles (series 1011-1 [breaking]). Squares are measured values, except for the highest and lowest velocity which are based on theoretical conditions and considerations. Positive velocity/transport is north/onshore, negative velocity/transport is south/offshore. Note that this example is one of the few of which the depth-integrated suspended sediment transport is *onshore* directed.

Formulae 5.11 and 5.12 are somewhat different from the interpolation functions used by Kroon (1994). A different interpolation method for the concentration was chosen because it represents the notion that the time-averaged concentration at the surface is not always zero, where Kroon's (1994) interpolation method assumed a zero concentration at the surface. Moreover, Formula 5.12 was chosen instead of a linear interpolation because it is more likely that the velocity varies more smoothly with depth than can be represented by a linear function. For the non-breaking wave series, a second order function was used to interpolate the velocities.

5.5.2 Results and discussion

The measured concentration and velocity data fit rather well into the computed concentration and velocity profiles. The average regression coefficient for the concentration is 0.63, for the cross-shore velocity 0.89 and for the longshore velocity 0.93. One series (0711-1) was removed from the dataset because of considerable scatter in the measured concentrations. As a result, a representative profile for this series could not be computed. An example of the computed concentrations, cross-shore and longshore velocities, and suspended sediment transport rates in the cross-shore and longshore direction is presented in Figure 5.19. In general, the lower part of the water column shows offshore directed fluxes while in the upper part they are either on- or offshore directed.

The depth-integrated, time-averaged cross-shore sediment fluxes vary between $0.03 \text{ kg s}^{-1} \text{ m}^{-1}$ onshore and $0.49 \text{ kg s}^{-1} \text{ m}^{-1}$ offshore (Fig. 5.20). Four depth-integrated fluxes are onshore directed while the remaining 33 fluxes are offshore directed. The depth-integrated, cross-shore suspended sediment fluxes increase from the non-breaking wave zone to the breaking wave zone and it is in the latter zone, that the highest offshore depth-integrated, suspended sediment fluxes are found. The depth-integrated, suspended sediment fluxes decrease from the breaking wave zone to the

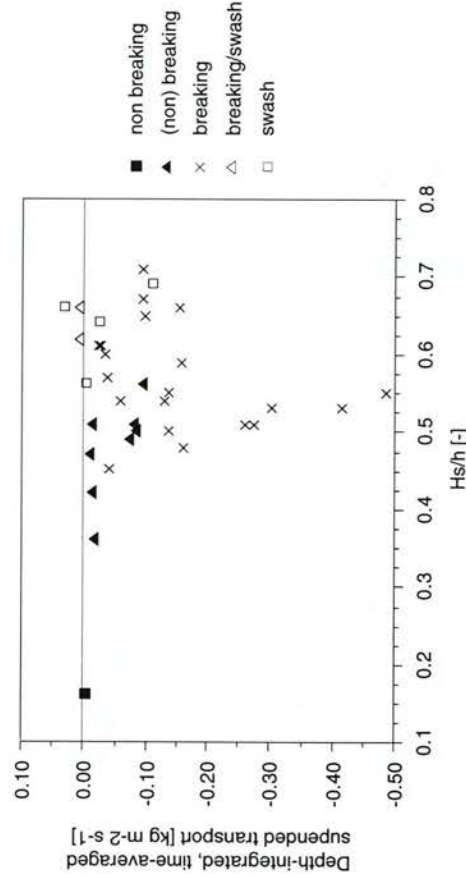


Figure 5.20 Relation between relative wave height (H_s/h) and depth-integrated, suspended-sediment transport in the cross-shore direction. Positive transport is onshore directed, negative transport is offshore directed.

swash zone and may even change from offshore to onshore. These results are in line with the results of most other investigators e.g. Dally and Dean (1984). Kroon (1994) observed a relation between relative wave height and depth-integrated, suspended sediment transport, in that the latter appeared to increase with increasing relative wave heights but Figure 5.20 shows that those findings are not confirmed by this study.

The previous section makes clear that suspended sediment transport in the inner nearshore zone at the four OBS elevations (0.05 m - 0.26 m above the bed) is predominantly dominated by the mean currents. Therefore, it is reasonable to assume that the depth-integrated transport is also dominated by the mean transport rate and the present calculations confirm this assumption. Figure 5.21 shows that there is a relation between the observed at 0.1 m above the bed, mean cross-shore currents and the depth-integrated, time-averaged suspended sediment transport in that a higher mean current leads to a higher depth-integrated, suspended sediment transport. The same figure indicates that some of the depth-averaged, suspended sediment transports were onshore which is caused by a combination of high concentrations and onshore velocities in the upper part of the water column. Thus a mean cross-shore current near the bed that is offshore directed may still be associated with an onshore sediment transport.

In conclusion, the direction and magnitude of the depth-integrated, time-averaged, suspended sediment transport is largely determined by the near bed (0.1 m), mean cross-shore current.

The observed depth-integrated, suspended sediment transport fluxes are compared with the depth-integrated, suspended sediment flux as calculated by the TRANSPOR model of Van Rijn (1993). Figure 5.22 shows that the TRANSPOR model only predicts offshore suspended sediment fluxes while the observed depth-integrated, suspended

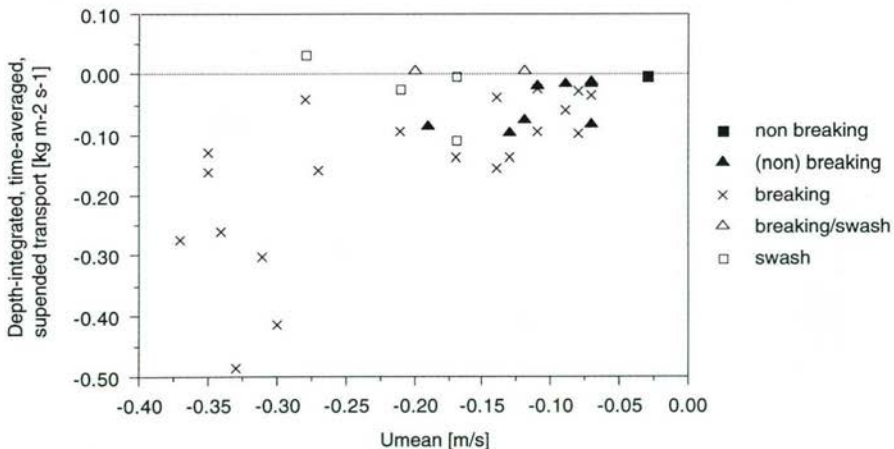


Figure 5.21 Relation between depth-averaged cross-shore mean current at 0.1 m above the bed (U_{mean}) and depth-integrated, suspended-sediment transport in the cross-shore direction. Positive transport is onshore directed, negative transport is offshore directed. Negative velocities are offshore directed.

sediment transports also include onshore fluxes. The largest deviation between computed and measured fluxes is at low transport rates. However, the observed and computed fluxes are generally in the same order of magnitude and the average ratio between the measured and computed depth-integrated, suspended sediment transport is about 8. This factor is rather high compared with Kroon's (1994) results where the ratio was within a factor of 2.

The large differences between the computed and measured depth-integrated sediment transport of this study and Kroon's results are due to a number of factors. First, there were a few series with very large differences between computed and measured depth-integrated sediment transport. In 7 of the 37 series the factor between the measured and computed depth-integrated sediment transport is higher than 20. Without these series the average difference between the computed and measured depth-integrated sediment transport is about 3, which is more in line with Kroon (1994).

Second, Kroon (1994) used a different interpolation technique to calculate the concentration and velocity profiles. To investigate this effect on the depth-integrated, suspended sediment transport, velocity profiles were computed using Kroon's (1994) method. The velocities between the bed and the first measuring point were represented by a power function. Those between the upper measuring point and the water surface were chosen to equal the velocity measured at the upper measuring point. Then a linear function was applied between the measuring points of the velocity. The difference between the depth-integrated, suspended sediment transport computed according to Kroon's method and that computed according to Formula 5.12 generally varies within a factor 1-4. Thus, using a different interpolation technique leads to differences in the depth-integrated, suspended sediment transport. However, the observed trends in the relation between the depth-integrated, suspended sediment transport and the various hydrodynamic parameters, did not change as a result of the different interpolation techniques. Thus, using Kroon's interpolation technique (1994) instead of the present interpolation to compute the depth-integrated, suspended sediment transport may result in different values but not in differences in the observed trends.

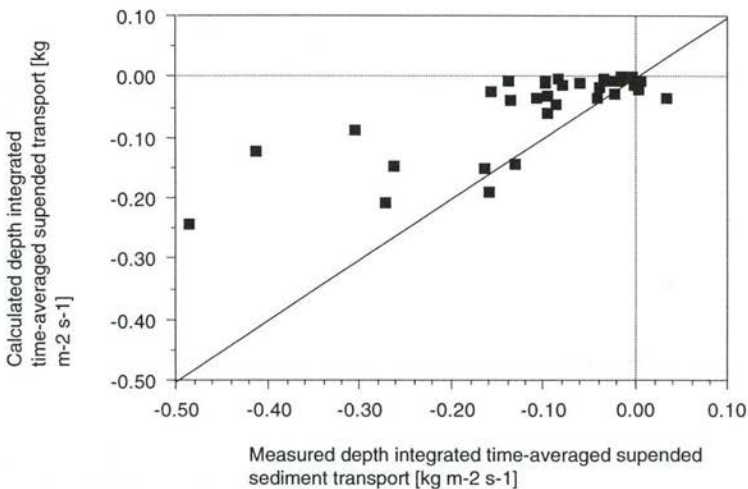


Figure 5.22 Relation between measured and computed (Van Rijn model) depth-integrated, suspended sediment transport in the cross-shore direction.

Finally, the TRANSPOR model uses empirical formulations based on Kroon's (1994) measurements. For instance the mixing layer thickness (δ_s) used in the TRANSPOR model is related to the relative wave height to represent the mixing effect of spilling and plunging waves. The formula that relates the thickness of the mixing layer with the relative wave height is based on Kroon's measurements. This study does not sustain all the relations found by Kroon (1994). Hence, larger differences between the TRANSPOR model and the measured results are more likely.

The observed cross-shore depth-integrated, suspended sediment transport is also compared with the longshore depth-integrated, suspended sediment transport. Figure 5.23 shows that the longshore and cross-shore sediment transport are correlated and in the same order. The magnitude of the longshore sediment transport increases with an increasing cross-shore sediment transport. The largest longshore sediment transport is found in the breaker zone; the lowest is found in the non-breaking zone. In the cross-shore direction, the largest depth-integrated, suspended sediment transport is also found in the breaking zone. Thus, while the largest suspended sediment concentrations are found in the swash zone, the largest depth-integrated, suspended sediment transport in both the cross-shore and longshore direction is found in this breaker zone. The largest velocities were measured in the breaking zone. Hence, the spatial distribution of depth-integrated, suspended sediment transport is dominantly determined by the spatial distribution of the velocities rather than that of the concentrations.

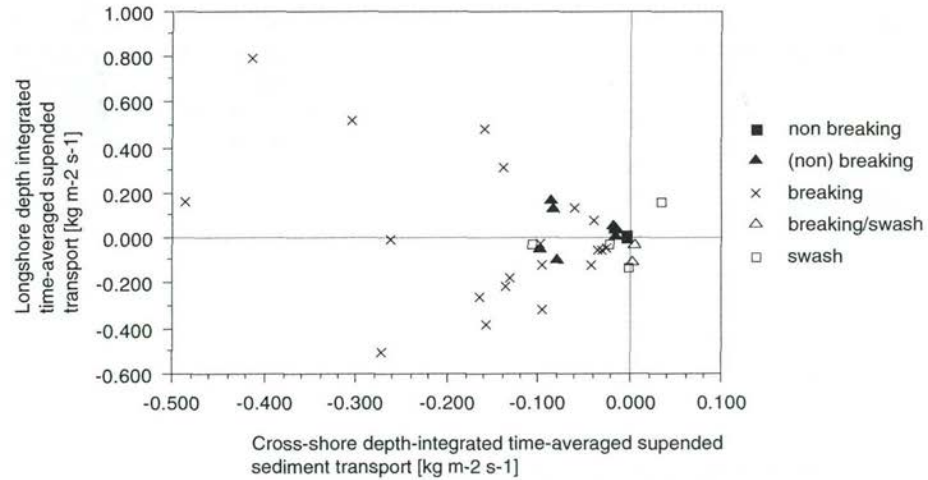


Figure 5.23 Relation between cross-shore and longshore depth-integrated, time-averaged, suspended sediment transport

5.5.3 Conclusions

The following conclusions are based on the measured cross-shore, depth-integrated, time-averaged, suspended sediment transport in the inner nearshore zone:

- The cross-shore, depth-integrated, time-averaged, suspended sediment transport varies between $0.03 \text{ kg s}^{-1} \text{ m}^{-1}$ onshore and $0.49 \text{ kg s}^{-1} \text{ m}^{-1}$ offshore.

- The cross-shore depth-integrated, suspended sediment transport is mainly offshore directed.
- The cross-shore, depth-integrated, suspended sediment transport increases from the non-breaking to the breaking zone and thereafter decreases from the breaker to the swash zone.
- The cross-shore depth-integrated, suspended sediment transport increases with increasing mean offshore directed currents (undertow).
- The spatial distribution of the depth-integrated, suspended sediment transport is more determined by the spatial distribution of the velocities than that of the concentrations.
- The TRANSPOR model (Van Rijn, 1993) is capable of predicting cross-shore depth-integrated, suspended sediment transport with the same order of magnitude as the measured cross-shore depth-integrated, suspended sediment transport; however, the actual differences remain significant (factor 2-8).
- Longshore sediment transport and cross-shore sediment transport are of the same order.

5.6 Bedload transport

5.6.1 Analysis and interpretation methods

The sediment transported by rolling, sliding and saltation is called the bedload transport (Van Rijn, 1984). In field conditions, however, there is no sharp division between the suspended and bedload part of the total sediment transport. Therefore, the distinction between bedload and suspended transport is made here by introducing an arbitrary boundary between what is considered to be the bedload and the suspended part of the transport. The inside height of the sampler is 0.044 m while the outside height is 0.05 m. So, for reasons of simplicity, bedload transport is here considered to be the sediment transport between the bed and 0.05 m.

The bedload transport was computed by using the next formula:

$$q_b = \frac{M}{\Delta t \cdot b} \quad (5.14)$$

where

- q_b = bedload transport [$\text{kg m}^{-1} \text{s}^{-1}$]
- M = total weight of the sediment [kg]
- Δt = sampling time [s]
- b = internal width of the bedload sampler (=0.094m) [m].

The bedload transport measurements were conducted from the BERT by using the bedload sampler, described in Section 3.6. The bedload transport was only measured in the cross-shore direction during 25, 40-minute lasting- sessions with the BERT when the bedload transport was sampled synchronously with the water level variations, the currents and the concentration. During each session about 8 bedload measurements were taken, each with a burst duration of about three minutes. Originally, it was the intention to use two bedload samplers at the same time: one

facing the waves and the other in the opposite direction. In this way it was thought possible to measure the onshore and offshore bedload transport synchronously. However, test measurements revealed that one of the samplers was too close to a pole of the BERT and the results of this sampler were heavily influenced by scour around the pole. The resulting scour hole around the leg developed in such a way that the sampler remained above the bottom. Therefore, one bedload sampler was used and alternately pointed onshore and offshore. After the bedload material had been collected, it was washed through a 1000 μm sieve to separate shells and organic matter from the sand. Thereafter, the sand was dried and weighed.

5.6.2 Results and discussion

The measured onshore and offshore bedload transport within a session was computed using the results of 1 to 4 sampling series. Despite the lengthy sampling time (3 - 12 minutes), the measured transport of an individual 3-minute measurement deviated by up to 100 percent of the session-averaged transport. The standard deviation of an individual measurement within any one session was 17.5 percent and the net transport had an error of 35 percent. These deviations may be due to the design and handling procedures of the bedload sampler.

Van Rijn (1993, in Van der Lee, 1994) tested the use of valves in the opening of this bedload sampler in an oscillating water tunnel. The metal valves were swung around a thin horizontal bar at the upper inner side of the sampler. Van Rijn (1993) found that without the valves and with peak velocities of 0.91 m s^{-1} , 40 percent and during peak velocities of 1.5 m s^{-1} , 60-80 percent of the sediment was lost. The latter velocity is about the same as that found during the field measurements where an average peak velocity of 1.15 m s^{-1} was measured. This loss occurs when sediment, trapped during the forward flow, was washed out during the reversed flow. Moreover, scouring around the corners of the sampler was observed which reduced the effective width of the bedload sampler by a factor 1.5 to 2. Initially, the bedload sampler used during the Egmond measurements in 1992 was also equipped with valves. However, due to the rather rough hydrodynamic conditions, the sand prevented the swinging mechanism from turning and the valves became stuck and had to be removed. Scour holes clearly influenced the amount of sand trapped by the sampler but as it was not monitored during the 3-minute measurements, the occurrence of scour holes and their influence on the measurements could not be verified. In all, bedload transports have to be interpreted with care.

The results of the bedload measurements are presented in Table 5.3. The onshore bedload transport varies between $2.5 \cdot 10^{-3}$ and $6.0 \cdot 10^{-3} \text{ kg s}^{-1} \text{ m}^{-1}$ and that of the offshore between $4.6 \cdot 10^{-3}$ and $3.6 \cdot 10^{-2} \text{ kg s}^{-1} \text{ m}^{-1}$. The variation of the net bedload transport is between $-3.4 \cdot 10^{-2} \text{ kg s}^{-1} \text{ m}^{-1}$ (offshore) and $+50 \cdot 10^{-2} \text{ kg s}^{-1} \text{ m}^{-1}$ (onshore). A negative net transport means that the sediment is transported in the offshore direction and a positive one that it is transported onshore. The measured transports are in the same order as those measured with the same sampler in a large oscillating water tunnel (Van der Lee, 1994). Table 5.3 also reveals that the gross bedload transports are about a factor 5 to 10 higher than the net bedload transport, the majority of the latter being onshore directed (Fig. 5.24). No hydrodynamic zone shows solely onshore or offshore bedload transport and the measured net transport is not related to the relative wave height.

Table 5.3 Hydrodynamic conditions, time-averaged suspended transport and bedload transport

Series	h	Hs	T	Wave conditions	Breaker type	% br waves	H_b/L_{br}	H_b/h	(1)	(2)	Onshore Bedload transport [kg m ⁻¹ s ⁻¹]	Offshore Bedload transport [kg m ⁻¹ s ⁻¹]	Net Bedload transport [kg m ⁻¹ s ⁻¹]
2310-1	0.65	0.43	6.91	swash	-	-	0.055	0.66	6.69E-03	1.72E-01	x	x	x
2310-2	1.33	0.87	6.37	breaking	plunging	61.2	0.072	0.65	-9.65E-02	-2.78E-02	x	x	x
2310-3	1.34	0.90	6.72	breaking	plunging	70.1	0.071	0.67	-9.48E-02	-3.27E-01	x	x	x
2310-4	1.23	0.81	6.90	breaking	plunging	82.6	0.065	0.66	-1.55E-01	-4.04E-01	x	x	x
2310-5	1.03	0.73	7.36	breaking	plunging	74.6	0.057	0.71	-9.58E-02	-1.50E-01	x	x	x
2510-2	1.95	0.32	5.78	non breaking	-	0.0	0.056	0.16	-3.79E-03	9.54E-03	x	x	x
2510-3	1.85	0.29	5.15	non breaking	-	0.0	0.056	0.16	-2.40E-03	2.88E-03	x	x	x
2610-1	0.77	0.53	7.08	swash	-	-	0.058	0.69	-1.07E-01	-2.81E-02	x	x	x
2610-2	1.57	0.66	6.11	(non) breaking	plung/spill	3.4	0.069	0.42	-1.56E-02	1.83E-03	x	x	x
2610-3	1.31	0.73	6.06	(non) breaking	plung/spill	32.8	0.071	0.56	-9.77E-02	-5.73E-02	x	x	x
0411-1	0.87	0.49	8.04	swash	-	-	0.043	0.56	-1.73E-03	-1.31E-01	x	x	x
0411-2	1.21	0.66	7.72	breaking	plung/spill	84.9	0.051	0.54	-1.31E-01	-1.79E-01	x	x	x
0411-3	1.40	0.72	7.73	breaking	plunging	82.6	0.053	0.51	-2.61E-01	2.60E-01	9.81E-03	2.93E-02	-1.95E-02
0411-4	1.37	0.70	7.71	breaking	plung/spill	84.6	0.052	0.51	-2.73E-01	-5.48E-01	2.47E-03	3.61E-02	-3.36E-02
0411-5	1.24	0.60	8.19	breaking	plung/spill	x	0.046	0.48	-1.63E-01	-2.85E-01	x	x	x
0411-6	1.05	0.47	8.28	breaking	spilling	93.1	0.040	0.45	-4.06E-02	-1.25E-01	5.14E-03	2.09E-02	-1.58E-02
0511-1	1.00	0.64	7.04	swash	-	-	0.060	0.64	-2.20E-02	-2.36E-02	2.00E-02	3.35E-02	-1.35E-02
0511-2	1.20	0.74	6.52	breaking	plung/spill	84.9	0.065	0.61	-2.45E-02	-4.78E-02	1.25E-02	1.16E-02	9.37E-04
0511-3	1.20	0.72	6.51	breaking	plunging	82.6	0.065	0.60	-3.30E+00	-5.29E-02	x	x	x
0511-4	1.08	0.67	6.73	breaking/swash	plunging	84.6	0.061	0.62	4.83E-03	-3.40E-02	2.61E-02	8.61E-03	1.75E-02
0511-5	0.89	0.58	6.77	breaking/swash	spilling	85.7	0.056	0.66	3.33E-03	-1.14E-01	1.83E-02	1.98E-02	-1.54E-03
0611-1	0.97	0.57	6.98	breaking	spilling	91.8	0.056	0.59	-1.58E-01	5.12E-01	1.82E-02	3.21E-02	-1.39E-02
0611-2	1.50	0.81	5.81	breaking	plung/spill	71.2	0.079	0.54	-5.91E-02	1.39E-01	3.23E-02	9.01E-03	2.33E-02
0611-3	1.58	0.81	5.90	(non) breaking	plung/spill	64.1	0.078	0.51	-1.63E-02	3.62E-02	x	x	x
0611-4	1.42	0.72	5.68	(non) breaking	plung/spill	69.1	0.075	0.51	-8.39E-02	1.25E-01	2.18E-02	1.29E-02	8.85E-03
0611-5	1.25	0.63	5.68	breaking	plung/spill	85.7	0.069	0.50	-1.37E-01	3.12E-01	1.07E-02	2.06E-03	2.06E-03
0711-1	1.06	0.68	6.64	swash	-	-	0.064	0.64	*	*	1.48E-02	6.25E-01	-6.10E-01
0711-2	1.61	0.88	6.26	breaking	plunging	35.5	0.075	0.55	-4.86E-01	1.71E-01	3.11E-02	2.96E-02	1.54E-03
0711-3	1.57	0.84	6.24	breaking	plunging	50.8	0.073	0.53	-4.14E-01	8.32E-01	1.32E-02	2.27E-02	-9.47E-03
0711-4	1.29	0.68	6.31	breaking	plunging	-	0.065	0.53	-3.04E-01	5.61E-01	2.75E-02	3.55E-02	-7.96E-03
0811-1	1.25	0.76	8.23	breaking	plung/spill	53.3	0.055	0.61	-2.85E-02	-5.20E-02	3.40E-02	1.40E-02	2.00E-02
0811-2	1.62	0.80	8.20	(non) breaking	plunging	62.7	0.056	0.49	-7.80E-02	-1.04E-01	1.69E-02	1.80E-02	-1.12E-03
0811-3	1.43	0.79	8.06	breaking	plung/spill	78.0	0.056	0.55	-1.36E-01	-2.31E-01	2.21E-02	7.26E-03	1.48E-02
0911-1	1.54	0.56	4.77	(non) breaking	plung/spill	36.0	0.084	0.36	-1.83E-01	5.95E-02	9.29E-03	4.62E-03	4.68E-03
0911-2	1.58	0.74	5.12	(non) breaking	plung/spill	10.4	0.087	0.47	-1.43E-02	4.22E-02	1.51E-02	1.05E-02	4.63E-03
0911-3	1.47	0.74	5.70	(non) breaking	plung/spill	23.1	0.077	0.50	-8.70E-02	1.86E-01	2.63E-02	1.71E-02	9.20E-03
1011-1	1.36	0.98	7.36	swash	-	-	0.065	0.72	3.36E-02	1.36E-01	5.94E-02	9.90E-03	4.95E-02
1011-2	1.69	0.97	7.22	breaking	plung/spill	19.4	0.069	0.57	-3.89E-02	7.49E-02	5.14E-02	9.10E-03	4.23E-02

x = not measured

- = not applicable

* = no representative velocity profile calculated

(1) Depth-integrated, cross-shore, suspended sediment transport

(2) Depth-integrated, longshore, suspended sediment transport

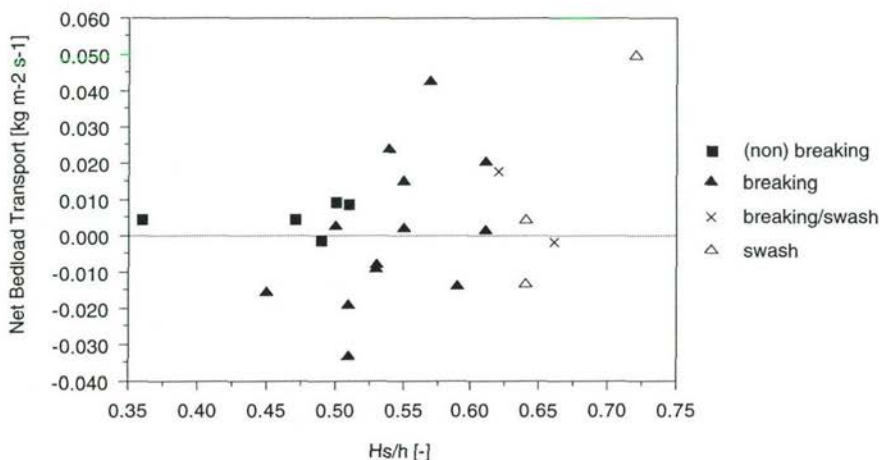


Figure 5.24 Relation between relative wave height (H_s/h) and net, cross-shore, bedload transport. Positive transport is onshore directed, negative transport is offshore directed.

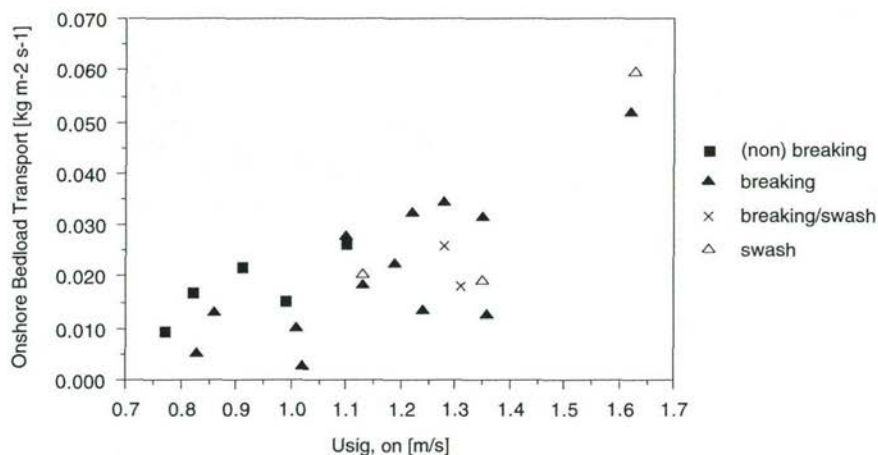


Figure 5.25 Relation between significant, onshore, orbital peak velocity ($U_{sig, on}$) and onshore bedload transport.

No relation is found between either the significant onshore peak velocity or the significant offshore velocity or either the duration- or amplitude-asymmetry of the velocity and the net bedload transport. The importance of wave related motion on net transport is further examined by considering the gross transport in the on- and offshore direction. It was found that although a larger onshore significant peak velocity results in a larger onshore bedload transport (Fig. 5.25), the offshore bedload

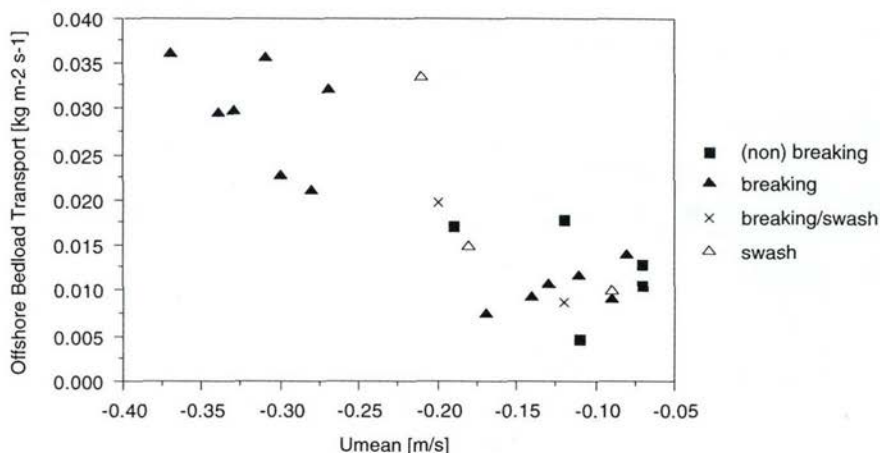


Figure 5.26 Relation between mean cross-shore velocity (U_{mean}) at 0.1 m and offshore bedload transport in the cross-shore direction.

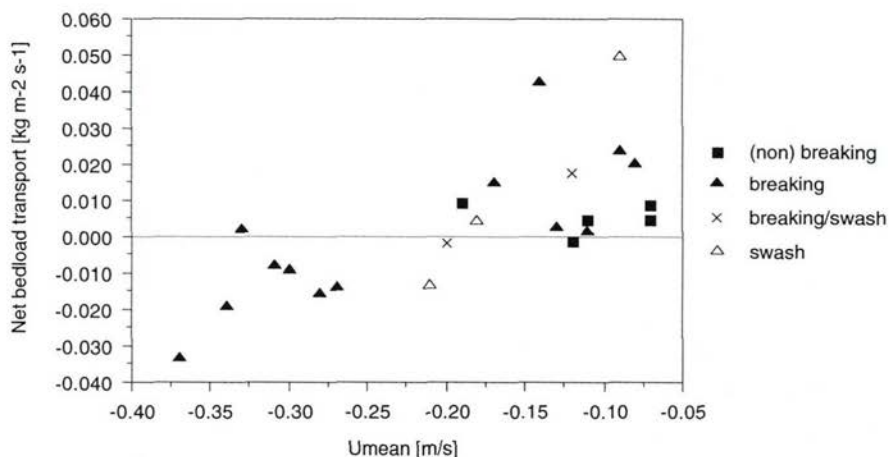


Figure 5.27 Relation between mean cross-shore velocity (U_{mean}) at 0.1 m and net bedload transport in the cross-shore direction. Positive transport/current is onshore directed, negative transport/current is offshore directed.

transport is not related to the offshore significant peak velocity, but shows a relation with the offshore directed mean currents (undertow) (Fig. 5.26). The net bedload transport (Fig. 5.27) shows no relation with the offshore or onshore significant velocity but is related to the mean, offshore directed currents and is always in the direction of the wave propagation as long as the undertow is not larger than 0.2 m s^{-1} . This suggests that without the undertow, the net bedload transport would be onshore directed, a conclusion also found by Ribberink and Al Salem (1992) who conducted experiments in a large oscillating water tunnel with an undertow in the order of cm s^{-1} .

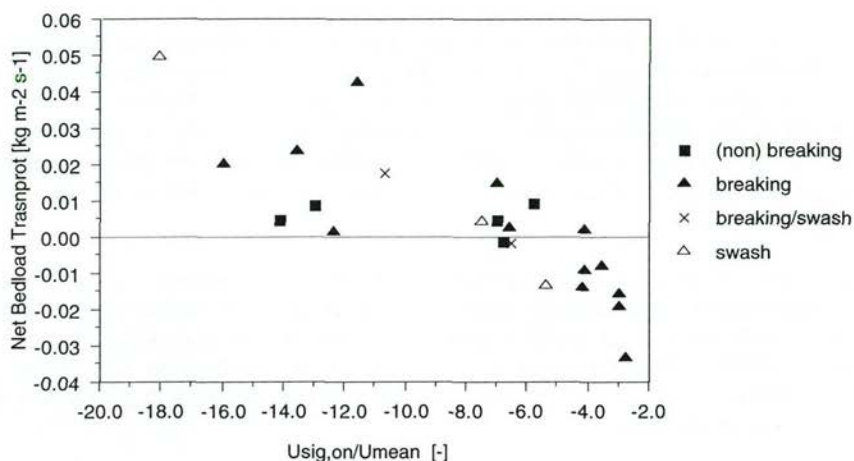


Figure 5.28 Relation between the ratio onshore significant, orbital peak velocity to mean velocity at 0.1 m, and net bedload transport in the cross-shore direction. Positive transport is onshore directed, negative transport is offshore directed.

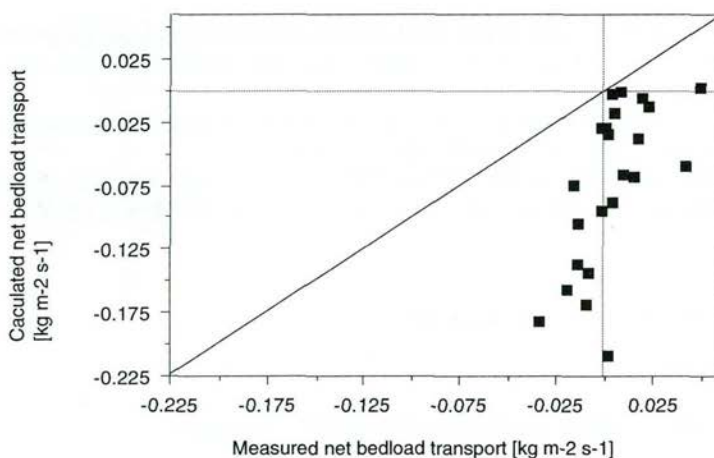


Figure 5.29 Relation between measured and computed (TRANSPOR model) bedload transport. Positive transport is onshore directed, negative transport is offshore directed.

Onshore bedload transport is related to onshore peak velocity and offshore bedload transport is related to the undertow. The net bedload transport, therefore, is likely to be determined by the ratio of onshore peak velocity to undertow and this proved to be the case (Fig. 5.28).

The measured net bedload transport was then compared with the net bedload transport computed by the TRANSPOR model (Van Rijn, 1993) (Fig. 5.29). The measured mean cross-shore current was used as input while the on- and offshore peak velocities were computed by the model. The most apparent difference between

the computed and the measured net bedload transport was found to be the direction of the net bedload transport. The TRANSPOR model predicts, except for one case, an offshore directed net bedload transport but the measured net bedload transport is both onshore and offshore directed. So, only a weak relation between the measured and computed values is present. In addition, the order of magnitude of the computed and measured transport differs significantly because the ratio between the two varies between 0.01 and 16.

In conclusion, the direction and magnitude of the net bedload transport is determined by the ratio between onshore peak velocity and undertow. If this ratio is higher than 4-6, the bedload transport is onshore directed. A ratio of less than 4-6 results in an offshore- directed bedload transport. However, these conclusions are based on samples with a sampling error of about 50 percent due to oscillating flow and the occurrence of scour holes.

5.6.3 Conclusions

- The measured net bedload transport varies between $-3.4 \cdot 10^{-2} \text{ kg s}^{-1} \text{ m}^{-1}$ and $+5.0 \cdot 10^{-2} \text{ kg s}^{-1} \text{ m}^{-1}$ while the majority of the measured bedload transport is onshore directed.
- The direction and magnitude of the net bedload transport are determined by the ration between the onshore peak velocity and the mean (offshore directed) currents.
- The bedload samples have an estimated sampling error of about 50 percent due to 'losses' by oscillating flow and the occurrence of scour holes.
- The measured and computed (TRANSPOR model) net bedload transport frequently have not the same order of magnitude, while the directions may also differ.

5.7 Total net sediment transport

5.7.1 Ratio between suspended and bedload transport

The distinction between bedload and suspended sediment transport is often difficult to make. A ratio between suspended load and bedload found in previous research is therefore subject to the definition used (Hallermeier, 1982). Nevertheless, when this definition is clear, as is here the case, the results can be used to indicate where in the water column the majority of the (net) sediment transport takes place. Note that the ratio suspended to bedload transport is calculated using the net values which incorporate the sediment transport direction. In addition, the total net sediment transport is here considered to be the total of the depth-integrated, time-averaged suspended sediment transport and the measured bedload transport, i.e. the oscillating suspended sediment transport is not incorporated.

It can be concluded from Table 5.3 that the ratio of suspended load to bedload transport varies largely, from -315 to +70. A negative ratio indicates that the net suspended transport takes place in the opposite direction to the net bedload transport.

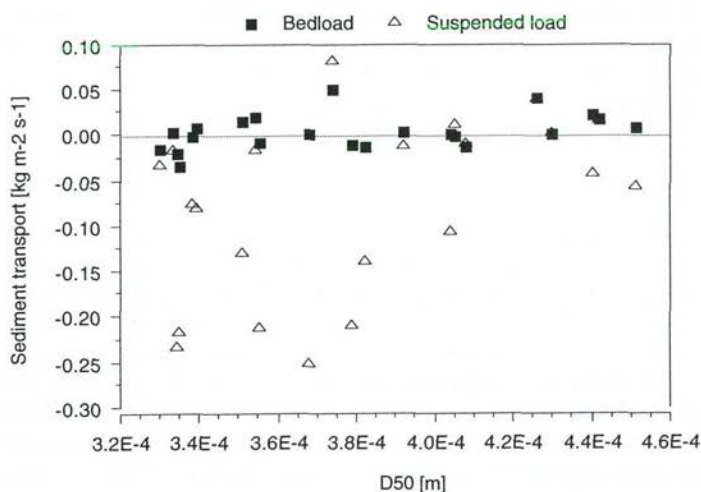


Figure 5.30 Relation between measured bedload and suspended sediment transport and diameter of the sediment (D_{50}). Negative transport means offshore directed transport, positive transport onshore directed transport.

Sediment transport in the bedload layer (0-0.05 m) may take place in an opposite direction due to the shoaling of waves which generate a quasi-steady weak current in the onshore direction near the bed. This current may lead to a net onshore transport in the case of a plane bed (Van Rijn, 1993). In 3 of the 22 series, the bedload transport is larger than that of the suspended load. These 3 series show a ratio of suspended to bedload transport between 0.3 and 1, indicating that the bedload transport is not substantially larger than the suspended transport in these 3 series. The measured and computed ratios were plotted against the measured hydrodynamic conditions to evaluate possible causes for the very large measured ratios. Unfortunately, these ratios could not be attributed to specific hydrodynamic conditions or the relative wave height but the large deviations in the ratio of suspended load to bedload transport may, according to some authors, be related to the D_{50} of the sediment (Komar, 1978; Walton and Chui, 1979, in Carter, 1988). The measured bedload and suspended transport rates show no clear relation with the grain size of the bed sediment, although the ratio suspended to bedload is larger for smaller grain sizes (Fig. 5.30). Hence, the difference in grain size over the series may explain the large variation of the ratio of suspended load to bedload transport but sampling errors made in the determination of the bedload and suspended load transport also contribute to this variation.

The computed ratio of suspended load to bedload transport (TRANSPOR model) is generally smaller than those ratios measured. The computed ratio varies between -8.0 and 2.0 and only for one case, the predicted bedload is directed in the opposite direction of the suspended load transport. The average ratio is 1.0. Thus, the TRANSPOR model predicts bedload and suspended load transports that are in the same order and in the same direction while according to the measured results different directions and magnitudes of suspended load and bedload transport are evident.

The measured and computed results regarding the ratio between the time-averaged, suspended load and bedload transport lead to the conclusion that in the nearshore zone suspended transport generally dominates the total transport but that the ratio between these transport modes varies largely .

5.7.2 Discussion

The total net transport, further referred to as total transport, was only considered in the cross-shore direction because no bedload measurements were taken in the longshore direction and a total of 22 series consisted of both bedload and suspended load measurements. The total sediment transport varied between $-0.48 \text{ kg s}^{-1} \text{ m}^{-1}$ (offshore) and $0.08 \text{ kg s}^{-1} \text{ m}^{-1}$ (onshore) with the total sediment transport showing largely the same trend as the total suspended sediment transport (cf. Fig. 5.31 and Fig. 5.20), i.e. an increase in magnitude from the non-breaking to the breaking zone with the direction of the total transport remaining offshore. The highest offshore directed transport was found in the breaker zone with the total transport reducing to the swash zone and changing direction from off- to onshore.

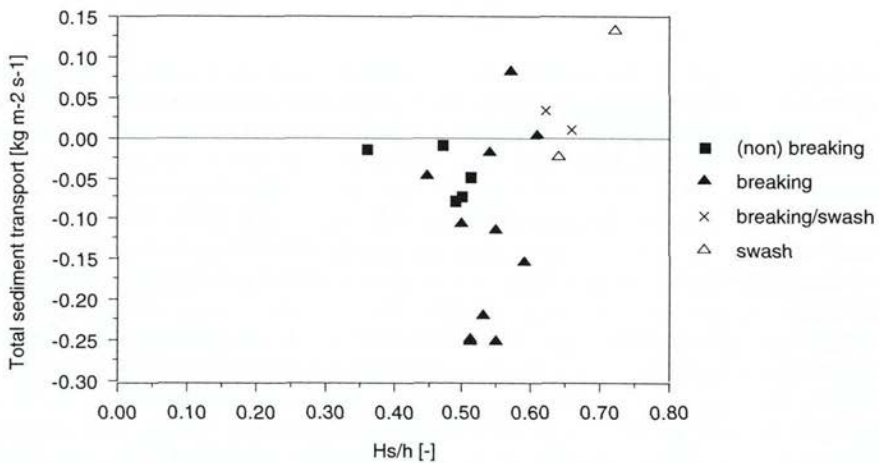


Figure 5.31 Relation between the relative wave height and total, cross-shore, sediment transport. Onshore transport is positive, offshore transport negative.

The measured total transport was compared with that predicted by the Van Rijn model and despite the large difference between the predicted and the measured suspended sediment transport and the predicted and measured bedload transport, the total transport shows reasonable agreement (Fig. 5.32). The ratio between the total measured transport and the total transport computed by the TRANSPOR model is between -4 and +30. This large variation, however, is mainly caused by a few series; 18 of the 22 series show a ratio of less than 2 and with the measured and computed sediment transport in the same direction. Hence, the TRANSPOR model reasonably predicts the total sediment transport in the nearshore zone.

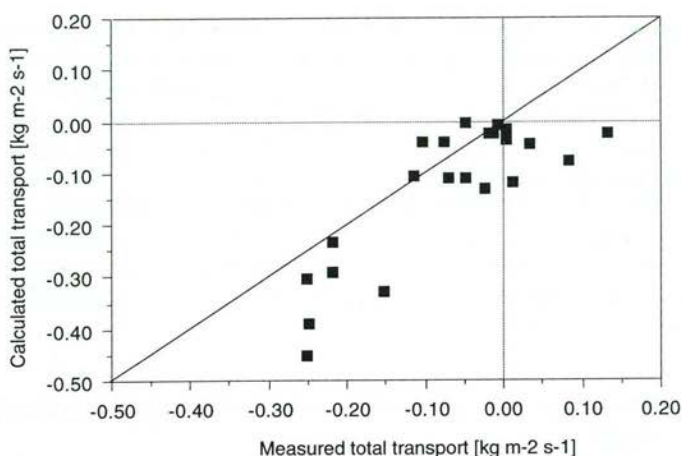


Figure 5.32 Relation between the measured and computed (TRANSPOR model) total, cross-shore, sediment transport. Negative transport means offshore directed transport, positive transport is onshore directed.

5.7.3 Conclusions

- The total sediment transport, i.e. the sum of the time-averaged, depth-integrated suspended sediment transport and the bedload transport, varied between $-0.48 \text{ kg s}^{-1} \text{ m}^{-1}$ (offshore) and $0.08 \text{ kg s}^{-1} \text{ m}^{-1}$ (onshore).
- The total sediment transport increases from the non-breaking to the breaking zone and is offshore directed but decreases and reverses in direction from the breaking zone to the swash zone
- The suspended sediment transport is generally larger than the bedload transport but their ratio varies largely.
- The total transport is reasonably predicted by the TRANSPOR model (Van Rijn, 1993) (generally within a factor of 2), in case of an offshore sediment transport.

5.8 Sediment transport patterns in the inner nearshore zone

5.8.1 Introduction

The previous analysis has considered the sediment transport on a small time scale and at the inter-tidal bar. It showed that the offshore directed total sediment transport increased towards the breaker zone which may lead to accumulation of sediment seaward of the breaker zone. At the same time and in the landward direction, the decrease of the offshore directed total sediment transport and an eventual onshore directed total transport will result in a divergence of sediment transport landward of the breaking zone. Potentially, this cross-shore distribution of the total sediment transport may lead to the formation of a bar at the seaward side and the formation of a trough landward of the breaker zone. The attention is now focused on the medium time scale by studying sediment transport patterns, i.e. convergence and divergence

of sediment in the inner nearshore under non-storm and storm conditions. Ideally, sediment transport measurements could have been performed closely around the breakpoint located near the inner nearshore bar. However, technical and operational constraints prohibited such an instrumental arrangement. Instead, surface wave and water level variables were measured on both sides but at larger distances from the inner nearshore bar (Fig. 3.7b) and were used to determine the relative wave height which in turn was used to calculate the direction and magnitude of the sediment transport. In addition, a coastal profile model (UNIBEST-TC, appendices A,B) was used to obtain a more detailed picture of the relative wave height variation in the inner nearshore. This model was first validated; the results are described in the next chapter.

5.8.2 Estimation of cross-shore sediment transport using relative wave height

The 40-minutes averaged values of the relative wave height and the sediment transport measured with the BERT were used to determine a curve representing the relation between relative wave height and net sediment transport. In the previous section, the net (total) sediment transport was considered to be the total of the depth-integrated, mean suspended sediment transport and the bedload transport, the depth-integrated, oscillating suspended sediment being disregarded. The reason for this was that the net sediment transport was compared with the TRANSPOR model which also excludes oscillating suspended sediment transport. Besides, this transport mode was only measured between 0.07 and 0.26 m above the bed and not in the entire vertical. Consequently, it is difficult to estimate the depth-integrated, oscillating suspended sediment transport. The instantaneous sediment transport analysis showed, however, that near the bed, the oscillating suspended load is significant for computing the net sediment transport (Section 5.4). Hence, integrating the sediment transport over days, the time scale of the morphological surveys, would lead to a considerable over- or underestimation of the integrated sediment transport. Thus, the following three relations between local hydrodynamics and the total sediment transport were evaluated:

- between the relative wave height and the depth-integrated, time-averaged suspended sediment transport
- between the relative wave height and the depth-integrated, oscillating suspended sediment transport
- between the relative wave height and the bedload transport

The depth-integrated, time-averaged suspended sediment transport was only measured during series where the relative wave height was between 0.35 and 0.7 (Section 5.5). Relative wave height values lower than 0.35 and higher than 0.7 were, however, measured at pole 1 (beach) and pole 2 (inner nearshore). Kroon (1994) measured the depth-integrated, time-averaged suspended transport during conditions with relative wave heights between 0.18 and 1.17. Kroon's (1994) data were, therefore, added and used to estimate the magnitude and direction of mean suspended sediment transport at values lower than 0.35 and higher than 0.7. In total, 67 measurements were used to establish a relationship between relative wave height and depth-integrated, time-averaged suspended sediment transport in the cross-shore direction (Fig. 5.33a).

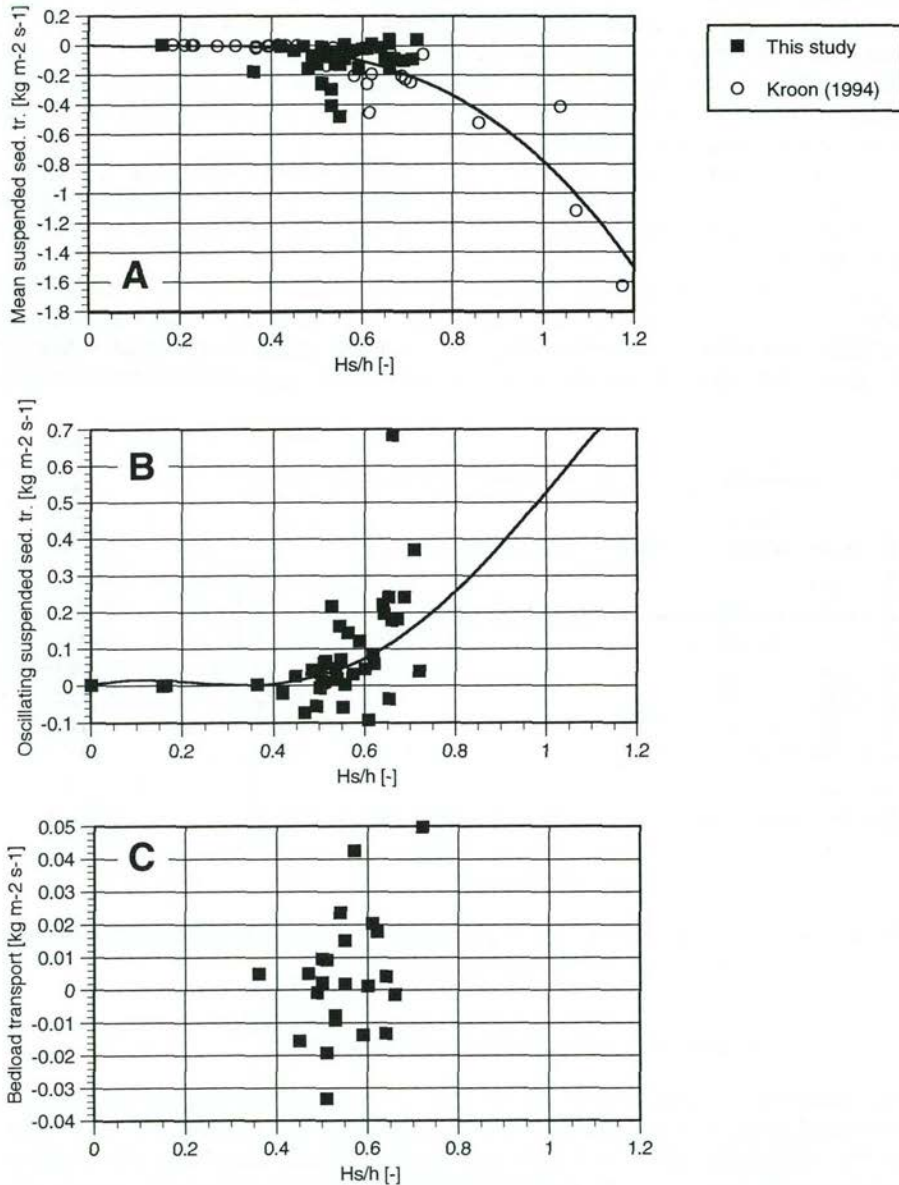


Figure 5.33 Relation between relative wave height (H_s/h) and:
 (A) depth integrated, mean suspended sediment transport,
 (B) depth-integrated, oscillating suspended sediment transport,
 (C) bedload transport
 and fitted curves. Positive transport is onshore directed, negative transport is offshore directed.

The oscillating suspended sediment transport was measured at 0.07, 0.12, 0.17 and 0.26 m above the bed but not higher in the vertical. Here, it is assumed that the depth-integrated, oscillating suspended sediment transport may be represented by the averaged oscillating suspended sediment transport between 0.07 m and 0.26 m. Kroon's (1994) data could not be used because he only measured oscillating suspended sediment transport at 0.05 - 0.09 m above the bed and the curve (Fig. 5.33b) is solely based on data of this study.

The bedload data showed no relation with relative wave height (Fig. 5.33c) and because Kroon did not measure bedload and bedload was found to be about a factor 10 smaller than the suspended sediment transport, it was decided to disregard bedload transport.

In short, in the relation between relative wave height and total sediment transport the latter is equal to the sum of the mean- and the oscillating suspended sediment transport. For lower relative wave heights (< 0.4) the sediment transport is onshore directed, while higher relative wave heights result in offshore sediment transport (Fig. 5.34).

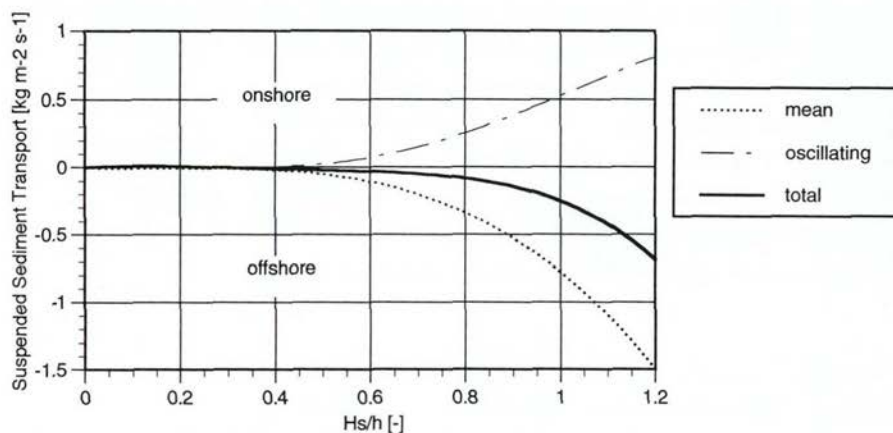


Figure 5.34 Relation between suspended sediment transport and relative wave height for different sediment transport modes.

5.8.3 Transport estimates based on observations

The convergence and divergence of sediment transport is studied for the inner nearshore zone development before, during and after a single storm in 1991 based on the relationship given in Figure 5.34. Further details about this storm and the resulting inner nearshore bar development will be discussed in the next chapter. Here, it is only of importance that the inner nearshore bar, located between pole 1 and pole 2 (see Fig. 3.7b), showed almost no changes before the storm, increased in height during the storm and migrated onshore after the storm. Patterns of sediment convergence or divergence can be derived (using Fig. 5.34) from the relative wave heights at poles 1 and 2 which determine the direction of the net, depth-integrated, suspended sediment transport (Fig. 5.35c-f). Note that due to technical difficulties and low water levels the recordings at pole 1 are discontinuous. The period between 14

and 23 October 1991 can be divided into three phases: pre-storm, storm and post-storm. The first phase was between 14 and 16 October when the relative wave height at pole 1 was between 0.1 and 0.7, resulting in both onshore and offshore transport. The relative wave height at pole 2 showed values of between 0.05 and 0.25 and the sediment transport at this pole was estimated to be always onshore directed, i.e. in the direction of the crest of the inner nearshore bar. Hence, the sediment transports at poles 1 and 2 indicate that some sediment might have accumulated in the inner nearshore at and around the inner nearshore bar.

The storm phase began on 16 October and ended on 20 October. Both at pole 1 and 2, the sediment transport was offshore directed. This means that the inner bar development during the storm was probably not caused by gradients of two opposing sediment transport vectors, as suggested by some bar forming theories (Fig. 2.2; e.g. Dally, 1973; Greenwood and Davidson-Arnott, 1979; Hattori and Kawamata, 1981). More likely, the morphologic changes during the storm were caused by a gradient in the offshore sediment transport because the relative wave heights at pole 1 are higher than at pole 2.

During the post-storm phase, 20 - 23 October, there was mostly offshore sediment transport at the beach and onshore sediment transport at pole 2. Consequently, there was a convergence of sediment in the inner nearshore zone during this period.

In conclusion, the above analysis suggests that inner nearshore bar development between pole 1 and pole 2 during a storm was mainly the result of a gradient in the predominantly offshore-directed sediment transport in the inner nearshore zone (Fig. 5.35e/f). Estimated sediment transport directions indicate that only the pre- and post storm bar development was the result of a convergence of sediment caused by opposing sediment transport vectors.

The estimated sediment transport directions can, however, only be used for a qualitative analysis of the processes. The volumetric gain between pole 1 and pole 2 from 14 to 23 October was, according to surveys with the SAP (see Section 3.7), about $7 \text{ m}^3 \text{ m}^{-1}$. According to the estimated sediment transports at poles 1 and 2, the estimated volumetric gain should have been approximately $42 \text{ m}^3 \text{ m}^{-1}$. Hence, a quantitative comparison between the volumetric changes obtained from the SAP profiles and the estimated sediment transport reveals that sediment transport estimations differ by a factor 5 from the profile results. Clearly, the present data are not accurate enough to perform a quantitative analysis, probably because of the scatter in the data and their sparsity for high relative wave heights. In addition, relative wave height is calculated using interpolated bed-levels, as the elevation of the bed was only measured once a day. A small change in bed-level and thus in water depth results in large changes in estimated sediment transport, especially when there is a large relative wave height. Finally, the measurements were not performed closely around a breakpoint which may have influenced the interpretation of the results. In order to make a more detailed study of sediment transport gradients and quantities around and at the inner nearshore bar, more information about changes in relative wave height is required. It is studied in the next section to which extent a physical-mathematical model can provide these data and how this may lead to new insights into the sediment transport patterns around the inner nearshore bar.

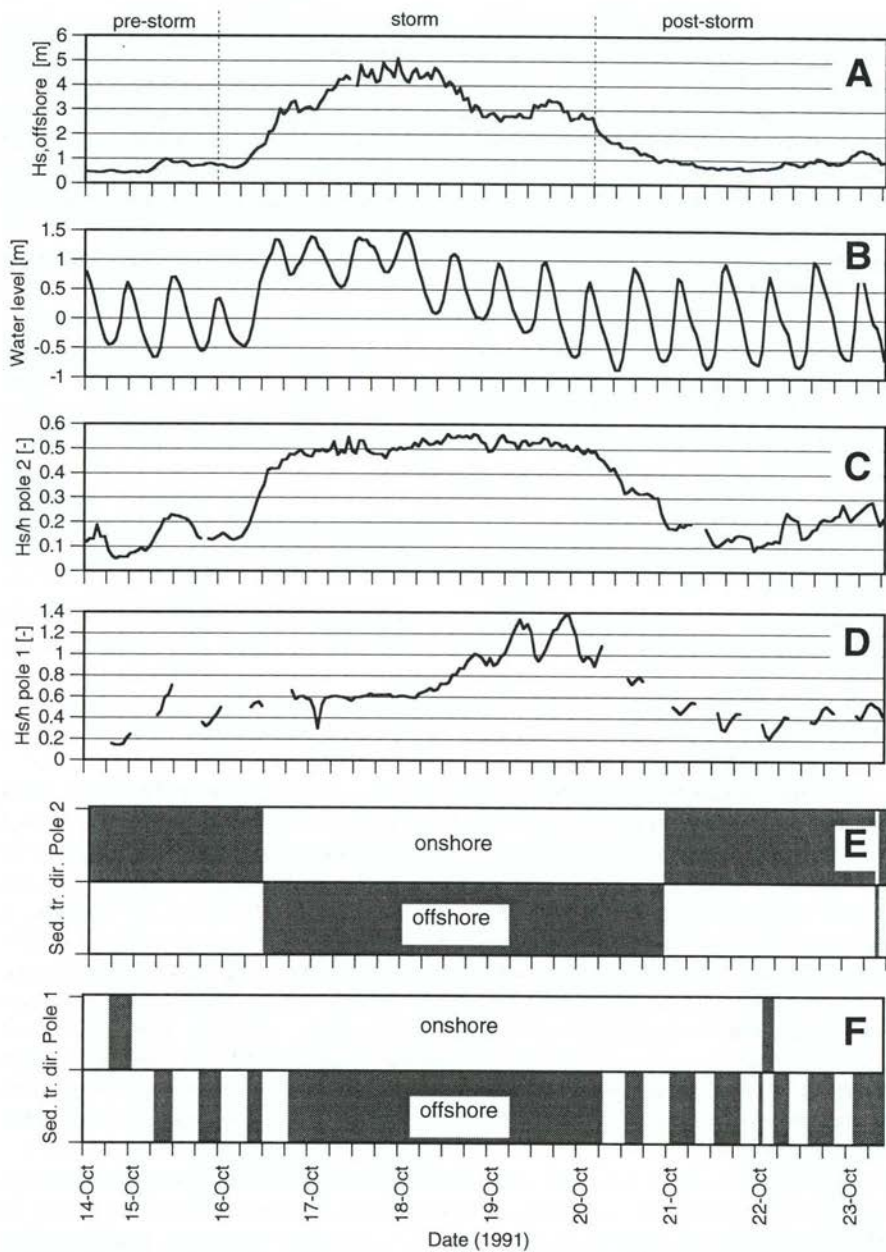


Figure 5.35 Sediment transport direction in the inner nearshore during 1991 storm

- (A) Offshore wave height
- (B) Water level fluctuations
- (C) Relative wave height at pole 2 (at seaward slope of inner nearshore bar)
- (D) Relative wave height at pole 1 (at lower beach)
- (E) Sediment transport direction at pole 2
- (F) Sediment transport direction at pole 1

5.8.4 Model computations

Model computations show (see Section 6.8) that the UNIBEST-TC model reasonably predicts the wave height in the surf zone, but the predicted sediment transport rates and morphologic developments are generally not in line with the observations. Therefore, to reveal sediment transport patterns in the nearshore zone and to establish a conceptual model regarding the sediment transports near the inner nearshore bar, the UNIBEST-TC model was used for the computation of wave height while the resulting sediment transport was computed by using the relation between the relative wave height and the total suspended sediment transport (Section 5.8.2; Fig. 5.34).

The relative wave height distribution and the resulting sediment transport patterns were calculated for three days (3, 9, and 15 October 1992) because these days showed a large variation in offshore wave height. The offshore wave conditions during these days were:

- 3 October
 $H_{s, \text{offshore}}$ = 0.1 - 1.0 m
 $T_{s, \text{offshore}}$ = 3.0 - 6.7 s
water level = -0.8 - +0.6 m
- 9 October
 $H_{s, \text{offshore}}$ = 1.2 - 2.1 m
 $T_{s, \text{offshore}}$ = 7 - 10 s
water level = -0.9 - +1.0 m
- 15 October
 $H_{s, \text{offshore}}$ = 1.7 - 3.6 m
 $T_{s, \text{offshore}}$ = 7 - 8.5 s
water level = -0.4 - +1.3 m

Very low offshore wave heights ($H_{s, \text{offshore}} < 0.5$ m) tend to flatten the inner nearshore bar because on both sides of the crest a small accumulation of sediment is predicted while the crest loses sediment (not shown). During moderate weather conditions ($H_{s, \text{offshore}} = 0.5 - 1.5$ m) the relative wave height increases towards the shore, resulting in a total suspended sediment transport which increases up to the inter-tidal bar (Fig. 5.36). The total suspended sediment transport around the inner nearshore bar (between $x=925$ and 1040 m) is always onshore directed which means that sediment transport gradients in this onshore transport must have caused the observed changes. Figure 5.36d shows that these gradients, calculated over a cross-shore distance of 5 m, result in a loss of sediment at the seaward side of the crest of the inner bar while an (small) increase in sediment volume is expected on the landward side of this bar, i.e. sediment transport gradients tend to increase the height of the bar while the bar's crest is to migrate onshore.

The computations of 9 (Fig. 5.37) and 15 (not shown) October show a remarkable consistency in the distribution of the total suspended sediment transport in the inner nearshore for higher offshore wave heights ($H_{s, \text{offshore}} > 1.5$ m). Wave heights between 1.5 and 2 m result in a distribution that shows an onshore directed sediment transport at the seaward and an offshore sediment transport at the landward side of the inner nearshore bar (between $x=925$ and $x=1050$; Fig. 5.37). For storm waves ($H_{s, \text{offshore}} > 2$ m), the net sediment transport direction over the bar is always offshore. The predicted sediment transport distribution suggests that the height of the inner nearshore bar will increase and the trough will be eroded (e.g. Fig. 5.37d). Such developments were indeed observed between 9 and 10 October 1992 and between 15 and 16 October, although the developments of 15-16 October were less pronounced. The location to

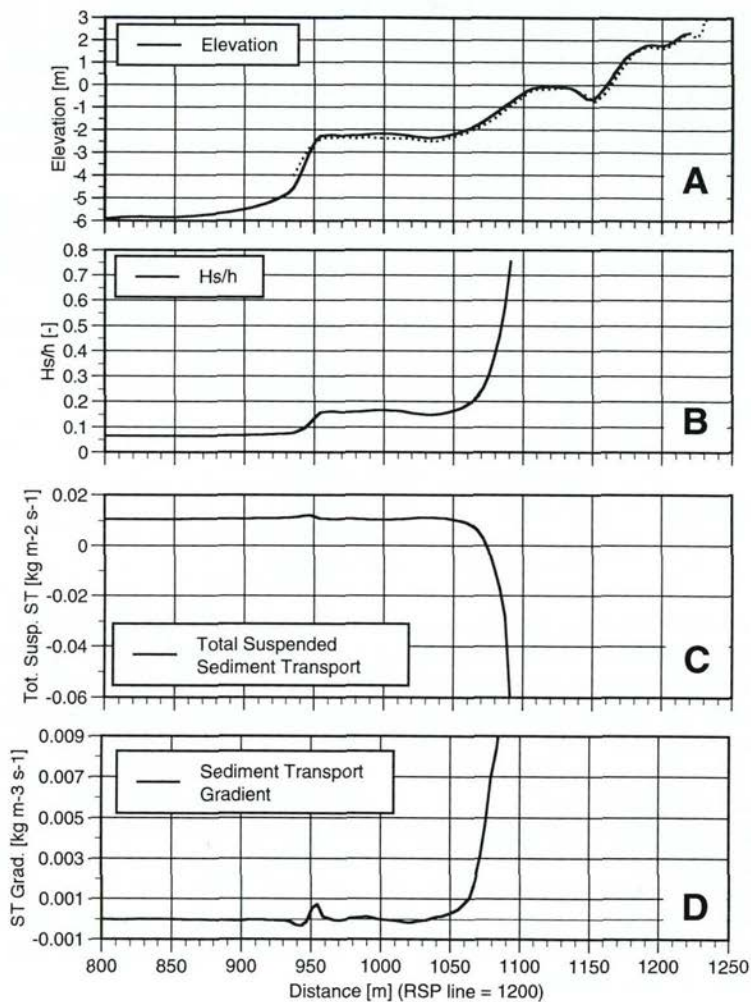


Figure 5.36 Measured nearshore profiles and calculated hydrodynamics and sediment transport on 3 October 1992 (1900h). Positive transport is onshore directed, negative transport is offshore directed.

(A) measured cross-shore profile (3 Oct. = full line, 4 Oct = dashed line)

(B) computed relative wave height (H_s/h)

(C) estimated total suspended sediment transport

(D) sediment transport gradient (+ = sedimentation, - = erosion)

$H_{s, \text{ offshore}}$ = 0.4 m

water level = -0.55 m NAP

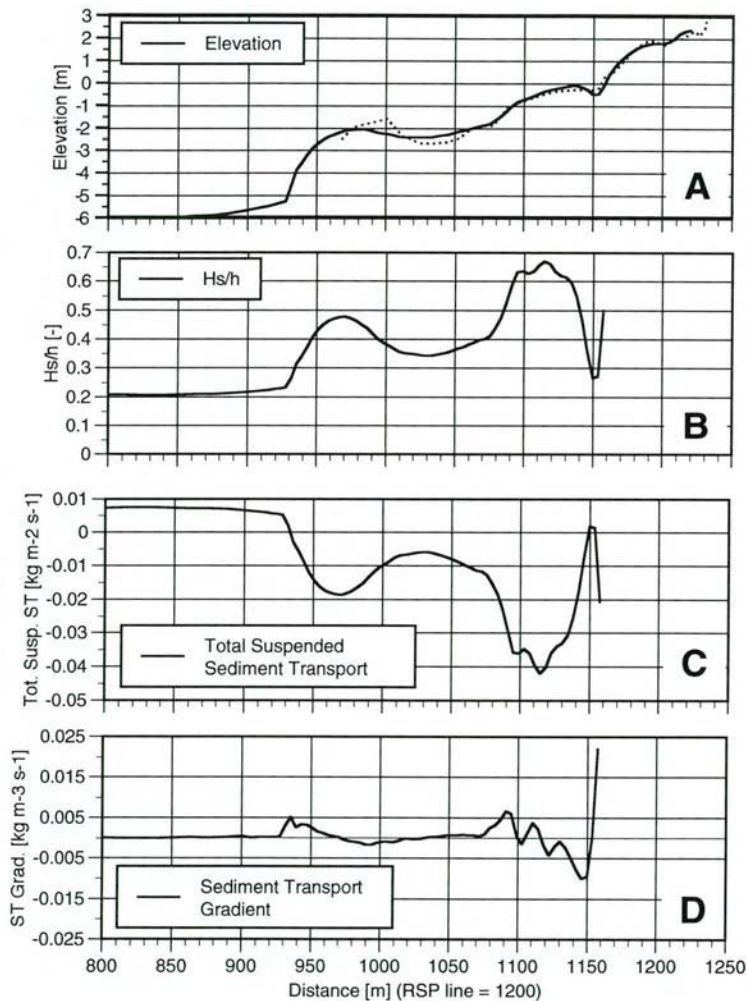


Figure 5.37 Measured nearshore profiles and calculated hydrodynamics and sediment transport on 9 October 1992 (0100h). Positive transport is onshore directed, negative transport is offshore directed.

(A) measured cross-shore profile (9 Oct. = full line, 10 Oct = dashed line)

(B) computed relative wave height (H_s/h)

(C) estimated total suspended sediment transport

(D) sediment transport gradient (+ = sedimentation, - = erosion)

$H_{s, \text{ offshore}} = 1.55 \text{ m}$

water level = +1.38 m NAP

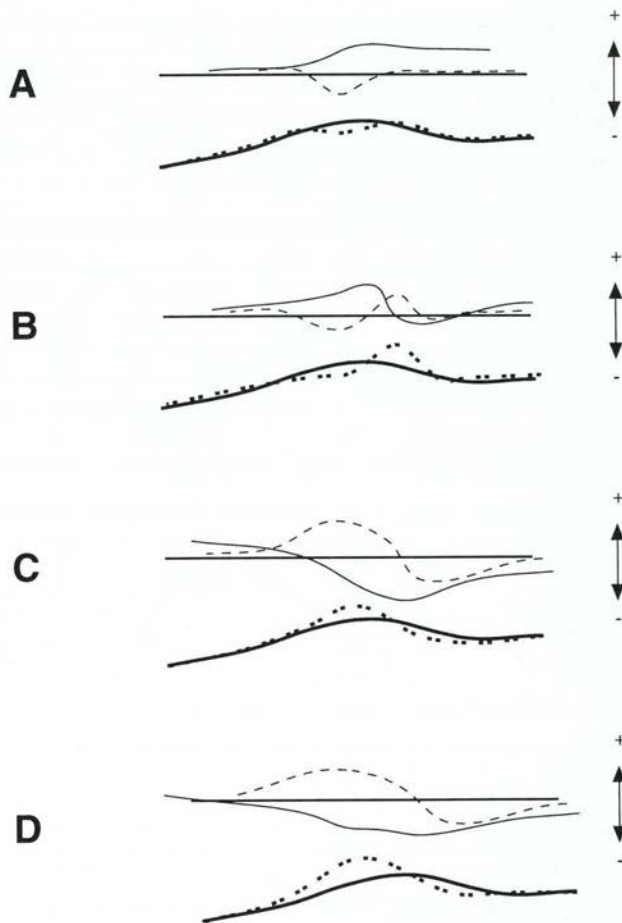


Figure 5.38 Sediment transport, sediment transport gradients at the inner nearshore bar during four different offshore wave height ranges. Plus means onshore sediment transport or gain of sediment; minus means offshore sediment transport or loss of sediment.

Legend:

- = sediment transport
- - - - = sediment transport gradient
- = initial morphology
- - - - = morphologic development

- (A) $H_{s, \text{offshore}} < 0.5 \text{ m}$
- (B) $H_{s, \text{offshore}} \sim 0.5 - 1.5 \text{ m}$
- (C) $H_{s, \text{offshore}} \sim 1.5 - 2 \text{ m}$
- (D) $H_{s, \text{offshore}} > 2 \text{ m}$

which the inner bar's crest will move can, however, not rightfully be predicted for either the 9 or 15 October case. For instance, the observations shows that on 9 October the inner nearshore bar crest will move onshore (Fig. 5.37a) while the predictions suggest that the crest will move offshore as the maximum sediment transport gradients (Fig. 5.37d) occur seawards of the crest of the initial profile (Fig. 5.37a).

In conclusion, the model computations, in combination with the H_s/h relation, suggest that the inner nearshore bar developments are steered by four groups of sediment transport gradients, each present during a particular range of offshore wave heights (see Fig. 5.38):

- $H_{s, \text{offshore}} < 0.5$ m; the local sediment transport gradient first decreases and then increases over the inner nearshore bar suggesting that the bar will be flattened. The local sediment transport gradients are the result of a variation in an onshore sediment transport (Fig. 5.38a).
- $H_{s, \text{offshore}} = \text{ca. } 0.5 - 1.5$ m; From offshore to onshore and over the inner nearshore bar, the local sediment transport gradient first decreases then increases, then decreases and finally increases again. These variations tend to move the crest of the bar onshore. The local sediment transport gradients are the result of a both onshore and offshore sediment transport vectors (Fig. 5.38b).
- $H_{s, \text{offshore}} = \text{ca. } 1.5 - 2$ m; The local sediment transport gradient first increases and then decreases and finally increases again over the inner nearshore bar. These variations may lead to an offshore migration of the bar possibly in combination with an increase in height. The local sediment transport gradients are the result of both onshore and offshore sediment transport vectors (Fig. 5.38c).
- $H_{s, \text{offshore}} > 2$ m; The local sediment transport gradients are the same as during offshore wave heights of 1.5 - 2 m and the bar is also moving offshore and the height of the bar may also increase. The local sediment transport gradients are, however, caused by an offshore sediment transport (Fig. 5.38d).

5.8.5 Conclusions

- inner nearshore bar developments during low offshore wave heights ($H_{s, \text{offshore}} < 0.5$ m) are the results of gradients in onshore sediment transport.
- inner nearshore bar developments during moderate offshore wave heights ($H_{s, \text{offshore}} = \text{ca. } 0.5 - 2$ m) are caused by an onshore sediment transport seaward and an offshore sediment transport landward of the inner nearshore bar.
- High offshore wave heights ($H_{s, \text{offshore}} > 2$ m) lead to gradients in an offshore sediment transport extending over the inner nearshore bar.

5.9 Final discussion and conclusions

The objective of this chapter was to identify the causes, modes, magnitudes and directions of cross-shore sediment transport in the different hydrodynamic zones present in the inner nearshore. To reach this goal, the sediment transport measurements, performed with the BERT in the inner nearshore zone, were analysed. First, the instantaneous and time-averaged sediment concentrations were studied. Second, an analysis was made of the suspended sediment transports in terms of

mean and oscillating transport. Next, the depth-integrated, suspended sediment transport and the bedload transport were examined. Finally, the total sediment transport and sediment transport patterns in the inner nearshore were analysed.

The analysis indicates that the instantaneous sediment concentrations near the bed vary not only on the time scales of the incident wave frequency but also on longer time scales. Consequently, sediment concentration is not simply a function of the instantaneous wave orbital velocity. The measured instantaneous concentration varied between 0.05 kg m^{-3} (background concentration in the non-breaking wave zone) and 40 kg m^{-3} (suspension event in the breaker zone), thereby agreeing with other studies (e.g. Jaffe et al., 1984; Sternberg et al., 1984, 1989; Beach and Sternberg, 1991). The concentration spectra show an increase in spectral density towards the lower frequencies, indicating that the instantaneous concentrations are determined by processes beyond the time scale of an individual wave. The time lag between the variation of the concentration at the lowest (0.07 m above the bed) and the highest OBS (0.26 m above the bed) is less than a second which means that the bed material is rapidly suspended to higher elevations.

The measured time-averaged concentrations increase towards the shore with concentrations varying between 0.01 kg m^{-3} (non-breaking wave zone) and 5 kg m^{-3} (swash zone); a trend also observed by Zampol and Inman (1989) and Kroon (1994). Higher concentrations near the bed are associated with higher concentrations in the upper part of the water column. Moreover, in case of a high concentration near the bed, the steepness of the concentration profile is larger than for lower near bed concentrations; a result also in agreement with other studies (e.g. Van Rijn et al., 1993; Osborne and Greenwood, 1993). The measured time-averaged concentration profiles were generally more uniform than those predicted by the TRANSPOR model (Van Rijn, 1993).

The suspended sediment transport near the bed (0.07 - 0.26 m) was analysed in terms of the oscillating, mean and a net transport. The mean sediment transport was found to dominate the oscillating sediment transport in the cross-shore direction, but the oscillating sediment transport was significant and cannot be ignored. The mean transport is nearly always directed offshore and the highest mean transport is found in the breaker zone. The oscillating sediment transport is predominantly onshore directed and its contribution to the total transport seems to increase with the relative wave height. The ratio low-frequency to high-frequency oscillating sediment transport is about 0.5 with the latter component mainly onshore directed and the former either offshore or onshore directed, in line with the study of Beach and Sternberg (1991).

The longshore sediment transport is almost totally determined by the mean transport. Thus, by measuring the mean suspended load and the mean longshore current a reasonable estimate of the longshore suspended sediment transport can be obtained. This result confirms the conclusions of other investigators e.g. Hanes and Huntley (1986), Sternberg et al. (1989) and Davidson et al., (1993).

Greenwood et al. (1990) and Beach and Sternberg (1991) suggest that the different sediment transport modes vary with elevation above the bed. This study, however, reveals that the transport modes vary only little between 0.26 and 0.12 m above the bed, but that there is a significant increase in the mean cross-shore suspended sediment transport and a decrease in the oscillating suspended sediment transport

between 0.12 and 0.07 m above the bed. These trends are opposite to those found by Huntley and Hanes (1987) and others who observed that oscillating transport is dominant near the bed while mean sediment transport was dominant higher in the water column. Huntley and Hanes's (1987) measurements were, though, performed outside the surf zone which may explain the differences between this study and theirs.

The depth-integrated, time-averaged, suspended sediment transport varies between $+0.03 \text{ kg s}^{-1} \text{ m}^{-1}$ (onshore) and $-0.49 \text{ kg s}^{-1} \text{ m}^{-1}$ (offshore) and is strongly dominated by the mean cross-shore currents ('undertow'). As the undertow is always offshore directed, the offshore depth-integrated, time-averaged, suspended sediment transport is also mainly offshore directed. The depth-integrated, time-averaged, suspended sediment transport increases from the non-breaking to the breaking zone and decreases from the breaking to the swash zone, thus, primarily depends on the distance from the breakpoint (cf. Kana, 1978, in Sternberg et al., 1989). The longshore and cross-shore depth-integrated, suspended sediment transports were correlated and found to be in the same order.

The bedload transport varies between $-3.4 \cdot 10^{-2} \text{ kg s}^{-1} \text{ m}^{-1}$ (offshore) and $+5.0 \cdot 10^{-2} \text{ kg s}^{-1} \text{ m}^{-1}$ (onshore). The direction and the magnitude of the net bedload transport are dominated by mean cross-shore currents ('undertow'), and this transport mode was found to coincide with the direction of wave propagation as long as the undertow did not exceed 0.2 m s^{-1} . Quick (1983, in Van Rijn et al., 1993) also found onshore transport as long as the undertow was less than 0.2 m s^{-1} .

The total sediment transport, i.e. the total of the net depth-integrated, time-averaged, suspended sediment transport and the net bedload transport, increases from the non-breaking to the breaking zone but decreases from the breaking to the swash zone while changing direction from off- to onshore. The ratio between suspended load and bedload transport varies largely over the measured series, but the majority showed that the suspended load rate dominates over the bedload rate. The ratio of suspended load to bedload is hard to estimate. In case of a large undertow, the TRANSPOR model (Van Rijn, 1993) predicts the magnitude of the total sediment transport ($> 0.2 \text{ m s}^{-1}$) fairly well.

The analysis of the sediment transport directions in the inner nearshore zone showed that around a breakpoint located at the inter-tidal bar, the offshore sediment transport increases towards the breaker zone and this pattern may lead to an accumulation of sediment seaward of the breaker zone. At the same time and in the landward direction, the decrease of the offshore directed total sediment transport and an eventual onshore directed total transport will lead to a divergence of sediment transport landward of the breaking zone. Note, however, that this analysis was based on measurements performed at the inter-tidal bar and that, for instance, the water depth at the landward side of the inner nearshore bar increases while at the landward side of the inter-tidal bar the water depth monotonically decreases towards the shoreline. Thus not all results regarding the net sediment transport direction may be directly extrapolated to the inner nearshore bar.

Analysis of the total suspended sediment transport directions at the seaward and landward side of the inner nearshore zone indicated that during periods with high relative wave heights ($H_{s, \text{ offshore}} > 2 \text{ m}$, i.e. storms) inner nearshore development was determined by gradients in the offshore directed sediment transport. During non-storm

periods ($H_{s, offshore} 0.5 - 2 \text{ m}$), an onshore sediment transport at the seaward side of the inner nearshore zone and an offshore directed sediment transport at the landward side of this zone lead to an convergence of sediment. During very low waves ($H_{s, offshore} < 0.5 \text{ m}$), sediment accumulation in the inner nearshore zone may be the result of gradients in the onshore sediment transport.

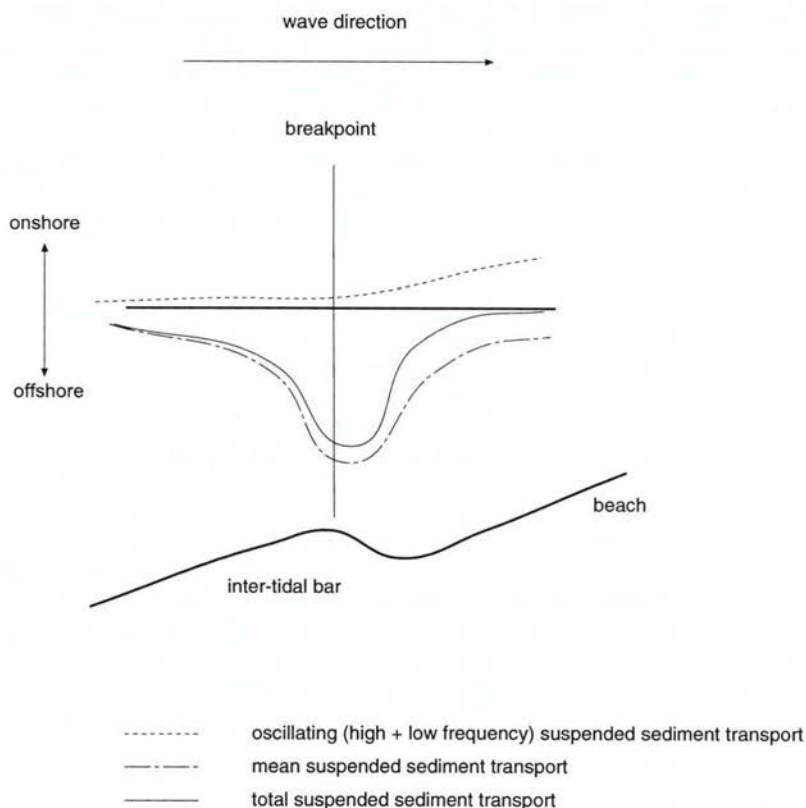


Figure 5.39 Spatial distribution of suspended sediment transport modes around a breakpoint, based on measurements at 0.17 m above the bed.

In all, the analysis of the sediment transport, measured at the inter-tidal bar under offshore wave height vaying from 0.5 to 2 m, has lead to the following answers to the research questions stated in the introduction of this chapter:

- Suspended sediment transport dominates over the bedload transport with a estimated factor of 10, although the ratio suspended load to bedload varied largely. The time-averaged (mean) suspended sediment transport slightly dominates the oscillating suspended sediment transport while the ratio high-frequency to low-frequency oscillating suspended sediment transport is about 0.5

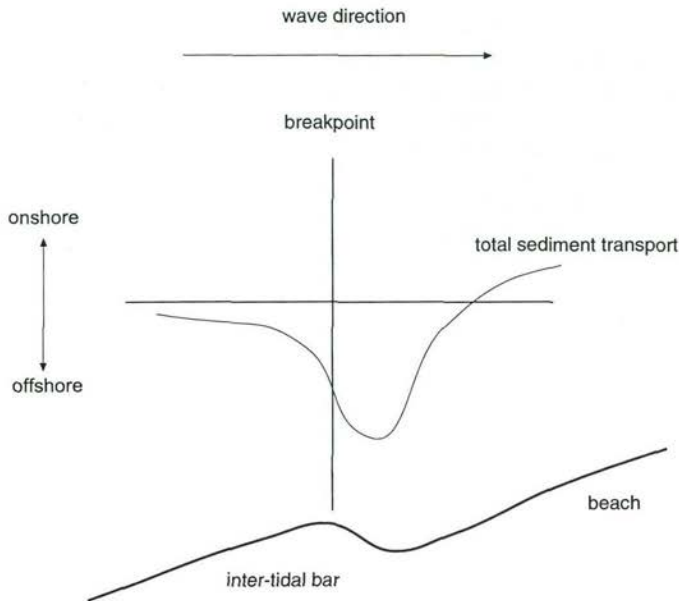


Figure 5.40 Spatial distribution around a breakpoint of the total sediment transport, i.e. the sum of the depth-integrated, time-averaged suspended sediment transport and bedload transport.

- The offshore directed total suspended sediment transport near the bed increases towards the breakpoint (Fig. 5.39) but decreases from the breaking zone to the swash zone. The mean suspended sediment transport shows the same trends while the onshore directed oscillating suspended sediment transport continuously increases from the non-breaking zone to the swash zone (Fig. 5.39). The mostly onshore directed high-frequency oscillating suspended sediment transport also increases towards the shore. The mostly offshore directed low-frequency oscillating suspended sediment transport and the bedload transport shows no relation with the hydrodynamic zones.
- The total sediment transport, i.e. the sum of the depth-integrated, time-averaged suspended sediment transport and the bedload transport varied between $0.08 \text{ kg m}^{-2} \text{ s}^{-1}$ (onshore) to $-0.48 \text{ kg m}^{-2} \text{ s}^{-1}$ (offshore). The total sediment transport increases towards the breakpoint but decreases from the breaking zone to the swash zone and eventually changes its direction from offshore to onshore (Fig. 5.40). Note that the oscillating suspended sediment transport is omitted in this 'total' sediment transport.
- During very low offshore wave heights ($H_{s, \text{offshore}} < 0.5 \text{ m}$), sediment diverges at the inner nearshore bar. Higher offshore wave heights, between 0.5 and 2 m, result in an offshore sediment transport at the beach and an onshore sediment transport at the seaward side of the inner nearshore bar leading to sediment convergence in the inner nearshore zone. Wave heights larger than 2 m lead to an overall offshore sediment transport in the inner nearshore zone. Gradients in this offshore transport lead to sediment convergence at the inner nearshore bar.

The bars in the inner nearshore zone are locations where the fluid and sediment dynamics change rapidly due to a nearby breaker zone. Such changes are essential in understanding beach and bar dynamics. This chapter and the previous chapter have analysed the hydrodynamics and sediment dynamics around a breaker zone which is located near an inter-tidal bar. This thesis concerns the processes steering the development of the inner nearshore bar. Therefore, in the next chapter the morphological developments of the inner nearshore bar will be studied and related to the high-frequency wave related hydrodynamics and sediment transport processes.

6. MORPHOLOGICAL DEVELOPMENTS AND MORPHODYNAMIC MODEL COMPUTATIONS

6.1 Introduction

The aim of the study described in this thesis is to understand the relation between the inner nearshore bar developments and the hydrodynamics and sediment transports associated with the shoaling and breaking of high-frequency waves. The hydrodynamics and sediment transport were studied in the previous two chapters. This chapter concentrates on inner nearshore bar developments on the medium scale. Experiments performed at Egmond (Kroon, 1994), at other field sites (e.g. Larson and Kraus, 1992; Lippmann et al, 1993) and in laboratories (e.g. Sunamura and Takeda, 1993) give no uniform clues regarding inner nearshore bar developments in response to varying hydrodynamic conditions. It is, therefore, necessary to address the next research questions (see also Chapter 2):

- how does the inner nearshore bar respond to daily changes in the shoaling and breaking of high-frequency waves over the bar, i.e. to non-storm and storm periods?
- how does the response of the inner nearshore bar to non-storm and storm periods depend on the antecedent cross-shore profile configuration?

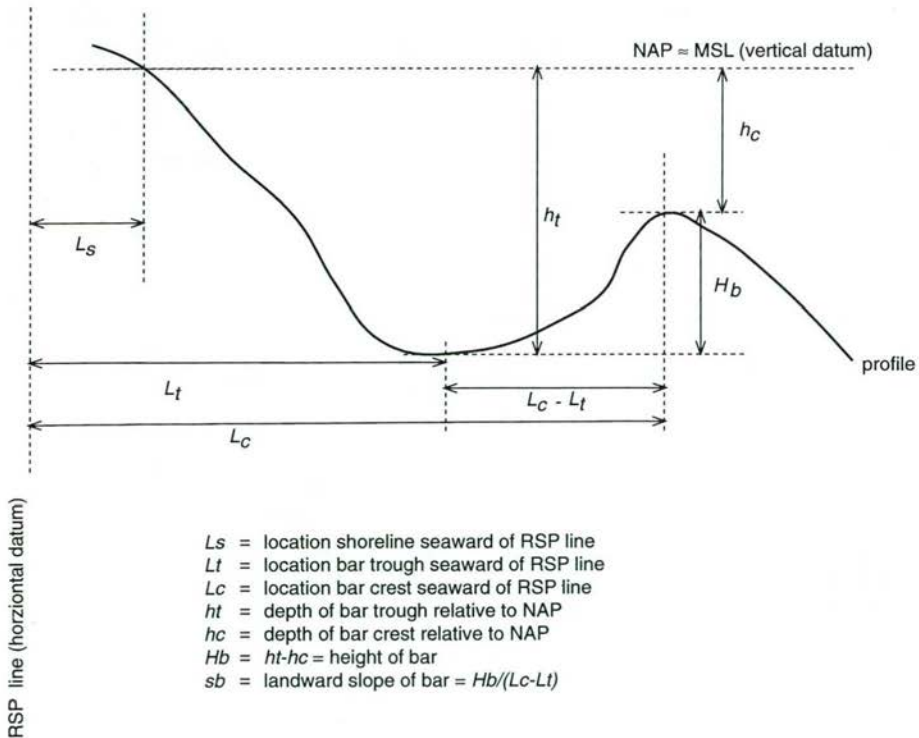


Figure 6.1 Definition sketch of morphometric bar properties

The analysis is concentrated on the response of a cross-shore profile in the centre of the field area (line 39.500). Other cross-shore profiles on both sides of this location were also surveyed, but on a less regular basis. The latter profiles have been used to study the longshore homogeneity in morphological response. The data were obtained during the 1991 and 1992 field experiments. In 1991, the morphological response following a single storm was documented while in 1992 the effect of a sequence of storms on the nearshore profile was measured. The movement of the bars is described in terms of the changes in elevation and migration of the bar's crest and trough. It is assumed that the behaviour of these variables represents the behaviour of the entire bar (cf. Birkemeier, 1985). The crest and trough are defined as the position at which the slope changes from seaward to landward (crest) and from landward to seaward (trough). The shoreline is defined as the intersection between the profile and the NAP ordnance level, i.e. the 0 m contour line. Other definitions are depicted in Figure 6.1. All elevations are relative to Dutch Ordnance Datum (NAP) and all distances are relative to a reference line, the so-called RSP reference line which consists of a series of beach poles that follow the coastline (Fig. 3.1) and are numbered according to their distance to Den Helder.

The previous chapter studied the sediment transport patterns in order to reveal regions with either a convergence or divergence of sediment. In order to compare the sediment transports associated with the inner nearshore bar developments in a quantitative manner, this chapter also evaluates a coastal profile model. To see if the model rightfully predicts the observed hydrodynamics, sediment transports and morphologic developments, model computations are compared with field observations.

6.2 Offshore wave conditions and initial cross-shore profiles

6.2.1 Single storm event (1991 data set)

The 1991 data set includes a single storm event. A storm is designated as a period in which the significant offshore wave height reaches values of more than 2 m. The 1991 period can be characterised by the data in Table 6.1 (see also Fig. 6.2).

Table 6.1 Offshore wave characteristics in 1991

Period	Date (1991)	$H_{s, \text{offshore}}$ [m]	$T_{s, \text{offshore}}$ [s]	Wave direction [deg]	Water level variation relative to NAP [m]
pre-storm	10 - 16 Oct.	0.25 - 1	4 - 12	250 - 350	-1 / +1
storm event	16 - 20 Oct.	2 - 5	4 - 12	250 - 330	-0.5 / +1.5
post-storm	20 - 25 Oct.	ca. 1	ca. 6	ca. 340	-1 / +1
fair weather	25 Oct. - 1 Nov.	0.25 - 1.5	3 - 8	220 - 320	-1.25 / +0.75

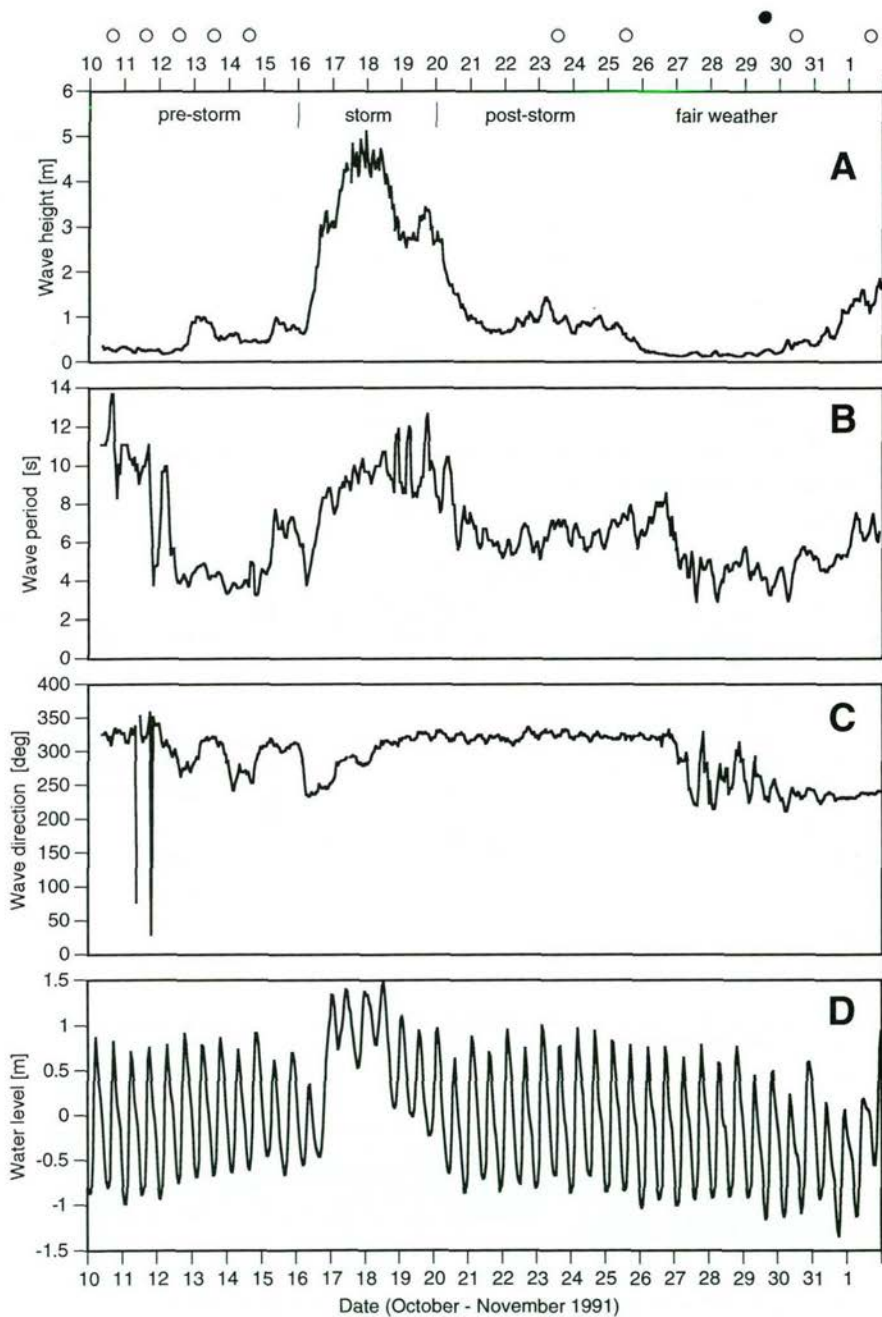


Figure 6.2 Offshore hydrodynamics and morphologic surveys in 1991. The dots above the graphs indicate the data of the surveys. Black dots refer to outer nearshore echo soundings; white dots are inner nearshore SAP surveys.

(A) wave height
 (B) wave period
 (C) wave direction
 (D) water level

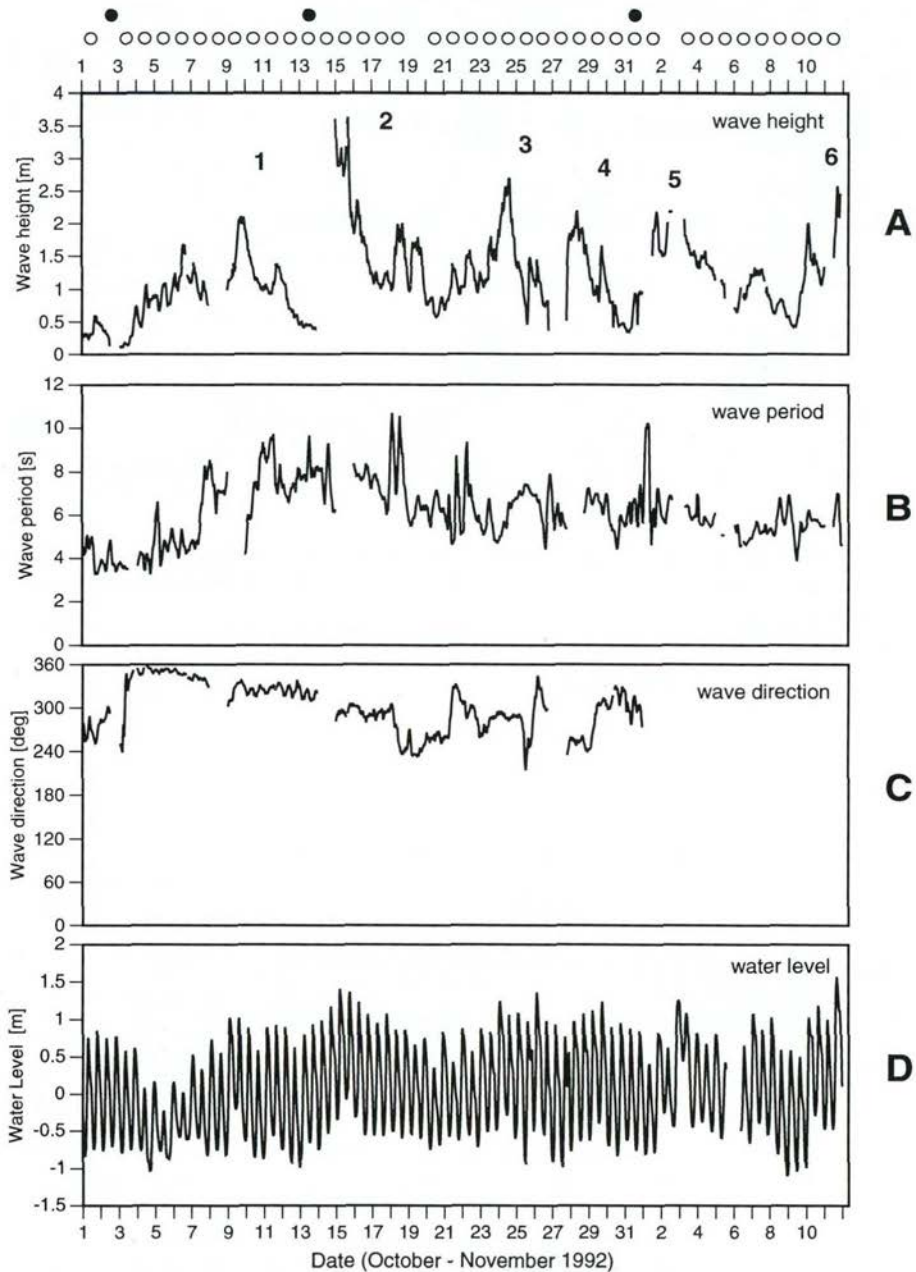


Figure 6.3 Offshore hydrodynamics and morphologic surveys in 1992. The numbers in the upper panel refer to storms. The dots above the graph indicate the date of the surveys. Black dots refer to outer nearshore echo soundings; white dots are inner nearshore SAP surveys.

Some remarks regarding these characteristics are:

- The wave period may vary considerably over hours, due partly to the low sampling frequency (1.28 Hz) and the short burst duration (20 min.)
- The wave height measured during the peak of the storm was extreme as it occurs less than 0.5% of the time along the Dutch coast (Roskam, 1988).
- The water level shown is the mean of the water level measured at IJmuiden and Petten (see Fig. 3.1), because of the malfunctioning of instruments at the field site.

6.2.2 Sequence of storms (1992 data set)

The period considered ranges from 1 October to 10 November 1992. The Wave buoy recorded the offshore wave height almost continuously during the period 1 October - 1 November but malfunctioned thereafter. The offshore wave height in the period 2 - 10 November, therefore, has been derived from the capacitance wire of the outer nearshore pole (pole 3, Fig. 3.7b). The entire study period showed moderate to high offshore wave conditions (Fig. 6.3) and six storms were observed. The characteristics of these storms are summarised in Table 6.2.

Table 6.2 Storm characteristics in 1992

Storm No.	Date	H _s , offshore	T _s , offshore	Wave direction	Water level variation relative to NAP	Storm duration
		[m]	[s]	[°]	[m]	[hours]
1	9 Oct.	2	6-8	340	-0.25/+1	2
2	14-15 Oct.	2-3.5	8	270-300	-0.5/+1.5	42*
3	24 Oct.	2-2.75	7-8	280-290	-0.5/+1.25	15
4	28 Oct.	2-2.25	6-7	240-250	-0.5/+1	3
5	2-3 Nov.	2-2.5*	6	x	-0.5/+1.25	20*
6	11 Nov.	2-2.5	6-7	x	-0.5/+1.5	>12

* estimated

x not measured

6.2.3 Initial profile characteristics 1991-1992

Figure 6.4 shows the cross-shore profiles at the start of the measurements in 1991 and 1992. The initial morphology of 1991 and 1992 differed considerably because of the yearly net offshore migration of the bars (see Section 3.2, Wijnberg and Wolf, 1994; Wijnberg, 1995). In 1991 and 1992, the profile was characterised by three bars: an outer nearshore bar, an inner nearshore bar and a swash bar or an inter-tidal bar. A swash bar is defined here as a bar that is formed and modified by swash-backwash processes, an inter-tidal bar as one that is formed and modified by swash-backwash processes (low tide) and breaking wave processes (high tide). This means that the crest of a swash bar is nearly always above Mean Sea Level (MSL) while the inter-tidal bar's crest is mostly below MSL. The inter-tidal bar had a much larger volume than the former swash bar.

The characteristics of the bars in 1991 and 1992 are presented in Table 6.3.

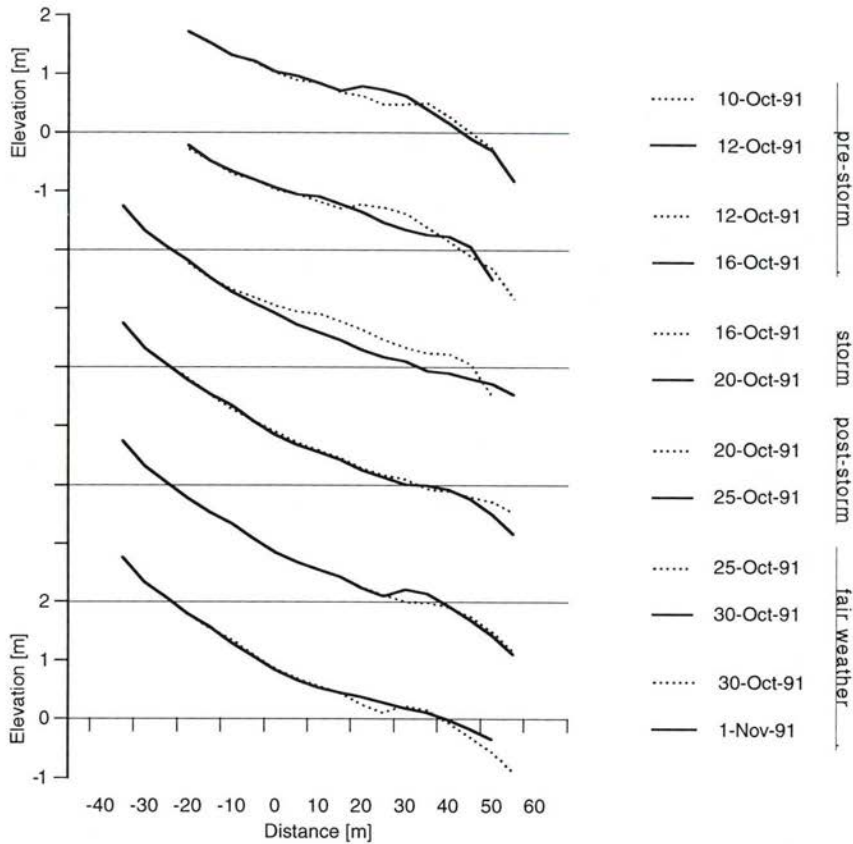


Figure 6.5 Beach profile response of profile 39.500 in 1991.

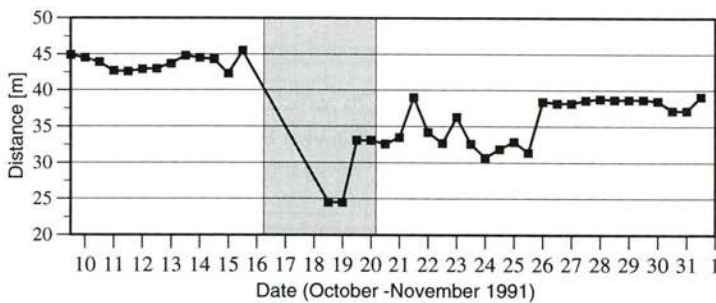


Figure 6.6 Position shoreline in 1991 (profile 39.500). Shaded area indicates storm.

From monitoring the beach in 1991 it is evident that the swash bar is eroded during a storm and built up again during the post-storm period. This sequence is accompanied by a retreat of the shoreline and a loss of beach sediments whereby the shoreline position moves towards its pre-storm position in the post-storm period. However, 12

days after the storm, the shoreline was still landward of its pre-storm position and the volumetric losses caused by the storm were still present. Thus, the net effect of the storm is a lowering of the beach profile although its shape is maintained.

The correlation between two different swash bar properties (Fig. 6.1) and between a swash bar property and the position of the shoreline was investigated for the 1991 data set. It was found that the location of the crest of this swash bar is well correlated with its elevation ($r^2 = 0.85$) and that the elevation increases when the crest of the swash bar moves in an onshore direction; an identical result to that found by Kroon (1994). No other significant correlations were found.

6.3.2 Response to a sequence of storms (1992)

The beach and shoreline response to the 1992 storms is (see also Figs. 6.7 and 6.8):

- Storm 1 (9 October):
 - berm : minimal erosion
 - shoreline : seaward shift 10 m
 - inter-tidal bar : remains present
 - volumes : net changes over entire profile (-50/+75 m) are small ($< 0.5 \text{ m}^3 \text{ m}^{-2}$)
- Storm 2 (14-15 October):
 - berm : completely eroded
 - shoreline : small landward shift (5 m)
 - inter-tidal bar : regains asymmetric shape
 - volumes : beach (-50/+25 m) lost $18 \text{ m}^3 \text{ m}^{-1}$ while inter-tidal bar region gained $3 \text{ m}^3 \text{ m}^{-1}$
- Storm 3 (24 October):
 - berm : has vanished
 - shoreline : large seaward shift of 30 m
 - inter-tidal bar : transformed into a low-tide terrace (LTT)
 - volumes : upper beach volume remained the same while entire profile gained $8 \text{ m}^3 \text{ m}^{-1}$
- Storm 4 (28 October):
 - berm : no longer present
 - shoreline : no changes
 - inter-tidal bar : old LTT was eroded and new inter-tidal bar emerged
 - volumes : no changes

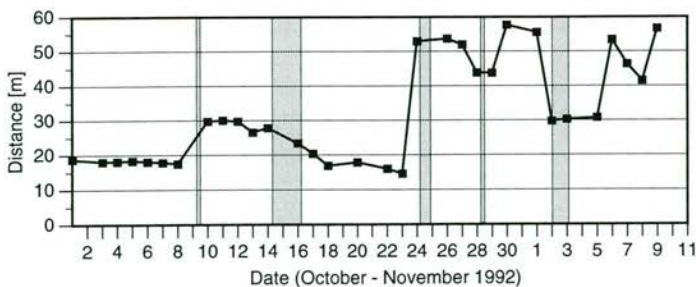


Figure 6.7 Location of the shoreline at 39.500 profile in 1992. Shaded areas indicate storms.

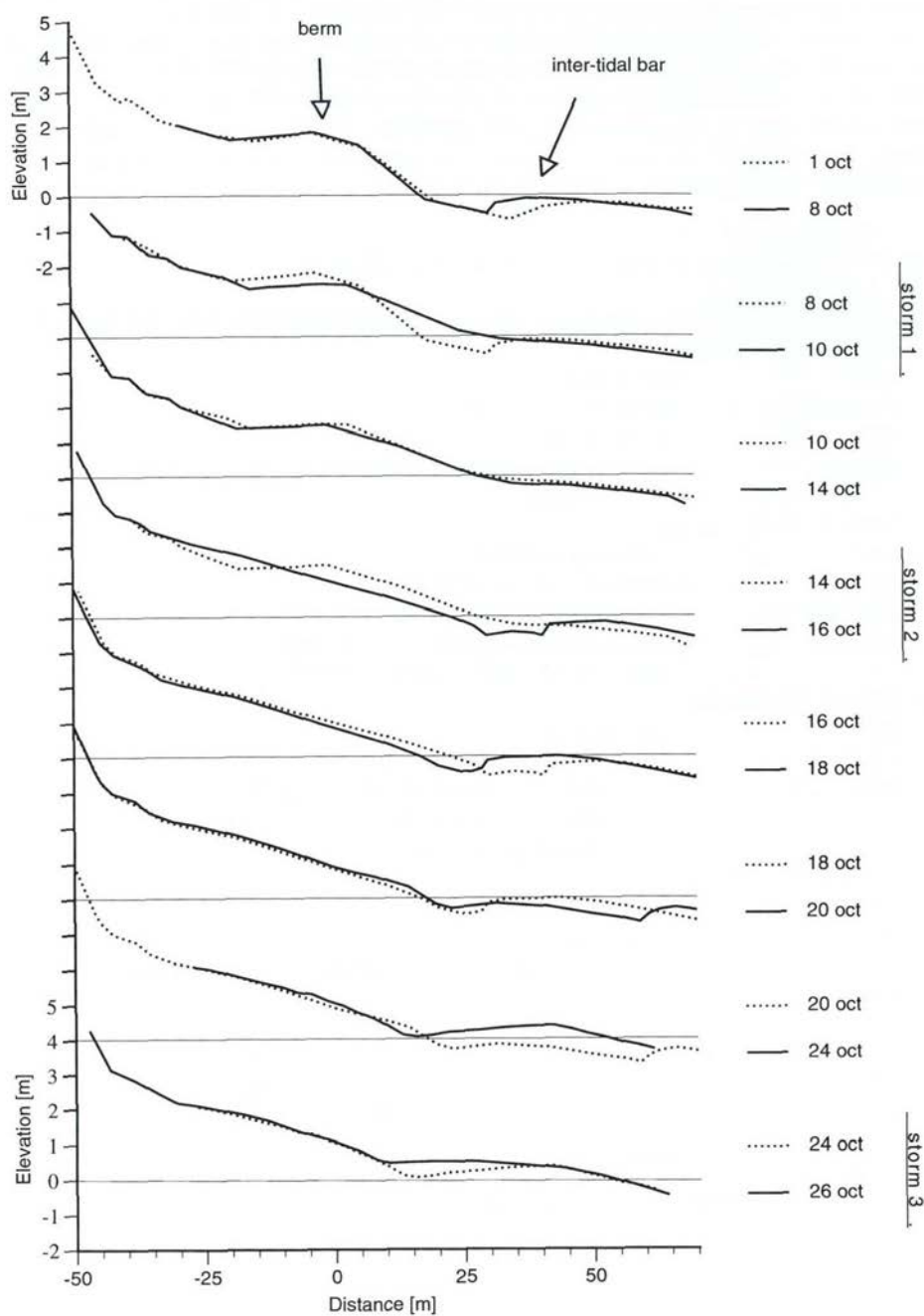


Figure 6.8 Beach profile response at profile 39.500 in 1992.

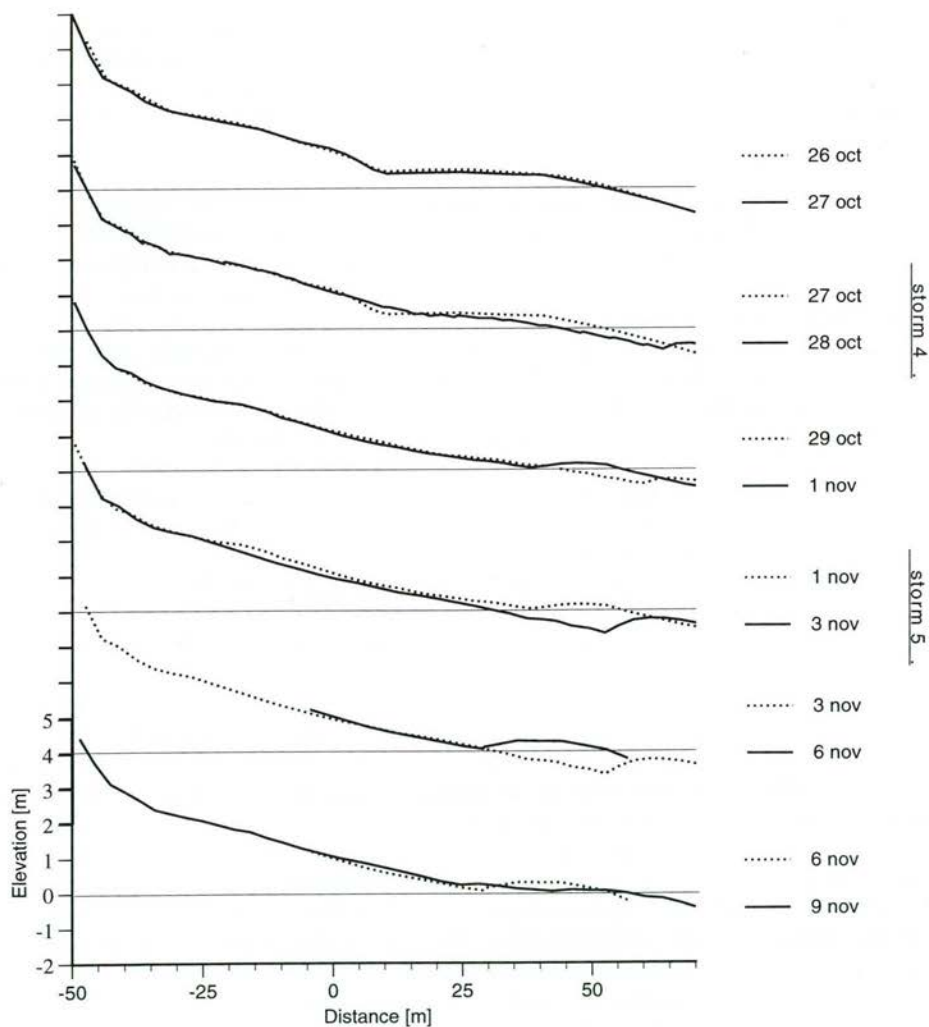


Figure 6.8 Beach profile response at profile 39.500 in 1992.
(continued)

- Storm 5 (2-3 November):
 berm: no longer present
 shoreline: large landward shift of 20 m
 inter-tidal bar: eroded but a new inter-tidal bar emerges soon after the storm
 volumes: large losses of sediment over entire profile: $21 \text{ m}^3\text{m}^{-1}$

No beach profiles were surveyed during and after the sixth storm so the impact of this event cannot be analysed. In the periods between the storms the shoreline was relatively stable compared to the storm developments (Fig. 6.7). The onshore migration of the inter-tidal bar took place mostly during the non-storm periods (e.g. 1-8 October, 3-6 November; Fig. 6.8) during which it either became welded to the shore or was transformed into a low-tide terrace (20-24 October). The volumetric changes over the entire profile were insignificant during the non-storm periods, giving an integrated result for the period 1 October - 10 November of a volumetric loss of about $15 \text{ m}^3\text{m}^{-1}$ over the entire profile.

In conclusion, the beach and shoreline developments do not show a uniform response to every storm. The presence of a berm in the beginning of the observation period had a definite influence on the shoreline and inter-tidal response. The inter-tidal bar behaves somewhat like a swash bar with onshore migration, an increase in volume during non-storm periods and partial erosion during storm periods. Recovery is often fast as, within 24 hours after the storm, a gain of sediment in the inter-tidal zone is visible (e.g. 3 November; Fig. 6.8). The volumetric losses of the beach are often more than the gain in the inter-tidal zone, which suggests that the sediment is deposited either further offshore than the inter-tidal bar or carried alongshore.

The correlation between two different inter-tidal bar properties and between a property and the position of the shoreline was analysed for the 1992 data set. In this case, significant linear correlations were found between:

- elevation of the trough and crest of the inter-tidal bar ($r^2=0.71$)
- location of the trough and crest of the inter-tidal bar ($r^2=0.70$)
- location the shoreline and the elevation of the trough of the inter-tidal bar ($r^2=0.89$)

A feature clearly visible in most of the scatter plots is the clustering of data into two groups. Additional analysis proved that these groups represented two particular situations, namely an inter-tidal bar at a certain distance from the shoreline and a welded inter-tidal bar, defined as welded from the day that its crest is above the NAP level. This definition is related to the definition of the shoreline, i.e. that it is the intersection of the SAP profile and the NAP level. When the crest of the inter-tidal bar is below NAP level it is situated seaward of the shoreline and when above, landward of the shoreline, i.e. the inter-tidal bar is then part of the beach. Examination of the correlation for both situations separately dramatically changes its strength. Hence, it became clear that the relations between different morphometric properties of the inter-tidal bar strongly depend on the position of the bar itself. In particular, the relation between the trough and crest position of the inter-tidal bar shows two trends (Fig. 6.9). When the inter-tidal bar is at some distance from the coastline (non-welded), the location of the crest may vary over 30 m, although there is hardly any change in the position of the trough. When the inter-tidal bar is welded to the coast, the crest and

trough location are linearly related. When the trough of the welded inter-tidal bar, which shows some resemblance to a runnel, moves farther onshore, the crest also moves onshore. The welded inter-tidal bar thus moves as a more or less coherent body, i.e. like a swash bar.

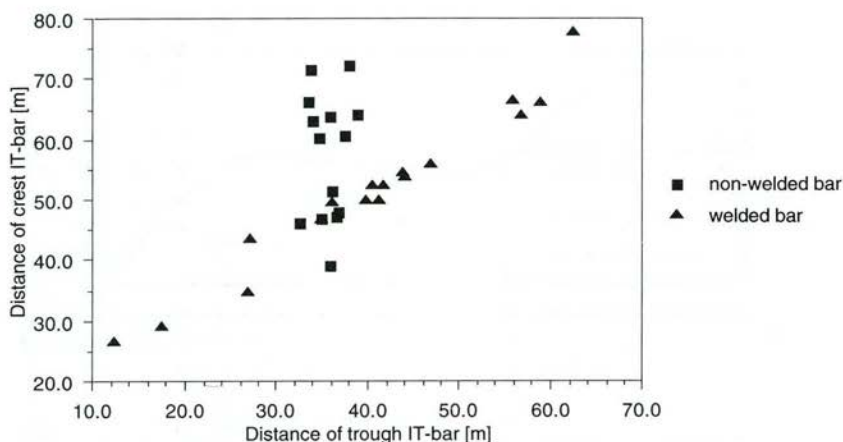


Figure 6.9 Relation between location of the crest and of the trough of the inter-tidal bar (IT-bar) (1992 data)

Only little correlation was found to be present between the offshore hydrodynamics and the different morphometric inter-tidal bar properties, which is somewhat surprising as the relaxation and reaction times are assumed to diminish when going from offshore to the shoreline (cf. Kroon, 1994).

Hence, it is probably not simply the magnitude of the hydrodynamics that is important but possibly more the chronological position of a event in a sequence of hydrodynamic events that is of higher importance.

6.4 Cross-shore morphological response of the inner nearshore bar

6.4.1 Response to a single storm (1991)

The response of the inner nearshore bar was monitored along a single cross-shore profile, located 50 m north of the instrumented transection, which was located in the centre of the field area (Fig. 3.10), coinciding with cross-shore profile 39.500. Due to the presence of the instrumented poles, a morphological monitoring of the inner nearshore bar was not possible along the instrumented transection itself. The cross-shore profile measurements were performed with the SAP (see Section 3.7). This profile will further be referred to as the 'SAP profile'.

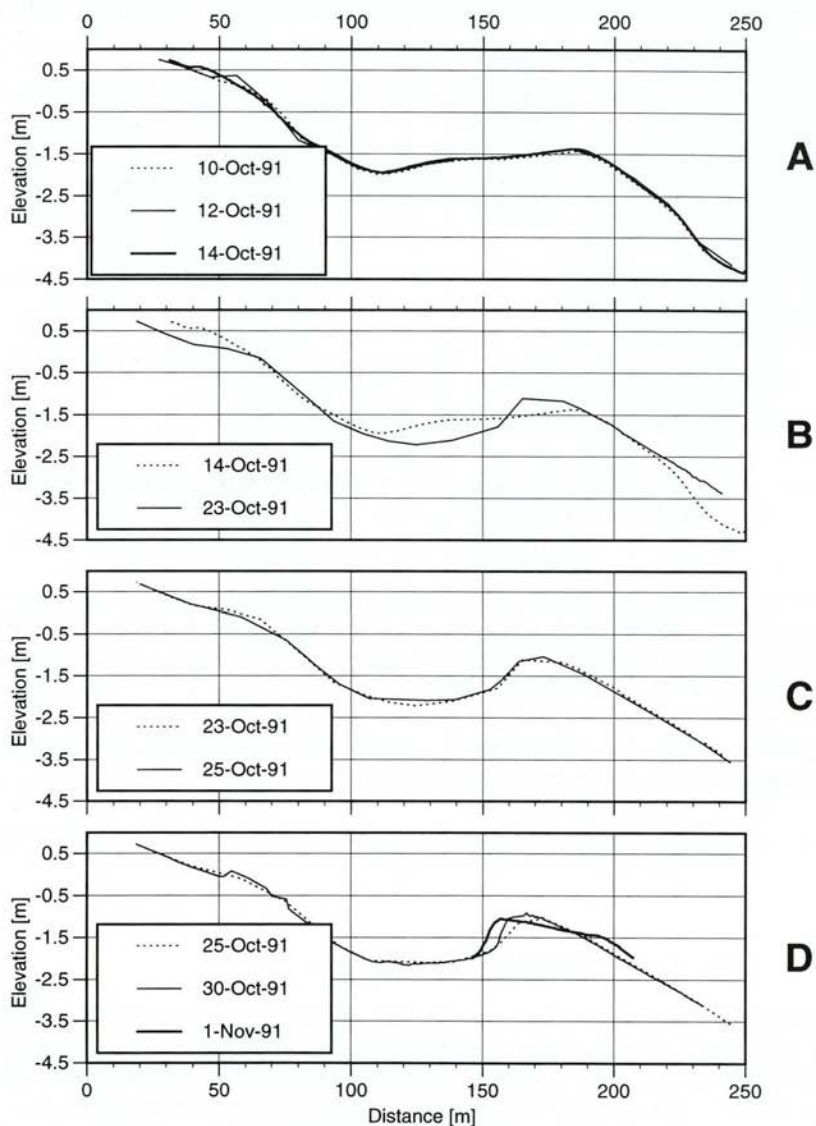


Figure 6.10 Morphologic response of the inner nearshore zone (SAP profile) in 1991. Storm occurred on 14-15 October.

The development of the inner nearshore bar can be described as follows:

- Pre-storm (10-14 October):
The SAP profile was monitored four times in the pre-storm period (Fig. 6.2). The sub-tidal part of the profile below -1 m showed hardly any changes (Fig. 6.10a) and the daily volume changes in the pre-storm period were also insignificant.
- Pre-storm - storm - post-storm (14-23 October):
During this period other measurements were required and there were difficulties with the tow-cable of the SAP, so the SAP profile could not be surveyed until 23 October. As this period also covered parts of the pre- and post-storm periods, the profile present on 23 October was not just the result of the single storm. This post-storm profile showed the development of a pronounced inner nearshore bar with a steep slip face (Fig. 6.10b), due to both an increase in the height of the bar and a deepening of the trough on its landward side. The crest of the inner nearshore bar migrated about 20 m in a landward direction and the beach elevation was reduced by 0.2 m. During the period 14-23 October, the volume of the beach was reduced by about $8 \text{ m}^3\text{m}^{-1}$, while the entire SAP profile lost about 15 m^3 per unit width (m^{-1}).
- Post-storm (23-25 October):
There were no significant changes at the inner nearshore bar and the beach had only lost a small amount of sediment (Fig. 6.10c).
- Fair weather (25 October - 1 November):
During the fair weather period, the inner nearshore bar moved onshore (Fig. 6.10c/d), its crest migrating about 8 m between 25-30 October ($1.6 \text{ m}\cdot\text{day}^{-1}$) and 10 m between 30 October - 1 November ($5 \text{ m}\cdot\text{day}^{-1}$). The onshore movement between 25 October and 1 November took place without any net volume changes for the entire SAP profile.

It is interesting to note that the inner nearshore bar moved onshore in the fair weather period while the wave height was about equal to the pre-storm period. However, during that period the bar's properties did not change. Thus it seems that the storm lead to a further elevation of the crest and as a result the sediment was thereafter also moved during lower wave conditions.

In conclusion, the single storm monitored during 1991 resulted in a net change in the properties of the inner nearshore bar due to both changes that occurred during the storm and during the post-storm period. Table 6.4, based on nine SAP profiles, summarises the inner nearshore bar properties during the period 10 October-1 November 1991.

The correlation analysis for the 1991 profiles reveals a high correlation coefficient (> 0.6) for various combinations of two bar properties. However, the results are influenced by the small number of SAP profiles involved; only eight profiles were surveyed. Besides, the data are clustered into two groups, resulting from the inactivity of the inner nearshore bar during the first SAP surveys, and this also contributes to the high correlation coefficient (Fig. 6.11). The correlation analysis reveals two trends. First the elevation of the crest of the inner nearshore bar increases when the bar moves onshore ($r^2=0.93$). Second, the steepness of the landward slope of the inner nearshore bar increases when the bar migrates onshore ($r^2=0.78$). These trends were also found by Houwing (1991) and Kroon (1994) for the Egmond field site.

Table 6.4 Descriptive statistics of the inner nearshore bar 1991

	Mean	Standard deviation	Minimum	Maximum	Range	Net
Location inner trough [m]	117.09	6.99	110.20	128.80	18.60	11.7
Elevation inner trough [m]	- 2.04	0.10	- 2.21	- 1.95	0.26	0.17
Location crest inner bar [m]	176.73	11.05	156.80	187.50	30.70	-
Elevation crest inner bar [m]	- 1.24	0.19	- 1.43	- 0.96	0.47	29.6
Height inner bar [m]	0.78	0.28	0.55	1.20	0.65	0.63
Landward slope inner bar [°]	0.70	0.64	0.43	1.56	1.94	0.77
Migration speed inner bar*	- 1.67	5.18	- 12.40	4.30	16.70	1.42
Onshore migr. speed*	- 3.63	4.37	- 12.40	- 0.80	11.60	-
Offshore migr. Speed*	4.20	0.14	4.10	4.30	0.20	-

* = in [m.day⁻¹]

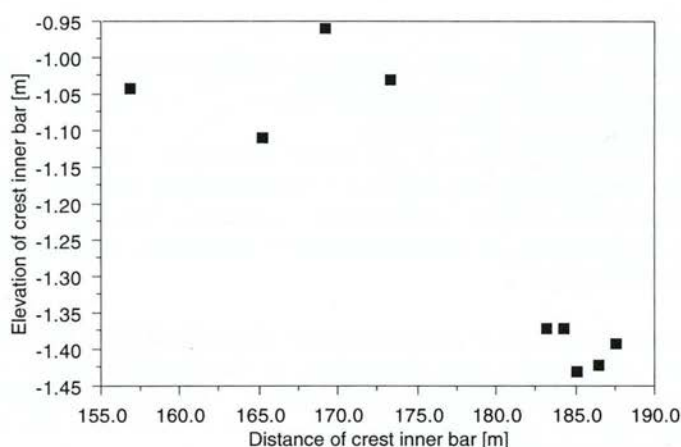


Figure 6.11 Relation between location and the elevation of the crest of the inner nearshore bar in 1991.

6.4.2 Response to a sequence of storms (1992)

The monitoring of the inner nearshore bar in 1992 was performed at the SAP profile of 1991 and was surveyed nearly every day between 1 October and 11 November with the exception of 19 October and 2 November when surveying was impossible due to mechanical difficulties. The profile of 2 October showed significant measurement errors that could not be corrected. Apart from these three days, profiles are available for the remainder of the period. From 1-14 October, the position was determined with the Elta total station (Section 3.7) so these profiles are based on discrete points, with a cross-shore spacing of 10 m. The remainder of the profiles were surveyed with the self-tracking Polartrack. They are more or less continuous but are smoothed using a moving average filter.

The response of the inner nearshore bar to the different storms can be characterised as follows (see also Figures 6.12 and 6.13).

- Storm 1 (9 October)
 - location crest : onshore migration (5 m)
 - elevation crest : increases with 0.5 m
 - height : increases from 0.3 to 1.1 m
 - volume (150-250 m): gain of $12 \text{ m}^3\text{m}^{-1}$
 - bar becomes more asymmetric with steeper landward slope
- Storm 2 (14-15 October)
 - location crest : offshore migration (10 m)
 - elevation crest : decreases with 0.4 m
 - height : decreases from 1 to 0.5 m
 - volume (150-250 m): loss of $10 \text{ m}^3\text{m}^{-1}$
 - all major changes take place in the first part of the storm
- Storm 3 (24 October)
 - location crest : offshore migration of a few metres
 - elevation crest : small increase
 - height : no changes
 - volume (150-250 m): gain of $10 \text{ m}^3\text{m}^{-1}$
- Storm 4 (28 October)
 - location crest : onshore migration of 15 m
 - elevation crest : increases 0.3 m
 - height : almost no change
 - volume (150-250 m): no changes
 - bar becomes more asymmetric with steeper landward slope
- Storm 5 (2-3 November)
 - location crest : offshore migration 35 m
 - elevation crest : decreases with 0.7 m
 - height : decreases from 0.8 to 0.6 m
 - volume (150-250 m): no changes
 - the shape of the bar dramatically changes, flattening of bar (Fig. 6.12).

Between the storms the inner nearshore bar mostly migrated onshore though its shape either remained asymmetric or changed gradually from symmetric to asymmetric. The elevation of the crest shows irregular behaviour with no specific trends. The onshore moving inner nearshore bar could bring about significant volumetric changes in the most seaward part of the profile (150-250 m).

Table 6.5 summarises the inner nearshore bar morphometrics.

In conclusion, the inner nearshore bar does not respond uniformly to each individual storm. The crest of the bar mostly moves offshore during storms but there are few changes in its elevation. The second storm indicates that there is a rapid (<24 h) morphological adjustment to large storms. During non-storm periods, the inner nearshore bar gradually moves onshore. Hence, the development of the inner nearshore bar on a medium time-scale is characterised by a gradual onshore moving crest interrupted by offshore migrations during storms. The offshore migration is faster than that in an onshore direction (Table 6.3) and days with offshore migration occur less frequently than those where the movement is onshore.

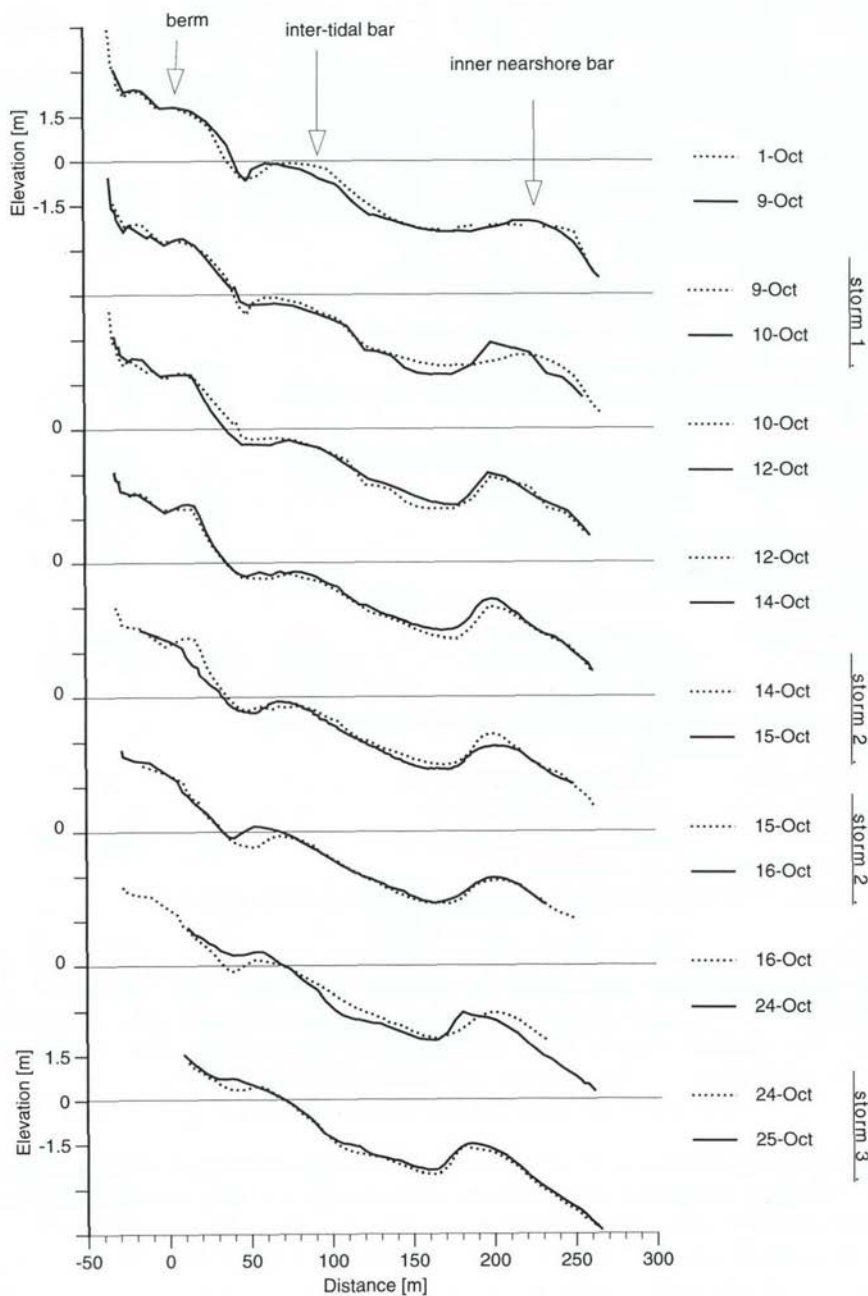


Figure 6.12 Morphological response of the inner nearshore zone (SAP profile) in 1992.

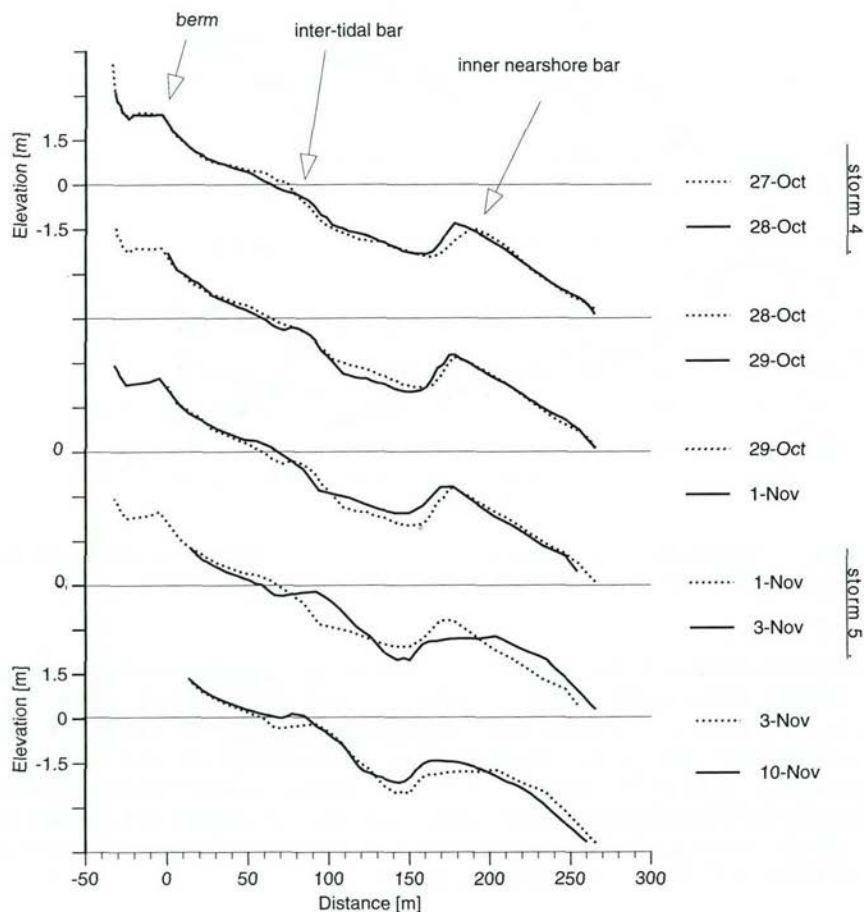


Figure 6.12 Morphological response of the inner nearshore zone (SAP profile) in 1992.
(continued)

Table 6.5 Descriptive statistics of the inner nearshore bar 1992

	Mean	Standard deviation	Minimum	Maximum	Range	Net
Location inner trough [m]	159.85	10.37	142.50	174.50	32.00	26.30
Elevation inner trough [m]	- 2.37	0.16	- 2.70	- 2.00	0.70	0.27
Location crest inner bar [m]	180.99	23.34	147.80	230.40	82.60	-
Elevation crest inner bar [m]	- 1.56	0.36	- 2.34	- 1.12	1.22	69.90
Height inner bar [m]	0.81	0.32	0.08	1.18	1.10	0.99
Slope inner bar [°]	1.77	1.02	0.06	4.36	4.30	-
Migration speed inner [m.day ⁻¹]	- 2.33	6.73	- 17.30	17.00	34.30	-
Onshore migr. speed [m.day ⁻¹]	- 4.99	4.49	- 17.30	- 0.20	17.10	-
Offshore migr. speed [m.day ⁻¹]	7.15	5.31	1.70	17.00	15.30	-

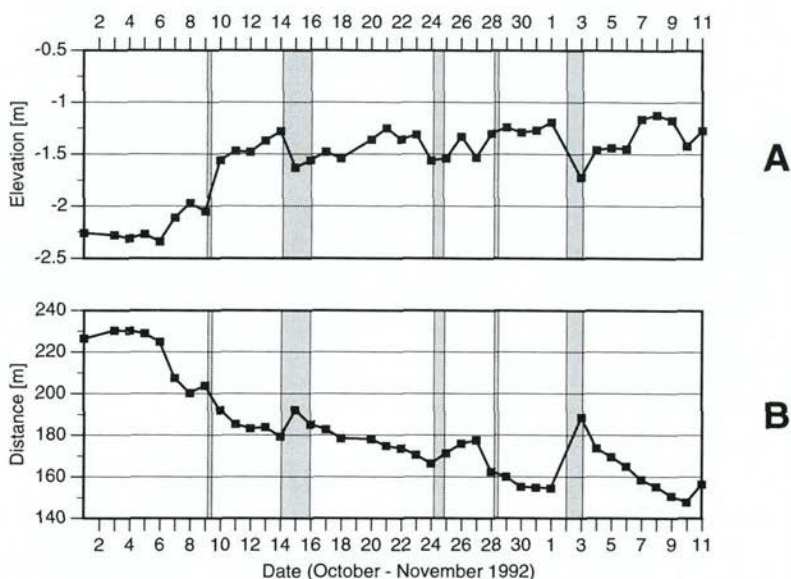


Figure 6.13 The elevation and location of the crest of the inner nearshore bar at SAP profile as a function of time (1992 data)

The correlation analysis of the 1992 data also shows high correlation between those bar properties that showed a high correlation for the 1991 dataset. Again, the elevation of the crest and the steepness of the landward slope of the inner nearshore bar increase when the distance between the inner nearshore bar and the shore decreases (Figs. 6.14, 6.15). However, analysis of other bar properties result in low ($r^2 < 0.5$) correlation coefficients. Kroon (1994) found relations between the location of the trough and the crest and between the height of the bar and the location of the crest but these relations were not confirmed by this study.

It is interesting to see that in both 1991 and 1992 several bar properties show a distinct temporal trend. The temporal development of the inner nearshore bar (Fig. 6.13) shows that there is a trend over weeks: the bar moves onshore. Yet, the correlation coefficients for any combination of offshore wave property (wave height, -period and -direction) and inner nearshore bar property (Fig. 6.1) for both the 1991 and the 1992 data sets are small (r^2 about 0.1-0.5). Thus, it seems that this trend is not related to daily averaged offshore wave characteristics but only requires a varying offshore wave climate.

The individual storms only determine the inner nearshore bar's development for a small number of days (<5). The long term trend (weeks) is not governed by individual storms, because during storm events the inner nearshore bar often shows a development opposite to that shown in the longer term. However, the storms may, in addition to the longer term development, induce a post-storm onshore movement which would not be present without the storms. For instance, it seems that from 30 October to 1 November there was no onshore movement. The fifth storm (2 November) induced, after an offshore movement, an onshore movement that went beyond the location reached on 30 October (Fig. 6.13). The latter storms also resulted

in larger offshore displacement of the crest than in the previous storms although at the same time, the onshore migration speed remained the same. This seems to indicate that, eventually, the onshore migration between two storms will be smaller than the offshore displacement during the first of the two storms, i.e. the net migration direction over weeks will be offshore.

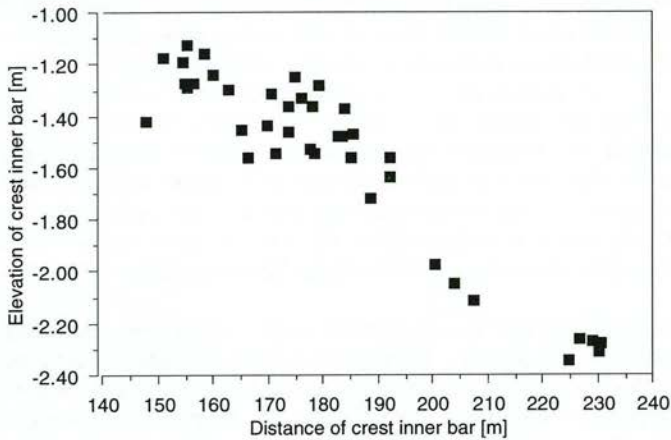


Figure 6.14 Relation between location and the elevation of the crest of the inner nearshore bar in 1992.

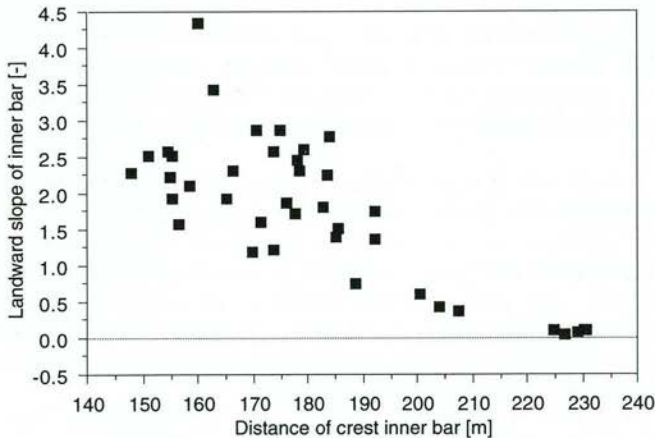


Figure 6.15 Relation between the location and the landward slope of the inner nearshore bar in 1992.

To gain an understanding of why there is no correlation between the offshore wave conditions and the inner nearshore bar morphology, some additional calculations were made. The offshore wave properties were calculated between 12.00 h of the previous day and 12.00 h on the day the SAP profile was surveyed. The wave properties were averaged over 24 hours because the inner nearshore profile was surveyed once a day. It is assumed that the bar properties are determined only by the wave conditions

preceding the survey. Results of previous studies (e.g. Birkemeier, 1984; Larson and Kraus, 1992) have clearly demonstrated that the reaction and response times for nearshore breaker bars are small when wave height is increasing. They found reaction and response times in the order of hours. Figure 6.12 shows that also at the Egmond field site, the reaction and response times during increasing wave heights are small. For instance, during the second storm of 1992 the inner nearshore bar was adjusted to higher wave conditions even before the peak of the storm. This means that the surveyed cross-shore profile is only partially determined by the offshore averaged wave conditions during the previous 24 hours and also depends on the wave conditions of earlier days ('beach memory'). Moreover, in using 24-hour averaged values, it is assumed that the offshore hydrodynamics does not vary much in 24 hours, i.e. that the averaged value is a good representation. The fast reactions and response times during erosional events, and the varying offshore wave conditions within 24 hours are a possible reason for the low correlations between observed offshore wave conditions and inner nearshore bar morphology.

In the preceding paragraph it was assumed that, under storm conditions, it is only the hydrodynamics in the 24-hour time span before the survey that determines the response of the bar. It might, though, be the case that, during periods of lower waves ('accretional state'), the profile is still (partially) adjusted to higher wave conditions and therefore not yet in equilibrium with present wave conditions. Thus, the initial shape and location of the bar itself, which is the integrated result of the preceding hydrodynamics over longer time scales before the survey, may also influence its further development (Lippmann and Holman, 1990). With this in mind, an additional correlation analysis was performed on the 1992 data in which the bar properties itself were taken into account by examining the correlation between the offshore wave characteristics (height, period, direction) and the *changes* in the bar properties. Unfortunately, analyses of relations between change in bar properties and offshore wave characteristics do not lead to significant results ($r^2 < 0.45$).

The above analysis shows that the relation between the offshore wave conditions and the inner nearshore bar developments is of a qualitative nature. It is not possible to quantify this relation, i.e. to define a parameter, incorporating offshore wave conditions and profile configurations, and parameter boundaries during which the inner nearshore bar moves either onshore or offshore. Sediment transport calculations (Section 5.9) seem to indicate that the inner nearshore bar generally moves offshore when the offshore wave heights are higher than 1.5 m but this could not be verified by the present morphological data.

6.5 Cross-shore morphological response of the outer nearshore bar

6.5.1 Response to a single storm (1991)

The outer nearshore zone was only surveyed on two occasions, 13 September and 29 October. It is thus impossible to determine the response of the outer nearshore zone to the single storm. However, to get an idea of the magnitude of the response of the outer nearshore zone, the integrated changes due to three storms occurring during

the period 13 September to 29 October are considered. It is assumed here that the observed changes were caused by the storms and that the calm weather periods had no influence on the morphology of the outer nearshore bar.

The integrated effect of the three storms was to increase the height of the landward slope of the outer nearshore bar by about 0.4 m (Fig. 6.16). Any changes in the elevation of the seaward slope of the crest of the outer nearshore bar, and also farther offshore, were insignificant. The crest of the bar increased 0.3 m and shifted over 10 m in a landward direction and the trough in front, i.e. on the landward side, was eroded and became wider and deeper. The maximum vertical change, observed at the landward side of the trough, was about 0.7 m.

There were no significant net volumetric changes of the entire outer nearshore profile although, within it, significant changes did occur. The trough (200-400 m) lost about $70 \text{ m}^3 \text{m}^{-1}$ while the landward slope of the bar (400-500 m) gained about $30 \text{ m}^3 \text{m}^{-1}$. This implies that there was a significant ($\sim 40 \text{ m}^3$) net longshore transport gradient during the one-and-a-half months, as the inner nearshore did not increase in volume (Section 6.4).

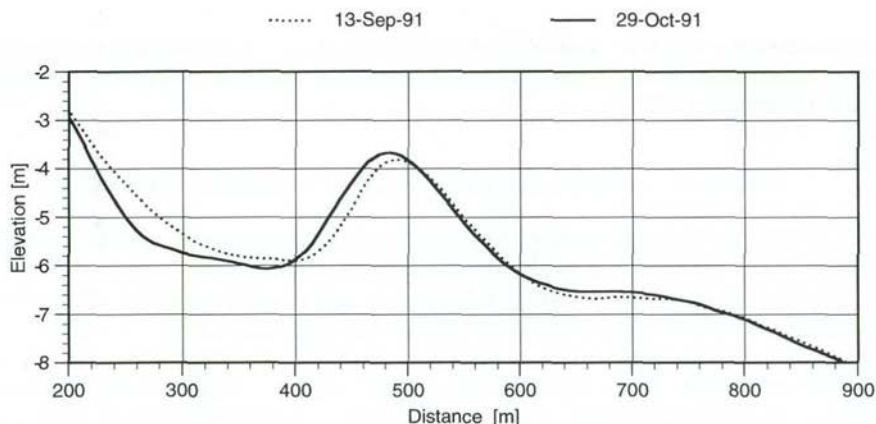


Figure 6.16 Outer nearshore zone development in 1991 (profile 39.500).

6.5.2 Response to a sequence of storms (1992)

Due to the rather rough weather, only three echo-sounding surveys were carried out during the field period. The outer nearshore zone was surveyed on 2, 13 and 31 October. However, due to the temporal spacing of these surveys, it is hard to relate these results to individual storms. The results (Fig. 6.17) show that there was no significant change in the position and elevation of the outer nearshore bar between 2 and 13 October but between 13 and 31 October, the crest of the outer nearshore bar became higher and moved onshore and the landward slope of the outer nearshore bar became steeper. There were no significant changes in the remainder of the profile.

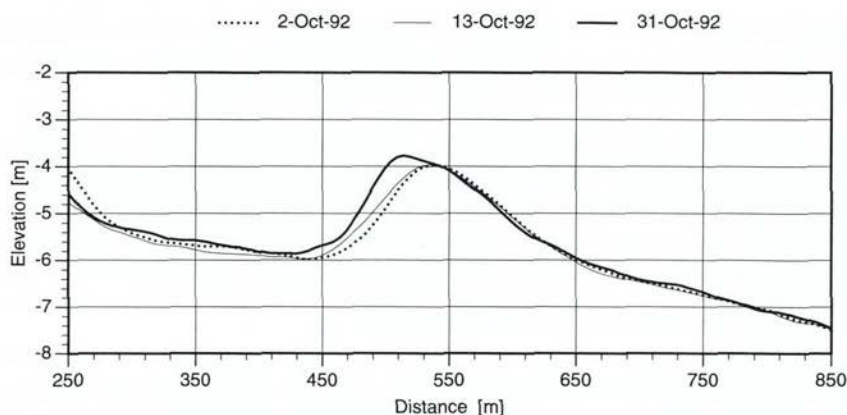


Figure 6.17 Outer nearshore zone development in 1992 (profile 39.500).

The net volumetric changes between 300 and 900 m and between either 2-13 or 13-31 October were insignificant.

It is concluded that the 1991 and 1992 storms had a small but significant influence on the outer nearshore bar. The storm(s) resulted in an onshore migrating bar that increased slightly in height.

6.6 Longshore variability of beach and outer nearshore response

The longshore variability in morphologic response to offshore wave conditions was examined to evaluate to what extent the 39.500 profile represents the morphological response of the entire field area. Moreover, it was studied to what extent the morphological characteristics of a certain profile are related to its own development. Unfortunately for this study, it was not possible to survey the longshore variability of the inner nearshore zone because the rough weather made wading surveys impossible. In addition, the water depth over the inner nearshore bar was so small that it was unfeasible to include the inner nearshore bar in the echo soundings. Only the longshore variability of the beach and the outer nearshore zone was evaluated, and then only for the 1992 data set as it is more complete than that for 1991.

First, the longshore variability of the beach was examined, based on the most comprehensive data set, namely that for shoreline variation. Figure 6.18 shows the shoreline variation at the profiles, which can be divided in two areas. The four profiles 39.000 to 39.417 show a large, though not simultaneous, displacement of the shoreline after which its position fluctuates around a new equilibrium. In contrast, no large displacement of the shoreline was shown in the profiles 39.583 to 40.000, where the fluctuation took place around a single equilibrium, the magnitude of which varied alongshore. The 39.500 profile is positioned in the transition zone between the two areas and the shoreline response at this profile is thus neither indicative for either of the two groups individually but is more regarded as being the average for the entire fieldsite.

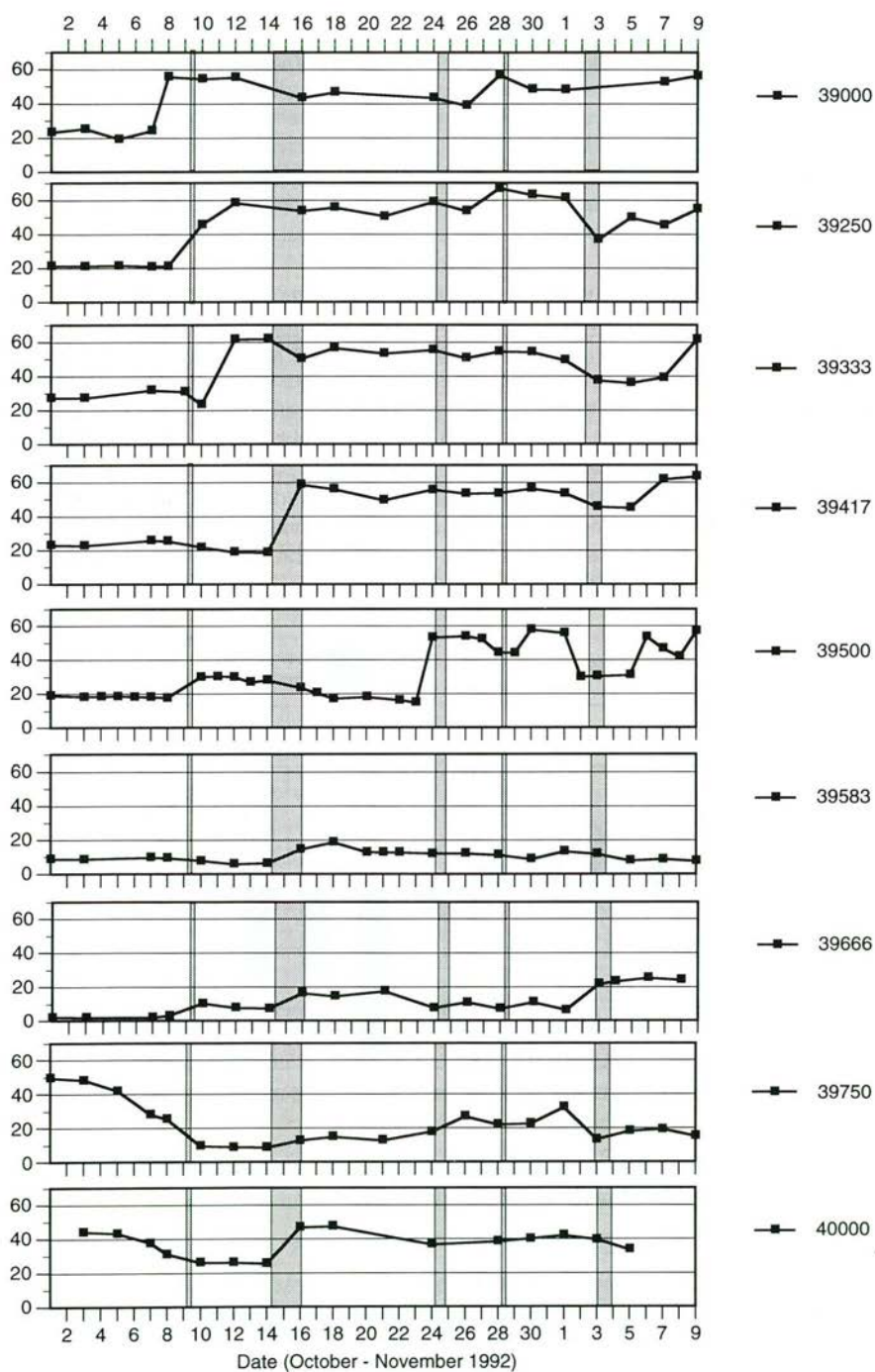


Figure 6.18 Variation in response of the shoreline along the field site in 1992. Vertical axis: location of shoreline in metres distance to RSP line.

which, as it varies along the field site, may partly explain the observed variances in volumetric changes. However, beach width, which largely determines beach volume, is not related to volumetric changes. Another factor affecting the results is that the transition area between the upper beach and the dunes (above +3 m NAP) is rarely included in the profile comparison, because this area was not surveyed on either days. A small amount of dune erosion ($< 2 \text{ m}^3\text{m}^{-1}$) was observed during the second and fourth storm. Hence, sediment eroded from the dunes and deposited on the beach may only have had a minor effect on the net changes.

Thus, despite an uniform chronology in the alongshore morphological development, there are large net volumetric changes of the beach alongshore. This means that volumetric changes are not representative of morphological developments and vice versa. The presence of an inter-tidal bar near the shoreline makes the latter invaluable as an indicator of erosion-accretion events. The 39.500 beach profile may, therefore, only be regarded as representative for the entire field area in a morphological sense and not in an volumetric sense.

Although there were significant morphometric changes, i.e. changes above the accuracy level of the soundings, in the crest position of the outer nearshore bar, these changes were rather small. The changes in elevation of the crest varied between about 0.2 and 0.5 m, which is slightly above the measuring accuracy (0.2 m), and showed an opposite migration direction (Fig 6.20) in the northern part of the study area (profiles 39.000 and 39.250) to that in the south, and a higher crest. The largest changes occurred between 13 and 31 October. In the southern part of study area (profiles 39.750 and 40.000), the crest migrated in an offshore direction (Fig. 6.20). The volumetric changes in the outer nearshore zone are not significant. Thus, although the outer nearshore bar did not behave uniformly along the coast, the observed changes were small.

In conclusion, the beach and outer nearshore bar development along the field site cannot be regarded as purely two dimensional. Three dimensional developments may be expected and the observed morphological developments may not be regarded as representative for the entire field site.

6.7 Conclusions morphological behaviour nearshore zone

The response of bars in the nearshore zone to a single storm and a sequence of storms was analysed. This analyses has lead to the following conclusions:

beach response

- beach and shoreline do not respond identically to every storm; a berm present on the upper beach affects the response of the beach and foreshore to the first few autumn storms.
- the inter-tidal bar largely determines the shoreline developments. This inter-tidal bar shows a swash bar-like behaviour when welded to the shore.
- beach recovery, i.e. the development of a new swash bar or of an inter-tidal bar takes place quickly (~days) after the peak of the storm.
- the beach response along the field site shows an identical chronology, although the development shows a time lag.

inner nearshore response

- the general response of the inner nearshore bar on a medium time scale to a sequence of storms and non-storm periods is to migrate gradually onshore during the non-storm periods interrupted by a (fast) offshore migration during storms. The integrated result is an onshore moving inner nearshore bar.
- both the non-storm and storm behaviour are more related to the position and shape of the inner nearshore bar than on the offshore wave conditions.
- the response of the inner nearshore bar to storms is rapid (relaxation time ~ 1 day).
- the onshore migration of the inner nearshore bar is accompanied by an increase of the crest's elevation while the landward slope of the bar becomes steeper.
- the inner nearshore bar movements take place without significant losses of sediment to the outer nearshore area.

outer nearshore bar response

- storms result in a small migration of the outer nearshore bar, the direction of which varies alongshore.

In all, the general behaviour of bars in the nearshore zone has been documented. Clearly, the outer bar may, on a medium time scale, be regarded as a more or less fixed boundary for the inner nearshore morphologic developments. The inner nearshore bar and the bars near the beach are highly mobile on the medium time scale but the response to non-storm periods is different from that to storm periods. A breaker zone near the inner nearshore bar may lead to convergence and divergence of sediment near the bar but also unidirectional gradients extending over the entire inner nearshore zone may contribute to the accumulation of sediments. In order to give a more definite answer to the research questions stated in the introduction of this chapter, it is necessary to study the morphodynamic processes in the inner nearshore zone in more detail. The morphodynamic processes will be studied by using a physical-mathematical model because detailed measurements are not available.

6.8 Morphodynamic computations in the nearshore zone

6.8.1 Introduction and methods

The feasibility of accurately simulating the above described processes by using a physical-mathematical model UNIBEST-TC (UNiform Beach Sediment Transport-Time dependent Cross-shore) (Reniers, 1993; Bakker, 1995; Delft Hydraulics, 1996) was explored. With this model, it is possible to predict wave propagation to the shore, cross-shore currents, cross-shore sediment transport and cross-shore profile development of alongshore uniform coasts. The application was performed by testing the behaviour and the accuracy of UNIBEST-TC. The 1991 and 1992 Egmond field observations were used as input and for comparison with the model output. The model calculations were divided in a hydrodynamic and morphodynamic part. The first examined the calculation of the root mean square wave height (H_{rms}) and the mean cross-shore currents (undertow) at different locations along the cross-shore profile. A bottom profile and boundary conditions such as an incident wave field, tidal and wind conditions are required to make this calculation. Sediment transport rates and the

resulting bottom changes were then computed using the computed hydrodynamics along the profile. However, the predicted bottom profile changes can only be considered accurate when the hydrodynamic part can be modelled with sufficient accuracy, so it is best to examine the hydrodynamics first. The resulting profile changes were then validated in the morphodynamic part. In order to find ways of improving the accuracy of the predictions, a sensitivity analysis was also performed. Field data from 1991 were used for the hydrodynamic evaluation while for the morphodynamic examination field data of 1992 were used. Thus the validations were carried out using two independent data sets. The UNIBEST-TC model is briefly described in Appendix A.

6.8.2 Model input

bottom profile

The cross-shore bottom profile was obtained by combining the SAP inner nearshore measurements with profiles surveyed by echo-sounding in the outer nearshore. In case of an overlap between both profiles, the SAP profile was used in its entirety in the combined profile; the higher accuracy of the SAP profiles compared with the echo-sounding profiles supports this choice.

offshore hydrodynamic conditions

The model requires an input of offshore wave height, -wave direction, and -wave period. Furthermore, the water level (tide), tidal current and wind speed and -direction are part of the input files.

The wave variables were obtained from the offshore Wavec buoy (Section 3.5). The model uses the root-mean-square wave height (H_{rms}) while the Wavec yields the significant wave height (H_s). It is assumed that the wave heights at the Wavec were Rayleigh distributed. According to Battjes (1982), the relation between H_s and H_{rms} is then given by:

$$H_s = 1.41 * H_{rms} \quad (6.1)$$

This relation was used to obtain the root mean square offshore wave height.

The direction of the incident waves at the offshore boundary has to be given relative to the shore normal at Egmond aan Zee (α_{cn}). The Wavec gives wave direction relative to North (α_{wavec}). The wave direction was rotated, therefore, following:

$$\alpha_{cn} = \alpha_{wavec} + 82^\circ \quad (6.2)$$

The pressure gauges failed to record the water level during a large part of the field campaigns in 1991 and 1992. Therefore, the water level was derived from tidal stations at IJmuiden (17 km South of Egmond) and Petten (16 km North of Egmond). It was assumed that the water level at Egmond could be calculated by taking the average of the recordings at these two stations.

The velocity measured at pole 3, near the outer nearshore bar, and a frame located at the -10 m depth contour in the cross-shore hydrodynamic array (see Houwman and Hoekstra, 1994) were used to obtain the tidal current. Reniers (1993) showed that for the Egmond field site, when there were no breaking waves, the tidal current was alongshore with hardly any variation cross-shore wise. Hence, the tidal current could thus only be obtained from the longshore velocity measurements. Because the tidal currents were, however, only available for a very limited period, the effect of their omission on the prediction of mean cross-shore currents was investigated as part of the hydrodynamic calculations.

parameter settings

It is possible to define a non-equidistant grid for the model computations. Near the bars, where large gradients in wave height are expected a smaller grid size was chosen. The grid size used in this validation varied between 50 m (beyond outer nearshore bar) and 3.2 m (inner nearshore).

The wave breaking parameter γ plays an important role in the computation of the wave height along the profile (Formula A.3, Appendix A). For the initial hydrodynamic calculations, γ was derived from the relation with the offshore wave steepness (Formula A.4, Appendix A). Bakker (1995), however, has shown that this relation is often absent or very weak. In the hydrodynamic validation, therefore, γ was either derived from the deep- water wave steepness or a fixed value was defined in order to analyse the effect on predicted wave heights. The friction factor (f_w) in the energy decay model was initially set at 0.01.

A detailed bottom sediment sampling of the Egmond field site was part of both the 1991 and the 1992 field campaigns. The results showed that, in the cross-shore as well as in the longshore direction, the D_{50} and D_{90} values of the bed sediment varied greatly (Wolf, 1992, 1993). For instance, the 1991 sampling showed that the D_{50} values varied between 147 μm (at the -10 m depth contour) and 488 μm (trough between outer and inner nearshore bar). For the UNIBEST-TC calculations the D_{50} and D_{90} values of all samples along the 39.500 profile (i.e. along the poles and frames of the hydrodynamic array) were averaged and used as input. The effect of sediment size on the predicted profiles was studied as part of the morphodynamic calculations.

A modification in the latest version of the UNIBEST-TC model is the breaking delay option (Roelvink et al., 1996). The previous version of the model calculated the fraction of broken waves (Q_b) using the local water depth; the fact that waves need a certain distance to actually start or stop breaking was disregarded. This feature has been taken into account by replacing local water depth by water depth, weighted over a certain distance seaward of the point in question. The effect of this feature was treated in the morphodynamic validation. The breaking delay only has a limited influence on the overall wave dissipation pattern (Reniers and Roelvink, in Hoekstra et al., 1996). Therefore, in the hydrodynamic validation the breaking delay option was not used.

Parameters needed for the input of the UNIBEST-TC model that could not be (accurately) determined for the 1991 and 1992 Egmond field campaigns were taken from input data used to validate the UNIBEST-TC model for the Terschelling

nourishment case (see Bakker, 1995; Reniers, pers. comm.). Appendix B gives an overview of all parameter settings.

6.8.3 Hydrodynamic calculations

The hydrodynamic calculations focus on wave height (H_{rms}) and mean cross-shore current (undertow) at different elevations above the bed. These variables were chosen because previous analysis showed that these variables determine important sediment transport processes in the inner nearshore zone.

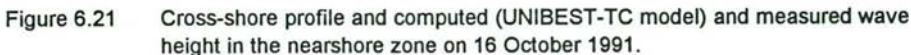
wave height

Wave height along the profile was computed for two days, chosen because the wave height was available at all measuring poles and there was a large variation in the offshore wave height (between 0.5 and 2.5 m). As a result, the hydrodynamics were validated for a wide range of boundary conditions. Figure 6.21 shows the cross-shore bottom profile, the measured offshore wave height, the tide and the measured and computed wave height at the three poles. The results for pole 1 showed that the model was only capable of computing a wave height for 20.00 h. At all other hours, the water depth near pole 1 was too shallow, i.e. less than 0.3 m, for the UNIBEST-TC model to carry out computations. The computed wave heights at pole 2 (inner nearshore) corresponded reasonably with the measurements taken on 16 October 1991. During low offshore wave heights, the model overestimated the measured wave heights at pole 2 by about 0.2 m, an overestimation that reduced almost to zero for higher offshore wave heights. It is very unlikely, therefore, that the initial overestimation is the result of a constant error in either the model or in the measured wave heights, e.g. an offset of the instruments. The results for pole 3 (outer nearshore) show that the model overpredicts wave height for low offshore waves but underpredicts it at pole 3 for higher offshore waves. Nevertheless, the computed wave heights at pole 3 are comparable with the measured ones.

In order to see whether the above results are consistent, a second data set was used showing a persistently high offshore wave height of 1.5 - 2 m (Fig. 6.22) and a bottom profile with a more asymmetric inner nearshore bar. At pole 1, the water depth was shallower than 0.3 m for two periods so no computational output could be generated. During the remaining hours, the predicted wave height was systematically lower (0.4 m) than the measured wave height, probably this was due to inaccuracies in the measured bottom profile.

However, the computed and measured wave heights at pole 2 correspond quite well, showing a difference of less than 0.1 m. The computed and measured wave heights at pole 3 were also comparable except those at between 8 and 11.00 h, when the measured wave heights were much higher (up to 0.5 m) than the computed ones. This increase in the wave height at pole 3 is somewhat awkward because the offshore wave height remained the same.

The sensitivity for varying bottom friction factors (f_w , Formula A.6, Appendix A) was tested by changing f_w in three steps between 0.005 and 0.03. The effect on the computed wave heights at pole 2 remained limited to 0.1 m (not shown) but up to an offshore wave height of 2 m; a higher bottom friction coefficient results in higher wave energy losses. Consequently, the predicted wave heights at pole 2 are smaller when



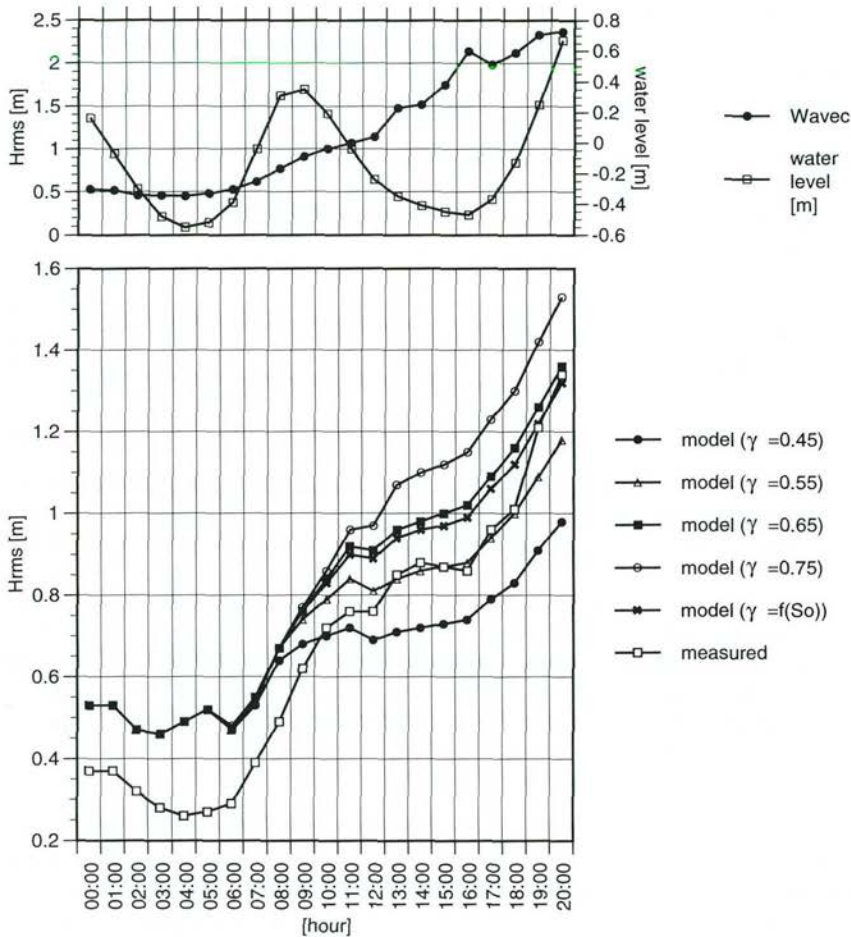


Figure 6.23 Influence of varying breaker coefficient (γ) on predicted wave height at pole 2 at inner nearshore bar. $F(S_o)$ means: is function of offshore wave steepness (Formula A.4, Appendix A). Data of 16 October 1991.

there is a higher bottom friction coefficient, and vice versa. The computed wave heights at pole 3 and pole 1 follow similar trends (not shown). In conclusion, the variation of the bottom friction coefficient may lead to improved predicted wave heights in individual cases, but not along the whole range of measured wave heights.

A second parameter which influences the estimated wave heights is the wave breaking parameter γ . This parameter was varied between 0.45 and 0.75 in three steps, with the bottom friction coefficient held constant at a value of 0.01. The results were compared with the earlier predicted wave heights which used the relation between the offshore wave heights, the wave breaking parameter (Battjes and Stive, 1985; Formula A.4, Appendix A) and the measured wave heights.

Because no waves break near the inner nearshore bar for low offshore wave heights, the wave breaking parameter had no effect on the predicted wave heights during the first hours of 16 October 1991 (Fig. 6.23). For breaking waves, the predicted wave heights may vary over a range of 0.6 m as a result of the variation of γ . The largest differences were found for the highest offshore wave heights. In general, lower values of the wave breaking parameter lead to lower predicted wave heights. Figure 6.23 shows that no single value of the wave breaking parameter or Battjes and Stive's (1985) relation gives the best computed wave height over the entire range of offshore wave conditions. For low offshore wave height, the model's predicted wave heights are about 0.15 m higher than the measured values. When the offshore wave height increases (from 0.5 to 1.25 m), a wave breaking parameter value of 0.45 gives the best results. For an offshore wave height of between 1.25 and 2.0 m, the wave heights produced by the model almost perfectly match the measured wave heights for γ having a value of 0.55. Using the relation between offshore wave steepness and the wave-breaking parameter gives the best results for offshore wave heights above 2.0 m. Similar trends are observed at pole 3 and pole 1 (not shown).

In conclusion, for an optimal prediction of the wave height in the nearshore zone, it is necessary to vary the wave breaking parameter γ along the profile and to vary the wave breaking parameter γ as a function of the offshore wave height. The present UNIBEST-TC model is not capable of doing this. The above analysis shows that for the inner nearshore bar (pole 2) a value of 0.55 gives the best results at higher offshore wave heights (Fig. 6.23) and it are these heights that will result in the most significant morphological changes. In addition, the inner nearshore is the main subject of this research. For the morphodynamic validation, therefore, a value of 0.55 was chosen. This is in line with the results of Chapter 4 which also indicated that 0.55 is a representative value for the averaged wave breaking parameter (Section 4.4.2).

mean cross-shore currents (undertow)

The predicted mean cross-shore currents were compared with the results of the frame on the outer nearshore bar and the EMF on pole 2 (Fig. 6.24). The computed and measured mean cross-shore currents at the outer nearshore bar were similar for low offshore wave heights. However, for high offshore wave heights (> 1.8 m), the UNIBEST-TC model largely underpredicted the measured mean cross-shore current velocity, resulting in differences of about 0.3 m s^{-1} . There was reasonable agreement between the measured and predicted mean cross-shore current at pole 2, with differences varying from 0.01 to 0.19 m s^{-1} . The largest disagreement between the measured and predicted mean cross-shore current was again found during the highest offshore wave height.

In short, the measured and computed mean cross-shore currents show reasonable agreement during low offshore wave conditions. It is likely that the observed disagreement is caused by inadequate formulations for the undertow and/or by measured processes that are not incorporated in the model, e.g. rip currents.

In conclusion, the predicted wave heights for the 1991 data agree reasonably well with the measured wave heights. The mean cross-shore currents, however, do not fit with the measured values for high offshore wave heights.

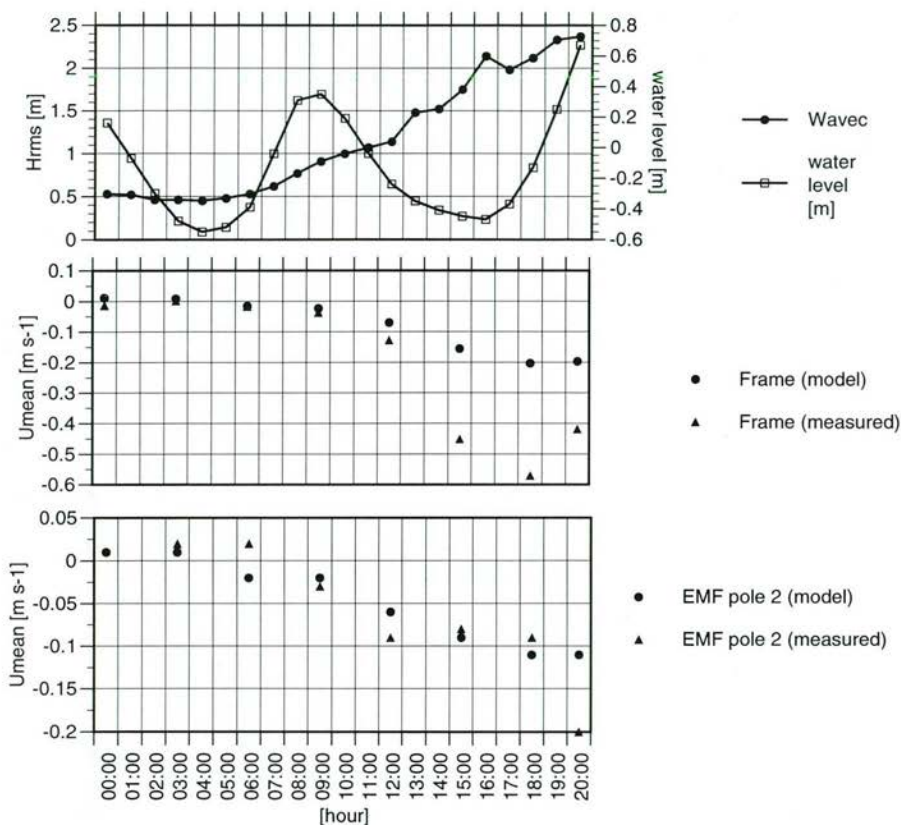


Figure 6.24 Computed (UNIBEST-TC model) and measured mean cross-shore velocity at frame on outer nearshore bar and at pole 2 at inner nearshore bar. Negative velocities are offshore directed; positive velocities are onshore directed. Data of 16 October 1991.

6.8.4 Morphodynamic calculations

The morphodynamic calculations address the profile development and are performed in three runs. The offshore hydrodynamics in these periods are presented in Figure 6.3 while the morphologic developments of the inner nearshore are presented in the Figures 6.12 and 6.13. In addition, the sensitivity of the model to breaking-wave delay and grain diameter was studied. The hydrodynamic and morphological characteristics of the three runs are:

- run 1 date: 3-8 October 1992
offshore wave height: 0.2 -1.5 m
inner bar development: small, onshore migration of bar crest
- run 2 date: 9-14 October 1992
offshore wave height: 0.5 -2 m (storm event)
inner bar development: considerable, bar height increases

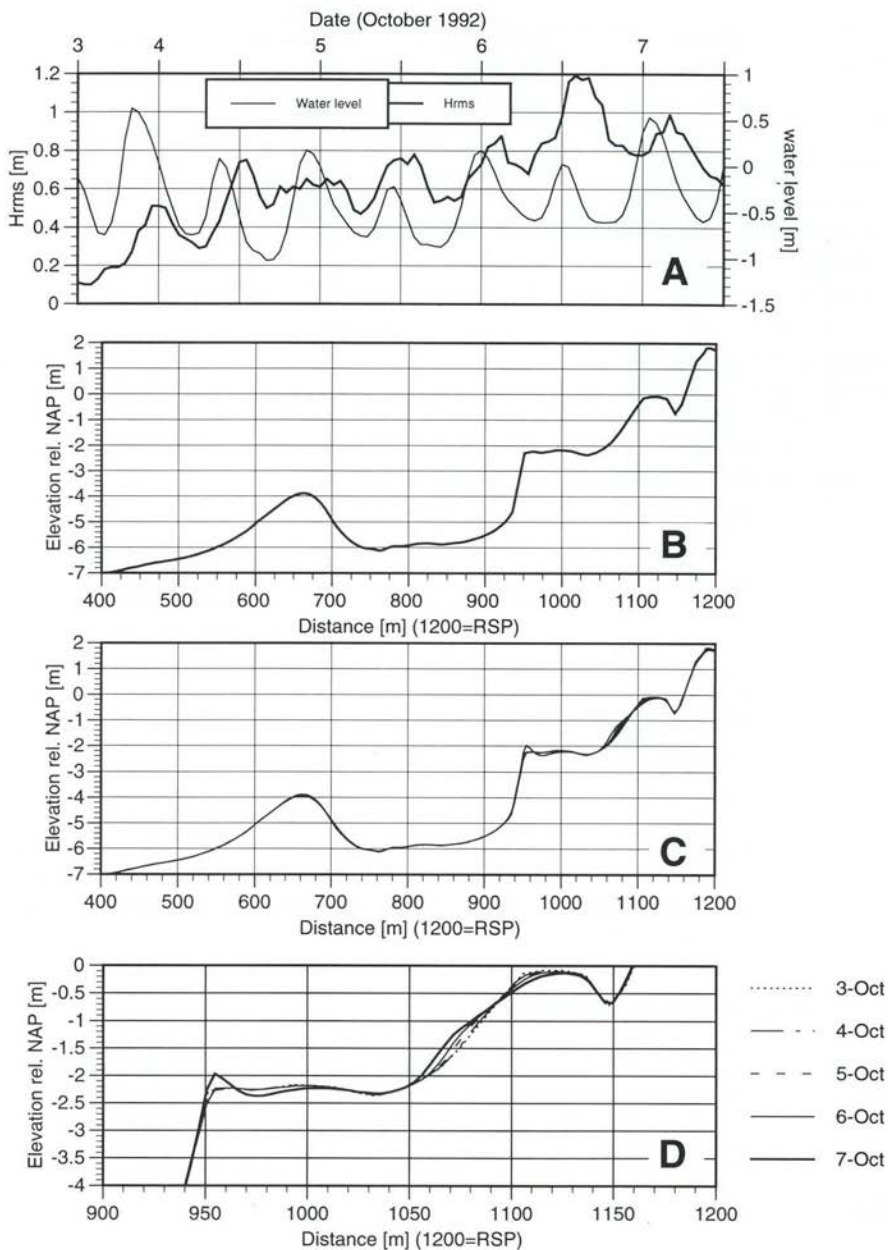


Figure 6.25 Computed (UNIBEST-TC model) and measured profile development 3 - 7 October 1992.

(A) Offshore wave and tidal conditions

(B) Initial profile (3 October)

(C) Predicted profile development in the entire nearshore zone

(D) Predicted profile development in the inner nearshore zone

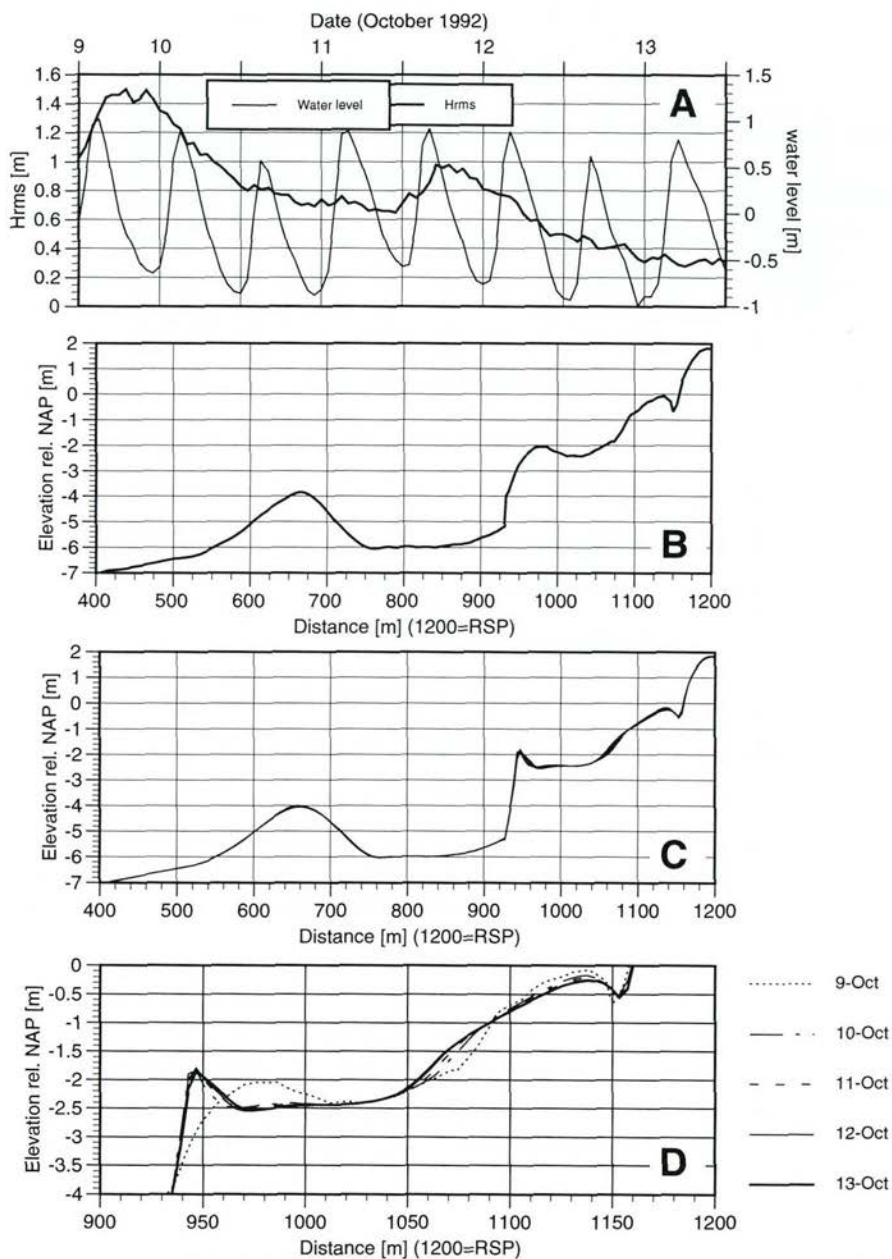


Figure 6.26 Computed (UNIBEST-TC model) and measured profile developments 9 - 13 October 1992.

(A) Offshore wave and tidal conditions

(B) Initial profile (9 October)

(C) Predicted profile development in the entire nearshore zone

(D) Predicted profile development in the inner nearshore zone

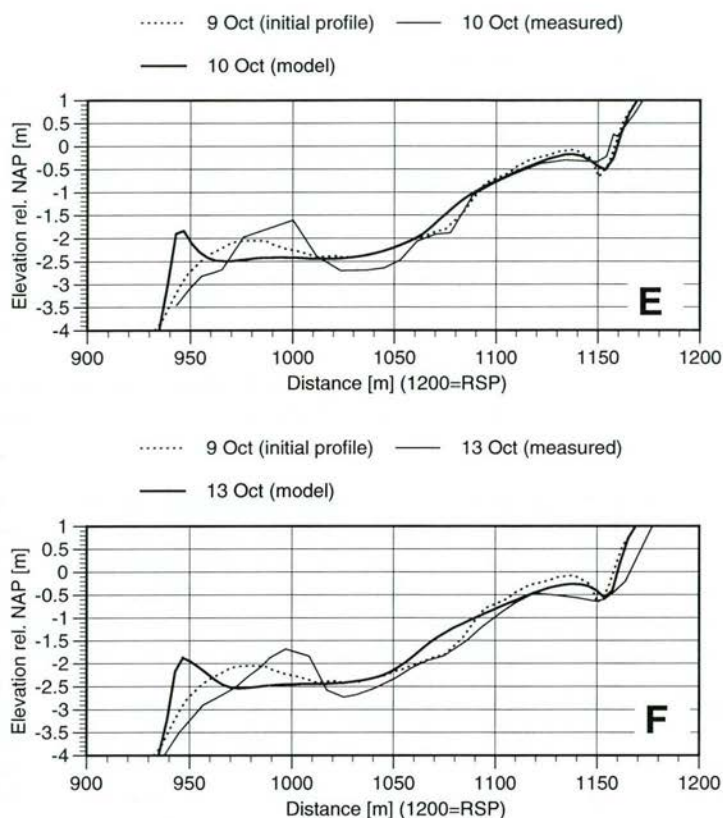


Figure 6.26 Computed (UNIBEST-TC model) and measured profile developments
(continued)
9 - 13 October 1992.
(D) Initial profile (9 Oct.) and computed and measured profile on 10 October
(E) Initial profile (9 Oct.) and computed and measured profile on 13 October

restricted to the last day but took place throughout the first run. There were only small differences between the measured and computed bottom profiles on 4 October (Fig. 6.25e). Landward of the inner nearshore bar's crest, the measured profile was lower than the predicted one but at the seaward side of the inner nearshore bar crest, it was just the opposite, there the predicted profile was lower than the measured one. Differences between the measured and predicted profiles increased on the last day of the first run (7 October; Fig. 6.25f). Both profiles show a more pronounced inner nearshore bar but the computed location of its crest differs 30 m from the measured position and a small difference in the elevation (~ 0.1 m) was also noticeable. The measured and computed developments of the inter-tidal bar showed large differences, especially at the seaward slope of the inter-tidal bar. In conclusion, the computed profiles incorporate the same inner nearshore developments as the measured profiles. However, the location and the shape of the predicted inner nearshore bar developments differ from the measured ones.

profile development - second run

The second run again showed morphological developments at the outer nearshore-, inner nearshore- and inter-tidal bar (Fig. 6.26). The outer nearshore bar showed the same developments as the previous run: a slight onshore migration. The crest of the inner nearshore bar became more pronounced, but the shape of the bar is hardly comparable to the measured one. As with the previous run, the crest of the inner nearshore bar was predicted to migrate offshore, a development most of which took place during the first day (Fig. 6.26d). Thus the model predicts a very rapid adaptation of the profile to high offshore waves. This prediction agreed with the observed reaction and relaxation time of the inner nearshore bar which were also estimated to be in the order of one day (Section 6.4). After the initial rapid development during the first day, the inner nearshore bar crest did not change very much, but nevertheless, the landward slope of the bar became less steep and the front of its seaward slope migrated seaward over about 10 m during the final three days of the second run. The trough between the inner nearshore bar and the inter-tidal bar remained largely unchanged.

The rather unfamiliar shape of the inner nearshore bar after the first day was very different from the measured cross-shore profile (Fig. 6.26e). Both the computed and measured profiles of 10 October (1st day) showed the development of a more pronounced inner nearshore bar, even though, the computed and measured morphometric properties of this bar were quite different -its predicted crest, for example, lay about 55 m seaward of the measured one- although its height only differed a little (< 0.05 m). Moreover, the volume of the predicted inner nearshore bar is considerably smaller than that of the measured one, differences which may be due to the underlying sediment transport processes. The predicted developments indicate that near the initial crest of the inner nearshore bar, seaward sediment transport will be larger than shoreward directed sediment transport (not shown) and that the former will probably be dominated by the mean transport which, in turn, is driven by the undertow (Chapter 5). The onshore transport is mainly the result of wave-related oscillating motions but the suspended sediment transport due to these motions is not included in the UNIBEST-TC model which only comprises the mean suspended sediment transport and the (oscillating and mean) bed load transport. The sediment transport analysis (Chapter 5) has shown that oscillating suspended sediment transport determines about half of the mean suspended transport in the inner nearshore. Thus, disregarding wave-related, suspended sediment transport may have led to these large deviations between the computed and measured bottom profiles. By including wave-related suspended sediment transport in the model, it may have resulted in a larger onshore directed sediment transport near the inner nearshore bar crest, thereby reducing the offshore sediment transport and causing a smaller and slower offshore migration of the inner nearshore bar than was observed in the measurements. Both the predicted and measured developments of the inter-tidal bar show it to be flattening but the measured and computed profiles show a systematic difference in detail during the days, in that the elevation of the measured profile is nearly always lower than that of the computed one, a difference especially visible at the beach face. Although measurement errors may provide an explanation, another possible reason for the difference between the measured and computed profile may be the longshore sediment transport rates, which together with the cross-shore sediment transport rates, may also have led to the observed differences. However, as the longshore sediment transport rates were neither measured nor validated, it is

difficult to address the influence of either the computed or measured longshore sediment transport rates on the observed and computed profile developments. Note that the model is also not designed to describe hydrodynamic and sediment transport processes in the vicinity of the shoreline.

In short, the second run reveals that the computed and measured inner nearshore profiles show large differences; the differences are introduced within a day.

profile development - third run

The profile changes of the third run are larger than the two previous runs (Fig. 6.27) which is due to the larger average wave height and the larger number of days included in this run. The model predicts a flattening of the outer nearshore bar. However, the outer nearshore measurements of 13 and 31 October (see Fig. 6.20) showed that the outer nearshore bar migrated somewhat onshore, at the same time increasing its height.

The landward side of the trough (at $x=950$) between the outer and inner nearshore bar showed a very odd development. The model predicts that, as the trough develops, the seaward slope of the inner nearshore bar will become steeper. This predicted development is very strange, because it has never been observed during the Egmond field campaigns (Kroon, 1994; Wolf, 1992, 1993) and may be due to numerical instabilities. At the field site, the inner nearshore bar, in fact, showed a very similar development to that observed during the first two runs. Again, the initial (computed) development of the inner nearshore bar was considerable (Fig. 6.27d) and its shape was almost nearly identical to that observed after a few days during the first and second run (Fig. 6.28). The location of the inner nearshore bar hardly varies even between the three runs. After one computation day, the crest of the inner nearshore bar was located at 960 (run 1), at 945 m (run 2) and at 960 m (run 3) despite the different initial profile. Thus, it seems that the model is aiming at a 'standard' or 'ideal' inner nearshore bar. The fact that many different model parameters were calibrated using the Terschelling nourishment data, which were not further considered in this analysis may provide an explanation.

The inner nearshore bar crest further changed again on the 17, 18 and 19 October, i.e. days 2 - 4, mainly due to the two periods of waves higher than 1.5 m on 18 and 19 October. Only minor developments were observed during the remainder of the third run (Fig. 6.27e/f). Even the increase in offshore wave height on the 24 October, with heights of more than 2.5 m did not lead to significant changes in the inner nearshore bar, which once rapidly (~days) adjusted to high (> 3 m) offshore wave conditions, it attains an 'ideal' shape which is only slightly changed by lower waves. Comparison between the measured and computed profiles shows that the latter does resemble the observation that a storm results in the growth of an inner nearshore bar (Fig. 6.27g/h). However, the shape and location of the computed inner nearshore bar largely disagrees with the measured one. Moreover, the model does not predict the observed onshore migration of the inner nearshore bar, and the measured inter-tidal bar developments do not compare with the computed developments.

It is concluded from the morphodynamic runs that the UNIBEST-TC model cannot accurately predict the observed inner nearshore developments. The predicted shape and location of the inner nearshore bar differs significantly from the measured developments. Numerical instabilities, ignoring important sediment transport processes (i.e. oscillating suspended sediment transport) and the use of parameter settings that were not validated for the Egmond field site are believed to be the main

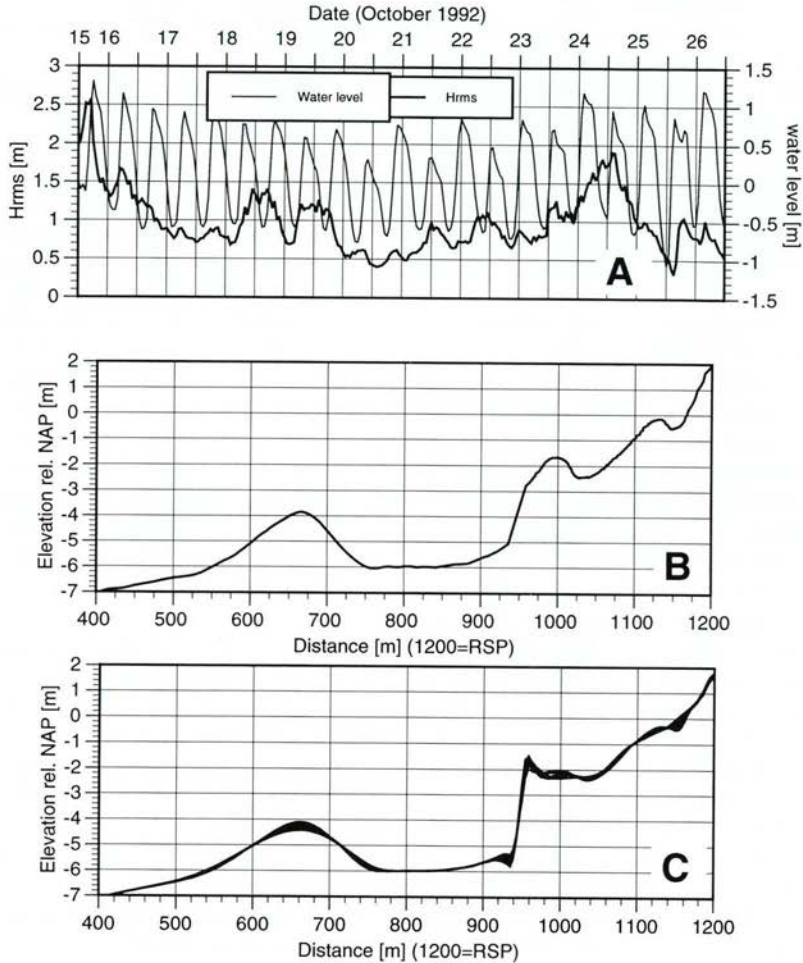


Figure 6.27 Computed (UNIBEST-TC model) and measured profile developments 15 - 26 October 1992.
 (A) Offshore wave and tidal conditions
 (B) Initial profile (15 October)
 (C) Predicted profile development in the entire nearshore zone

factors causing the lack of agreement. Note that only situations with an onshore migrating inner nearshore bar were computed.

sensitivity analysis

This sensitivity analysis studies the effect of sediment size and the breaking delay concept on predicted profiles. Grain size varied considerably at the field site (Table 3.1), so to study the effect of grain size on predicted profiles, two runs were computed in which the D_{50} and the D_{90} of the bed sediment and the D_{50} of the suspended

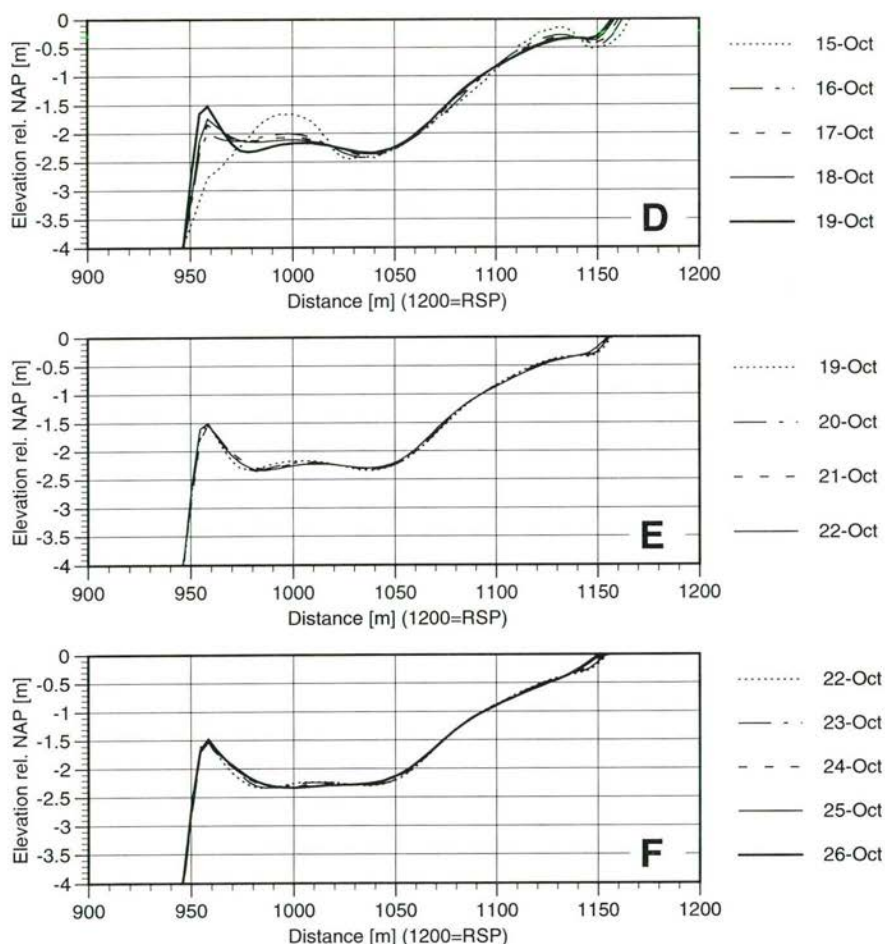


Figure 6.27 Computed (UNIBEST-TC model) and measured profile developments
(continued) 15 - 26 October 1992.

(D) 15-19 October (computed)

(E) 19-22 October (computed)

(F) 22-26 October (computed)

sediment were varied. The D_{50} of the bed sediment was varied by $50 \mu\text{m}$, and the D_{90} of the bed sediment and the D_{50} of the suspended sediment by $40 \mu\text{m}$. The model itself assumes a linear decrease of the D_{50} value with depth. The results reveal that the influence of grain size on the bottom profile development is very small, the differences in elevation being less than 0.05 m (not shown). A reduced grain size leads to somewhat less steep slopes, but the general shape and location of the inner nearshore bar development did not change very much. Hence, the UNIBEST-TC

model indicates that the observed grain size variation has little influence on the profile development.

The breaking delay concept spreads the wave energy released by wave breaking over a larger profile distance. By including this concept in the model, predictions lead to less sharp inner nearshore bar crests, compared to the results of the first run (Fig. 6.29a, Fig. 6.25), which indicates that the wave breaking delay may result in much better predictions as far as inner nearshore bar development is concerned (compare Figs. 6.29b and 6.25e); The development of the inter-tidal bar is, however, not much better predicted and the results of the second run reveal that the wave-breaking delay does not always lead to a higher degree of coherence between the measured and predicted profile (Fig. 6.29c).

In conclusion, the variation in sediment size and the use of the wave breaking delay concept does not lead to an overall improvement in the predicted profiles where large differences remain.

In all, the validation of the UNIBEST-TC model shows that wave height in the surf zone can be reasonably predicted by the model. The mean cross-shore currents are less well predicted, but this may also be due to inaccurate measurements or the presence of rip-currents. Moreover, only a few mean cross-shore current measurements were available. After examining the model's bottom friction coefficient and the wave breaking parameter γ , the morphodynamic validation illustrated that the model is incapable of accurately predicting the observed profile developments. The model can primarily be used to detect trends, rather than as an accurate quantitative predictor (cf. Hoekstra et al., 1996). The model predictions show that its parameters have to be adjusted before the model can be used successfully at other field sites. For the Egmond field site, the predicted hydrodynamics were particularly sensitive for the wave breaking parameter γ while the predicted bottom profile development was very much influenced by the breaking-wave delay. Identical conclusions were drawn by Hoekstra et al. (1996) in their study of the long-term development of the Terschelling nourishment site. Clearly, more systematic and synoptic field data are necessary to carry out a full calibration of the model for the Egmond field site. The model computations analysed here can be seen as an ongoing part of process of model calibration and validation.

6.9 Conclusions morphodynamic computations

The extent to which the observed hydrodynamics and morphological developments could be simulated by a coastal profile model was examined. These analyses have lead to the following conclusions:

- measured wave heights at the inner nearshore bar and outer nearshore bar were, generally, reasonably well predicted.
- the measured mean cross-shore currents were quite adequately predicted for low offshore wave heights but the model largely underpredicted the measured mean cross-shore currents during higher offshore wave heights ($H_{s, offshore} > 1$ m).
- certain aspects of the morphological development of the inner nearshore bar, e.g. the growth of the bar, can be qualitatively described by the model. Quantitatively, however, there is no agreement between the measured and predicted inner nearshore bar development.

6.10 Final discussion and conclusions

morphological developments during non-storm and storm conditions

The impact of a single storm and of a sequence of storms on a barred coastal profile was documented using beach surveys, a sea sled and echo soundings.

The beach is mostly eroded during storms and the beach slope decreases at the same time (e.g. Fig. 6.8; Komar, 1976) but beach erosion has little effect on the position of the shoreline. This is similar to the impact of tropical storms on US Atlantic beaches (Savage and Birkemeier, 1987; Birkemeier et al., 1991). In the Egmond case, apart from a large displacement due to the welding of the inter-tidal bar, the shoreline remains rather stable.

A swash bar, present in 1991, was eroded during storms but recovered, within a few days during the post-storm conditions. The 1992 inter-tidal bar was enlarged during the first storm and welded to the shore during the second one. Once welded, it then showed a similar response to varying offshore wave conditions as the 1991 swash bar.

However, the swash bar/welded inter-tidal bar did not show a distinctive accretion-erosion cycle, as found by e.g. Owens and Frobel (1977) and Kroon (1994) as the migration and growth of this bar on the beach was only rarely observed, probably because of the rough wave conditions. Such conditions diminish the relative influence of the tide on the development of the swash bar (cf. Kroon, 1994), as an increase in the tidal range (i.e. in mean water level) is essential for the development of a swash bar. Nevertheless, the fact that a swash bar developed at all is indicative of the net sediment transport direction. For instance, the swash bar recovered quickly after storms which means that sediment rapidly began to return to the (lower) foreshore. The volumetric computations have shown (sections 6.3 and 6.4) that, during periods of swash bar erosion, sediment is mostly deposited near the inner nearshore bar rather than being carried away by the longshore currents. This indicates that during erosion events the net cross-shore transport is much stronger than gradients in the net longshore sediment transport. The latter is confirmed by the sediment transport analysis (Chapter 5) which showed that the longshore and cross-shore sediment transports are in the same order, i.e. only very large gradients in the longshore sediment transport could have caused the observed cross-shore developments. Hence, the cross-shore morphologic developments are very likely the result of cross-shore sediment transport processes.

The inner nearshore bar's development over weeks showed a gradual onshore movement, temporarily interrupted by storms which caused an offshore movement as was also reported by e.g. Birkemeier (1984), Davis and Fox (1975), Sallenger et al (1985) and Short (1979). The migration rates of the crest of the inner nearshore bar in the present study range from 3.4 to 17.0 m.day⁻¹ in the offshore direction and from 0.2 to 17.3 m.day⁻¹ in the onshore direction. These values were obtained under the assumption that the movement is constant between consecutive surveys. However, the actual migration rate may have been higher as the relaxation times during storms were short (< 1 day). The onshore rates are comparable with bar migration rates along the Japanese coast (Sunamura and Takeda, 1984), but much lower than those observed along the east and west coast of the United States (Orme, 1985; Sallenger et al., 1985). Sallenger et al. (1985) reported onshore migration rates of 24 m.day⁻¹ and offshore migration rates of 48 m.day⁻¹. However, onshore migration rates under

swell are generally higher than under sea conditions, a phenomenon attributed to wave asymmetry, which is higher under swell waves. Velocity asymmetry at the bottom is also higher than under sea waves, because of the higher wave period of swell waves. The differences in onshore rates, reported by the American researchers may, therefore, be attributed to higher wave periods in the (post) storm period along the US coast (10-15 s) than those measured at the Egmond site (8-9 s). Although the offshore wave heights reported by the Americans during post-storm conditions are comparable with the Egmond site, the offshore migration rates were probably higher because Sallengers' (1985) rates were observed on a coast with a single bar, i.e. without an outer nearshore bar reducing the wave heights. The volume of the bar may also play an important role as smaller bars show a faster response and migrate over larger distances. Finally, an inter-tidal bar may act as a temporary storage for eroded beach sediment thereby influencing the development of the inner nearshore bar. This suggestion should be relatively easy to verify because when the inter-tidal bar welds to the shore this barrier disappears and different relations between the shoreline and the inner nearshore bar developments should be found before and after this welding. Indeed such changes were found. For instance, the shoreline is relatively stable before the inter-tidal bar welds to the shore and becomes part of the beach. Thereafter, the shoreline is more related to the position of the inner nearshore bar crest (Fig. 6.30). The development of the trough seaward of the inter-tidal bar also suggests that this bar interferes with the relation between the inner nearshore bar and the shore. Figure 6.31 shows that the position of the inner trough seems to be steady before the inter-tidal bar is welded, but afterwards moves gradually towards the shore. The inter-tidal bar not only hinders the onshore movement of the trough of the inner nearshore bar as long as it is not welded to the shore, but also might affect the development of the entire bar (cf. Lippmann et al., 1993).

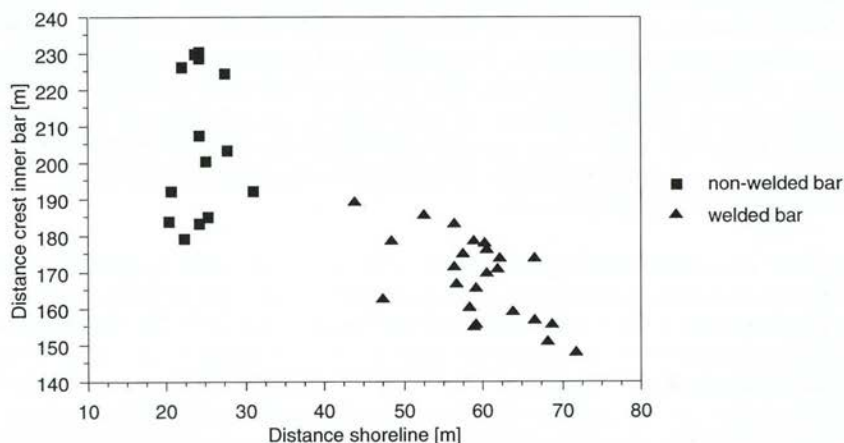


Figure 6.30 Relation between location of the shoreline and location of the crest of the inner nearshore bar in 1992.



Figure 6.31 The location of the trough of the inner nearshore bar at SAP profile as function of time in 1992. Shaded areas indicate storms.

The inner nearshore bar at Egmond is not destroyed during storms, as suggested by some researchers (e.g. Davis and Fox, 1972; Orme, 1985), but is generally enlarged during the first autumn storms. Succeeding storms may change its shape further but they do so less dramatically than during the first storm. The shape of the inner nearshore bar is mostly asymmetric (cf. Orme, 1985), but its asymmetry decreases when moving offshore (Houwing, 1991).

The outer nearshore bar remained inactive compared to the more dynamic inner nearshore bar, as is common in multi-barred coasts (e.g. Larson and Kraus, 1992; Short and Aagaard, 1993). Besides, larger bars usually have a longer relaxation time (cf. Ahnert, 1994) and the outer nearshore bar may still be out of equilibrium with the offshore hydrodynamics. The outer nearshore bar showed small changes in response to storms and may be regarded as stable over weeks. This suggests that the yearly net offshore movement of this bar (Wijnberg, 1995) is not gradual, but episodic. The average depth at the outer nearshore bar was about -4 m (Fig. 6.17) which means that breaker heights should have been in the order of 2.5 m in order to modify the outer nearshore bar ($h_{br} = \alpha h$, $\alpha = 0.6$) so that it would only be exposed to breaking waves during the largest storms. As transport was minimal during non-storm conditions it showed a less rapid movement than the inner nearshore bar. Nevertheless, Hoekstra et al. (1994) suggest, using data from a multiple bar system along a barrier island in the north of the Netherlands, that when the crest of an outer nearshore bar is at a depth of -4 m it still affects the dynamics of the inner nearshore. Additional analysis is needed to verify this suggestion. The suggestion that the elevation of the crest of the outer nearshore bar affects the inner nearshore developments could explain the longshore variability of the shoreline response, because the position of the outer nearshore bar varied alongshore.

- the general response of the inner nearshore bar during non-storm conditions is to move onshore while storm conditions tend to move this bar offshore.

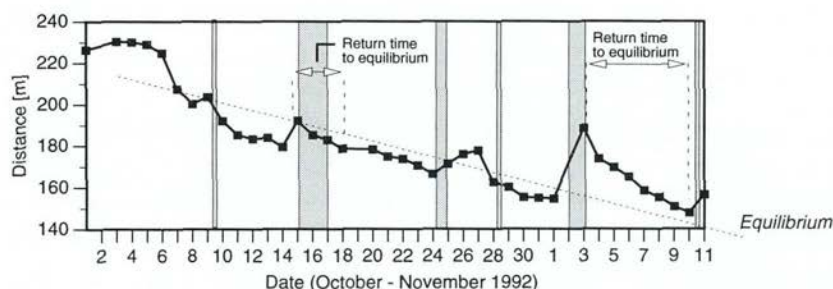


Figure 6.32 Position of the crest of the inner nearshore bar and suggested dynamic equilibrium. Shaded areas indicate storms.

influence of antecedent morphology on the response of the inner nearshore bar

To study the influence of the antecedent profile configuration which incorporates the antecedent wave conditions one has to consider the medium scale development of the inner nearshore bar because the profile configuration clearly changes on this scale. The medium scale development shows a persistent onshore moving bar interrupted by an offshore movement during storms (Fig. 6.13). To which equilibrium the inner nearshore bar is moving during the non-storm conditions is unclear. Evidently this equilibrium did not change during the 1992 field measurements because the inner nearshore bar nearly always showed the same trend during non-storm conditions, namely an onshore migration. It is interesting, though that this bar migration did not stop at its pre-storm position but moved further onshore. Hence, the processes related to this equilibrium must have been acting on a time scale that is larger than the period of observation. Although it was not possible to determine the magnitude of this scale, it is clear from the yearly observations (Fig. 6.4) that it must have been less than a year, because on a yearly scale, the net migration direction of the inner nearshore bar is offshore (cf. Wijnberg, 1995) and not onshore, as observed in this study. Hence, the most probable time-scale associated with the onshore movement will be in the order of months. Figure 6.32 shows that the offshore displacement of the inner nearshore bar increases with every storm and that the time needed to return to the dynamic equilibrium also increases. Both trends are not related to the magnitude of the succeeding storms. The time scales of offshore and onshore movements tend to diverge the nearer the bar is to the shore. For instance, the fifth storm resulted in larger offshore displacement of the crest than in the previous storms although at the same time, the onshore migration speed remained the same. This suggests that the processes contributing to the offshore migration were stronger when the bar was closer to the shore, but the strength of the processes resulting in the *onshore* migration were not influenced by the position of the inner nearshore bar. Thus, the antecedent morphology was found to be determining the offshore migration distance while it does not seem to affect the onshore migration which is in contrast to the notion that post-storm recovery is determined by the post-storm profile configuration (Birkemeier, 1984; Lippmann and Holman, 1990).

Clearly, to reveal which part of the cross-shore profile has been responsible for the observed trend in the offshore migration distance one has to look at the beach because the sediment transport analysis (Section 5.8) made clear that it is beach sediments which largely contribute to the inner nearshore bar developments while the

outer nearshore zone is of less importance. It was earlier revealed that it was only after the fifth storm of 1992 that caused the shoreline to retreat at most profiles along the field site (Fig. 6.18). During the first four storms, the upper beach acted as a reservoir for the lower beach thus preventing shoreline retreat, but apparently, this reservoir was 'empty' by the time the fifth storm approached the coast. Thus, after a few storms the beach loses its sand 'buffer' resulting in a reduced offshore transport of beach sediment. Because offshore sediment transport at the bar will be approximately the same, the offshore migration of the inner nearshore bar during each next storm will increase (Fig. 6.32).

In conclusion, storms with an equal magnitude are likely to have a smaller impact on the beach if they are located at the end of a storm-sequence because the beach profile has adapted itself to the first few storms. As a result, the amount of beach sediments that contribute to the development of the inner nearshore bar *decreases* with each next storm and the impact on the inner nearshore bar *increases* with each next storm. Hence, the impact of a single storm on a coast and on a medium time-scale depends, therefore, on the shape of the coastal profile before the storm, i.e. its position in the sequence of storms.

- the response of the inner nearshore bar during *non-storm* conditions shows only little relation with the antecedent profile configuration. The response during *storm* conditions, i.e. an offshore migration, seems to increase with every succeeding storm because it depends on the offshore transport of beach sediment. The latter depends on the availability of beach sediment, i.e. the beach volume which decreases during each storm. Hence, the inner nearshore bar response during storms depends on the antecedent (beach) profile configuration.

limitations and suggestions for further research

The short time scales of response of the inner nearshore bar and inter-tidal bar and the sampling rate of one survey a day suggests that aliasing effects cannot be ruled out. These aliasing effects may, together with measurement errors, have influenced the correlation analysis and may express the low correlation coefficients. At the onset of a storm, a sampling rate of 2-3 surveys a day is particularly desirable. Moreover, three dimensional developments, e.g. crescentic bar formation, could have been present during the measurements (cf. Birkemeier, 1984; Sallenger, 1985), since there is no definite evidence that the inner nearshore bar was linear during the observations. The SAP profile may, therefore, not be fully representative of the behaviour of the inner nearshore bar. Yet the migration distance of the inner nearshore bar (~80 m) suggests that rhythmic features alone cannot be responsible for the observed movements. Nevertheless, since the SAP profile is the only extensive and continuous data set available, it is, from a practical view, advisable to regard the inner nearshore bar as linear. In conclusion, the application of instruments and observation techniques that make rapid and three dimensional sampling of the inner nearshore zone under all weather conditions possible should be given high priority. Such techniques and instruments are already available, e.g. the CRAB (Birkemeier, 1984) and the video system of Lippmann and Holman (1992). The latter technique makes it possible to obtain long records that are invaluable for understanding the morphological behaviour of bars. At the same time, hydrodynamic and sediment transport measurements with a high spatial accuracy are necessary to get a more accurate picture of the gradients of these processes.

7. SYNTHESIS

7.1 Introduction

Longshore breaker bars are present in the surf zone of the central part of the Dutch coast. These bars are expected to play an important role in the coastal development because they may reduce coastal erosion by acting as a natural breakwater. In addition, these bars incorporate large volumes of sand which can play a role in the natural recovery of the beach and nearshore zone after periods of coastal erosion. Despite numerous field- and laboratory studies, the behaviour of these bars is poorly understood and the main processes responsible for bar development have not been clearly identified. Several studies have related the migration and development of these bars to low-frequency waves but these studies are often theoretical and based on unrealistic boundary conditions. Most *field* studies have not been able to produce support for these theories. Another group of theories links the morphological development of bars to the breaking of high-frequency (wind-) waves. These theories hypothesise that sudden hydrodynamic changes occur when waves break, thereby inducing a convergence in the sediment transport that will lead to bar development. Despite the simplicity and attractiveness of this second group of theories, they have not been thoroughly validated in the field.

The primary research goal of this study is to reveal inner nearshore bar development on the short and medium scale and relate this development to hydrodynamic and sediment transport processes. The study concentrates on hydrodynamic and sediment transport processes associated with the shoaling and breaking of wind-waves. Two field experiments were executed near Egmond aan Zee to collect the data needed for this study; hydrodynamic, sediment transport and morphological processes were measured under a wide range of weather conditions in the autumn of 1991 and of 1992.

7.2 Main results

hydrodynamic processes of breaking and shoaling waves

The inner nearshore hydrodynamics of high-frequency waves shows a spatial cross-shore zonation ranging from non-breaking waves (seaward of the breakpoint) via breaking waves to swash (landward from the breakpoint). High-frequency motions (surface waves and orbital excursions) in these hydrodynamic zones dominate the spectra, although the contribution of low-frequency energy increases toward the coast. The hydrodynamic zones can be distinguished by the relative wave height parameter (H_s/h). Low relative wave heights indicate a non-breaking zone while high relative wave heights are observed in the swash zone. An increase in the relative wave height leads to a larger onshore and offshore peak velocity near the bed. Up to the breaker zone ($H_s/h \sim 0.55$), an increase in the relative wave height also results in more asymmetric waves and higher mean cross-shore currents near the bed (0-0.3 m). The waves typically have short and sharp-peaked crests and larger extended troughs with a smaller amplitude but large duration. The breaking of waves reduces the wave- and orbital excursion asymmetries, although waves and excursions remain asymmetric. The shape of the waves and orbital excursions can not be described

using existing wave theories. Moreover, the mean cross-shore currents, which are offshore directed due to the undertow, can also not be predicted by existing theories.

sediment concentrations and sediment fluxes

The suspended sediment concentrations near the bed vary on time-scales of incident wave frequencies and lower frequencies. High-frequency oscillations dominate the velocity field and little correlation is, therefore, present between the instantaneous concentration and velocity. A large vertical diffusivity exists in all hydrodynamic zones which implies that a higher time-averaged concentration near the bed is associated with a steeper and more uniform vertical concentration profile. The near bed concentration increases with the relative wave height and the highest concentrations are, therefore, found in the swash zone.

The mean suspended sediment transport dominates the sediment transport within 0 - 0.3 m of the bed, being about twice as large as the oscillating suspended sediment transport. Within the oscillating transport mode, the high frequency transport is about twice as much as the low-frequency oscillating transport. The total oscillating suspended sediment transport increases with an increasing relative wave height, while the mean suspended sediment transport depends on the strength of the mean cross-shore current. The highest time-averaged suspended sediment transports near the bed are, therefore, found in the breaking wave zone as in this zone also the highest mean cross-shore currents are measured.

The time-averaged, depth-integrated, suspended sediment transport in the cross-shore direction was largely determined by the mean currents. Hence, time-averaged suspended sediment transports were all offshore directed and the largest quantities were found in the breaking wave zone. In general, the suspended sediment transport mode dominates the total net sediment transport, i.e. the sum of the suspended and bedload transports. There is, however, a great variation in the ratio between the depth-integrated suspended sediment transport and the bedload transport. The total onshore transport is likely to be generated by wave and orbital excursion asymmetry because no other transport mechanism is known that can generate the observed onshore transport quantities. Nonetheless, the wave asymmetry and the onshore sediment transport are not observed to correlate well. The offshore sediment transport is steered by the mean cross-shore current.

The estimated sediment transports indicate that inner nearshore bar development does not always result from a convergence of sediment caused by opposing sediment transport vectors, as suggested by some bar generating theories. The inner nearshore bar developments may also be the result of gradients in a unidirectional sediment transport (either onshore or offshore).

morphological response and morphodynamic computations

The beach, shoreline and inner nearshore bar do not respond identically to every storm, because the response also depends on the antecedent cross-shore profile. Sediment from a berm, initially present at the upper beach, but eroded during the successive storms, is deposited near the shoreline, causing a prograding shoreline. After the berm is completely eroded by the first few storms, successive storms resulted in a retreat of the shoreline. In these conditions, an inter-tidal bar may act as a temporary barrier in the exchange of sediments between the beach and the inner nearshore bar. However, the eroded beach sediments are eventually also transported farther offshore resulting in a build-up of the inner nearshore bar. During storms, the inner nearshore bar mostly migrates offshore while during non-storm periods this bar

moves onshore. The offshore migration speed during storms is higher than the onshore migration speeds during non-storm conditions. Non-storm conditions occur, however, more frequently than storm conditions. Nonetheless, the integrated result of the inner bar development after several weeks is an onshore migration. The offshore migration distance of the inner bar increased during each successive storm, probably because the quantities of offshore transported beach sediment, replacing the offshore transported sediments at the bar, decreased with each storm. The response of the outer nearshore bar to storms was small, compared with the inner nearshore developments and varied along the field site.

The reaction and relaxation times of the inner nearshore during accretional stages were short. For instance, it was not uncommon that one or two days after the peak of the storm, for a new swash bar or inter-tidal bar to have emerged, and for the inner nearshore bar to have stopped its offshore migration (Fig. 6.32). Despite such rapid response, it was not possible to establish quantitative relations between the inner nearshore developments and the offshore wave conditions.

The tested mathematical-physical model (UNIBEST-TC, Delft Hydraulics) accurately predicts the wave height in the nearshore zone; the mean cross-shore current and the morphological developments were, however, unsatisfactorily predicted. Detailed calibration is required for realistic results.

7.3. Small and medium scale morphodynamic processes involved in the inner nearshore bar development

Morphological developments of the inner nearshore bar during storm and non-storm conditions are strongly influenced by high frequency wind-waves. The net sediment transport direction is determined by the balance between the orbital wave asymmetry (causing an onshore sediment transport) and the mean cross-shore current (causing an offshore transport). During lower wave conditions, the offshore directed mean cross-shore current induced by wave breaking (undertow) is not strong enough to dominate over the wave asymmetry and the local sediment transport direction is, therefore, onshore. During higher wave conditions, more waves will break and it is then that the undertow dominates the velocity field, resulting in an offshore sediment transport. Hence, the distribution of the net sediment transport direction over the inner nearshore zone is mainly related to the probability of breaking of the waves. The latter is largely determined by the bathymetry and the offshore wave height.

In all, an increase of the offshore wave height will result in the following sequence of inner nearshore processes (cf. Fig. 5.38):

- During periods of low offshore wave heights ($H_{s, \text{offshore}} < 0.5 \text{ m}$), waves do not break on the inner nearshore bar and the net sediment transport direction in the entire nearshore zone is directed onshore. This results in an onshore moving inner nearshore bar and a heightening and widening of the beach.
- If the offshore wave height increases ($H_{s, \text{offshore}} = 0.5 - 1.5 \text{ m}$), waves will break on the inner nearshore bar, generating a (small) offshore sediment transport at the landward side of the inner nearshore bar, while the sediment transport at the seaward side is still onshore directed. As a result, the inner nearshore bar migrates onshore. Its onshore migration speed will strongly reduce, however, for higher waves because a larger offshore sediment transport at the landward side of the inner bar may be expected when the intensity of breaking increases. At the beach,

the relative wave height will be larger than at the inner nearshore bar. Therefore, with increasing wave heights, the net sediment transport direction will reverse from onshore to offshore and erode the beach. The result is a retreating shoreline; however, in the case when enough sediment transported from the upper beach to the lower beach to resupply the beach face (erosion of a berm), the shoreline will be stable or may even prograde. It is unlikely, though, that eroded beach sediments largely contribute to the inner bar development, because the sediment transport direction in the trough between the inner nearshore bar and the beach may be still onshore. Besides, an inter-tidal bar may act as a temporal blockage in the transport of sediment between the beach and inner nearshore bar.

- Offshore wave heights between 1.5 and 2 m will be large enough to generate an undertow in the inner nearshore zone that extends from the beach up to the crest of the inner nearshore bar. As a result, the sediment transport at the landward side of the crest of the inner nearshore bar is offshore directed and because onshore sediment transport only takes place at some distance seaward of the inner nearshore bar, the inner nearshore bar will migrate offshore. The beach will be eroded and the offshore transport of beach sediments will play an important role in the development of the inner nearshore bar because these sediments are likely to be transported towards and incorporated into the nearshore bar.
- Offshore wave heights larger than 2 m generate an offshore-directed sediment transport up to and over the inner nearshore bar, with high rates of offshore transport near the shore and lower rates in the direction of the inner nearshore bar. Hence, gradients in the offshore directed sediment transport will steer the inner nearshore bar developments. These sediment transports result in an offshore moving bar, in erosion of the beach and, if present, of the inter-tidal bar.

The above sequence of morphodynamic processes is based on a synthesis of field studies at Egmond aan Zee under particular offshore wave conditions and cross-shore profile configurations. In reality, the transformation from one group of processes to the next will vary with the shape and location of the nearshore bars and beach, and will occur gradually. The offshore wave heights at which one group of processes is being replaced by another must, therefore, be seen as indicative.

Nevertheless, these results make clear that, basically, inner nearshore bar movements are related to the breaking of high-frequency wind-waves, the so-called 'break point hypothesis'. However, this hypothesis explains bar development by using two opposing sediment transport vectors, i.e. an onshore movement of sediment at the seaward side of the bar and a landward sediment transport at the landward side of the bar. This study concludes that when there are very low ($H_{s, offshore} < 0.5$ m) or very high ($H_{s, offshore} > 2$ m) waves, the development of the inner nearshore bar is steered by gradients of *unidirectional* (onshore or offshore) sediment transport rather than by two opposing sediment transport fluxes. Only in the case of moderate offshore wave heights (between 0.5 and 2 m) the development of the inner nearshore bar could be explained by two opposing sediment transport vectors.

The presence and source of long waves were not studied in this thesis. Nevertheless, low frequency energy and low frequency oscillating sediment transport only formed a small part of the total sediment transport in the inner nearshore zone. In explaining inner nearshore bar behaviour these findings do not favour the infragravity theories.

7.4 Development of inner nearshore bar on a medium to large time scale

The integrated result of a sequence with storm events and non-storm periods is a net beach erosion. The swash bar or an inter-tidal bar is eroded by storms but reappears during the following non-storm conditions. Thus the beach displays cyclical behaviour (new swash bar, new inter-tidal bar) as well as unidirectional behaviour (lowering of beach) on a medium time-scale. The integrated result for the inner nearshore bar is an onshore migration, which is associated with an increase in volume. The entire sediment volume in the inner nearshore zone is, however, unaffected by the storm sequence.

On the medium time scale (days to weeks), the beach and an inner nearshore bar strive to achieve dynamic equilibrium. The non-storm processes, directed towards a low energy equilibrium occur more frequently, but are weaker compared to the storm processes directed towards high-energy equilibrium. Yet, non-storm periods dominate the inner nearshore bar development on the medium scale and the inner nearshore bar is part of a development that creates a 'fair-weather' beach state. The impact of a single storm varies and depends on the position of the inner nearshore bar at the onset of the storm; each successive storm has a stronger impact on the inner nearshore bar than its predecessor. At the same time, the onshore migration rates during non-storm periods remain the same. As the measurements were conducted in the autumn, and the occurrence of storms is higher in the winter season, the frequency of storms will also increase. Thus, at some point during the winter, the net migration direction on a medium time-scale will change from onshore to offshore and the net migration direction after the autumn and winter season (large time scale) will be offshore. The latter is clearly confirmed by studies analysing the yearly coastal surveys (JARKUS data base; e.g. Wijnberg, 1995).

This study has shown that the offshore transport of beach sediments plays an important role in the inner nearshore bar development. It is hypothesised, therefore, that the change in the net migration of the inner nearshore bar on the medium time scale is caused by a (temporal) decrease in offshore sediment transport from the beach to the inner nearshore bar. The first storm of every autumn erodes beach sediments which have been deposited during the summer. These sediments are eventually deposited on the inner nearshore bar. After a number of storms, the beach is in equilibrium with most storm conditions, i.e. only higher magnitude storms can erode greater quantities of sediment from the beach. At that condition, the offshore sediment transport at the inner nearshore bar during storms is no longer compensated by beach sediments, and the bar moves offshore (Fig 7.1). Storms with an equal magnitude are likely to have a smaller impact on the beach, if they occur at the end of a storm sequence, because by then the beach profile has adapted itself to the first few storms. Hence, bar dynamics not only depend on offshore wave conditions but also on the antecedent morphology, in particular the beach state and its associated sediment volume. As bar dynamics also determine the entire coastal profile development, it may also be concluded that the impact of a single storm on a coast over a medium time-scale depends on the shape of the coastal profile before the storm, i.e. the position of the storm in the sequence of storms. An identical conclusion can be drawn for the large time scale. The impact of autumn/winter storms depends on the shape of the coastal profile at the end of the summer.

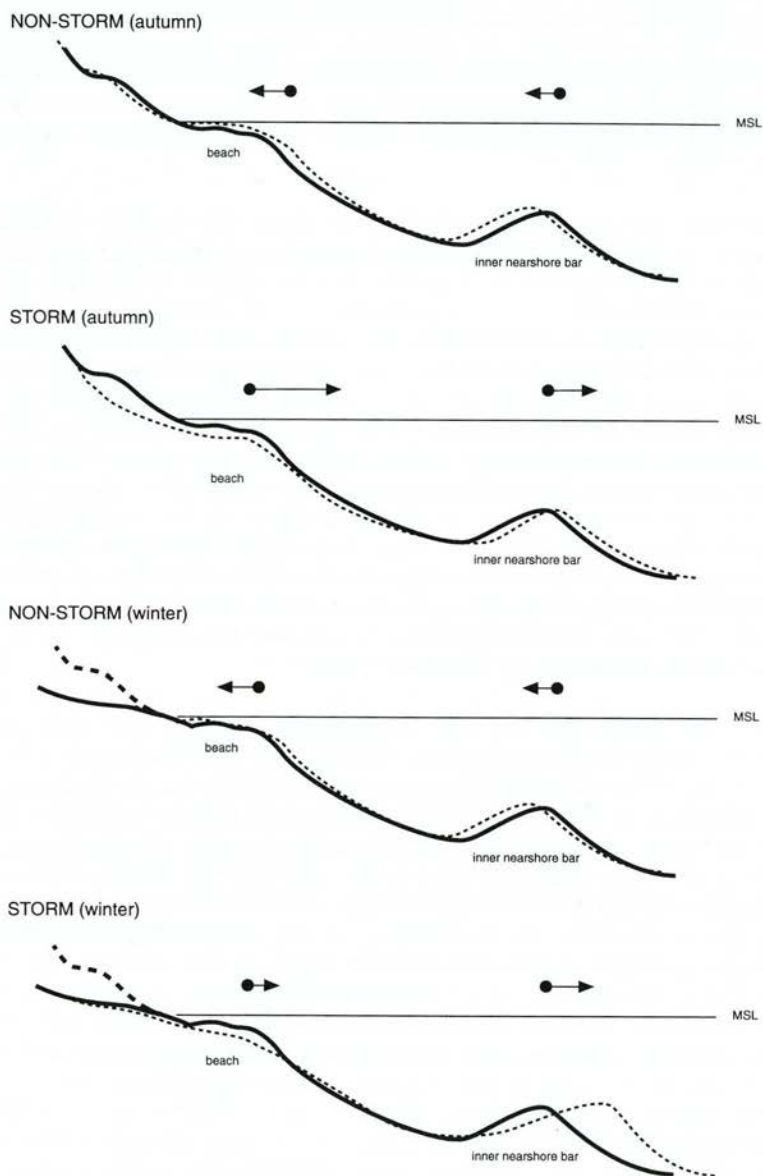


Figure 7.1 Sediment transport vectors and the resulting morphologic development of the shoreline and inner nearshore bar during non-storm and storm-periods in the autumn and winter. Thick dotted lines indicate beach volume losses.

7.5 Final remarks and recommendations

In short, the development of the inner nearshore bar is the result of two delicate balances, one present on the small scale, the other on the medium to large scale. The first is a balance between the onshore sediment transport induced by the wave asymmetry and the offshore sediment transport induced by the mean cross-shore current. This balance determines the local net sediment transport direction. The medium to large time scale distribution of the local net sediment transport direction is determined by the balance between non-storm and storm periods in relation to the antecedent morphology and sediment volumes. In other words, it is determined by the balance between the offshore transport of sediments in the inner nearshore and the supply of eroded beach sediments. This medium scale balance determines the development of the nearshore bars and, consequently, the development of nearshore profiles. The development of nearshore profiles determines, in turn, the development of the entire coast. To understand the development of the coast on a large time scale, it is of essential importance to know which knowledge about the small scale balance is important for the determination of the large scale developments. An identical scale problem is present regarding the two-dimensional approach of this study as it is not clear to what extent the results of this study may be extrapolated to three-dimensional situations. To answer these questions, more research is necessary and particularly the next topics should be studied in the near future:

- Verification of the proposed sequence of morphodynamic processes that determine inner nearshore bar development by collecting field data and improving morphodynamic models. These data should reveal the net sediment transport direction close to the inner nearshore bar, thereby analysing the proposed correlations between the orbital asymmetry and the onshore sediment transport, and between the undertow and the offshore sediment transport at the bar, preferably in non-equilibrium conditions.
- Evaluation of the conceptual model for the inner bar movement during the autumn and winter (Fig. 7.1), i.e. study if the loss of beach sediments is indeed the main factor changing the net migration direction of the inner nearshore bar on the medium time scale. This requires more morphologic data which can be obtained through video-monitoring systems (ARGUS system, cf. Lippmann and Holman, 1989) and beach surveys and may link developments at different (interacting) time scales
- Investigation of the three-dimensional character of inner nearshore bar and the extent to which the development of inner nearshore bars is a two-dimensional or three-dimensional process. A CRAB-like profiling system (cf. Birkemeier, 1984), capable of surveying the inner nearshore under low and high wave conditions is then essential to obtain the required data.

unidirectional offshore sediment transport throughout the inner nearshore zone. Hence, the morphologic development of the inner nearshore bar is not necessary the results of a convergence of two opposite sediment transport vectors but may also be the results of gradients in a unidirectional transport.

The response of nearshore bars and the inner nearshore sediment transport patterns, induced by a single storm and a series of storms, was analysed. The beach, shoreline and inner nearshore bar do not respond identically to every storm because their response is influenced by sediment eroded from a berm. Sediment from this berm, initially present at the upper beach, but eroded during the successive storms, is deposited near the shoreline, causing a prograding shoreline. After the berm is completely eroded by the first few storms, the successive storms result in a retreat of the shoreline. An inter-tidal bar may act as a temporary barrier in the exchange of sediments between the beach and the inner nearshore bar. However, the eroded beach sediments are eventually also transported farther offshore and contribute to the development of the inner nearshore bar. During storms, the inner bar mostly migrates offshore but the onshore migration during the non-storm periods and the larger number of days with non-storm conditions result in a net onshore migration after several weeks. The offshore migration of the inner bar increases during each successive storm probably because the quantities of offshore transported beach sediment decreases with each storm. The outer nearshore bar response to storms is small compared with the inner nearshore developments.

Finally, a physical mathematical model (UNIBEST-TC, Delft Hydraulics) was analysed to see whether it could accurately predict the observed hydrodynamics and morphologic developments. The surface wave hydrodynamics were reasonably predicted by the model but the computed mean cross-shore current and morphological development largely differed from the observations.

HYDRODYNAMICA, SEDIMENT TRANSPORT EN DAGELIJKSE MORFOLOGISCHE ONTWIKKELING VAN EEN BRANDINGSBANK-STRAND SYSTEEM - SAMENVATTING

De brandingszone langs de Noord- en Zuidhollandse kust wordt gekenmerkt door de aanwezigheid van brandingsbanken. Deze banken spelen in de kustontwikkeling een voorname rol omdat zij de golven breken waardoor minder kustafslag plaatsvindt. Daarnaast is het zandvolume van deze banken belangrijk omdat dit volume kan worden gebruikt om het herstel van de kust, na een periode van kustafslag, te bespoedigen.

Ondanks het feit dat er veel onderzoek heeft plaatsgevonden naar het morfologisch gedrag van deze banken en naar de fysische processen die dit gedrag sturen, is het nog niet mogelijk het gedrag van deze banken op korte (dagen) en langere termijn (jaren) met een voldoende nauwkeurigheid te voorspellen.

Het doel van het onderzoek, beschreven in dit proefschrift, is het vergroten van de kennis van het gedrag van brandingsbanken op de korte tot middellange (weken) termijn. Daarnaast is het bedoeling om een (kwalitatief) inzicht te verkrijgen in de fysische processen die dit gedrag sturen. Daarbij heeft dit onderzoek zich gericht op de processen die samenhangen met de transformatie en het breken van korte ($T < 20$ s) golven rondom de binnenste van twee brandingsbanken in de brandingszone nabij Egmond aan Zee. Er is bovendien gekozen voor een tweedimensionale benadering, dat wil zeggen dat de morfologische veranderingen en de fysische processen in een kustdwars profiel zijn beschouwd.

Uit de *hydrodynamische analyse* van processen die een rol spelen bij de transformatie en het breken van korte golven is gebleken dat rond een breekpunt, gelegen in de nabijheid van het strand, vijf zones kunnen worden onderscheiden. Van zeewaarts naar landwaarts gezien zijn deze zones:

- zone waarin golven niet breken ('non-breaking zone')
- zone waarin sommige golven breken ('(non)-breaking zone')
- zone waarin alle golven breken ('breaking zone')
- zone waarin alle golven breken of als golfploop passeren ('breaking/swash zone')
- golfploop zone ('swash zone')

In alle zones was het aandeel van de korte golf energie, zowel aan het oppervlak als aan de bodem, groter is dan van de lange golven ($T > 20$ s). Het aandeel van de lange golf energie nam echter naar de kust wel toe. De hydrodynamische zones konden worden gerelateerd aan de relatieve golfhoogte (H_s/h) waarbij lage relatieve golfhoogten werden gemeten in de niet-brekende zone en hoge relatieve golfhoogten in de golfploop zone. Een toename van de relatieve golfhoogte heeft tot gevolg dat de orbitale snelheden bij de bodem toenemen. De asymmetrie van de golven en van de orbitale bodemsnelheden nam toe van de niet-brekende zone tot aan de brekende zone. Door het breken van de golven neemt de asymmetrie af maar zowel de golven als de snelheden bij de bodem blijven asymmetrisch. Het breken van golven leidt bovendien tot een toename van de tijdsgemiddelde kustdwarse stroming. De golven en orbitale snelheden hadden een golfdal dat meestal meer vervormd was dan de

golftop en deze vorm kon niet worden beschreven door bestaande golftheorieën. Omdat er ook geen duidelijk empirisch (lineair) verband bestond tussen de golf- en snelheid parameters was het niet mogelijk om golf- en snelheid karakteristieken aan elkaar te relateren. Bestaande formules om de gemiddelde kustdwarse stroming ('undertow') te berekenen, die zo'n relatie vooronderstellen, bleken dan ook niet te voldoen.

Naast de hydrodynamica werd ook de *sediment concentraties en -transporten* onderzocht. Bovendien werden ook sediment transport patronen onderzocht die van belang zijn voor de morfologische ontwikkeling van de binnenste brandingsbank om een middellange termijn en waarbij gebruikt werd gemaakt van een fysisch-mathematisch model.

Omdat de sediment concentraties varieerden op de tijd schaal van de golven (6-10 s) maar ook op die van de lange golven (> 20 s) bleek er geen duidelijke relatie te bestaan tussen de snelheid bij de bodem en de concentratie. De verticale sediment uitwisseling was groot en een hoger suspensieve sediment concentratie nabij de bodem betekende ook dat het verticale concentratie profiel steiler werd. De suspensieve sediment concentraties bij de bodem namen toe met de relatieve golfhoogte en de hoogste concentraties werden daarom gemeten in de golfoploop zone.

Het netto suspensieve sediment transport kan worden verondersteld opgebouwd te zijn uit een hoogfrequent ($T < 20$ s), oscillerend, suspensief transport (HFST), een laag-frequent ($T > 20$ s), oscillerend, suspensief sediment transport (LFST) en een tijdsgemiddeld suspensief transport (TGST). Het LFST was ongeveer de helft van het HFST terwijl het totale oscillerende suspensieve transport (LFST+HFST) ongeveer half zo groot was als het TGST. Het oscillerende transport nam toe met de relatieve golfhoogte terwijl het TGST groter werd naarmate de tijdgemiddelde kustdwarse stroming groter werd. Aangezien deze laatste altijd zeewaarts gericht was, was het TGST ook altijd van de kust af gericht. De verhouding tussen het suspensieve transport en het bodem transport varieerde met een factor 100 maar het suspensieve transport was vrijwel altijd dominant. Het zeewaarts gerichte sediment transport wordt dus bepaald door de tijdgemiddelde kustdwarse stroming terwijl het landwaarts gerichte transport vermoedelijk wordt veroorzaakt door de golfasymmetrie. Deze laatste relatie kon echter niet worden bevestigd door de metingen.

Op de middellange termijn wordt het netto sediment transport in het binnenste deel van de brandingszone bepaald door de golfhoogte op diep water. Bij lage golfhoogten (< 0.5 m) was het sediment transport in de gehele brandingszone landwaarts gericht terwijl hogere golfhoogten (0.5 - 2 m) resulteerde in zones met of een zeewaarts of een landwaarts transport. Stormen, dat wil zeggen perioden met een offshore golfhoogte groter dan 2 m, resulteerde in een zeewaarts transport in binnenste deel van de brandingszone. De morfologische ontwikkeling van de binnenste brandingsbank is dus niet altijd het resultaat van een convergentie van sediment maar kan ook veroorzaakt worden door gradienten in het sediment transport.

Tenslotte werd de *morfologische ontwikkeling van banken* in het kustdwarse profiel bestudeerd en werden er *morfodynamische model berekeningen* uitgevoerd met een fysisch-mathematisch model.

De ontwikkeling van het strand, de kustlijn en de binnenste brandingsbank werd, gedurende de eerste najaarsstormen, sterk beïnvloed door sediment dat afkomstig is van een berm. Deze berm, oorspronkelijk aanwezig nabij de duinvoet, erodeerde door

de opeenvolgende stromen waarbij het geërodeerde zand werd afgezet nabij de kustlijn. Het strand werd gedurende de eerste stormen daardoor breder terwijl tijdens de latere stormen, als de berm volledig verdwenen is, de kustlijn migreerde in de richting van de duinen. Het geërodeerde strandzand droeg bij aan de ontwikkeling van de binnenste brandingsbank alhoewel een bank, gelegen vlak voor het strand, in het intergetijde gebied, dit zand tijdelijk gebruikte voor zijn eigen opbouw. De binnenste bank migreerde zeewaarts gedurende de meeste stormen en landwaarts gedurende de rustiger golfcondities. De zeewaartse migratie snelheden waren groter dan die in landwaartse richting maar het aantal dagen met storm was relatief klein zodat de netto bewegingsrichting van de bank op de middellange termijn toch landwaarts is. De binnenste bank reageert snel (binnen 1 dag) op veranderingen in de offshore golfcondities maar desondanks kon geen kwantitatieve relatie worden vastgesteld tussen offshore golf-parameters en morfologische bank-parameters. De buitenste brandingsbank was relatief stabiel en kan op de middellange termijn worden beschouwd als een vaste randvoorwaarde voor de processen in het binnenste deel van de brandingszone.

Het geteste fysisch-mathematisch model (UNIBEST-TC, Waterloopkundig Laboratorium) was in staat om een betrouwbare schatting te geven van de golfhoogte veranderingen in de brandingszone. De gemiddelde kustdwarse stroming en de morfologische ontwikkeling konden echter niet goed worden voorspeld.

Het al dan niet breken van de korte golven wordt bepaald door de golfhoogte en de aanwezigheid van banken. Het breken van korte golven is vervoglens van grote invloed op het gemiddelde stromingsbeeld in kustdwarse richting. Omdat de lokale sediment transport richting wordt bepaald door de balans tussen de golfasymmetrie en de tijdsgemiddelde kustdwarse stroming betekent dit dat het netto sediment transport richting sterk beïnvloed wordt door het breken van golven. De morfologische veranderingen in de binnenste deel van de brandingszone, inclusief de binnenste brandingsbank, worden dus bepaald door de transformatie en het breken van korte golven.

REFERENCES

- Aagaard, T., 1988. A study on nearshore bar dynamics in a low energy environment : Northern Sealand, Denmark, *Journal of Coastal Research* 4, 115-128.
- Aagaard, T., 1988. Nearshore bar morphology on the low energy coast of northern Zealand, Denmark, *Geografiska Annaler* 70A, 59-67.
- Aagaard, T., 1989. Infragravity waves and nearshore bars, Thesis, University of Copenhagen, Denmark.
- Aagaard, T., 1990. Infragravity waves and nearshore bars in protected, storm-dominated coastal environments, *Marine Geology* 94, 181-203.
- Aagaard, T., 1991. Multiple-bar Morphodynamics and it's relation to low-frequency edge waves, *Journal of Coastal Research* 7, 801-813.
- Aagaard, T. and B. Greenwood, 1994. Suspended sediment transport and the role of infragravity waves in a barred surf zone, *Marine Geology* 118, 23-48.
- Ahnert, F., 1994. Equilibrium, scale and inheritance in geomorphology, *Geomorphology* 11, 125-140.
- Allen, J.R. and N.P. Psuty, 1987. Morphodynamics of a single-barred beach with a rip channel, Fire Island, NY. *Proceedings Coastal Sediments '87*, New Orleans, ASCE, 1964-1975.
- Allen, J.R., B.O. Bauer, N.P. Psuty and R.W.G. Carter, 1991. Process variation across a barred, tidal nearshore. *Proceedings Coastal Sediments '91*, Seattle, ASCE, 498-511.
- Augustein, B., H. Daan, B. van Mourik, D. Messerschmidt and B. Zwart, 1990. Stormenkalender. Chronologisch overzicht van alle stormen (windkracht 8 en hoger) langs de Nederlandse kust voor het tijdvak 1964-1990. (Storm-calendar. Chronological summary of all storms (> windforce 8) along the Dutch coast during 1964-1990). KNMI, centrale weerdienst, de Bilt, Report publicatie 176.
- Bagnold, R.A., 1963. Beach and Nearshore processes, Part I Mechanics of Marine Sedimentation. In : Hill, M. N. (ed.), *The Sea* (3), London. Wiley Interscience, 507-553.
- Bailard, J.A. and D.L. Inman, 1981. An energetics bedload model for a plane sloping beach: Local transport, *Journal of Geophysical Research* 86, 2035-2043.
- Bailard, J.A., 1981. An energetics total load sediment transport model for a plane beach, *Journal of Geophysical Research* 86, 10938-10954.
- Bakker, R., 1995. Verifications of the Unibest-TC model, Msc. Thesis, Delft University of Technology, Department of Civil Engineering.
- Basco, D.R., 1985. A qualitative description of wave breaking, *Journal of Waterway, Port, Coastal and Ocean Engineering* 111, 171-188.
- Battjes, J.A., 1975. Surf Similarity. *Proceedings 13th Coastal Engineering Conference*, ASCE 466-88.
- Battjes, J.A. and J.P.F.M. Jansen, 1978. Energy losses and set-up due to breaking of random waves. *Proceedings 16th Coastal Engineering Conference*, ASCE, 569-587.
- Battjes, J.A., 1982. Windgolven (Windwaves). TU Delft, Faculteit Civiele Techniek, Report b78.
- Battjes, J.A. and M.J.A. Stive, 1985. Calibration and verification of a dissipation model for random breaking waves, *Journal of Geophysical Research* 90, 9159-9167.
- Battjes, J.A., 1988. Surf zone dynamics, *Annual review of Fluid Mechanics* 20, 257-293.
- Bauer, B.O. and B. Greenwood, 1990. Modification of a linear bar-through system by a standing edge wave, *Marine Geology* 92, 177-204.
- Beach, R.A. and R.W. Sternberg, 1988. Suspended sediment transport in the surf zone : response to cross-shore infragravity motion, *Marine Geology* 80, 61-79.

- Fredsøe, J. and R. Deigaard, 1992. *Mechanics of Coastal Sediment Transport*, World Scientific, Singapore.
- Galvin, C.J., 1972. Wave breaking in shallow water. In : (ed.), *Waves on beaches and resulting sediment transport*, Academic press, 413-456.
- Goldsmith, V., D. Bowman and K. Kiley, 1982. Sequential stage development of crescentic bars: Hahoterin beach, southeastern Mediterranean, *Journal of Sedimentary Petrology* 52, 233-249.
- Greenwood, B. and R.G.D. Davidson-Arnott, 1975. Marine bars and nearshore sedimentary processes, Kouchibouguac Bay, New Brunswick. In : (ed.), *Nearshore sediment dynamics and sedimentation*, Wiley and Sons, New York, 123-150.
- Greenwood, B. and R.G.D. Davidson-Arnott, 1979. Sedimentation and equilibrium in wave-formed bars: a review and case study, *Canadian Journal of Earth Sciences* 16, 313-332.
- Greenwood, B. and P.B. Hale, 1980. Depth of activity, sediment flux, and morphological change in a barred nearshore environment. In : McCann, S. B. (ed.), *The Coastline of Canada*, paper 80-10. Geological Survey of Canada, 89-109.
- Greenwood, B., 1987. Sediment balance and bar morphodynamics in a multiple bar system: Georgian Bay, Canada. *Proceedings International Geomorphology*, John Wiley & Sons Ltd, --.
- Greenwood, B., P.D. Osborne, A.J. Bowen, D.G. Hazen and A.E. Hay, 1990. Nearshore sediment flux and bottom boundary dynamics - the Canadian coastal sediment transport programme (C-Coast). *Proceedings Coastal Engineering Conference, Delft, ASCE*, 2227-2241.
- Greenwood, B. and P. Osborne, 1990. Vertical and horizontal structure in cross-shore flows: an example of undertow and wave set-up on a barred beach, *Coastal Engineering* 14, 543-580.
- Greenwood, B. and P.D. Osborne, 1991. Equilibrium slopes and cross-shore velocity asymmetries in a storm-dominated, barred nearshore system, *Marine Geology* 96, 211-235.
- Guillén, J. and A. Palanques, 1993. Longshore bar and through systems in a microtidal, storm wave dominated coast: The Ebro delta (Northwestern Mediterranean), *Marine Geology*, 115, 239-252.
- Guillén, J. and P. Hoekstra, 1996. The 'equilibrium' distribution of grain size fractions and its implication for cross-shore sediment transport: a conceptual model, *Marine Geology* 135, 15-33.
- Guza, R.T. and E.B. Thornton, 1981. Wave set-up on a natural beach, *Journal of Geophysical Research* 86, 4133-4137.
- Guza, R.T. and E.B. Thornton, 1982. Swash oscillation on a natural beach, *Journal of Geophysical research* 87, 483-491.
- Guza, R.T. and E.B. Thornton, 1985. Velocity moment in nearshore, *Journal of Waterway, Port, Coastal and Ocean Engineering* 111, 235-256.
- Hallermeier, R.J., 1982. Oscillatory bedload transport: Data review and simple formulation, *Continental Shelf research* 1, 159-190.
- Hamm, L., P.A. Madsen and D. Howell Peregrine, 1993. Wave transformation in the nearshore zone: a review, *Coastal Engineering* 21, 5-39.
- Hanes, D.M. and D.A. Huntley, 1986. Continuous measurement of suspended sand concentration in a wave dominated nearshore environment, *Continental Shelf Research* 6, 585-596.
- Hanes, D.M., 1988. Intermittent sediment suspension and its implications for sand tracer dispersal in wave-dominated environments, *Marine Geology* 81, 175-183.
- Hanes, D.M., 1991. Suspension of sand due to wave groups, *Journal of Geophysical Research* 96, 8911-8915.

- Hattori, M. and R. Kawamata, 1981. Onshore-Offshore transport and beach profile change. *Proceedings 17th Coastal Engineering Conference*, Sydney, Australia, ASCE, 1175-1193.
- Hayes, M.O., 1972. Forms of sediment accumulation in the beach zone. In : Meyer, R. E. (ed.), *Waves on Beaches*, Academic Press, New York, N. Y., 297-356.
- Hazen, D.G., B. Greenwood and A.J. Bowen, 1990. Nearshore current patterns on barred beaches. *Proceedings Coastal Engineering Conference*, Delft, ASCE, 2061-2073.
- Hoekstra, P., K.T. Houwman, A. Kroon, P. van Vessem and B.G. Ruessink, 1994. The Nourtec experiment of Terschelling: Process-oriented monitoring of a shoreface nourishment. *Proceedings Coastal Dynamics 1994*, Barcelona, ASCE, 402-416.
- Hoekstra, P. and K.T. Houwman, 1994. Hydrodynamic processes on the lower shoreface of the Dutch coast. *Proceedings Coastal Dynamics 1994*, Barcelona, ASCE, 852-866.
- Hoekstra, P., K.T. Houwman, A. Kroon and B.G. Ruessink, 1996. *Morphodynamic Behaviour of the Terschelling Shoreface Nourishment*. Institute for Marine and Atmospheric Research, Report R 96.14.
- Holman, R.A., 1981. Infragravity energy in the surf zone, *Journal of Geophysical Research* 86, 6442-6450.
- Holman, R.A. and A.J. Bowen, 1982. Bars, bumps and holes : Models for the generation of complex beach geomorphology, *Journal of Geophysical Research* 87, 457-468.
- Holman, R.A. and A.H. Sallenger, 1993. Sand Bar Generation: A discussion of the Duck Experiment Series, *Journal of Coastal Research*, Special Issue no. 15, 76-92.
- Horikawa, K., 1988. *Nearshore dynamics and coastal processes*, University of Tokio Press, Tokio.
- Hotta, S. and M. Mizuguchi, 1980. A Field study of waves in the surf zone. In : (ed.), *Coastal Engineering in Japan*, 23. Japan Society of Civil Engineers, Tokyo.
- Houwing, E.J., 1991. Analyse van TAW-profielen, Egmond aan Zee, Katwijk aan Zee. (Analysis of TAW-profiles, Egmond aan Zee, Katwijk aan Zee). Utrecht University, Dept. Physical Geography, Report GEOPRO-1991.09.
- Houwman, K. and P. Hoekstra, 1994. Shoreface Hydrodynamics, Part I field measurements Egmond aan Zee. Institute for Marine and Atmospheric Research, Utrecht University, Report R 94-2.
- Houwman, K.T. and G. Ruessink, in prep. Cross-shore sediment transport mechanisms in the surf zone. *Proceedings 25th International Conference on Coastal Engineering*, Orlando.
- Howd, P.A. and W.A. Birkemeier, 1987. Beach and nearshore survey data: 1981-1984. CERC Field Research Facility, Technical Report CERC-87-9.
- Huntley, D.A. and A.J. Bowen, 1975. Comparison of the Hydrodynamics of steep and shallow beaches. In : Hail, J. and Carr, A. (ed.), *Nearshore sediment dynamics and sedimentation*, Wiley and Sons, London, 69-109.
- Huntley, D.A., 1976. Long-period waves on a natural beach, *Journal of Geophysical Research* 81, 6441-6449.
- Huntley, D.A., R.T. Guza and E.B. Thornton, 1981. Field observations of surf beat 1: Progressive Edge waves., *Journal of Geophysical Research* 85, 6451-6466.
- Huntley, D.A. and D.M. Hanes, 1987. Direct measurements of suspended sediment transport. *Proceedings Coastal Sediments '87*, New Orleans, LA, ASCE, 723-737.
- Jaffe, B.E., R.W. Sternberg and A.H. Sallenger, 1984. The role of suspended sediment in shore normal beach profile changes. *Proceedings Coastal Engineering Conference*, Houston, USA, ASCE, 1983-1996.
- Jaffe, B.E., D.M. Rubin and A. Sallenger, 1994. How much velocity information is necessary to predict sediment suspension in the surf zone. *Proceedings 24th Coastal Engineering Conference*, Kobe, Japan, ASCE, 2085-2099.

- Rienecker, M.M. and J.D. Fenton, 1981. A Fourier approximation method for steady water waves, *Journal of Fluid mechanics* 104, 119-137.
- Roelvink, J.A., 1987. Large-scale investigation of cross-shore sediment transport. Delft Hydraulics, Delft, The Netherlands, Report H596.
- Roelvink, J.A. and M.J.F. Stive, 1989. Bar-Generating cross-shore flow mechanisms on a beach, *Journal of Geophysical Research* 94, 4785-4800.
- Roelvink, J.A., T.J.G.P. Meijer, K. Houwman, R. Bakker and R. Spanhoff, 1996. Field validation and application of a coastal profile model. *Proceedings Coastal Dynamics, ASCE*, 818-828.
- Roskam, A.P., 1988. Golfklimaten voor de Nederlandse kust. Rijkswaterstaat, Report GWA0 88.046.
- Ruessink, B.G. and A. Kroon, 1994. The behaviour of a multiple bar system in the nearshore zone of Terschelling, the Netherlands: 1965-1993, *Marine Geology* 121, 187-197.
- Ruessink, B.G., M.G. Kleinhan and P.G.L. Van den Beukel, submitted to *Journal of Coastal Research*. Observations of swash under highly dissipative conditions.
- Rusell, P.E., 1993. Mechanisms for beach erosion during storms, *Continental Shelf Research* 13, 1243-1265.
- Sallenger, A.H., R.A. Holman and W.A. Birkemeier, 1985. Storm-induced response of a nearshore-bar system, *Marine Geology* 64, 237-257.
- Sallenger, A.H. and R.A. Holman, 1985. Wave energy saturation on a natural beach of variable slope, *Journal of Geophysical Research* 90, 11939-11944.
- Sallenger, A.H. and R.A. Holman, 1987. Infragravity waves over a natural barred profile, *Journal of Geophysical Research* 92, 9531-9540.
- Sallenger, A.H. and P.A. Howd, 1989. Nearshore bars and the break-point hypothesis, *Coastal Engineering* 12, 301-313.
- Sanchez-Arcilla, A., J.A. Roelvink, B.A. O'Connor, A. Reniers and J.A. Jimenez, 1994. The Delta Flume '93 Experiment. *Proceedings Coastal Dynamics, ASCE*, 448-502.
- Sand, S.E., 1982. Long waves problems in laboratory models, *Journal of Waterways, Port and Coastal Engineering* 108, 492-503.
- Savage, R.J. and W.A. Birkemeier, 1987. Storm erosion data from the United States Atlantic Coast. *Proceedings Coastal Sediments 1987, New Orleans, ASCE*, 1445-1459.
- Seymour, R.J. and D.G. Aubrey, 1987. Beach morphology observations during NSTS. *Proceedings Coastal Sediments '87, New Orleans, ASCE*, 668-681.
- Shepard, F.P., 1950. Longshore-bars and longshore troughs. In : Schwarz, M. L. (ed.), *Spits and bars*, Dowden, Hutchinson & Ross, Inc., Stroudsburg, Pennsylvania, 1-31.
- Shepard, F.P. and D.L. Inman, 1950. Nearshore circulation related to bottom topography and wave refraction. *Transactions American Geophysical Union* 31, 555-565.
- Sherman, D.J. and B.O. Bauer, 1993. Coastal Geomorphology through the looking glass, *Geomorphology* 7, 225-249.
- Shi, N.C. and L.H. Larsen, 1984. Reverse sediment transport induced by amplitude modulated waves, *Marine Geology* 54, 181-200.
- Shore Protection Manual, 1984. 4th ed., US Army Engineer Waterways Experiment Station, Coastal Engineering Research Center, US Government Printing Office, Washington, DC,
- Short, A.D., 1975. Multiple offshore bars and standing waves, *Journal of Geophysical Research* 80, 3838-3840.
- Short, A., 1979. Three dimensional beach state model, *Journal of Geology* 87, 553-571.
- Short, A.D., 1985. Rip-current type, spacing and persistence, Narrabeen beach, Australia, *Marine Geology* 65, 47-71.

- Short, A.D., 1991. Beach morphodynamic systems of the central Netherlands coast, Den Helder to Hoek van Holland. Rijksuniversiteit Utrecht, vakgroep fysische geografie, Report GEOPRO 1991.01.
- Short, A.D., 1992. Beach systems of the central Netherlands coast : Processes, morphology and structural impacts in a storm driven multi-bar system, *Marine Geology* 107, 103-137.
- Short, A.D. and T. Aagaard, 1993. Single and Multi-bar Beach Change Models, *Journal of Coastal Research*, Special Issue no. 15, 141-157.
- Soulsby, R.L., L. Hamm, G. Klopman, D. Myrhaug, R.R. Simons and G.P. Thomas, 1993. Wave current interaction within and outside the bottom boundary layer, *Coastal Engineering* 21, 41-69.
- Sternberg, R.W., N.C. Shi and J.P. Downing, 1984. Field investigations of suspended sediment in the nearshore zone. *Proceedings 19th Coastal Engineering Conference*, Houston, Texas, ASCE, 1782-1798.
- Sternberg, R.W., N.C. Shi and J.P. Downing, 1989. Suspended sediment measurements. A. Continuous measurements of suspended sediment. In : Seymour, R. J. (ed.), *Nearshore sediment transport*, Plenum, New York, 231-257.
- Stive, M.J.F. and H.G. Wind, 1986. Cross-shore mean flow in the surf zone, *Coastal Engineering* 10, 325-340.
- Stokes, G.G., 1847. On the theory of oscillatory waves, *Transactions of the Cambridge Philosophical Society* 8, 441-455.
- Stolk, A., 1989. Zandsysteem Kust, een morfologische karakterisering (Sandsystem Coast, a morphological characterisation). Rijksuniversiteit Utrecht, Vakgroep Fysische Geografie, Report GEOPRO 1989.02.
- Stolk, A., 1991. TAW profielen : Selectie- en Analyse-methoden (TAW-profiles : Methods for selection and analysis). Department Physical Geography Utrecht University, Report GEOPRO 1991.027.
- Sunamura, T. and K. Horikawa, 1974. Two dimensional beach transformation due to waves. *Proceedings 14th international Conference on Coastal Engineering*, 920-938.
- Sunamura, T. and I. Takeda, 1984. Landward migration of inner bars, *Marine Geology* 60, 63-78.
- Sunamura, T., 1985. Predictive relationships for position and size of longshore bars. *Proceedings 31st Japanese Conference on Coastal Engineering*, JSCE, 316-320 (in Japanese).
- Sunamura, T. and K. Maruyama, 1987. Wave-induced geomorphic response of eroding beaches- with special reference to seaward migrating bars. *Proceedings Coastal Sediments '87*, New Orleans, LA, 789-801.
- Sunamura, T. and I. Takeda, 1993. Bar movement and shoreline change: Predictive relations, *Journal of Coastal Research*, S.I. 15, 125-140.
- Svendsen, I.A., 1984. Mass flux and undertow in a surf zone, *Coastal Engineering* 8, 347-365.
- Swart, D.H. and J.B. Crowley, 1990. Time and Frequency domain analysis of shallow water waves on a slope. *Proceedings 21st Coastal Engineering Conference*, Delft, the Netherlands, ASCE, 293-305.
- Takeda, I. and T. Sunamura, 1992. Conditions for beach erosion on a barred beach, *Zeitschrift für Geomorphologie* 36, 453-464.
- Thornton, E.B., R.T. Humiston and W. Birkemeier, 1996. Bar/trough generation on a natural beach, *Journal of Geophysical Research*, 101, 12097-12110.
- Van Alphen, J., 1987. the morphology and lithology of the surf zone between Terheide and Egmond aan Zee (in Dutch). Rijkswaterstaat, Notitie NZ-N-87.28.
- Van Bemmelen, C.E., 1988. De Korrelgrootte-samenstelling van het strandzand langs de Nederlandse kust (the sediment size distribution of beach sand along the Dutch

- coast). Rijkswaterstaat, dienst getijdewateren/Utrecht University, department physical geography,
- Van de Graaff, J., 1988. Sediment Concentration due to wave action, Ph. D. Thesis, Delft University of Technology.
- Van de Meene, J.W.H., 1994. The Shoreface connected ridges along the central Dutch coast, Ph. D. Thesis, Utrecht University.
- Van den Berg, J.H., 1977. Morphodynamic development and preservation of physical sedimentary structures in two prograding recent ridge and runnel beaches along the Dutch coast, *Geologie en Mijnbouw*, 56, 185-202.
- Van der Lee, W., 1994. The Measurement of Bedload Sand Transport and Concentration Under Waves Using a Bedload Sampler and a Conductivity Concentration Meter (CCM). Institute for Marine and Atmospheric Research Utrecht (IMAU), Utrecht University, Report V 94-4.
- Van der Velden, E.T.J.M., 1993. Ontgroningen rond pijpleidingen op slibhoudend zand (erosion near pipelines on sand-mud mixtures). Delft University of Technology, Department Coastal Engineering.
- Van Rijn, L., 1984. Sediment transport, Part II: Suspended load transport, *Journal of Hydraulic Engineering*, 110, 1613-1641.
- Van Rijn, L., 1990. Principles of fluid flow and surface waves in rivers, estuaries, seas and oceans, first edition, Aqua Publications, Amsterdam.
- Van Rijn, L.C., M. Nieuwjaar W.C., T. Van der Kaay, E. Nap and A. Van Kampen, 1993. Transport of fine sands by currents and waves, *Journal of Waterways, Port, Coastal and Ocean Engineering*, 119,
- Van Rijn, L.C., 1993. Principles of Sediment Transport in Rivers, Estuaries and Coastal Seas, Aqua Publications, Amsterdam.
- Van Rijn, L.C. and A. Kroon, 1993. Sediment Transport by Waves and Currents. Proceedings 22nd Coastal Engineering Conference, Venice, Italy,
- Van Vessem, P., 1989. Indeling Hollandse kust in erosie en sedimentatie gebieden (classification of the Holland coast in areas of erosion and sedimentation). Rijkswaterstaat, dienst getijdewateren.
- Wiersma, J. and J.S.L.J. van Alphen, 1988. The Morphology of the Dutch shoreface between Hook of Holland and Den Helder, the Netherlands. In : de Boer, P. L., van Gelder, A. and Nio, S. D. (ed.), *Tide-Influenced Sedimentary Environments and Facies*, D. Reidel Publishing Co., 101-111.
- Wijnberg, K.M. and F.C.J. Wolf, 1994. Three Dimensional behaviour of a nearshore bar system. Proceedings Coastal Dynamics, Barcelona, ASCE, 59-73.
- Wijnberg, K.M., 1995. Morphologic behaviour of a barred coast over a period of decades, Ph. D. Thesis, Utrecht University.
- Wijnberg, K.M. and J.H.J. Terwindt, 1995. Extracting decadal behaviour from high-resolution, long-term bathymetric surveys along the Holland coast using eigenfunction analysis, *Marine Geology*, 126, 301-330.
- Wolf, F.C.J., 1991. Evaluation field test (April 1991) Sub Aquatic Profiler (SAP) Egmond aan Zee, the Netherlands. Department Physical Geography, University of Utrecht, The Netherlands, Technical Report GEOPRO 1991.14.
- Wolf, F.C.J., 1992. Field measurements Egmond aan Zee, Fall 1991. Data summary morphological measurements. Institute for Marine and Atmospheric Research (IMAU), Department Physical Geography, University of Utrecht, The Netherlands, Report
- Wolf, F.C.J., 1993. Data summary field measurements Egmond aan Zee, September-November 1992 (4 Volumes). Institute for Marine and Atmospheric Research (IMAU), Department Physical Geography, University of Utrecht, The Netherlands, Report
- Wright, L.D. and A.D. Short, 1984. Morphodynamic variability of surf zones and beaches: a synthesis, *Marine Geology*, 56, 93-118.

- Wright, L.D., J.D. Boon, S.C. Kim and J.H. List, 1991. Modes of cross-shore sediment transport on the shoreface of the Middle Atlantic Bight, *Marine Geology*, 96, 19-51.
- Yu, Y., R.W. Sternberg and R.A. Beach, 1993. Kinematics of breaking waves and associated suspended sediment in the nearshore zone, *Continental Shelf Research*, 13, 1219-1242.
- Zampol, J.A. and D.L. Inman, 1989. Suspended sediment measurements. In : Seymour, R.J. (ed.), *Nearshore Sediment Transport*, Plenum Press, New York, 387-401.

APPENDIX A

SHORT DESCRIPTION OF UNIBEST-TC MODEL

A complete description of the UNIBEST-TC model is given in Delft Hydraulics (1996) and Bakker (1995). This appendix gives a brief overview of the physics that are of importance for the validation of the model.

The model assumes that the coast is uniform in the longshore direction. The wave model of UNIBEST-TC consists of three different equations describing the wave energy balance (Battjes and Janssen, 1978), the roller energy balance (Nairn et al., 1990) and the momentum balance equation. The wave energy balance, for waves incident perpendicular to a the coast can be written as.

$$\frac{\partial P_x}{\partial x} + D = 0 \quad (\text{A.1})$$

with: P_x = x component of the time-mean energy flux per unit length
 x = a horizontal co-ordinate, normal to the still water line
 D = time-mean dissipated power per unit area (= D_w [A.2] + D_r [A.6])

The energy dissipation for *breaking* waves is given by:

$$D_w = \frac{1}{4} \rho g \alpha f_p H_{\max}^2 Q_b \quad (\text{A.2})$$

with:

g = gravitational acceleration
 ρ = density of water
 f_p = spectral peak frequency
 α = constant of order one
 H_{\max} = maximum wave height
 Q_b = fraction of breaking waves

The maximum wave height is calculated using:

$$H_{\max} = \frac{0.88}{k} \tanh\left(\frac{\gamma k h}{0.88}\right) \quad (\text{A.3})$$

with:

k = wave number
 h = water depth
 γ = breaker index

γ controls the breaking of the waves and therefore the fraction of breaking waves (Q_b). In the UNIBEST-TC model γ is a fixed value or may be calculated using the relation with the deep water wave steepness (s_0) (Battjes, and Stive, 1985):

$$\gamma = 0.5 + 0.4 \tanh(33s_0) \quad (\text{A.4})$$

with:

$$s_0 = \frac{H_{\max,0}}{L_0}$$

in which $L_0 = \frac{g}{(2\pi f_p)^2}$ = deep water wave length

$H_{rms,0}$ = deep water root mean square wave height

The fraction of breaking waves is calculated by assuming that this fraction at any point is related to the quotient of the root mean square wave height (H_{rms}) and the maximum wave height (H_{max}).

$$\frac{1 - Q_b}{\ln Q_b} = - \left(\frac{H_{rms}}{H_{max}} \right)^2 \quad (A.5)$$

with:

Q_b = fraction of breaking waves

The mean energy dissipation due to bottom friction is calculated with:

$$D_f = \frac{1}{8} \rho f_w \pi^{-1/2} \left(\frac{\omega_p H_{rms}}{\sinh(kh)} \right)^3 \quad (A.6)$$

with:

f_w = bottom friction factor

ω_p = peak frequency

With equations A.1-A.6 it is possible to obtain a cross-shore distribution of the wave heights.

In UNIBEST-TC, the vertical velocity distribution due to wave height, wave set-up and dissipation is computed using the eddy viscosity, i.e. the relation between the shear stress and the velocity gradient:

$$\tau = \frac{\rho \nu}{h} \frac{\partial u}{\partial z} \quad (A.7)$$

τ = shear stress

ν = viscosity

u = velocity

z = elevation above the bed

In order to calculate the depth averaged eddy viscosity a three layer eddy viscosity model is used which is based on earlier work of De Vriend and Stive (1987), Svendsen (1985, in Bakker, 1985), Stive and Wind (1986) and Battjes (1975). The depth averaged viscosity is derived by combining the effects of slope driven currents, wind driven currents and a wave breaking induced turbulence. The computation of the shear stress includes the effect of wind and streaming.

The near bed orbital velocity due to non-linear short waves and bound long waves, is based on a concept of Roelvink and Stive (1989). For the non-linear short waves, the near bed orbital velocity is calculated using Rienecker and Fenton's (1981) model. This model, originally for non-breaking monochromatic waves is adapted whereby the mean wave energy and the peak period are used as input for random waves. In case

of breaking waves, the asymmetry is reduced as function of the fraction of breaking waves. The contribution due to bound long waves is based on Sand (1982) and an empirical relationship for the computation of the phase of the bound wave relative to the short wave envelope.

Both velocity models are used to calculate the sediment transport rates. The sediment transport is divided in a suspended- and a bedload sediment transport and are calculated according to the model Van Rijn (Van Rijn, 1993).

Parameter	input file name	value
transport at shoreward boundary	(JCLOSE)	0 (no transport)
relative wave period	(TDR)	40
wave breaking delay (if on)	(KEY-NAIJL)	1
integration length	(F-LAM)	2
weighting function	(POW)	1
internal friction at location 1	(TANPHI1)	0.3
internal friction at location 2	(TANPHI2)	0.63
location 1	(XF1)	0
location 2	(XF2)	200
viscosity coefficient velocity profile	(FACVISC)	0.1
wave breaking parameter	(GAMMA)	0.55
wave breaking parameter	(ALFAC)	1
friction factor for wave dissipation due to bottom friction	(FWEE)	0.01
friction factor for mean current computation	(RKVAL)	
reference depth for tidal velocity	(DIEPV)	3.05
layer in which sediment transport is reduced to zero (fixed bed)	(REMLAAG)	0
factor used in roller formulation, expressing the steepness of the wave front	(BETD)	0.1
D_{50} grain diameter [m]	(D50)	0.000284
D_{90} grain diameter [m]	(D90)	0.000429
D_{50} grain diameter of the suspended sediment [m]	(DSS)	0.000227
current related roughness for sediment transport computation [m]	(RC)	0.01
wave related roughness for sediment transport computation [m]	(RW)	0.002
density gradient in x-direction [kgm^{-3}m]	(DRHODX)	0.0
density gradient in y-direction [kgm^{-3}m]	(DRHODY)	0.0

temperature of the water	(TEMP)	14
salinity of the water [0/00]	(SALIN)	31
correlation coefficient between wave envelope and bound long waves	(C_R)	0.25

CURRICULUM VITAE



Felix Wolf was born on February, 7th 1962 in Arnhem, the Netherlands. He attended primary and secondary education in his beautiful home-town Arnhem. He graduated on two types of secondary schools: on HAVO in 1980 and on VWO in 1982 at the Katholiek Gelders Lyceum.

After the secondary education, he went to the Senior Nautical College in Amsterdam to follow a four year course for hydrographic surveyor. As part of the course he worked, in 1984-1985 for the Dutch Oil Company (NAM) and the Eastern Scheldt Storm Surge Barrier Building Company (DOSBOUW). During these trainee-periods, he executed land-based and hydrographic surveys in construction-docks, on offshore production-platforms and from a number of survey vessels. In 1986, he graduated at the Senior Nautical College and was specialised in maritime meteorology and oceanography, hydrographic surveying, hydrographic measuring systems, land surveying and informatics.

In September 1986, Felix started the study Physical Geography at the Utrecht University. He specialised in physical-geographical processes of coastal and riverain areas with examination in e.g. morphodynamic systems in rivers and coasts, fluid-mechanics and Geographical Information Systems (GIS). During a trainee-period at Delft Hydraulics he executed sediment-transport measurements in the river Nile, Egypt. His M.Sc. thesis dealt with eolian and hydraulic processes related to coastal erosion for which he executed two field studies in the Carmargue (Rhône-delta, France). He earned his 'drs' (~M.Sc.) degree in August 1990.

In May 1990, he got a position as a Ph.D. -fellow at the department Physical Geography at the Utrecht University. He focused on the research described in this thesis. Besides, he gave lectures and supervised undergraduate students. In May 1994 he was appointed associated researcher at the same department.

Besides his Ph.D.-research, Felix tried to be busy with computers (mainly games and the Internet), squash, scuba-diving, skiing, speed-cycling and drinking wit beer with taco chips.

available titles

- 1 G MIK & J H STIKKELBROEK Verkiezingen in Rotterdam -- Amsterdam/Rotterdam 1985: Knag/Economisch-Geografisch Instituut Erasmus Universiteit Rotterdam. 130 pp, 51 figs, 8 tabs. ISBN 90-6809-009-7 Dfl 17,50
- 2 S MUSTERD Verschillende structuren en ontwikkelingen van woongebieden in Tilburg -- Amsterdam 1985: Knag/Geografisch en Planologisch Instituut VU. 292 pp, 104 figs, 44 tabs. ISBN 90-6809-010-0 Dfl 27,75
- 3 M J TITUS Urbanisatie, integratie en demografische respons in Jakarta -- Amsterdam/Utrecht 1985: Knag/Geografisch Instituut Rijksuniversiteit Utrecht. 380 pp, 14 figs, 202 tabs. ISBN 90-6809-012-7 Dfl 39,50
- 4 H SCHENK Views on Alleppey -- Amsterdam 1986: Knag/Instituut voor Sociale Geografie Universiteit van Amsterdam. 246 pp, 41 figs, 36 tabs. ISBN 90-6809-011-9 Dfl 29,50
- 5 P J BOELHOUWER & F M DIELEMAN (red) Wonen in de stad -- Amsterdam/Utrecht 1986: Knag/Geografisch Instituut Rijksuniversiteit Utrecht. 138 pp, 41 figs, 32 tabs. ISBN 90-6809-013-5 Dfl 19,50
- 7 P P P HUIGEN Binnen of buiten bereik? Een sociaal-geografisch onderzoek in ZW-Friesland -- Amsterdam/ Utrecht 1986: Knag/Geografisch Instituut Universiteit Utrecht. 276 pp, 58 figs, 72 tabs. ISBN 90-6809-014-3 Dfl 34,00
- 8 V M VAN DALEN & L VAN DER LAAN (red) Werken aan de kust; verslag van het Knag-symposium over de plannen tot uitbreiding van de Ned. kust -- Amsterdam 1986: Knag. 78 pp, 8 figs, 2 tabs. ISBN 90-6809-016-X Dfl 14,00
- 9 H KNIPPENBERG Deelname aan het lager onderwijs in Nederland gedurende de 19e eeuw -- Amsterdam 1986: Knag/Instituut Sociale Geografie Universiteit Amsterdam. 268 pp, 29 fig, 81 tab. ISBN 90-6809-017-8 Dfl 29,00
- 11 M DE SMIDT (red) Regionale statistiek: organisatie en onderzoek -- Amsterdam/Utrecht 1986: Knag/Geografisch Instituut Rijksuniversiteit Utrecht. 86 pp, 17 figs, 9 tabs. ISBN 90-6809-020-8 Dfl 14,95
- 13 J J HARTS & L HINGSTMAN Verhuizingen op een rij -- Amsterdam/Utrecht 1986: Knag/Geografisch Instituut Rijksuniversiteit Utrecht. 312 pp, 54 figs, 108 tabs. ISBN 90-6809-022-4 Dfl 38,50
- 14 A VAN SCHAIK Colonial control and peasant resources in Java -- Amsterdam 1986: Knag/Instituut voor Sociale Geografie Universiteit van Amsterdam. 214 pp, 14 figs, 31 tabs. ISBN 90-6809-021-6 Dfl 27,00
- 16 J G BORCHERT, L S BOURNE & R SINCLAIR (eds) Urban Systems in Transition -- Amsterdam/Utrecht 1986: Knag/Geografisch Instituut Rijksuniversiteit Utrecht. 248 pp, 41 figs, 48 tabs. ISBN 90-6809-028-3 Dfl 24,90
- 17 P W BLAUW Suburbanisatie en sociale contacten -- Amsterdam/Rotterdam 1986: Knag/Faculteit der Economische Wetenschappen Erasmus Universiteit Rotterdam. 168 pp, 68 tabs. ISBN 90-6809-024-0 Dfl 25,00
- 18 H J SCHOLTEN, R J VAN DE VELDE & P PADDING Doorstroming op de Nederlandse woningmarkt; geanalyseerd en gemodelleerd -- Amsterdam/Utrecht 1986: Knag/Geografisch Instituut Rijksuniversiteit Utrecht. 116 pp, 38 figs, 22 tabs. ISBN 90-6809-025-9 Dfl 13,00
- 20 E VOS, M NIEUWENHUIS, M HOOGENDOORN & A SENDERS Vele handen; vrouw en werk in Latijns Amerika -- Amsterdam 1986: Knag/Geografisch en Planologisch Instituut VU. 210 pp, 9 figs, 7 tabs. ISBN 90-6809-027-5 Dfl 30,00
- 21 J H J VAN DINTEREN & H W TER HART (red) Geografie en kantoren 1985 -- Amsterdam/Nijmegen 1986: Knag/Geografisch en Planologisch Instituut Katholieke Universiteit. 144 pp, 15 fig, 15 tabs. ISBN 90-6809-029-1 Dfl 17,00
- 22 J VIJGEN, R VAN ENGELSDORP GASTELAARS Stedelijke bevolkingscategorieën in opkomst; stijlen en strategieën in het alledaagse bestaan -- Amsterdam 1986: Knag/Instituut voor Sociale Geografie Universiteit van Amsterdam. 122 pp, 3 figs, 40 tabs. ISBN 90-6809-031-3 Dfl 15,00
- 24 P HENDRIKS De relationele definitie van begrippen -- Amsterdam/Nijmegen 1986: Knag/Geografisch en Planologisch Instituut Katholieke Universiteit Nijmegen. 282 pp, 28 figs, 7 tabs. ISBN 90-6809-033-X Dfl 30,00
- 25 J M G KLEINPENNING (ed) Competition for rural and urban space in Latin America; its consequences for low income groups -- Amsterdam/Nijmegen 1986: Knag/Geografisch en Planologisch Instituut Katholieke Universiteit Nijmegen. 178 pp, 36 figs, 11 tabs. ISBN 90-6809-034-8 Dfl 22,50
- 26 J BUURSINK & E WEVER (red) Regio en ontwikkeling -- Amsterdam/Nijmegen 1986: Knag/Geografisch-Planologisch Instituut Katholieke Universiteit Nijmegen. 160 pp, 41 figs, 50 tabs. ISBN 90-6809-035-6 Dfl 20,00
- 27 G CLARK, P DOSTAL & F THISSEN (eds) Rural research and planning: the Netherlands and Great Britain -- Amsterdam 1987: Knag/Instituut voor Sociale Geografie Universiteit van Amsterdam. 88 pp, 6 figs, 4 tabs. ISBN 90-6809-037-2 Dfl 10,00
- 28 W M KARREMAN & M DE SMIDT (red) Redevoeringen en kleine geschriften van Prof A C de Voors -- Amsterdam/Utrecht 1987: Knag/Geografisch Instituut Rijksuniversiteit Utrecht. 156 pp, 8 figs, 5 tabs. ISBN 90-6809-036-4 Dfl 21,70
- 29 G PEPPERKAMP (red) Mens en milieu in de derde wereld -- Amsterdam/Nijmegen 1987: Knag/Geografisch en Planologisch Instituut Katholieke Universiteit Nijmegen. 146 pp, 17 figs, 11 tabs. ISBN 90-6809-038-0 Dfl 20,00
- 31 W J VAN DEN BREMEN & P H PELLENBURG (red) Het geografisch plechtanker: eenheid in verscheidenheid. Liber amicorum Rob Tamsma -- Amsterdam/Groningen 1987: Knag/Geografisch Instituut Rijksuniversiteit Groningen. 336 pp, 58 figs, 22 tabs. ISBN 90-6809-040-2 Dfl 35,00
- 32 G MIK Segregatie in het grootstedelijk milieu -- Amsterdam/Rotterdam 1987: Knag/Economisch-Geografisch Instituut Erasmus Universiteit Rotterdam. 252 pp, 48 figs, 45 tabs. ISBN 90-6809-041-0 Dfl 25,00
- 33 H J M GOVERDE Macht over de Markerruimte -- Amsterdam/Nijmegen 1987: Knag/Geografisch en Planologisch Instituut Katholieke Universiteit Nijmegen. 480 pp, 26 figs, 22 tabs. ISBN 90-6809-042-9 Dfl 57,50
- 35 R TER BRUGGE & E WEVER (red) Energiebeleid; het Nederlandse energiebeleid in ruimtelijk perspectief -- Amsterdam/Groningen/Nijmegen 1987: Knag/Geografisch Instituut Rijksuniversiteit Groningen/Geografisch en Planologisch Instituut Katholieke Universiteit. 132 pp, 21 figs, 18 tabs. ISBN 90-6809-044-5 Dfl 18,00
- 36 J A VAN DER SCHEE Kijk op kaarten -- Amsterdam 1987: Knag/Geografisch en Planologisch Instituut van de Vrije Universiteit Amsterdam. 312 pp, 42 figs, 58 tabs. ISBN 90-6809-045-3 Dfl 39,50
- 37 O VERKOREN & J VAN WEESEP (eds) Spatial mobility and urban change -- Amsterdam/Utrecht 1987: Knag/Geografisch Instituut Rijksuniversiteit Utrecht. 180 pp, 17 figs, 45 tabs. ISBN 90-6809-051-8 Dfl 24,75
- 38 M W DE JONG New economic activities and regional dynamics -- Amsterdam 1987: Knag/Economisch-Geografisch Instituut Universiteit van Amsterdam. 200 pp, 26 figs, 27 tabs. ISBN 90-6809-046-1 Dfl 29,00

- 39 A C M JANSEN Bier in Nederland en België; een geografie van de smaak -- Amsterdam 1987: Knag/Economisch-Geografisch Instituut Universiteit van Amsterdam. 282 pp, 14 figs, 7 tabs. ISBN 90-6809-047-X Dfl 37,50
- 40 Y C J BROUWERS, M C DEURLOO & L DE KLERK Selectieve verhuisbewegingen en segregatie; de invloed van de etnische samenstelling van de woonomgeving op verhuisgedrag -- Amsterdam 1987: Knag/Instituut voor Sociale Geografie Universiteit van Amsterdam. 112 pp, 9 figs, 22 tabs. ISBN 90-6809-048-8 Dfl 16,00
- 41 R J SCHOUW & F M DIELEMAN Echtheid en woningmarkt -- Amsterdam/Utrecht 1987: Knag/Geografisch Instituut Rijksuniversiteit Utrecht. 98 pp, 8 figs, 21 tabs. ISBN 90-6809-049-6 Dfl 14,95
- 42 J G GROENENDIJK De positie van dorpen in het beleid van Nederlandse plattelandsgemeenten -- Amsterdam 1987: Knag/Instituut Sociale Geografie Universiteit Amsterdam. 314 pp, 22 fig, 55 tab ISBN 90-6809-050-X Dfl 31,50
- 44 J J M ANGENET & A BONGENAAR (eds) Planning without a passport: the future of European spatial planning -- Amsterdam 1987: Knag/Siswo. 184 pp, 26 figs, 7 tabs. ISBN 90-6809-053-4 Dfl 24,90
- 45 R C VAN DER MARK, A H PERRELS & J J REYNDERS Kansen voor het Noorden; een beleidsstrategisch onderzoek naar nieuwe technologie -- Amsterdam/Utrecht 1987: Knag/Geografisch Instituut Rijksuniversiteit Utrecht/Economische Faculteit Vrije Universiteit Amsterdam. 168 pp, 54 figs, 41 tabs. ISBN 90-6809-054-2 Dfl 22,50
- 47 C CORTIE Alkmaar, van streekcentrum naar groeikern -- Amsterdam 1987: Knag/Instituut voor Sociale Geografie Universiteit van Amsterdam. 204 pp, 28 figs, 39 tabs. ISBN 90-6809-056-9 Dfl 25,00
- 49 T DIETZ Pastoralists in Dire Straits; survival strategies and external interventions in a semi-arid region -- Amsterdam 1987: Knag/Instituut voor Sociale Geografie Universiteit van Amsterdam. 332 pp, 34 figs, 66 tabs. ISBN 90-6809-057-7 Dfl 43,00
- 50 F J J H VAN HOORN Onder anderen; effecten van de vestiging van Meditranen in naoorlogse wijken -- Amsterdam/Utrecht 1987: Knag/Geografisch Instituut Rijksuniversiteit Utrecht. 226 pp, 36 figs, 55 tabs. ISBN 90-6809-060-7 Dfl 29,70
- 51 M J DIJST & C CORTIE Universiteit en revitalisering -- Amsterdam 1987: Knag/Instituut voor Sociale Geografie Universiteit van Amsterdam. 140 pp, 6 figs, 13 tabs. ISBN 90-6809-058-5 Dfl 17,00
- 52 Planologie als kleurbeplanning; de rol van toonaangevende instellingen en bedrijven op de ontwikkeling van de Amsterdamse Museum- en Concertgebouwuurt -- Amsterdam 1987: Knag/Centrum Beleidsadviserend Onderzoek. 164 pp, 2 figs, 23 tabs. ISBN 90-6809-061-5 Dfl 25,00
- 53 J VERHORST & M H STIJNENBOSCH Bedrijvigheid en stadsvernieuwing; analyse van de bedrijvigheidsontwikkeling in enkele stadsvernieuwinggebieden in Utrecht en Den Haag -- Amsterdam/Utrecht 1987: Knag/Geografisch Instituut Rijksuniversiteit Utrecht. 112 pp, 47 figs, 25 tabs. ISBN 90-6809-063-1 Dfl 15,70
- 54 B G J DRIESSEN, R VERHOEF & J G P TER WELLE-HEETHUIS Overheid en bevolkingsontwikkelingen; een onderzoek naar autonome en niet-autonome bevolkingsontwikkelingen in Arnhem en Utrecht -- Amsterdam/Utrecht 1987: Knag/Geografisch Instituut Rijksuniversiteit Utrecht. 166 pp, 53 figs, 42 tabs. ISBN 90-6809-064-X Dfl 23,30
- 55 O A L C ATZEMA, P P P HUIGEN, A G A DE VOCHT & C R VOLKERS De bereikbaarheid van voorzieningen in Noord-Nederland -- Amsterdam/Utrecht 1987: Knag/Geografisch Instituut Rijksuniversiteit Utrecht. 220 pp, 49 figs, 122 tabs. ISBN 90-6809-065-8 Dfl 24,00
- 56 P C BEUKENKAMP, G A HOEKVELD & A MUDDE (red) Geografie en onderwijsstelevisie -- Amsterdam/Utrecht 1987: Knag/Geografisch Instituut Rijksuniversiteit Utrecht. 222 pp, 29 figs, 6 tabs. ISBN 90-6809-066-6 Dfl 26,50
- 57 G CARDOL Ruimte voor agribusiness-complexen; structuur, positie en dynamiek van het Noordlimburgse tuinbouwcomplex -- Amsterdam/Nijmegen 1988: Knag/Geografisch en Planologisch Instituut Katholieke Universiteit Nijmegen. 312 pp, 34 figs, 57 tabs. ISBN 90-6809-067-4 Dfl 30,00
- 59 A H H M KEMPER-WARMERDAM Vergrijzen in het groen; het bereik van ouderen en de bereikbaarheid van voorzieningen in landelijke gebieden -- Amsterdam/Utrecht 1988: Knag/Geografisch Instituut Rijksuniversiteit Utrecht. 236 pp, 47 figs, 70 tabs. ISBN 90-6809-069-0 Dfl 29,50
- 60 P J BOELHOUWER De verkoop van woningwetwoningen -- Amsterdam/Utrecht 1988: Knag/Geografisch Instituut Rijksuniversiteit Utrecht. 208 pp, 49 figs, 122 tabs. ISBN 90-6809-070-4 Dfl 29,30
- 61 A G J DIETVORST & M C JANSEN-VERBEKE De binnenstad: kader van een sociaal perpetuum mobile; een literatuurstudie naar tijdsbesteding en binnenstadsgebruik -- Amsterdam/Nijmegen 1988: Knag/Geografisch en Planologisch Instituut Katholieke Universiteit Nijmegen. 240 pp, 10 tabs. ISBN 90-6809-071-2 Dfl 30,00
- 63 H J A BERENDSEN & H VAN STEUN (red) Nieuwe karteringsmethoden in de fysieke geografie -- Amsterdam/Utrecht 1988: Knag/Geografisch Instituut Utrecht. 176 pp, 56 figs, 24 tabs. ISBN 90-6809-073-9 Dfl 22,50
- 64 A G J DIETVORST & J P M KWAAD (eds) Geographical research in the Netherlands 1978-1987 -- Amsterdam. 1988: Knag/IGU Netherlands. 262 pp, 7 figs, 2 tabs. ISBN 90-6809-074-7 Dfl 33,00
- 65 J VAN WEESEP Appartementsrechten; het gebruik van het splitsingsregime -- Amsterdam/Utrecht 1988: Knag/Geografisch Instituut Rijksuniversiteit Utrecht. 94 pp, 4 figs, 16 tabs. ISBN 90-6809-075-5 Dfl 14,50
- 66 T W A EPPINK Choice of mathematical models in geographic research considering alternatives -- Amsterdam/Nijmegen 1988: Knag/Geografisch en Planologisch Instituut Katholieke Universiteit Nijmegen. 244 pp, 74 figs, 49 tabs. ISBN 90-6809-076-3 Dfl 30,00
- 67 J HINDERINK & E SZULC-DABROWIECKA (eds) Successful rural development in Third World Countries - Amsterdam/Utrecht 1988: Knag/Geografisch Instituut Rijksuniversiteit Utrecht. 256 pp, 14 figs, 20 tabs. ISBN 90-6809-077-1 Dfl 31,50
- 68 S BARENS, J D H HARTEN, J RENES, J VERHORST & K E VAN DER WIELEN (red) Planning in het verleden -- Amsterdam/Utrecht 1988: Knag/Geografisch Instituut Universiteit Utrecht. 192 pp, 71 figs. ISBN 90-6809-078-X Dfl 26,00
- 69 J MANSVELT BECK The rise of a subsidized periphery in Spain -- Amsterdam 1988: Knag/Instituut voor Sociale Geografie Universiteit van Amsterdam. 286 pp, 15 figs, 28 tabs. ISBN 90-6809-079-8 Dfl 37,50
- 70 S SMITH Kleinschalige industrie in Latijns Amerika; een studie van de ontwikkelingsmogelijkheden in Aguascalientes, Mexico -- Amsterdam/Nijmegen 1988: Knag/Geografisch en Planologisch Instituut Katholieke Universiteit Nijmegen. 422 pp, 4 figs, 16 tabs. ISBN 90-6809-080-1 Dfl 42,50
- 72 P J KORTEWEG Dynamiek en immobiliteit in naoorlogse woonwijken in Alkmaar, Haarlem en Purmerend -- Amsterdam/Utrecht 1988: Knag/Geografisch Instituut Rijksuniversiteit Utrecht. 144 pp, 21 figs, 34 tabs. ISBN 90-6809-082-8 Dfl 20,90

- 73 P J WIJERS Land prices in Tokyo -- Amsterdam 1988: Knag/Economisch-Geografisch Instituut Universiteit van Amsterdam. 84 pp, 12 figs, 8 tabs. ISBN 90-6809-084-4 Dfl 47,50
- 74 J VAN MOURIK (red) Landschap in beweging; ontwikkeling en bewoning van een stuifzandgebied in de Kempen -- Amsterdam 1988: Knag/Faculteit Ruimtelijke Wetenschappen Universiteit van Amsterdam. 197 pp, 95 figs, 1 tab. ISBN 90-6809-083-6 Dfl 30,00
- 75 W J M OSTENDORF Het sociaal profiel van de gemeente; woonmilieudifferentiatie en de vorming van het stadsgeest -- Amsterdam -- Amsterdam 1988: Knag/Instituut voor Sociale Geografie Universiteit van Amsterdam. 192 pp, 12 figs, 26 tabs. ISBN 90-6809-085-2 Dfl 23,00
- 76 J DE BRUIN & J A KOETSIER (red) De kracht van de regio; sociaal-economische ontwikkelingsmogelijkheden van de regio -- Amsterdam 1988: Knag/Instituut voor Sociale Geografie Universiteit van Amsterdam. 104 pp, 12 figs, 6 tabs. ISBN 90-6809-086-0 Dfl 15,00
- 77 A G M VAN DER SMAAT & P H J HENDRIKS (red) Methoden op een keerpunt; opstellen aangeboden aan prof drs P J W Kouwe -- Amsterdam/Nijmegen 1988: Knag/Geografisch en Planologisch Instituut Katholieke Universiteit Nijmegen. 170 pp, 29 figs, 10 tabs. ISBN 90-6809-087-9 Dfl 25,00
- 78 C VAN DER POST, Migrants and migrant-labour absorption in large and small centres in Swaziland -- Amsterdam/Utrecht 1988: Knag/Geografisch Instituut Utrecht. 310 pp, 32 figs, 84 tabs. ISBN 90-6809-088-7 Dfl 35,00
- 79 L J DE HAAN Overheid en regionale integratie van de savanne in Togo 1885-1985 -- Amsterdam 1988: Knag/Instituut v Sociale Geografie Universiteit van Amsterdam. 304 pp, 31 figs, 65 tabs. ISBN 90-6809-089-5 Dfl 33,00
- 80 L H VAN WINGAARDEN-BAKKER & J J M VAN DER MEER (eds) Spatial sciences, research in progress: Proceedings of the symposium "Spatial sciences, research in progress" -- Amsterdam 1988: Knag/ Faculteit Ruimtelijke Wetenschappen Universiteit van Amsterdam. 112 pp, 16 figs, 2 tabs. ISBN 90-6809-091-7 Dfl 24,00
- 81 F M H M DRIESSEN & J H VAN HOUWELINGEN Vrije tijd en korte verblijfsrecreatie -- Amsterdam/Utrecht 1988: Knag/Bureau Driessen. 256 pp, 25 figs, 146 tabs. ISBN 90-6809-095-X Dfl 15,00
- 82 P K DOORN Social structure and spatial mobility: composition and dynamics of the Dutch labour force -- Amsterdam/Utrecht 1989: Knag/Geografisch Instituut Rijksuniversiteit Utrecht. 262 pp, 72 figs, 41 tabs. ISBN 90-6809-092-5 Dfl 31,50
- 83 A LOEVE Buitenlandse ondernemingen in regionaal perspectief; vestigingsstrategieën en regionale effecten van buitenlandse bedrijven in Nederland -- Amsterdam/Utrecht 1989: Knag/Geografisch Instituut Rijksuniversiteit Utrecht. 272 pp, 49 figs, 78 tabs. ISBN 90-6809-093-3 Dfl 32,00
- 84 D H DE BAKKER Ruraal nederzettingenpatroon en beleid; ontwikkelingen in ZW-Friesland -- Amsterdam/Utrecht 1989: Knag/Geografisch Instituut Universiteit Utrecht. 230 pp, 32 figs, 68 tabs. ISBN 90-6809-094-1 Dfl 29,00
- 85 L J PAUL (ed) Post-war development of regional geography; with special attention to the United Kingdom, Belgium, and the Netherlands -- Amsterdam/Utrecht 1989: Knag/Geografisch Instituut Rijksuniversiteit Utrecht. 88 pp, 15 figs, 5 tabs. ISBN 90-6809-096-8 Dfl 14,00
- 86 P HOEKSTRA River outflow, depositional processes and coastal morphodynamics in a monsoon-dominated deltaic environment, East Java, Indonesia -- Amsterdam/Utrecht 1989: Knag/Geografisch Instituut Rijksuniversiteit Utrecht. 220 pp, 77 figs, 24 tabs. ISBN 90-6809-097-6 Dfl 28,50
- 87 E LENSINK Intermediaire diensten in landelijke gebieden -- Amsterdam/Nijmegen 1989: Knag/Faculteit Beleids-wetenschappen Katholieke Universiteit Nijmegen. 246 pp, 21 figs, 65 tabs. ISBN 90-6809-098-4 Dfl 30,00
- 88 J H J VAN DINTEREN Zakelijke diensten en middelgrote steden, een onderzoek naar dienstverleningsbedrijven in Noord-Brabant, Gelderland en Overijssel -- Amsterdam/Nijmegen 1989: Knag/Faculteit der Beleidswetenschappen Katholieke Universiteit Nijmegen. 312 pp, 28 figs, 84 tabs. ISBN 90-6809-099-2 Dfl 40,00
- 89 L VAN DER LAAN, H SCHOLTEN & G A VAN DER KNAAP Het regionaal arbeidsaanbod in Nederland -- Amsterdam/Rotterdam 1989: Knag/Economisch-Geografisch Instituut Erasmus Universiteit Rotterdam. 128 pp, 27 figs, 28 tabs. ISBN 90-6809-101-8 Dfl 17,50
- 90 C CLARK, P HUIGEN & F THISEN (eds) Planning and the future of the countryside: Great Britain and the Netherlands -- Amsterdam 1989: Knag/Instituut voor Sociale Geografie Universiteit van Amsterdam. 240 pp, 25 figs, 43 tabs. ISBN 90-6809-102-6 Dfl 35,00
- 91 J A VAN DEN BERG Variability of parameters for modelling soil moisture conditions; studies on loamy to silty soils on marly bedrock in the Ardèche drainage basin, France -- Amsterdam/Utrecht 1989: Knag/Geografisch Instituut Rijksuniversiteit Utrecht. 214 pp, 76 figs, 16 tabs. ISBN 90-6809-103-4 Dfl 28,50
- 92 O VERKOREN Huizen op de hoogvlakte; een residentieel-geografische verkenning van La Paz, Bolivia -- Amsterdam/Utrecht 1989: Knag/Geografisch Instituut Rijksuniversiteit Utrecht. 210 pp, 29 figs, 16 tabs. ISBN 90-6809-104-2 Dfl 32,00
- 93 G MIK (red) Herstructurering in Rotterdam; modernisering en internationalisering en de Kop van Zuid -- Amsterdam/Rotterdam 1989: Knag/Economisch Geografisch Instituut Erasmus Universiteit Rotterdam. 324 pp. 86 figs, 54 tabs. ISBN 90-6809-105-0 Dfl 30,00
- 94 P BEEKMAN, P VAN LINDERT, J POST & W PRINS Huisvestingsbeleid en informele bouw in de derde wereld -- Amsterdam 1989: Knag/Instituut voor Sociale Geografie Universiteit van Amsterdam. 174 pp, 9 figs, 25 tabs. ISBN 90-6809-106-9 Dfl 30,00
- 95 J G L PALTE Upland farming on Java, Indonesia -- Amsterdam/Utrecht 1989: Knag/Geografisch Instituut Rijksuni-versiteit Utrecht. 256 pp, 15 figs, 38 tabs. ISBN 90-6809-107-7 Dfl 34,50
- 96 P VAN GENUCHTEN Movement mechanisms and slide velocity variations of landslides in varved clays in the French Alps -- Amsterdam/Utrecht 1989: Knag/Geografisch Instituut Rijksuniversiteit Utrecht. 160 pp, 70 figs, 17 tabs. ISBN 90-6809-108-5 Dfl 25,00
- 97 M DE SMIDT & E WEVER (eds) Regional and local economic policies and technology -- Amsterdam/Utrecht/Nijmegen 1989: Knag/Geografisch Instituut Rijksuniversiteit Utrecht/Geografisch en Planologisch Instituut Katholieke Universiteit Nijmegen. 156 pp, 53 figs, 36 tabs. ISBN 90-6809-109-3 Dfl 24,00
- 98 P J H RIEMENS On the foreign operations of third world firms -- Amsterdam 1989: Knag/Instituut voor Sociale Geografie Universiteit van Amsterdam. 148 pp, 20 tabs. ISBN 90-6809-110-7 Dfl 30,00

- 101 G B M PEDROLI The nature of landscape; a contribution to landscape ecology and ecohydrology with examples from the Strijper Aa landscape -- Amsterdam 1989: Knag/Fysisch-Geografisch en Bodemkundig Laboratorium Universiteit van Amsterdam. 164 pp, 43 figs, 18 tabs. ISBN 90-6809-111-5 Dfl 25,00
- 102 H LEENAERS The dispersal of metal mining wastes in the catchment of the river Geul, Belgium-the Netherlands -- Amsterdam/Utrecht 1989: Knag/Geografisch Instituut Rijksuniversiteit Utrecht. 230 pp, 95 figs, 52 tabs. ISBN 90-6809-112-3 Dfl 30,00
- 104 P C J DRUUVEN Mandenvlechters en Mexcalstokers in Mexico -- Amsterdam 1990: Knag/Instituut voor Sociale Geografie Universiteit van Amsterdam. 294 pp, 21 figs, 55 tabs. ISBN 90-6809-114-X Dfl 38,50
- 105 W BLEUTEN De verwatering van meststoffen; analyse en modellering van de relaties tussen landgebruik en waterkwaliteit in het stroomgebied van de Langbroeker Wetering -- Amsterdam/Utrecht 1990: Knag/Geografisch Instituut Rijksuniversiteit Utrecht. 262 pp, 80 figs, 31 tabs. ISBN 90-6809-115-8 Dfl 37,00
- 107 M VAN HERWIJNEN, R JANSSEN & P RIJVELD Herbestemming van landbouwgrond -- Amsterdam 1990: Knag/Instituut Milieuvraagstukken Vrije Universiteit. 110 pp, 33 figs, 12 tabs. ISBN 90-6809-117-4 Dfl 25,00
- 108 D H DRENTHE De informatica-sector in Nederland tussen rijp en groen -- Amsterdam/Nijmegen 1990: Knag/Faculteit Beeldswetenschappen Katholieke Universiteit. 268 pp, 24 figs, 87 tabs. ISBN 90-6809-118-2 Dfl 37,50
- 109 H KNOL & W MANSHANDEN Functionele samenhang in de noordvleugel van de Randstad -- Amsterdam/Utrecht 1990: Knag/Economisch-Geografisch Instituut Universiteit van Amsterdam/Geografisch Instituut Rijksuniversiteit Utrecht. 112 pp, 26 figs, 27 tabs. ISBN 90-6809-119-0 Dfl 19,50
- 110 C D EYSBERG The Californian wine economy -- Amsterdam/Utrecht 1990: Knag/Geografisch Instituut Rijksuniversiteit Utrecht. 272 pp, 64 figs, 26 tabs. ISBN 90-6809-121-2 Dfl 29,75
- 111 J W A DIJKMANS Aspects of geomorphology and thermoluminescence dating of cold climate eolian sands -- Amsterdam/Utrecht 1990: Knag/Geografisch Instituut Rijksuniversiteit Utrecht. 256 pp, 119 figs, 19 tabs. ISBN 90-6809-120-4 Dfl 36,50
- 112 H TER HEIDE (ed) Technological change and spatial policy -- Amsterdam/Utrecht 1990: Knag/Geografisch Instituut Rijksuniversiteit Utrecht. 218 pp, 9 figs, 31 tabs. ISBN 90-6809-122-0 Dfl 29,00
- 113 L M VAN HEES De ontwikkeling van een woningmarktmodel en zijn toepassing op Italië -- Amsterdam/Nijmegen 1990: Knag/Faculteit der Beeldswetenschappen Katholieke Universiteit Nijmegen. 196 pp, 12 figs, 26 tabs. ISBN 90-6809-123-9 Dfl 35,00
- 114 M R HENDRIKS Regionalisation of hydrological data: effects of lithology and land use on storm runoff in east Luxembourg -- Amsterdam/Utrecht 1990: Knag/Geografisch Instituut Rijksuniversiteit Utrecht. 174 pp, 23 figs, 50 tabs. ISBN 90-6809-124-7 Dfl 26,00
- 115 P H RENOVOY The informal economy -- Amsterdam 1990: Knag/Regioplan. 204 pp, 12 figs, 21 tabs. ISBN 90-6809-125-5 Dfl 35,00
- 116 J H T KRAMER Luchthavens en hun uitstraling -- Amsterdam/Nijmegen 1990: Knag/Faculteit der Beeldswetenschappen Katholieke Universiteit Nijmegen. 312 pp, 47 figs, 60 tabs. ISBN 90-6809-126-3 Dfl 55,00
- 117 M DE KWAATENIET Denomination and primary education in the Netherlands 1870-1984 -- Amsterdam/ Florence 1990: Knag/Instituut voor Sociale Geografie Universiteit van Amsterdam/European University Institute Florence. 268 pp, 28 figs, 39 tabs. ISBN 90-6809-127-1 Dfl 36,00
- 118 W P M F IVENS Atmospheric deposition onto forests: an analysis of the deposition variability by means of throughfall measurements -- Amsterdam/Utrecht 1990: Knag/Geografisch Instituut Rijksuniversiteit Utrecht. 156 pp, 53 figs, 36 tabs. ISBN 90-6809-128-X Dfl 25,00
- 119 R HASSINK Herstructurering en innovatiebevordering in het Ruhrgebied -- Amsterdam/Utrecht 1990: Knag/Geografisch Instituut Rijksuniversiteit Utrecht. 122 pp, 20 figs, 18 tabs. ISBN 90-6809-120-8 Dfl 24,00
- 120 P P SCHOT Solute transport by groundwater flow to wetland ecosystems; the environmental impact of human activities -- Amsterdam/Utrecht 1991: Knag/Geografisch Instituut Rijksuniversiteit Utrecht. 136 pp, 27 figs, 9 tabs. ISBN 90-6809-130-1 Dfl 25,00
- 121 S DEN HENGST & B DE PATER (red) Externe relaties en regionale ontwikkeling: voorbeelden uit Spanje en Portugal -- Amsterdam/Utrecht 1991: Knag/Geografisch Instituut Rijksuniversiteit Utrecht. 198 pp, 31 figs, 27 tabs. ISBN 90-6809-131-X Dfl 29,50
- 122 J KROES Onvolledige opstrek op de Nederlandse zandgronden -- Amsterdam/Utrecht 1991: Knag/Geografisch Instituut Rijksuniversiteit Utrecht. 256 pp, 65 figs. ISBN 90-6809-132-8 Dfl 35,00
- 123 H S VERDUIN-MULLER Serving the knowledge-based society: research on knowledge products -- Amsterdam/Utrecht 1991: Knag/Geografisch Inst. Universiteit Utrecht. 116 pp, 3 figs. ISBN 90-6809-133-6 Dfl 24,00
- 124 F MULDER Assessment of landslide hazard -- Amsterdam/Utrecht 1991: Knag/Geografisch Instituut Rijksuniversiteit Utrecht. 156 pp, 59 figs, 25 tabs. ISBN 90-6809-134-4 Dfl 29,50
- 125 M VIS Processes and patterns of erosion in natural and disturbed Andean forest ecosystems -- Amsterdam 1991: Knag/Fysisch Geografisch en Bodemkundig Laboratorium Universiteit van Amsterdam. 190 pp, 70 figs, 40 tabs. ISBN 90-6809-136-0 Dfl 12,00
- 126 V EIFF Beleid voor bedrijfsterrainen -- Amsterdam 1991: Knag/Instituut voor Sociale Geografie Universiteit van Amsterdam. 214 pp, 13 figs, 18 tabs. ISBN 90-6809-135-2 Dfl 37,50
- 127 O ATZEMA Stad uit, stad in; residentiële suburbanisatie in Nederland -- Amsterdam/Utrecht 1991: Knag/ Geografisch Instituut Rijksuniversiteit Utrecht. 274 pp, 57 figs, 80 tabs. ISBN 90-6809-137-9 Dfl 37,50
- 128 M HULSHOF Zatopec moves; networks and remittances of US-bound migrants from Oaxaca, Mexico -- Amsterdam 1991: Knag/Instituut voor Sociale Geografie Universiteit van Amsterdam. 106 pp, 6 figs, 14 tabs. ISBN 90-6809-138-7 Dfl 18,50
- 129 J M J DOOMERNIK Turkse moskeeën en maatschappelijke participatie; de institutionalisering van de Turkse Islam in Nederland en de Duitse Bondsrepubliek -- Amsterdam 1991: Knag/Instituut voor Sociale Geografie Universiteit van Amsterdam. 200 pp, 30 figs, 1 tab. ISBN 90-6809-139-5 Dfl 32,50
- 130 M DE SMID, A GRANBERG & E WEVER (eds) Regional development strategies and territorial production complexes: a Dutch-USSR perspective -- Amsterdam 1991: Knag. 216 pp, 25 figs., 40 tabs. ISBN 90-6809-140-9 Dfl 29,50
- 131 P MISDORP Centrale begrippen in de sociale geografie; een conceptuele analyse van Engelstalige leerboeken -- Amsterdam 1991: Knag/Iparto 316 pp, 39 figs, 51 tabs. ISBN 90-6809-141-7 Dfl 39,50

- 133 I I Y CASTEL Late Holocene eolian drift sands in Drenthe -- Amsterdam/Utrecht 1991: Knag/Geografisch Instituut Rijksuniversiteit Utrecht. 162 pp, 49 figs, 15 tabs. ISBN 90-6809-143-3 Dfl 29,50
- 134 J G BORCHERT & M DE KRUYF Bevolkingsgroei ter wille van het voorzieningsniveau? -- Utrecht 1991: Knag/Faculteit Ruimtelijke Wetenschappen Rijksuniversiteit Utrecht. 78 pp, 4 figs, 15 tabs ISBN 90-6809-144-1 Dfl 18,00
- 135 R VAN DER VAART Educatief ontwerpen met geografie; een studie betreffende de structurering van geografische kennis voor educatieve doeleinden -- Utrecht 1991: Knag/Faculteit Ruimtelijke Wetenschappen Rijksuniversiteit Utrecht. 256 pp, 84 figs. ISBN 90-6809-145-X Dfl 36,00
- 136 P VAN LINDERT Huisvestingsstrategieën van lage-inkomensgroepen in La Paz -- Utrecht 1991: Knag/Faculteit Ruimtelijke Wetenschappen Rijksuniversiteit Utrecht. 320 pp, 34 figs, 26 tabs. ISBN 90-6809-146-8 Dfl 34,50
- 137 J M M VAN AMERSFOORT & H KNIPPENBERG (eds) States and nations: the rebirth of the 'nationalities question' in Europe -- Utrecht/Amsterdam 1991: Knag/Instituut voor Sociale Geografie Universiteit van Amsterdam. 198 pp, 20 figs, 12 tabs. ISBN 90-6809-147-6 Dfl 29,50
- 138 P VAN TEEFFELEN Dienstencentra en rurale ontwikkeling; een onderzoek naar het aanbod en gebruik van overheidssdiensten in Mali, Afrika -- Utrecht 1992: Knag/Faculteit Ruimtelijke Wetenschappen Rijksuniversiteit Utrecht. 256 pp, 70 figs, 40 tabs. ISBN 90-6809-148-4 Dfl 34,50
- 139 T H M VAN DER LOOP Industrial dynamics and fragmented labour markets. Construction firms and labourers in India -- Utrecht/Amsterdam 1992: Knag/Instituut voor Sociale Geografie Universiteit van Amsterdam. 350 pp, 30 figs, 71 tabs. ISBN 90-6809-149-2 Dfl 49,50
- 140 H VAN DER WUSTEN (ed) The urban political arena; geographies of public administration -- Utrecht/Amsterdam 1992: Knag/Instituut voor Sociale Geografie Universiteit van Amsterdam. 192 pp, 28 figs, 12 tabs. ISBN 90-6809-150-6 Dfl 35,00
- 141 B D HOEKSTRA Informatienetwerken rondom bedrijven; de bibliotheek als informatieleverancier voor het bedrijfsleven -- Utrecht/Groningen 1992: Knag/Faculteit Ruimtelijke Wetenschappen Rijksuniversiteit Groningen. 112 pp, 16 figs, 8 tabs. ISBN 90-6809-151-4 Dfl 25,00
- 142 H SCHRETTENBRUNNER & J VAN WESTRHENEN (eds) Empirical research and geography teaching -- Utrecht/Amsterdam 1992: Knag/Centrum voor Educatieve Geografie Vrije Universiteit Amsterdam. 190 pp, 48 figs, 38 tabs. ISBN 90-6809-152-2 Dfl 30,00
- 143 J VAN BECKUM & C VAN DER BURG Naar een online videotex geografisch informatiesysteem voor educatieve toepassingen; het Giset Project 1987-1992 -- Utrecht 1992: Knag/Faculteit Ruimtelijke Wetenschappen Rijksuniversiteit Utrecht. 224 pp, 19 figs, 30 tabs. ISBN 90-6809-153-0 Dfl 29,50
- 146 H REITSMA, T DIETZ & L DE HAAN (eds) Coping with semi-aridity; how the rural poor survive in dry season environments -- Utrecht/Amsterdam 1992: Knag/Instituut voor Sociale Geografie Universiteit van Amsterdam. 202 pp, 18 figs, 19 tabs. ISBN 90-6809-154-9 Dfl 32,00
- 147 M HESSELS Locational dynamics of business services; an intrametropolitan study on the Randstad Holland -- Utrecht 1992: Knag/Faculteit Ruimtelijke Wetenschappen Rijksuniversiteit Utrecht. 232 pp, 25 figs, 79 tabs. ISBN 90-6809-157-3 Dfl 34,50
- 148 J KANT Geografen en planologen op de arbeidsmarkt; het succes op de arbeidsmarkt van geografen en planologen, afgestudeerd in de periode september 1987 - augustus 1990 -- Utrecht 1992: Knag/Stichting Geografenwerk. 176 pp, 39 figs, 41 tabs. ISBN 90-6809-158-1 Dfl 26,00
- 149 R VAN DER VAART (red) Aardrijkskunde in de basisvorming -- Utrecht 1992: Knag/ Faculteit Ruimtelijke Wetenschappen Rijksuniversiteit Utrecht. 176 pp, 44 figs, 2 tabs. ISBN 90-6809-159-X Dfl 32,50
- 151 P P GROENEWEGEN & P P P HUIGEN (eds) Micro-macro vraagstukken in de sociologie en de sociale geografie -- Utrecht 1992: Knag/Faculteit Ruimtelijke Wetenschappen Rijksuniversiteit Utrecht. 140 pp, 15 figs, 9 tabs. ISBN 90-6809-161-1 Dfl 25,00
- 154 P LUCAS & G M R A VAN OORT Dynamiek in een stadsrandzone; werken en wonen in de stadsrandzone van de agglomeratie Utrecht -- Utrecht 1993: Knag/Faculteit Ruimtelijke Wetenschappen Universiteit Utrecht. 396 pp, 105 figs, 41 tabs, 20 photographs. ISBN 90-6809-164-6 Dfl 48,00
- 156 G DRAAIJERS The variability of atmospheric deposition to forests; the effects of canopy structure and forest edges -- Utrecht 1993: Knag/Faculteit Ruimtelijke Wetenschappen Universiteit Utrecht. 208 pp, 54 figs, 26 tabs. ISBN 90-6809-166-2 Dfl 34,00
- 158 R VERHOEFF De weg naar de podia; ruimtelijke aspecten van het bezoek aan podiumkunsten in Nederland -- Utrecht 1993: Knag/Faculteit Ruimtelijke Wetenschappen Universiteit Utrecht. 208 pp, 20 figs, 48 tabs. ISBN 90-6809-168-9 Dfl 35,00
- 159 H ZONDAG Regio en bedrijfseconomische vitaliteit -- Utrecht 1993: Knag/Faculteit Ruimtelijke Wetenschappen Universiteit Utrecht. 208 pp, 17 figs, 24 tabs. ISBN 90-6809-169-7 Dfl 34,50
- 160 T SPIT Strangled in structures; an institutional analysis of innovative policy by Dutch municipalities -- Utrecht 1993: Knag/Faculteit Ruimtelijke Wetenschappen Universiteit Utrecht. 192 pp, 36 figs, 11 tabs. ISBN 90-6809-170-0 Dfl 32,50
- 162 A BARENDREGT Hydro-ecology of the Dutch polder landscape -- Utrecht 1993: Knag/Faculteit Ruimtelijke Wetenschappen Universiteit Utrecht. 208 pp, 34 figs, 31 tabs. ISBN 90-6809-175-1 Dfl 34,50
- 164 J R RITSEMA VAN ECK Analyse van transportnetwerken in GIS voor sociaal-geografisch onderzoek -- Utrecht 1993: Knag/Faculteit Ruimtelijke Wetenschappen Universiteit Utrecht. 206 pp, 56 figs, 17 tabs. ISBN 90-6809-177-8 Dfl 35,00
- 165 P VAESSEN Small business growth in contrasting environments -- Utrecht/Nijmegen 1993: Knag/Faculteit Beeldswetenschappen Katholieke Universiteit Nijmegen. 228 pp, 9 figs, 3 tabs. ISBN 90-6809-178-6 Dfl 35,00
- 166 T E TÖRNQVIST Fluvial sedimentary geology and chronology of the Holocene Rhine-Meuse delta, The Netherlands -- Utrecht 1993: Knag/Faculteit Ruimtelijke Wetenschappen Universiteit Utrecht. 176 pp, 66 figs, 13 tabs. ISBN 90-6809-179-4 Dfl 32,00
- 167 P J M VAN STEEN (red) Geografie in beweging; liber amicorum Pieter Lukkes -- Utrecht/Groningen 1993: Knag/Faculteit Ruimtelijke Wetenschappen Rijksuniversiteit Groningen. 216 pp, 36 figs, 17 tabs. ISBN 90-6809-180-8 Dfl 35,00

- 168 E J A HARTS-BROEKHUIS & A A DE JONG Subsistence and survival in the Sahel; responses of households and enterprises to deteriorating conditions and development policy in the Mopti Region of Mali -- Utrecht 1993: Knag/Faculteit Ruimt. Wetenschappen Universiteit Utrecht. 464 pp, 42 figs, 69 tabs. ISBN 90-6809-181-6 Dfl 49,50
- 169 F FILIUS Huishoudensopheffing en woningverlating in een vergrijzende samenleving -- Utrecht 1993: Knag/Faculteit Ruimtelijke Wetenschappen Universiteit Utrecht. 224 pp, 28 figs, 37 tabs. ISBN 90-6809-182-4 Dfl 32,50
- 170 V SCHUTTIENS Dynamiek in het draagvlak; huishoudensontwikkelingen en winkelbestedingen in oudere na-oorlogse wijken -- Utrecht 1993: Knag/Faculteit Ruimtelijke Wetenschappen Universiteit Utrecht. 240 pp, 19 figs, 31 tabs. ISBN 90-6809-183-2 Dfl 34,50
- 172 E C A BOLSIUS, G CLARK & J G GROENENDIJK (eds) The retreat: rural land-use and European agriculture -- Utrecht/Amsterdam 1993: Knag/Department of Human Geography Faculty of Environmental Sciences University of Amsterdam. 168 pp, 12 figs, 26 tabs. ISBN 90-6809-185-9 Dfl 33,50
- 173 P HOOIMEIJER, G A VAN DER KNAAP, J VAN WEESEP & R I WOODS (eds) Population dynamics in Europe; current issues in population geography -- Utrecht 1994: Knag/Faculteit Ruimtelijke Wetenschappen Universiteit Utrecht. 192 pp, 29 figs, 36 tabs. ISBN 90-6809-187-5 Dfl 35,00
- 174 J W H VAN DE MEENE The shoreface-connected ridges along the Dutch coast -- Utrecht 1994: Knag/Faculteit Ruimtelijke Wetenschappen Universiteit Utrecht. 246 pp, 83 figs, 28 tabs. ISBN 90-6809-188-3 Dfl 44,00
- 175 F R BRUINSMA De invloed van transportinfrastructuur op ruimtelijke patronen van economische activiteiten -- Utrecht/Amsterdam 1994: Knag/Vakgroep Ruimtelijke Economie Vrije Universiteit. 272 pp, 33 figs, 64 tabs. ISBN 90-6809-189-1 Dfl 42,50
- 176 H CLOUT (ed) Europe's cities in the late twentieth century -- Utrecht/Amsterdam 1994: Knag/Department of Human Geography University of Amsterdam. 218 pp, 50 figs, 39 tabs. ISBN 90-6809-190-5 Dfl 35,00
- 177 S M DE JONG Applications of reflective remote sensing for land degradation studies in a Mediterranean environment -- Utrecht 1994: Knag/Faculteit Ruimtelijke Wetenschappen Universiteit Utrecht. 256 pp, 64 figs, 31 tabs. ISBN 90-6809-191-3 Dfl 39,00
- 178 A KROON Sediment transport and morphodynamics of the beach and nearshore zone near Egmond, the Netherlands -- Utrecht 1994: Knag/Faculteit Ruimtelijke Wetenschappen Universiteit Utrecht. 284 pp, 138 figs, 9 tabs. ISBN 90-6809-192-1 Dfl 39,00
- 179 C P TERLOUW (eds) Methodological exercises in regional geography: France as an example -- Utrecht/Amsterdam 1994: Knag/Faculteit Ruimtelijke Wetenschappen Universiteit Utrecht/Centrum voor Educatieve Geografie Vrije Universiteit Amsterdam. 226 pp, 96 figs, 15 tabs. ISBN 90-6809-193-X Dfl 36,00
- 180 H HUISMAN Planning for rural development: experiences and alternatives; Cases from Indonesia and Lesotho -- Utrecht 1994: Knag/Faculteit Ruimtelijke Wetenschappen Universiteit Utrecht. 240 pp, 9 figs, 36 tabs. ISBN 90-6809-194-8 Dfl 37,00
- 181 P DICKEN & M QUÉVIT (eds) Transnational corporations and European regional restructuring -- Utrecht 1994: Knag/Faculteit Ruimtelijke Wetenschappen Universiteit Utrecht. 168 pp, 5 figs, 54 tabs. ISBN 90-6809-195-6 Dfl 30,00
- 182 H TER HEIDE & D WUNBELT Tussen kennen en kunnen: over de verbinding van onderzoek en ruimtelijk ontwerp: verslag van een verkenning en van een symposium -- Utrecht/Den Haag 1994: Knag/Faculteit Ruimtelijke Wetenschappen Universiteit Utrecht/Rijksplanologische Dienst. 160 pp, 11 figs, 1 tab. ISBN 90-6809-196-4 Dfl 29,00
- 183 M GROTHE, H J SCHOLTEN & M VAN DER BEEK GIS, noodzaak of luxe? Een verkenning naar het gebruik van geografische informatiesystemen bij private ondernemingen in Nederland -- Utrecht/Amsterdam 1994: Knag/Vakgroep Ruimtelijke Economie Vrije Universiteit Amsterdam. 128 pp, 21 figs, 27 tabs. ISBN 90-6809-199-9 Dfl 49,95
- 184 M F P BIERKENS Complex confining layers; a stochastic analysis of hydraulic properties at various scales -- Utrecht 1994: Knag/Faculteit Ruimtelijke Wetenschappen Universiteit Utrecht. 272 pp, 102 figs, 29 tabs. ISBN 90-6809-200-6 Dfl 39,00
- 185 F BARNHOORN, R JANSSEN, H TH RIEZEBOS & J J STERKENBURG Sustainable development in Botswana; an analysis of resource management in three communal development areas -- Utrecht 1994: Knag/Faculteit Ruimtelijke Wetenschappen Universiteit Utrecht. 160 pp, 21 figs, 46 tabs. ISBN 90-6809-201-4 Dfl 35,00
- 186 A HARTS-BROEKHUIS & O VERKOREN (eds) No easy way out; essays on Third World development in honour of Jan Hinderink -- Utrecht 1994: Knag/Faculteit Ruimtelijke Wetenschappen Universiteit Utrecht. 392 pp, 21 figs, 16 tabs. ISBN 90-6809-202-2 Dfl 59,00
- 187 A C M VAN WESTEN Unsettled: low-income housing and mobility in Bamako, Mali -- Utrecht 1995: Knag/Faculteit Ruimtelijke Wetenschappen Universiteit Utrecht. 336 pp, 31 figs, 48 tabs. ISBN 90-6809-203-0 Dfl 43,00
- 188 F VAN DAM Meer voor minder; schaalverandering en bereikbaarheid van voorzieningen in landelijke gebieden in Nederland -- Utrecht 1995: Knag/Faculteit Ruimtelijke Wetenschappen Universiteit Utrecht. 346 pp, 119 figs, 56 tabs. ISBN 90-6809-204-9 Dfl 45,00
- 189 F VAN REISEN & M TACKEN (eds) A future of telework; towards a new urban planning concept? -- Utrecht/Delft 1995: Knag/Faculteit Bouwkunde TU Delft. 194 pp, 46 figs, 22 tabs. ISBN 90-6809-205-7 Dfl 37,50
- 190 W P A VAN DEURSEN Geographical Information Systems and Dynamic Models; development and application of a prototype spatial modelling language -- Utrecht 1995: Knag/Faculteit Ruimtelijke Wetenschappen Universiteit Utrecht. 206 pp, 44 figs, 8 tabs. ISBN 90-6809-206-5 Dfl 38,00
- 191 F THISSSEN Bewoners en nederzettingen in Zeeland: op weg naar een nieuwe verscheidenheid -- Utrecht/Amsterdam 1995: Knag/Instituut voor Sociale Geografie Universiteit van Amsterdam. 200 pp. ISBN 90-6809-207-3 Dfl 37,50
- 192 A ROMÉIN Labour markets and migrant absorption in small towns: the case of northern Costa Rica -- Utrecht 1995: Knag/Faculteit Ruimtelijke Wetenschappen Universiteit Utrecht. 190 pp, 24 figs, 47 tabs. ISBN 90-6809-208-1 Dfl 36,00
- 193 G J ASHWORTH & J WAALKENS (red) Geografie en milieu: trend of traditie? -- Utrecht/Groningen 1995: Knag/Faculteit der Ruimtelijke Wetenschappen Rijksuniversiteit Groningen. 152 pp, 14 figs, 9 tabs. ISBN 90-6809-209-X Dfl 32,50

- 194 A FEDDES Woningmarkt, regulering en inflatie: het na-oorlogse volkshuisvestingsbeleid van tien Noordwest-Europese landen vergeleken -- Utrecht 1995: Knag/Faculteit Ruimtelijke Wetenschappen Universiteit Utrecht. 464 pp, 69 figs, 75 tabs. ISBN 90-6809-210-3 Dfl 60,00
- 195 K M WINBERG Morphologic behaviour of a barred coast over a period of decades -- Utrecht 1995: Knag/Faculteit Ruimtelijke Wetenschappen Universiteit Utrecht. 254 pp, 131 figs, 25 tabs. ISBN 90-6809-211-1 Dfl 45,00
- 196 M DUST Het elliptisch leven; actieruimte als integrale maat voor bereik en mobiliteit - modelontwikkeling met als voorbeeld tweeverdieners met kinderen in Houten en Utrecht -- Utrecht/Delft 1995: Knag/Faculteit Bouwkunde Technische Universiteit Delft. 264 pp, 32 figs, 36 tabs. ISBN 90-6809-213-8. Out of print
- 197 L BLOEMBERG Tussen traditie en verandering; Hindostaanse zelforganisaties in Nederland -- Utrecht/Amsterdam 1995: Knag/Instituut voor Sociale Geografie Universiteit van Amsterdam. 244 pp, 13 fig, 17 tabs. ISBN 90-6809-214-6 Dfl 38,00
- 198 M K BANDMAN, V MALOV, G A VAN DER KNAAP & E WEVER (eds) Lower Angara Region: A new approach to regional development in Russia -- Utrecht/Rotterdam 1995: Knag/Faculteit of Geographical Sciences Utrecht University/Economic Geographical Institute Rotterdam. 144 pp, 37 figs, 18 tabs. ISBN 90-6809-215-4. Out of print
- 199 E J PEBESMA Mapping groundwater quality in the Netherlands -- Utrecht 1996: Knag/Faculteit Ruimtelijke Wetenschappen Universiteit Utrecht. 128 pp, 35 figs, 11 tabs. ISBN 90-6809-216-2 Dfl 29,50
- 200 M VAN DER PERK Muddy waters; uncertainty issues in modelling the influence of bed sediments on water composition -- Utrecht 1996: Knag/Faculteit Ruimtelijke Wetenschappen Universiteit Utrecht. 190 pp, 38 figs, 51 tabs. ISBN 90-6809-218-9 Dfl 34,00
- 201 G F GLAS Industriële netwerken; ruimte, regio's, cultuur en beleid -- Utrecht/Groningen 1996: Knag/Faculteit Ruimtelijke Wetenschappen Rijksuniversiteit Groningen. 276 pp, 37 fig, 37 tab. ISBN 90-6809-219-7 Dfl 39,95
- 202 R M HOOTSMANS Fuzzy sets and series analysis for visual decision support in spatial data exploration -- Utrecht 1996: Knag/Faculteit Ruimtelijke Wetenschappen Universiteit Utrecht. 192 pp, 50 figs, 8 colour plates, 19 figs. ISBN 90-6809-220-0 Dfl 34,50
- 203 H DE MARS Chemical and physical dynamics of fen hydro-ecology -- Utrecht 1996: Knag/Faculteit Ruimtelijke Wetenschappen Universiteit Utrecht. 176 pp, 40 figs, 23 tabs. ISBN 90-6809-221-9 Dfl 35,00
- 204 M GROTHE & H J SCHOLTEN GIS in de publieke sector; een inventarisatie naar gebruik van geo-informatie en GIS bij de Nederlandse overheid -- Utrecht/Amsterdam 1996: Knag/Vakgroep Ruimtelijke Economie Vrije Universiteit Amsterdam. 268 pp, 24 figs, 173 tabs. ISBN 90-6809-222-7 Dfl 35,00
- 205 W MANSHANDEN Zakelijke diensten en regionaal-economische ontwikkeling; de economie van nabijheid -- Utrecht/Amsterdam 1996: Knag/Faculteit der Economische Wetenschappen en Econometrie Universiteit van Amsterdam. 182 pp, 20 figs, 24 tabs. ISBN 90-6809-223-5 Dfl 32,50
- 206 V BERDOULAY & J A VAN GINKEL (eds) Geography and professional practice -- Utrecht 1996: Knag/Faculteit Ruimtelijke Wetenschappen Universiteit Utrecht. 270 pp, 5 figs. ISBN 90-6809-224-3 Dfl 55,00
- 207 G A VAN DER KNAAP & E WEVER (eds) Industrial organization: the firm and its labour market -- Utrecht/Rotterdam 1996: Knag/Faculteit of Geographical Sciences Utrecht University/Economic Geographical Institute Rotterdam. 126 pp, 33 figs, 22 tabs. ISBN 90-6809-227-8 Dfl 45,00
- 208 J VAN DER SCHEE, G SCHOENMAKER, H TRIMP & H VAN WESTRHENEN (eds) Innovation in geographical education -- Utrecht/Amsterdam 1996: Knag/IGU Commission on Geographical Education/Centrum voor Educatieve Geografie Vrije Universiteit Amsterdam. 280 pp, 41 figs, 1 tab. ISBN 90-6809-228-6 Dfl 45,00
- 209 J MARKUSSE Zuid-Tirol: de pacificatie van een multi-etnische regio -- Utrecht/Amsterdam 1996: Knag/Instituut voor Sociale Geografie Universiteit van Amsterdam. 246 pp, 21 figs, 42 tabs. ISBN 90-6809-229-4 Dfl 38,50
- 210 A COERTS Analysis of static cone penetration test data for subsurface modelling; a methodology -- Utrecht 1996: Knag/Faculteit Ruimtelijke Wetenschappen Utrecht. 272 pp, 110 figs, 47 tabs. ISBN 90-6809-230-8 Dfl 49,50
- 211 P GROOTE Infrastructure and Dutch economic development; a new long run data set for the Netherlands 1800-1913 -- Utrecht/Groningen 1996: Knag/Faculteit der Ruimtelijke Wetenschappen Rijksuniversiteit Groningen. 240 pp, 36 figs, 74 tabs. ISBN 90-6809-231-6 Dfl 30,00
- 212 T VAN DER ZIJP Het trainen van kaartvaardigheden; de effecten van inhoudelijke differentiatie en strategische hulp op het verwerven van kaartvaardigheden door leerlingen in het eerste jaar van het voortgezet onderwijs -- Utrecht/Amsterdam 1996: Knag/Centrum voor Educatieve Geografie Vrije Universiteit Amsterdam. 192 pp, 29 figs, 12 tabs. ISBN 90-6809-232-4 Dfl 35,00
- 213 H J T WEERTS Complex confining layers; architecture and hydraulic properties of Holocene and Late Weichselian deposits in the fluvial Rhine-Meuse delta, the Netherlands -- Utrecht 1996: Knag/Faculteit Ruimtelijke Wetenschappen Universiteit Utrecht. 198 pp, 86 figs, 20 tabs. ISBN 90-6809-233-2 Dfl 44,50
- 214 P H PELLENBARG, F SCHUURMANS & J DE VRIES (red) Reisgenoten; liber amicorum prof dr W J van den Bremen -- Utrecht/Groningen 1996: Knag/Faculteit Ruimtelijke Wetenschappen Rijksuniversiteit Groningen. 606 pp, 71 figs, 51 tabs. ISBN 90-6809-234-0 Dfl 62,50
- 215 J B NYAKAANA Kenya's development centre policy: the case of Eldoret; an assessment of its implementation and impact -- Utrecht/Amsterdam 1996: Knag/Instituut voor Sociale Geografie Universiteit van Amsterdam. 312 pp, 93 figs, 55 tabs. ISBN 90-6809-235-9 Dfl 47,50
- 216 T BÉNEKER "Buscar mejor ambiente" - Migratie naar, uit en langs een kleine stad in Costa Rica -- Utrecht 1997: Knag/Faculteit Ruimtelijke Wetenschappen Universiteit Utrecht. 208 pp, 45 figs, 32 figs. ISBN 90-6809-236-7 Dfl 29,50
- 217 H RENSEN The climate during the Younger Dryas stadial; Comparing global atmospheric simulation experiments with climate reconstructions based on geological evidence -- Utrecht 1997: Knag/Faculteit Ruimtelijke Wetenschappen Universiteit Utrecht. 192 pp, 59 figs, 6 tabs. ISBN 90-6809-237-5 Dfl 38,00
- 218 I VAN DER WAAL Vrouwen en werk in Hulu Terengganu, Maleisië; arbeidsinzet van vrouwen in een veranderende plattelandseconomie -- Utrecht 1997: Knag/Faculteit Ruimtelijke Wetenschappen Universiteit Utrecht. ca. 192 pp, 12 figs, 63 tabs. ISBN 90-6809-238-3 Dfl 39,50
- 219 C O OMBURA Towards an environmental planning approach in urban industrial siting and operations in Kenya: The case of Eldoret town -- Utrecht/Amsterdam 1997: Knag/Instituut voor Sociale Geografie Universiteit van Amsterdam. 276 pp, 68 figs, 42 tabs. ISBN 90-6809-239-1 Dfl 46,50

- 220 F VAN STEENBERGEN Institutional change in local water resource management: Cases from Balochistan -- Utrecht 1997: Knag/Faculteit Ruimtelijke Wetenschappen Universiteit Utrecht. 240 pp, 19 figs, 6 tabs. ISBN 90-6809-240-5 Dfl 47,00
- 221 A A VAN DER WOUDE Three small towns in Central Java; A comparative study of their economic structure and regional importance -- Utrecht 1997: Knag/Faculteit Ruimtelijke Wetenschappen Universiteit Utrecht. 208 pp, 26 figs, 41 tabs. ISBN 90-6809-241-3 Dfl 36,50
- 222 M J DOUGLAS A change of system: Housing system transformation and neighbourhood change in Budapest -- Utrecht 1997: Knag/Faculteit Ruimtelijke Wetenschappen Universiteit Utrecht. 236 pp, 24 figs, 57 tabs. ISBN 90-6809-242-1 Dfl 48,50
- 223 P J F TERHORST & J C L VAN DE VEN Fragmented Brussels and consolidated Amsterdam; A comparative study of the spatial organization of property rights -- Utrecht/Amsterdam 1997: Knag/Instituut voor Sociale Geografie Universiteit van Amsterdam. 382 pp, 3 figs, 6 tabs. ISBN 90-6809-243-X Dfl 60,00
- 224 H MIDDELKOOP Embanked floodplains in the Netherlands; Geomorphological evolution over various time scales -- Utrecht 1997: Knag/Faculteit Ruimtelijke Wetenschappen Universiteit Utrecht. 352 pp, 154 figs, 49 tabs. ISBN 90-6809-244-8 Dfl 69,00
- 225 S VAN BEURDEN Hydrology, soil mechanics and kinematics of slow mass movements in the Widenbach catchment, Switzerland -- Utrecht 1997: Knag/Faculteit Ruimtelijke Wetenschappen Universiteit Utrecht. 262 pp, 107 figs, 78 tabs. ISBN 90-6809-245-6 Dfl 52,00
- 226 F VAN REISEN Ruim baan door telewerken? Effecten van flexibele werkvormen op ruimtelijke ordening en mobiliteit als gevolg van veranderend tijd-ruimtegedrag -- Utrecht/Delft 1997: Knag/Faculteit Bouwkunde TU Delft. 240 pp, 55 figs, 34 tabs. ISBN 90-6809-246-4 Dfl 42,50
- 227 G P WESTERT & R N VERHOEFF (eds) Places and people: multilevel modeling in geographical research -- Utrecht 1997: Knag/Faculteit Ruimtelijke Wetenschappen Universiteit Utrecht. 128 pp, 39 figs, 18 tabs. ISBN 90-6809-247-2 Dfl 27,50
- 228 J KLAVER From the land of the sun to the city of the angels; The migration process of Zapotec Indians from Oaxaca, Mexico to Los Angeles, California -- Utrecht/Amsterdam 1997: Knag/Instituut voor Sociale Geografie Universiteit van Amsterdam. ca 288 pp. ISBN 90-6809-248-0 Dfl 39,00
- 229 R ISARIN The climate in north-western Europe during the Younger Dryas; A comparison of multi-proxy climate reconstructions with simulation experiments -- Utrecht/Amsterdam 1997: Knag/Faculteit der Aardwetenschappen Vrije Universiteit Amsterdam. ca 160 pp. ISBN 90-6809-249-9 Dfl 32,00
- 230 W HOEK Palaeogeography of Lateglacial vegetations; Aspects of Lateglacial and Early Holocene vegetation, abiotic landscape, and climate in The Netherlands -- Utrecht/Amsterdam 1997: Knag/Faculteit der Aardwetenschappen Vrije Universiteit Amsterdam. ca 160 pp. ISBN 90-6809-250-2 Dfl 32,00
- 231 W HOEK Atlas to palaeogeography of Lateglacial vegetations; Maps of Lateglacial and Early Holocene landscape and vegetation in The Netherlands, with an extensive review of available palynological data -- Utrecht/Amsterdam 1997: Knag/Faculteit der Aardwetenschappen Vrije Universiteit Amsterdam. ca 176 pp, ISBN 90-6809-251-0 Dfl 38,00
- 232 F WOLF Hydrodynamics, sediment transport, and daily morphological development of a bar-beach system -- Utrecht 1997: Knag/Faculteit Ruimtelijke Wetenschappen Universiteit Utrecht. ca 200 pp. ISBN 90-6809-252-9, Dfl 40,00
- 233 B VAN DER WATEREN-DE HOOG Quantification of catchment discharge sensitivity to climate variability -- Utrecht 1997: Knag/Faculteit Ruimtelijke Wetenschappen Universiteit Utrecht. ca 200 pp. ISBN 90-6809-253-7 Dfl 41,00
- 234 N E M ASSELMAN Suspended sediment in the river Rhine; the impact of climate change on erosion, transport, and deposition -- Utrecht 1997: Knag/Faculteit Ruimtelijke Wetenschappen Universiteit Utrecht. ca 200 pp. ISBN 90-6809-254-5, Dfl 42,00

Publications of this series can be ordered from KNAG / NETHERLANDS GEOGRAPHICAL STUDIES, P.O. Box 80123, 3508 TC Utrecht, The Netherlands (Fax +31 30 253 5523; E-mail knag@frw.ruu.nl). Prices include packing and postage by surface mail. Orders should be prepaid, with cheques made payable to "Netherlands Geographical Studies". Please ensure that all banking charges are prepaid. Alternatively, American Express, Eurocard, Access, MasterCard, BankAmericard and Visa credit cards are accepted (please specify card number, name as on card, and expiration date with your signed order).

100-1000

100-1000

100-1000

100-1000

100-1000

100-1000

100-1000

100-1000

100-1000

100-1000

100-1000

100-1000



